TOWARDS ROBUST AND SPECIFIC ENZYMATIC OXIDATION OF HYDROCARBONS

Thesis submitted for the degree of
Master of Philosophy
at the University of Leicester

by

Susan Antonia Murray BSc, MPhil Res

November 2009

TOWARDS ROBUST AND SPECIFIC ENZYMATIC OXIDATION OF HYDROCARBONS

Susan Murray

Selective hydroxylation/epoxidation of hydrocarbons generates useful chiral intermediates for the production of high value chemicals. The use of mono-oxygenase enzymes to add functional groups in a regio-and stereo-selective manner has the benefits of specificity, with yields in high enantiomeric excess. Two enzymes were investigated with a view to developing a robust and specific biocatalyst for the mono-oxidation of hydrocarbons; the membrane bound alkane hydroxylase from *Pseudomonas oleovorans* and the soluble cytochrome P450 BM3 from *Bacillus megaterium*.

A histidine tag was engineered to the C-terminus of the alkane hydroxylase in an attempt to isolate it for structural characterisation. Despite successful insertion of the his tag and good protein expression solubilisation and isolation proved unsuccessful. Therefore, the strategy was altered to focus on the more robust and soluble cytochrome P450 BM3.

Cytochrome P450 BM3 was analysed for activity with various alkenes and styrene and the reaction products were determined by gas chromatography and mass spectrometry (GC/MS). A point mutant, $BM3_{F87G}$, was then expressed and purified, and analysed with the same substrates. The mutant demonstrated increased activity towards these non-natural substrates and a reduction in regio-selectivity. The mutant also showed an increase in enantio-selectivity with a preference for *R*-styrene oxide.

A number of cysteines were then engineered into the heme domain of P450 BM3 to allow for attachment of photo-sensitive agents to enable light-induced electron transfer. The mutants did not appear to alter the enzymes ability to bind fatty acid; neither did they alter the enzymes redox potential to any large degree. Initial tests showed that three of the mutated cysteines were solvent accessible and available for attachment of photo-sensitive thiol modifying agents.

ACKNOWLEDGEMENTS

There are many people I owe my gratitude to and without whom I would never have completed this work. I would like to take this opportunity to thank them all.

Firstly I should thank Professors Andrew Munro & Nigel Scrutton for supervising the experimental part of this work and Dr David Leys for his guidance regarding membrane protein purification and advice on structure-guided mutagenesis.

I would also like to mention all members of the Munro group for their friendship, advice and helpful discussion. In particular Dr Ker Marshal for guidance with molecular biology; Kirsty Mclean for her abundance of knowledge and patience of all things 'Redox'; Hazel Girvan for 'showing me the ropes' and making me laugh; Harriet Seward for help understanding and interpreting the EPR data; and Joe McVey for being my friend and confidant.

I would like to thank my industrial supervisor, Dr Robert Holt, for his guidance throughout the project and for providing the opportunity to perform analysis in his laboratory at Avecia. I would also like to mention the members of his research team for their guidance and support on the preparation of samples for analysis and for making me feel welcome during my stay.

I would like to thank Professor Clive Bagshaw for undertaking the supervision of my thesis writing upon Professors Munro and Scrutton's move to Manchester University. He, along with Dr Christine Wells, have provided support and encouragement throughout this time.

During the writing up period, my work colleagues in the Department of Health Sciences have been especially supportive, many of whom know what it is like to write a for a postgraduate degree and work at the same time. They have all been extremely supportive and have each, in one way or another, kept me going when I was flagging. In particular I would like to thank Prof Paul Burton, Janet Jones, Clare Jackson, Emma Angell and Dr Carolyn Tarrant for their support, encouragement and friendship.

I also owe a huge debt of gratitude to Dr's Janet and Gary Willars. Janet has helped me recognise my strengths and how to get the best from characteristics that could turn to weakness. Gary has been extremely generous with his time, helping me to understand the process of writing and guide me through the minefield (I will have to buy him a new red pen!). Without his support I can honestly say I would have given up a long time ago.

Finally, I would like to thank my family, especially my loving husband Jake, for his belief in me and his unwavering support. Thank you with all my heart.

This project was financially supported by the EPSCR and Bell Technology.

DEDICATION

For Brian and Francis Murray.

CONTENTS

ABBREVIATIONS

Amino Acids

Amino acid	three-letter code	single-Letter code
Alanine	Ala	A
Arginine	Arg	R
Aspartate	Asp	D
Asparagine	Asn	N
Cysteine	Cys	C
Glutamate	Glu	E
Glutamine	Gln	Q
Glycine	Gly	G
Histidine	His	H
Isoleucine	Ile	I
Leucine	Leu	L
Lysine	Lys	K
Methionine	Met	M
Phenylalanine	Phe	F
Proline	Pro	P
Serine	Ser	S
Threonine	Thr	T

Tryptophan	Trp	W
Tyrosine	Tyr	Y
Valine	Val	V

Oligonucleotides

A - Adenine

C – Cytosine

G – Guanine

T – Thymine

Textual Abbreviations

A_{280}	Absorbance at 280 nm (similarly for other wavelengths)
bp	Base pairs
CD	Circular dichroism
Co(sep)3+	Cobalt (II) sepulchrate trichloride
CPR	Cytochrome P450 Reductase
Da	Daltons
ddH20	Distilled, deionised water
DNA	Deoxyribonucleic acid
DTNB	5, 5'-dithiobis-(2-nitrobenzoic acid) or Ellman's reagent
EPR	Electro Paramagnetic Resonance

ET	Electron transfer
FAD	Flavin adenine dinucleotide
FeS	Iron-sulphur
FMN	Flavin Mononucleotide
IPTG	Isopropyl β-D-thiogalactoside
IPTS	1-isothiocyanatopyrene-3,6,8-trisulphonate
K	Kelvin
kb	Kilobases
kbp	Kilobase pairs
NAD	Nicotinamide adenine dinucleotide ((H)-reduced)
NADP	Nicotinamide adenine dinucleotide phosphate
nm	Nanometers
NMR	Nuclear magnetic resonance
OD_{600}	Optical density at 600 nm
PAGE	Polyacrylamide gel electrophoresis
PCR	Polymerase Chain Reaction
PFOR	Phthalate-family mono-oxygenase reductase
Pfu	Pyrococcus furiousus DNA polymerase
PMSF	Phenylmethylsulfonyl fluoride
RMSD	Root mean standard deviation
RR	Rubredoxin reductase

SDS	Sodium dodecyl sulphate
TAE	Tris Acetate buffer
TBE	Tris Borate buffer
TCA	Trichloroacetic acid
Tm	Melting temperature
TNB	2-nitro-5-mercaptobenzoic acid
TUPS	Thiouredopyrene-3,6,8-trisulfonate
TUPS*	excited triplet state of thiouredopyrene-3,6,8-trisulfonate
UV	Ultraviolet

1 Introduction

1.1 Hydrocarbons: a natural resource

The regio- and stereo-selective functionalisation of the ubiquitous but inert hydrocarbon bond into more functional groups has widespread practical application in the world of chemical synthesis. Primarily the by-product of decaying organic material, aliphatic, branched and cyclic hydrocarbons are found in abundance in nature. For example, alkanes constitute up to 50% of crude oil [1]. These saturated hydrocarbons can be readily converted to the slightly more reactive alkene counterparts with the introduction of carbon-carbon double bonds by thermal cracking and catalytic dehydrogenation. Their widespread availability makes them a cheap feedstock to the chemicals industry for the synthesis of chiral intermediates in pharmaceuticals and agricultural chemicals.

Selective hydroxylation and epoxidation of alkanes and alkenes can generate valuable chiral synthons that are used as the building blocks in, for example, the chemical synthesis of complex pharmacologically active compounds [2-5]. Of particular interest are epoxidation reactions on carbon-carbon double bonds. Epoxides can be readily incorporated, in a stereo-specific manner, into a wide variety of industrially useful compounds. They are reactive, far more so than their precursors, and form key intermediates in the preparation of, for instance, chiral 1,2-diols and beta-amino alcohols, both of which are common structures found in pharmacologically active compounds. One such example is the protease inhibitor Crixivan® (indinavir sulphate) (Merk & Co) which is used in antiretroviral therapy to treat HIV infection. Crixivan® has one of the most complex stereo-chemical structures of any commercially available drug. With five asymmetric centres and a total of 32 diastereoisomers, the necessity of enatiomerically pure precursors is fundamental to its manufacture [6]. One of the precursors, *cis*-(1S,2R)-1 amino indan-2-ol, can be synthesised from an epoxide of indene. The traditional chemical epoxidation reaction can be replaced using a mono-oxygenase enzyme (Figure 1.1).

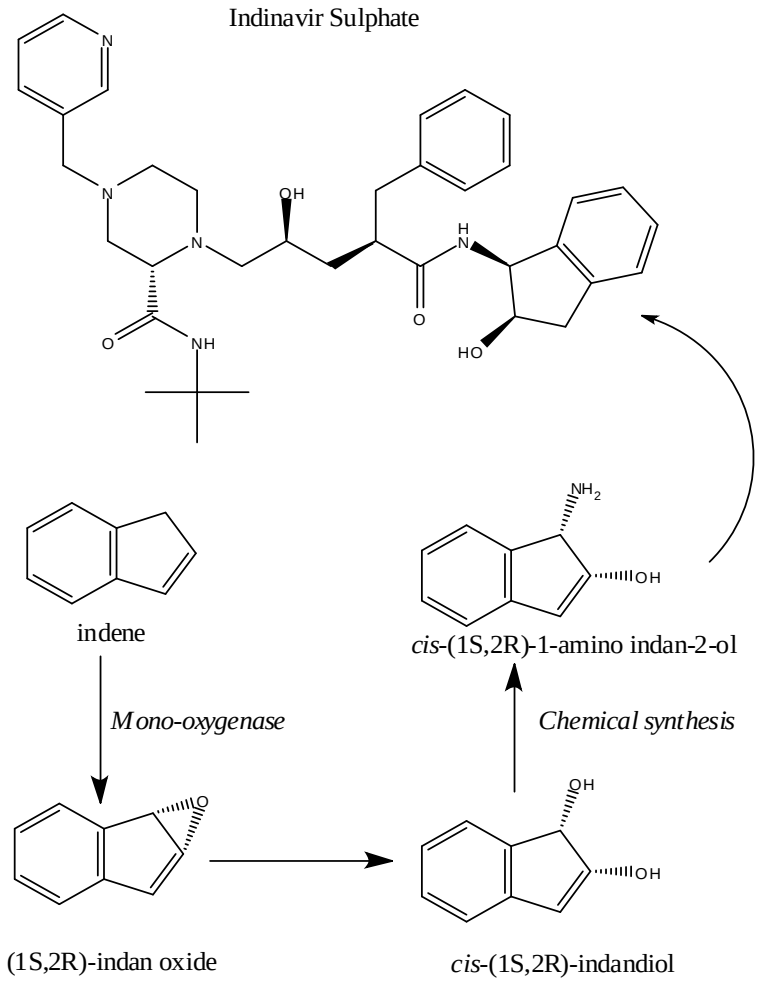

Figure 1.1 Proposed biocatalytic pathway for synthesis of *cis*-aminoindanol.

In the synthetic pathway, indene is subject to asymmetric epoxidation using a Jacobsen Salen catalyst followed by amination using acetonitrile under acidic conditions. The hypothetical biosynthetic pathway uses a mono-oxygenase isolated from *Rhodococcus sp*. I24 converting indene to indan oxide which resolves, via non-enzymatic processes to cis-indandiol. Amination can then continue via the synthetic route or potentially via a second stereo-specific transaminase [7, 8]. The enatiomeric product, cis-(1S,2R)-1-amino indan-2-ol, is subsequently used in the production of the protease inhibitor indinavir sulphate.

1.2 Chirality in biological systems

The asymmetry of chiral molecules is important in pharmacologically active compounds as different enantiomers can have dramatically different effects in biological systems [9]. One classic example is the anti-angiogenic drug Thalidomide. Originally introduced as an anti-emetic and hypnotic, it was administered in its racemic form (a mixture of the *R*- and *S*- enantiomers) to pregnant women towards the late 1950's to combat morning sickness and aid sleep. The drug caused widespread birth defects and was subsequently withdrawn. It was later found that the two enantiomers effect alternate biological consequences with the sedative effect conferred by the *R*-enantiomer and the teratogenic effect caused only by the S-enantiomer [10] (Figure 1.2). The asymmetric control of epoxidation reactions is, therefore, critical in drug development and manufacture.

In another example, epoxidation of styrene at the vinyl position produces styrene oxide which can adopt either *S*- or *R*-enantiomeric conformations. Each enantiomer displays different toxicological effects in mammals [11, 12] and in some prokaryotes with the *R*-enantiomer being more mutagenic [13]. Therefore, the ability to control the stereo-specificity of styrene epoxidation has implications not just in the synthesis of fine chemicals but also in the bioremediation of styrene contamination in the environment.

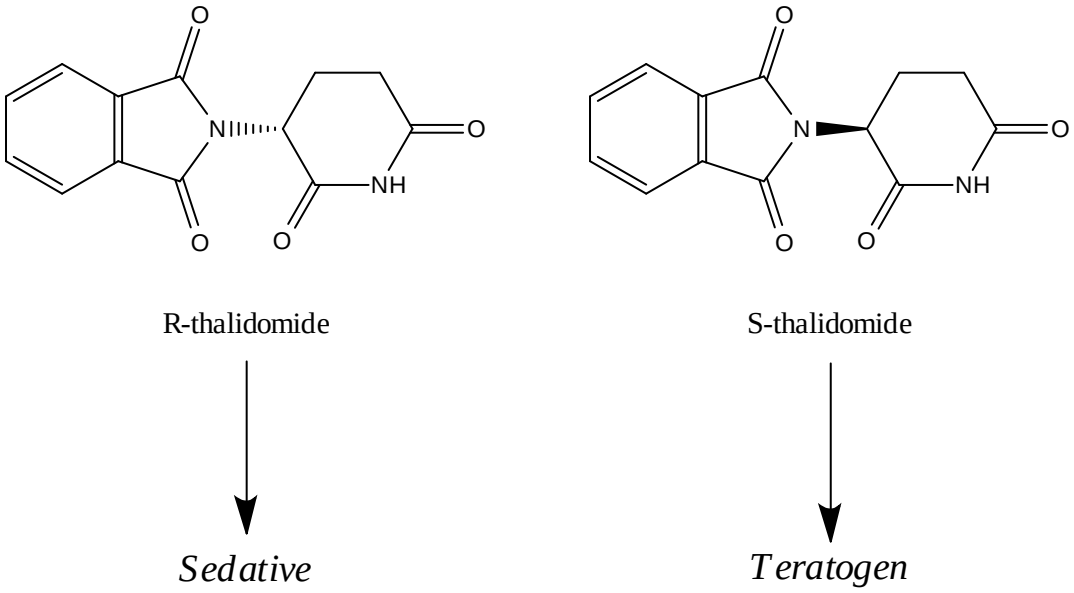

Figure 1.2 The *S*- and *R*-enantiomers of the drug thalidomide have dramatically different biological effects.

The *R*-enantiomer confers a sedative effect whilst the *S*-enantiomer causes congenital abnormalities.

1.3 Enzyme driven chiral synthesis

The synthetic chemistry used to perform epoxidation reactions is predominantly based on toxic metal ions and both regio- and stereo-specificity are difficult to attain. Several synthetic methods exist for asymmetric epoxidation e.g. Sharpless [14] and the Jacobsen Salen catalyst [15] but there are difficulties in scale-up from laboratory to manufacture and in the case of Sharpless, the method is limited to allylic alcohols. Therefore, methods for economically viable, environmentally friendly, scalable asymmetric epoxidation are highly prized.

Oxidative biotransformations, using enzymes to catalyse these oxidation reactions in a stereo-and regio-specific manner have a vast commercial potential within the fine chemicals industry. In general, enzymes are extremely efficient catalysts, accelerating the rate of chemical reactions by as much as 10^{12} [16]. The majority use oxygen as an oxidant, which has the advantage of being cheaper and much more environmentally friendly than the toxic chemical oxidants often used. Enzymes are able to catalyse reactions under mild conditions (~pH 5-8, 20-40^{o}C) which not only makes the processes cheaper and more environmentally friendly but, also reduces the possibility of side reactions often associated with the harsh conditions of synthetic reactions e.g. isomerisation and racemisation. Enzymes also have the potential to be used in large-scale fermentation schemes and because the majority of enzymes are active under the same or similar conditions, it makes them well-suited for sequential reactions in the same cell or flask.

Enzymes as a family are able to catalyse a wide spectrum of reactions e.g. hydrolysis, oxidation/reduction, isomerisation, dehalogenation and decarboxylation and they often display tremendous regio- and stereo-selectivity in their mode of action. They are inherently selective and can be manipulated to prefer one or other substrate/product combination through genetic engineering and/or by performing the reactions in non-aqueous solvents [17]. Genetic screening of organisms among microbial populations can also be used to locate naturally occurring iso-enzymes that are already fit for purpose [18, 19].

Companies like DSM in the Netherlands and Avecia in the UK already exploit enzymes in their production of chiral intermediates for the pharmaceutical and

nutrition industries, with production ranging from several- to several hundred tonnes per year [20]. However, only 2% of the fine chemicals market is currently made up of products manufactured by bio-processing and the use of oxygenases is hampered by the need for co-factors, commonly NADH and NADPH which necessitates a mechanism for recycling [20].

The majority of enzymes explored for their potential use in biotransformations originate from microbial populations. The ability to use alkanes as an energy source is widespread amongst bacteria and not confined to any particular group [21-23]. Medium chain (C10-C18) length hydrocarbons are the easiest to oxidise. Longer chain (>C20) hydrocarbons become increasingly less water soluble and therefore difficult to oxidise due to solubility constraints, whereas the shorter chain lengths (C5-10), although more soluble, are consequently more toxic to the organism. However, it is still possible to find organisms in nature that are able to grow on very long and very short chain hydrocarbons e.g. *P. putida* [22]. The first stage of alkane degradation in these organisms is the addition of oxygen to add a functional group (hydroxide or epoxide), which is followed by sequential hydroxylations, eventually converting the alkane to a fatty acid which can be used as an energy source via the β-oxidation pathway (Figure.1.3).

A variety of enzyme systems that are able to perform this initial oxidation have been identified from bacterial and fungal populations including; heme-containing mono-oxygenases (cytochromes P450), non-heme iron-containing oxygenases (both membrane bound and soluble), flavin-dependant mono-oxygenases and copper-containing oxygenases (Table 1.1). Of these microbial systems, only the membrane-bound alkane hydroxylase system of *Pseudomonas putida* GPo1 has been studied in depth. Originally termed ω-hydroxylase because of its ability to hydroxylate fatty acids at the ω position, the alkane mono-oxygenase system of *P. putida* GPo1 has since been shown to perform mono-oxidation reactions on a huge range of substrates, revealing tremendous potential for exploitation as an industrial biocatalyst [24]. A more recent discovery is the ability of mutant forms of the flavo-cytochrome P450 BM3 to hydroxylate short-chain fatty acids and alkanes [25, 26]. The wealth of information available regarding this enzyme's structure and enzymology coupled with

its high activity and efficiency, make it an excellent prospect for the generation of an adaptable biocatalyst.

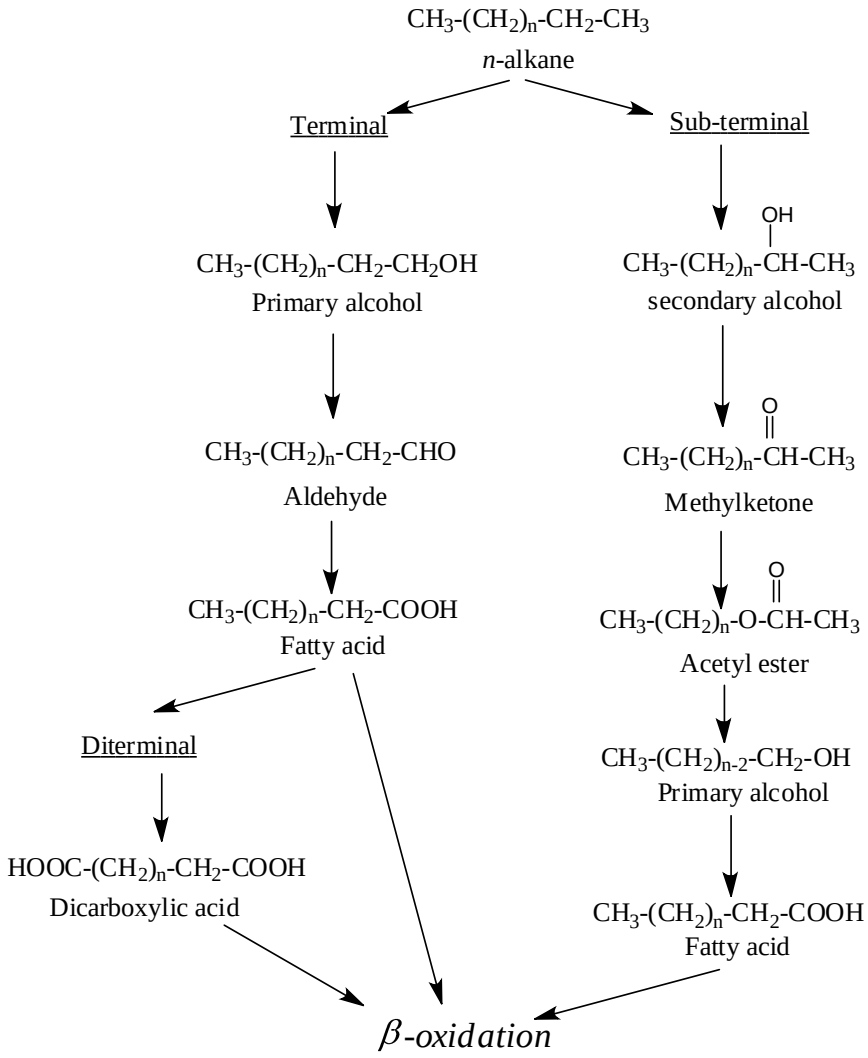

Figure.1.3 Alkane degradation pathways.

The main microbial degradation pathway is via ω-hydroxylation which leads to formation of fatty acids which feed into the *β*-oxidation cycle. Alternatively, sub-terminal oxidation may lead to formation of associated ketones leading into *β*-oxidation. Some organisms are able to oxidise both ends of the substrate and form dicarboxylic acids. (Adapted from [27]).

Table 1.1. Microbial enzyme systems known to perform alkane oxidation.

The Alkane hydroxylase from *Pseudomonas putida* belongs to the membrane-bound bi-nuclear iron containing mono-oxygenases (emboldened).

Enzyme class	Substrate range (in vivo)	Organisms showing presence	References
Eukaryotic cytochromes P450	C10-C16 *n*-alkane	Candida maltosa, Candida tropicalis, Yarrowia lipolytica	[28]
Bacterial cytochromes P450	C4-C16 *n*-alkanes	R. rhodochrous 7E1C Acinetobacter sp. EB104	[29, 30]
Copper-containing butane monooxygenase	Probably C4-C10 *n*-alkanes	Nocardioides sp. CF8	[29, 31, 32]
Butane monooxygenase	C2-C8 *n*-alkanes	Pseudomonas butanovora	[29, 31, 33]
Membrane-bound bi-nuclear iron containing mono-oxygenases	C5-C16 *n*-alkanes	Acinetobacter, Burkholderia, **Pseudomonas**, Rhodococcus, Mycobacterium, Alcanivora,	[34]
Copper-containing dioxygenase	C10-C30 *n*-alkanes	Acinetobacter sp. M-1	[35]

1.4 Overview

The work detailed here was aimed at developing an enzyme-based system for the specific functionalisation of hydrocarbons for use in industrial biosynthesis, with specific emphasis on epoxidation reactions. The two systems chosen to be investigated were the alkane hydroxylase system from *Pseudomonas putida* GPo1 and the fatty-acid hydroxylase P450 BM3 from *Bacillus megaterium.*

Much of the literature available regarding the *P. putida* system has focused on the genetics and regulation of alkane oxidation e.g. [35-42] and a significant amount is known about induction and expression of the system *in vivo* and the enzymology of the soluble electron transfer components of the system e.g. [43-53]. However, little is known about the structure or enzymology of the membrane-bound hydroxylase component, how it interacts with the electron transfer components or the mechanism of the enzyme's regio- and stereo-selectivity. Structural characterisation combined with structure guided mutation can often lead to an understanding of an enzyme's functional mechanism [54]. With these points in mind, the preliminary goal of this work was the isolation and characterisation (structural and kinetic) of the membrane-bound component of the alkane hydroxylase system.

Chapter 3 introduces the *P. putida* alkane hydroxylase system, the tri-component structure of its electron transport chain and the current understanding of the structure-function relationships. The isolation and purification of the soluble components of the system are described, followed by an account of the methods employed in attempting the isolation of the membrane alkane hydroxylase, including the engineering of a histidine tag for the purposes of purification by affinity chromatography.

Chapter 4 introduces the enzymology of cytochromes P450 in general before focussing on flavo-cytochrome P450 BM3. Despite its later discovery [55], a considerable amount is known about the enzymology of P450 BM3. The enzyme is soluble and easily expressed in heterologous hosts, see for example reference[56]; structural and functional characterisation has lead to significant advances in the understanding of the reaction mechanism of the enzyme and of cytochromes P450 in general, as well as identification of key structural components responsible for the enzyme's substrate specificity, see for example references [57-61]. The enzyme is

unique within the cytochrome P450 super-family in that its obligate redox donor protein is covalently fused to the hydroxylase component (the heme-domain) of the enzyme, making it catalytically self-sufficient and providing it with remarkably fast reaction kinetics [62].

A range of P450 BM3 mutants have been shown to have altered substrate specificity, pushing the enzyme's preference away from mid/long-chain fatty acids towards short-chain fatty acids and alkanes. One amino acid in particular, phenylalanine 87 (F87), has been identified as a key player in the regio-selectivity of the hydroxylation reaction. The preliminary goal for this section was to analyse the activity of the wild-type P450 BM3 and a F87 mutant using styrene and alkene substrates to evaluate the kinetics and product profile of the enzyme and explore the effect of the mutation on this activity. The isolation and characterisation of the wild-type and F87 mutant forms of the enzyme are described, followed by the analysis of their products after reaction with styrene and various alkenes.

Chapter 5 describes investigation of the potential of P450 BM3 to become cofactor-independent to eliminate the need for NADPH as an electron donor. A major obstacle to the economical use of redox enzymes as biocatalysts is their requirement for expensive cofactors such as NAD(P)H. Several methods can be employed to reduce the costs involved including conducting whole cell biotransformations (where the co-factors are recycled by the living cells' own metabolic functions) and employing cofactor recycling enzymes in cell-free biocatalysis. A variety of approaches to explore cofactor-independent biocatalysis have been published. For instance, engineering peroxygenase activity to enable the reaction to be driven by peroxide, see for example references [63, 64] or using electrodes to drive catalysis either directly or using mediators, see for example references [65-68]. To this end, P450 BM3 was engineered to enable the attachment of photo-sensitive reducing agents to explore the possibility of NADPH-independent, light-driven biocatalysis. Cysteines were introduced at a number of locations to enable attachment of thiol-modifying, photo-sensitive agents. The effect of the mutations on the enzyme/substrate relationship were analysed and the solvent accessibility of the newly engineered thiol groups was measured using UV/visible and EPR spectroscopy.

2 Methods

2.1 Materials

2.1.1 Chemicals & Reagents

Yeast extract, tryptone and agar were from Oxoid, Cambridge. Agarose, Ampicillin and IPTG (Isopropyl β-D-thiogalactoside) were from Melford Laboratories, Ipswich, UK. Chromatography materials were from Pharmacia. All substrates for P450 BM3 reactions (alkenes and arachidonic acid) were purchased from Sigma-Aldrich. All other Chemicals were purchased from Sigma unless otherwise stated and were of analytical grade wherever possible. Water used was glass-distilled and deionised.

2.1.2 Media

All media were mixed according to protocols described by Sambrook *et al* [69]. LB broth contained per litre: 10 g tryptone, 10 g NaCl and 5 g yeast extract, supplemented where appropriate with 50 μg/ml ampicillin or in the case of BL21(DE3)pLysS, 100 μg/ml ampicillin and 34 μg/ml chloramphenicol. LB agar solid media contained per litre: 10 g tryptone, 5 g yeast extract, 10 g NaCl and 7 g agar, supplemented where appropriate with 100 μg/ml ampicillin. Liquid media 2xYT contained, per litre: 16 g tryptone, 10 g yeast extract and 5 g NaCl, supplemented where appropriate with 50 μg/ml ampicillin. Terrific broth [70] contained per litre: 12 g tryptone, 24 g yeast extract, 4 ml glycerol and 900 ml H_2O, made up to 1 L after autoclaving by the addition of 100 ml TB buffer (0.17 M KH_2PO_4, 0.72 M K_2HPO_4) [70].

2.1.3 Bacterial Strains

The *E. coli* strains used in this study and their genotypes are listed in Table 2.1.

Table 2.1 Bacterial Strains

Strain	Genotype	Source/Reference
TG1	[*sup*E, *hsd*D5, *thi*, D(*lac-pro*AB), F' [*tra*D36, *pro*AB^{+}, *lac*I^{q}, *lac*ZDM15]]	(Stratagene, Cambridge, UK)
XL1-Blue	[recA1 endA1 gyrA96 thi-1 hsdR17 supE44 relA1 lac [F' proAB laci^{q} ZD15 Tn10 (Tet^{r})]]	(Stratagene, Cambridge, UK)
BL21 (DE3)	*E.coli* BF' *dcm ompT hsdS* (r_B-m_B-) *gall* (DE3)] and BL21 (DE3) pLysS [F-, *omp*T, *hsd*Sβ(rβ-mβ-), *dcm*, *gal*, (DE3), pLysS(CmR) tonA]	(Stratagene, Cambridge, UK) [71]
NovaBlue	[endA1 hsdR17 ($r_{K12}^{-}m_{K12}^{+}$) supE44 thi-1 recA1 gyrA96 relA1 lac F'[$proA^{+}B^{+}$ $lacI^{q}ZDM15$ ::Tn10(Tc^{R})]]	(Novagen, Merck, Darmstadt, Germany).
C41 (DE3)	[*E.coli* BF' *dcm ompT hsdS* (r_B-m_B-) *gall* (DE3)] plus at least one additional uncharacterised mutation	(AVIDIS S A, Saint Beauzire, France) [72]
JM109	(F´ traD36 proAB lacI Δ(lacZ)M15/ Δ(lac-proAB) glnV44 e14 gyrA96 recA1 relA1 endA1 thi hsdR17^{++q-})	(Promega)

2.1.4 DNA Modifying Enzymes and Molecular Weight Markers

Pfu DNA polymerase and *Dpn* I restriction endonuclease were supplied by Stratagene (Cambridge, UK). DNA ladders and protein marker were obtained from New England Biolabs (NEB, Hitchin, UK) with the following size and concentration ranges: 1 kb DNA ladder, 10.0 (42 ng), 8.0 (42 ng), 6.0 (50 ng), 5.0 (42 ng), 4.0 (33 ng), 3.0 (125 ng), 2.0 (48 ng), 1.5 (36 ng), 1.0 (42 ng) and 0.5 kb (42 ng); Broad

Range Protein Marker, 212, 158, 116, 97.2, 66.4, 55.6, 42.7, 34.6, 27.0, 20.0, 14.3, 6.5, 3.4 and 2.3 kDa.

2.1.5 Plasmid vectors

The expression vectors pBM20 and pBM23 were the source of heme-domain and full-length P450 BM3 respectively [62]. Plasmid pBM23 contains a 5 kbp fragment of *B. megaterium* chromosomal DNA encoding the entire P450 gene plus its own internal promoter [62] inserted in the vector pUC119 [73]. Plasmid pBM20 contains a 1.5 kbp fragment of chromosomal DNA from *B. megaterium* encoding the heme-domain (residues 1-472) of P450 BM3 inserted into the vector pUC118 [73] but does not contain the *Bacillus* promoter. Plasmid clone encoding full-length P450 $BM3_{F87G}$ (hence forth referred to as pBMF87G) was originally obtained by Professor Andrew Munro (Dept. of Biochemistry, University of Leicester) from Dr. David Mullin and Professor William Alworth (Dept. of Chemistry, Tulane University, New Orleans, USA), expression is under the control of T7 promoter [60]. The plasmid clone for heme-domain P450 $BM3_{F87G}$ (hence forth referred to as pBMHF87G) was constructed in-house Dr Hazel Girvan (Dept. of Biochemistry, University of Leicester). Vectors for the expression of rubredoxin, rubredoxin reductase and alkane hydroxylase were kindly donated by Ashley Perry and Winston Tambraya (Dept. Biochemistry, University of Leicester). The genes encoding rubredoxin and rubredoxin reductase (*alkG* and *alkT* respectively) were amplified from the OCT plasmid (*P. putida)* and inserted independently into cloning vector pKK223-3 (Pharmacia, Stockholm, Sweden), creating pKR10 and pKRR5 for the expression of rubredoxin and rubredoxin reductase respectively (Perry)[50, 53].

The gene encoding alkane hydroxylase (alkB) was amplified from the OCT plasmid (P. putida) and inserted into the expression vector pET3a to make pAlkB-3a (Tambraya) [74]. Expression in this plasmid in under the control of IPTG-inducible T7 promoter. Figure 2.1 to Figure 2.6 describe the plasmids used in this study and show the location of gene inserts, promoter and the restriction site used for cloning. The expression vectors used are summarised in Table 2.2.

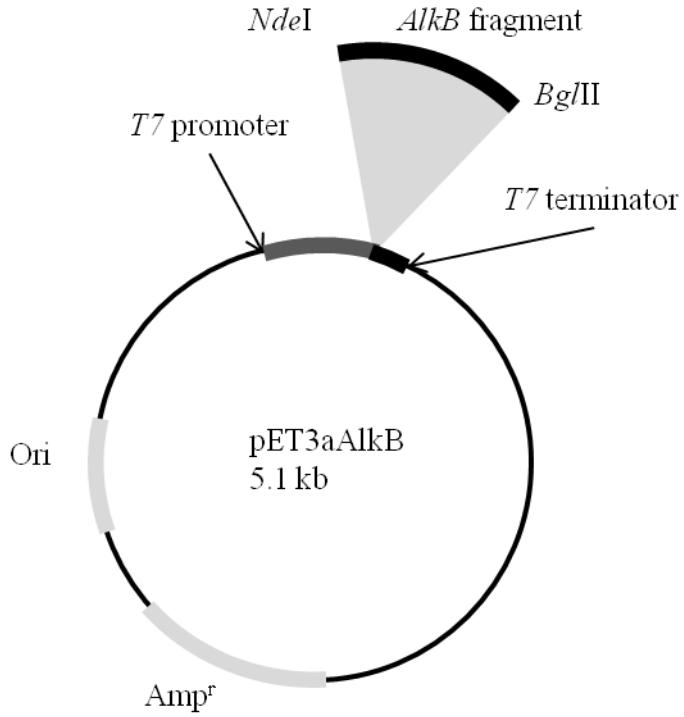

Figure 2.1 Plasmid pET3aAlkB for expression of Alkane Hydroxylase

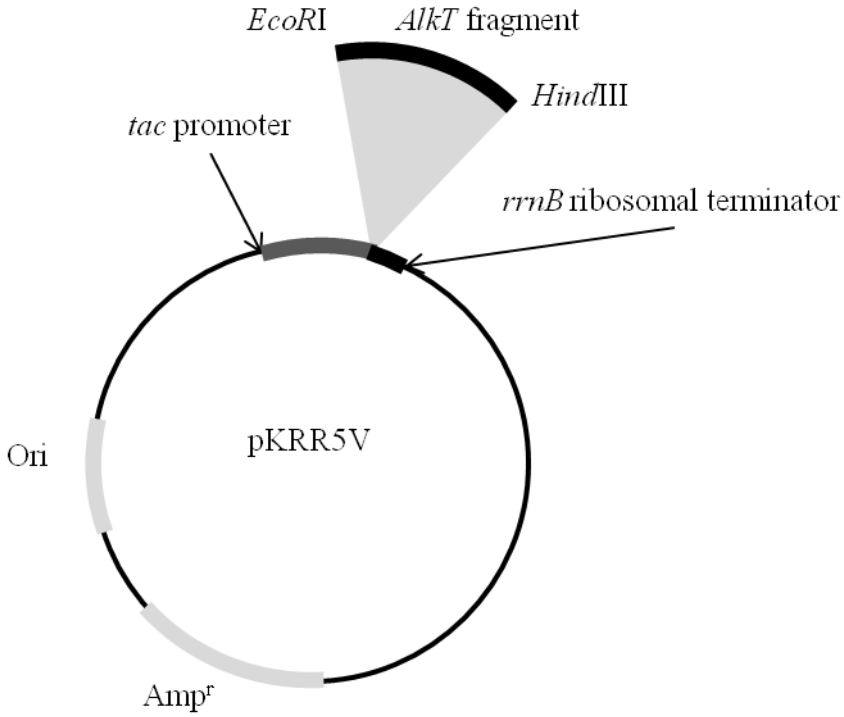

Figure 2.2 Plasmid PKRR5V for expression of rubredoxin reductase.

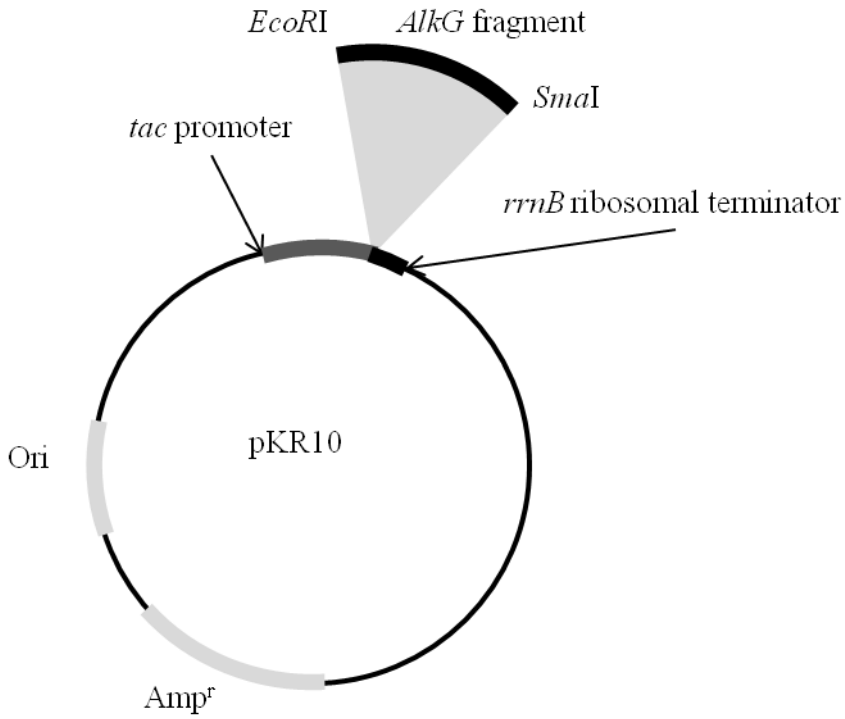

Figure 2.3 Plasmid pKR10 for expression of rubredoxin.

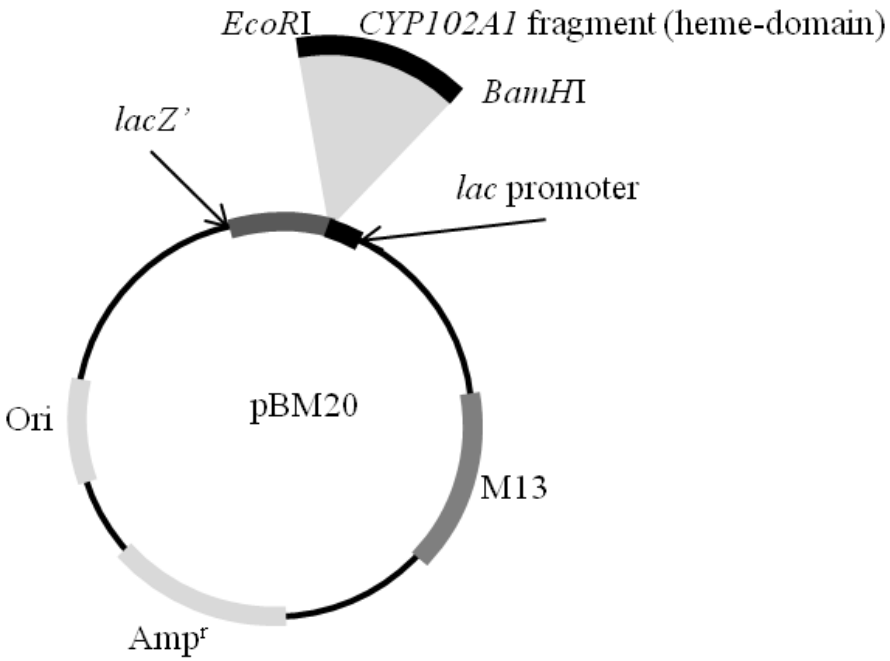

Figure 2.4 Plasmid pBM20 for expression of full-length P450BM3.

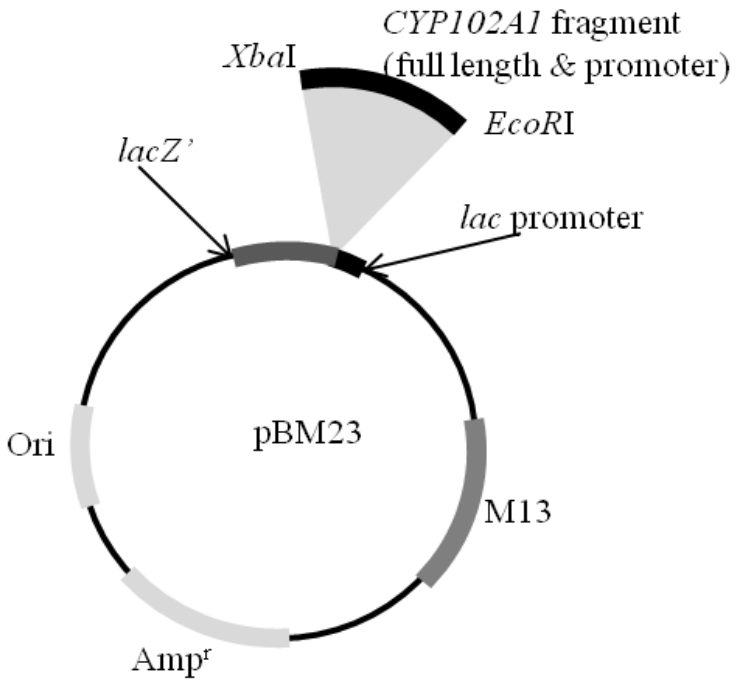

Figure 2.5 Plasmid pBM23 for expressionof heme-domain P450BM3.

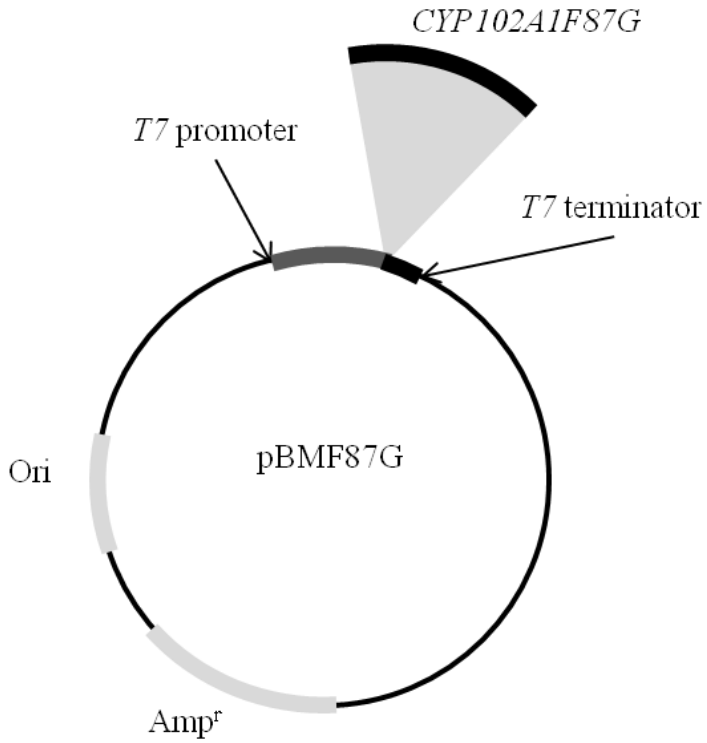

Figure 2.6 Plasmid pBMF87G for expression of Full-length BM3F87G.

Table 2.2 Genotypes of expression vectors used in this study.

Amp^r indicates presence of β-lactamase gene (conferring ampicillin resistance), the prefix "His-" indicates the gene is attached to a histidine linker encoded at the C-terminal of the protein.

Plasmid	Genotype	Source/Reference
pKR10	Amp^r, *AlkG*, pKK223-3	Dr A Perry (University of Leicester) [50]
pKRR5V	Amp^r, *AlkT*, pKK223-3	Dr A Perry (University of Leicester) {Lee, 1997 #402
pAlkB-3a	Amp^r, *AlkB*, pET3a	Dr W Tambraya (University of Leicester), [74]
pAlkB3H	Amp^r, His-*AlkB*, pAlkB-3a	This study
pBM20	Amp^r, *CYP102A1* (heme-domain), pUC119	[62]
pBM23	Amp^r, *CYP102A1*, pUC119	[62]
pBMHF87G	Amp^r, *CYP102A1F87G* (heme-domain), pBM20	Dr Hazel Girvan (University of Leicester)
pBMF87G	Amp^r, *CYP102A1F87G*, pTZ18U	[62]
pBM20Q387C	Amp^r, *CYP102A1Q387C*, pBM20	This study
pBM20Q397C	Amp^r, *CYP102A1Q397C*, pBM20	This study
pBM20Q403C	Amp^r, *CYP102A1Q403C*, pBM20	This study
pBM20Q404C	Amp^r, *CYP102A1Q404C*, pBM20	This study

2.2 Molecular biology methods

2.2.1 Preparation of plasmid DNA

All molecular biology methods, unless otherwise stated, were carried out using standard protocols [69].

All DNA preparations were performed using the Qiagen mini-prep kit (Qiagen, Hilden, Germany), for diagnostic purposes and the Qiagen Midi-prep kit, for obtaining DNA stocks and quantities for sequencing. The kits were used according to manufacturer's instructions. Briefly, single colonies of the relevant *E. coli* strain transformants were used to inoculate 5 ml (50 ml) of LB media and left to grow overnight (12 – 16 hours). Cells were harvested by centrifugation before resuspension in buffer (supplied with the kit), followed by DNA extraction. The extraction method employed by Qiagen in the kits is based on the alkaline lysis method [75, 76], the final DNA sample being stored (-20 ^{o}C) in EDTA free buffer.

2.2.2 PCR and Sequencing

All primers were obtained from the Protein and Nucleic Acid Chemistry Laboratory (PNACL) at the University of Leicester or Invitrogen. Sequencing reactions were performed by PNACL, using the di-deoxy chain termination method [77]. All PCR reactions were performed in a Techne Genius thermal cycler with a heated lid (Techne Ltd, Cambridge, UK). Sequences were aligned and compared using Clustawl [78] and chromatograms analysed using Chromas v. 1.62 (Technelysium, Helensvale, Australia).

2.2.2.1 Blunt end cloning into pGEM-T

The gene coding alkane hydroxylase (AlkB) was amplified from plasmid template pAlkB-3a by PCR using *Pfu* DNA Polymerase and the following primer; ANF, $^{5'}$CATATGCTTGAGAAACACAGAGTTCTGGATTCCGC$^{3'}$ and ASR, $^{5'}$GTCGACTGCTACCGCAGAGGTACTCGAACTATGACC$^{3'}$. Thermal cycler conditions were a single cycle of 30 s at 95 ^{o}C followed by 30 cycles of 30 s at 95 ^{o}C, 1 min at 59 ^{o}C, 1.5 min at 72 ^{o}C. The reaction mixture contained 0.5 μg DNA template, 0.2 mM dNTP mix, 0.8 μM each primer and 1 unit *Pfu* DNA polymerase in

a total volume of 50 µl. PCR product was separated using agarose gel electrophoresis (Section 2.2.3) and the amplified DNA was purified using a gel extraction spin kit (Qaigen, Hilden, Germany).

A 7 µl sample of *Pfu* DNA Polymerase-generated, gel purified, PCR fragment was incubated with *Taq* DNA Polymerase for 30 min at 70 ^{o}C in the presence of 0.2 dATP's in order to add dATP nucleotides to the 3' end of the PCR fragment (A-tailing) for insertion into pGEM-T. The A-tailed fragment was then ligated into vector pGEM-T using DNA ligase. A-tailed insert was incubated with pGEM-T in a 1:1 and 1:3 insert/plasmid ratios in separate reactions, alongside 1 µl DNA ligase in a total volume of 10 µl for 16 hr at 4 ^{o}C. Ligated plasmid was then used to transform *E. coli* JM109 cells using standard protocol as described (Section 2.2.6).

2.2.2.2 Site-directed mutagenesis

Each mutagenic PCR reaction mixture contained 5 µl of 10 x reaction buffer, 50 ng of backbone plasmid DNA, 125 ng each of the relevant forward and reverse oligonucleotide primers, 0.2 µM dNTPs and ddH_2O distilled water to a final volume of 50 µl. Finally 2.5 U of Pfu turbo DNA polymerase were added immediately prior to thermal cycler condition commencing. A 5 µl sample of the resultant PCR product was analysed by agarose gel-electrophoresis and the sample concentration estimated using comparison with the DNA ladder as described (Section 2.2.3).

Mutagenic PCR was performed on pAlkB-3a to construct a $(His)_6$ tag and stop codon in the C-terminus of AlkB. PCR was performed using the primers AHF and AHR in Table 2.3. Primers were designed to anneal to the C-terminal end of the protein as it lies within the plasmid in order to introduce 6 histidine residues and a stop codon into end of the gene. Thermal cycler conditions were as follows; a single cycle of 30 s at 95 ^{o}C followed by 20 cycles of 30 s at 95 ^{o}C, 60 s at 55 ^{o}C, 8 min at 68 ^{o}C.

The four glutamine residues, 387, 397, 403 and 404 in the heme-domain of P450 BM3 were mutated to cysteine by site-directed mutagenesis, using pBM20 as the plasmid template. Primers were designed to anneal to the centre of the gene fragment as it lies within the plasmid pBM20. Thermal cycler conditions were as follows; a single cycle of 30 sec at 95 ^{o}C followed by 16 - 18 cycles of 30 s at 95 ^{o}C, 60 s at annealing temperature, 5 min at 68 ^{o}C. The annealing temperatures used for each

mutant were 53 ^{o}C, 57 ^{o}C and 59^{o}C for Q403C, Q387C and Q397C/Q404 respectively.

Where DNA was present of anticipated size the remaining PCR product was digested with *Dpn* I as described in Section 2.2.4 to remove the parent methylated DNA and transformed into either *E. coli* TG1 (for pAlkB3H) or *E. coli* NovaBlue (for pBM20 derivatives). Following transformation of the DNA into *E. coli*, transformants were selected on LB media containing ampicillin at a final concentration of 100 mg/ml. Transformant colonies (6 of each) were picked to prepare plasmid DNA using the Qaigen mini-prep kit (Section 2.2.1). Following analysis by agarose gel electrophoresis (section 2.2.3) a minimum of two plasmid samples were sent for sequencing as described (Section 2.2.1).

Table 2.3 Oligonucleotide primers for site directed mutagenesis. Codon mismatches are shown in bold, stop codons are underlined.

Mutation	Name	Primer Sequence (5'→ 3')
AlkB(His)$_6$	AHF	CTGCGGTAGCATCG**CATCATCATCATCACCAT**TAG CTAACAAAGCCCG
	AHR	CGGGCTTTGTTAGCTA**ATGGTGATGATGATGATG**C GATGCTACCGCAG
BM3$_{Q387C}$	Q387CF	CCAAGTGCGATTCCG**TGT**CATGCGTTTAAACCG
	Q387CR	CGGTTTAAACGCATG**ACA**CGGAATEGEACTTGG
BM3$_{Q397C}$	Q397CF	GCGTTTAAACCGTTTGGAAACGGT**TGT**CGTGCGTGT ATCGG
	Q397CR	CCGATACACGCACG**ACA**ACCGTTTCCACCAGGTTTA AACGC
BM3$_{Q403C}$	Q403CF	GCGTGCGTGTATCGGT**TGT**CAGTTCGCTC
	Q403CR	GCGAACTG**ACA**ACCGATACACGCACG
BM3$_{Q404C}$	Q404CF	GCGTGTATCGGTCAG**TGT**TTCGCTCTTCATGAAGCA ACGC
	Q404CR	GCGTTGCTTCATGGAGAGCGAA**ACA**CTGACCGATA CACGC

2.2.2.3 Sequencing

For plasmid DNA, 0.6 μg of DNA was supplied alongside the relevant sequencing primer(s) (10 pmoles per reaction). Primers used for sequencing were as follows; TUPseq $^{5'}$GCGTTTAAACCGTTTGGAAACGGTTGTCGTGCGTGTATCGG$^{3'}$ for heme-domain cysteine mutants; BM1 $^{5'}$TTCACACAGGAAACAGCTAT$^{3'}$, BM2

$^{5'}$TCCTGCGTTTTCCCTATAT$^{3'}$, BM3 $^{5'}$TACCGGAAGACATGACACG$^{3'}$ for full sequencing of heme-domain BM3 in pBM20 and derivatives (heme-domain P450 BM3); T7 $^{5'}$AATACGACTCACTATAGGG$^{3'}$ (supplied by PNACL) for pAlkBH.

2.2.3 DNA agarose gel-electrophoresis

DNA produced from PCR reactions, restriction digests and frozen stocks (for verification of quality/integrity and estimation of DNA concentration), was analysed by running samples on 0.8 % agarose gel containing 0.6 μg/ml ethidium bromide submerged in 1 x TAE buffer (50x TAE buffer consisted of 242 g tris base, 18.6 g EDTA and 57.1 ml glacial acetic acid made up to 1 litre). Typically, a 10 μl sample of DNA (appropriately diluted if needed to approximately 0.5-1 μg) was prepared by adding 2 μl of 6 x loading buffer (consisting of 0.25 % bromophenol blue, 0.25 % xylene cyanol and 30 % glycerol in 50 mM EDTA) was run alongside a 1 kb DNA ladder (0.5 μg in same volume) at 150 V for 30 – 60 minutes. Visualisation, image capture and band analysis of gels was performed on a G:Box gel documentation system using GeneSnap and GeneTools software (Syngene, Cambridge, UK).

2.2.4 Restriction Digest

Restriction digests were performed as recommended by the enzyme suppliers using the buffer components supplied with the restriction enzymes (NEB). The digested DNA was analysed by DNA agarose gel electrophoresis. *Hind*III endonuclease was used to digest plasmids pBM20 and pBM23 before analysis; *Bam*HI and *Ase*I endonuclease was used to digest AlkB plasmid; the correct fragmentation pattern being used to confirm the identity of the plasmid DNA.

2.2.5 Preparation of competent *E. coli* cells

Competent cells were prepared using the method published by Sambrook *et al* [69]. A single colony was used to inoculate 5 ml of LB medium and grown overnight at 37 ^{o}C with gentle shaking. This overnight culture was used to inoculate fresh LB medium (1 ml into 100 ml LB) and incubated with shaking at 37 ^{o}C until the optical density (OD) reach 0.6-0.8. The cell suspension was then immediately cooled by transfer to ice then the cells collected by centrifugation (6000 g, for 10 minutes) in a pre-cooled rotor (4 ^{o}C). The supernatant was discarded and cells gently re-suspended

in sterile, ice-cold calcium chloride solution (0.1M $CaCl_2$, 10% glycerol) and left on ice for 15 minutes. The cells were centrifuged as before and re-suspended in 1 ml of the same CaCl2 solution. Aliquots of the cells (50 μl) were stored @ -80 ^{o}C in sterile, pre-cooled microfuge tubes and used within one month.

2.2.6 Transformation of competent *E. coli* cells

Transformations of competent cells were performed according to the method described by Sambrook *et al* [69]. Aliquots (50 μl) of competent *E. coli* cells (strains TG1, C41 (DE3) and BL21) were allowed to thaw on ice. Plasmid DNA (~10–50 ng) was added to the cell suspension. The tube was gently mixed by flicking before returning to ice for 30 min. The cell suspension containing the DNA was then heat-shocked in a water-bath at 42 ^{o}C for 2 min, then returned to ice for a further 3 min. Fresh LB medium (400 μl) was added to the cell suspension which was then incubated at 37 ^{o}C for 30 min. Aliquots of (100–200 μl) cell suspension were plated onto LB agar plates supplemented with ampicillin (100 μg/ml). The plates were allowed to stand on the bench for 15 min before incubation overnight at 37 ^{o}C.

2.3 Protein preparation

All liquid chromatography was carried out at 4 ^{o}C in a temperature controlled room using either gravity flow or flow controlled by peristaltic pumps (Amersham Biosciences, Berks, UK). All chromatography media was packed in either XK 26/70 or XK 26/100 glass columns internal diameter (i.d.) 26 mm and length 70 cm or 100 cm respectively (Pharmacia, USA) except affinity media which was packed in 10mm i.d. 30 cm length glass column (Omnifit, Cambridge, UK) and run under gravity flow only. Fractions (typically 2-5 ml) were collected automatically using a GradiFrac fraction collector (Pharmacia) unless otherwise stated.

2.3.1 Expression and purification of rubredoxin

Rubredoxin was expressed in *E. coli* TG1 cells transformed with pKR10, expression is under the control of the *tac* promoter. Location of rubredoxin during the purification was identified using spectroscopy. Starter cultures (5 ml LB, containing 50 μg/ml ampicillin) were inoculated from freshly transformed cells. The overnight culture was used to inoculate 2 x YT media (2.1.2) supplemented with ampicillin to 50 μg/ml (500 ml in 2 L Erlenmeyer flasks, typically 6 L total culture). After inoculation with an overnight culture, cells were allowed to grow for 24-26 h at 37 ^{o}C with shaking at 230 RPM. The cells were then harvested by centrifugation at 10,000 g for 20 min at 4 ^{o}C (5,000 rpm in a Sorvall RC5B using FAS10C rotor). The harvested cells were washed once by re-suspension in buffer A (50 mM potassium phosphate buffer, pH 7.5). Centrifugation was repeated and cell pellets frozen at -20 ^{o}C overnight.

All subsequent processes were carried out at 4 ^{o}C or on ice, unless otherwise stated. Cell pellets were defrosted on ice and resuspended in buffer A with the addition of 1mM phenylmethylsulfonyl fluoride (PMFS). Cells were lysed using a combination of French press (2 passes at 950 lb/in^2) followed by sonication at 40% power for 10 x 20 second bursts with 2 min rest gaps to allow cooling. Unbroken cells and cellular debris were separated from soluble protein by centrifugation for 90 min at 12,000 g (18,000 rpm in a Sorvall RC5B using FAS20C rotor). The supernatant containing rubredoxin was then removed to a clean pre-cooled container ready for purification.

Purification of rubredoxin was achieved following the protocol described by Tambraya [79] which is a modification of that published by Lee *et al* [50]. Cell free lysate was fractionated using ammonium sulphate ($(NH_4)_2SO_4$). Lysate was brought slowly to 40% saturation $(NH_4)_2SO_4$ with gentle stirring, the supernatant, containing rubredoxin, was separated from precipitate by centrifugation (10 min at 8,000 g) and the precipitate discarded. The $(NH_4)_2SO_4$ saturation in the supernatant was then increased to 60% and precipitate was again separated by centrifugation. The precipitate from this 40-60% fraction, which contained rubredoxin (as denoted by a rich red colour) was kept and the protein gently re-suspended in buffer A (~ 100 ml) and dialysed against 2 x 5 L of buffer A for at least 3 hours each, or overnight prior to chromatography.

The protein was then loaded onto anion exchange resin (Q-Sepharose, ~ 250 ml col. vol. Pharmacia) pre-equilibrated with buffer A. The column was then washed with at least two column volumes of buffer A. Protein was eluted using a multi-step gradient of 0 – 0.5 M KCl in buffer A over 300 ml followed by 150 ml holding at 0.5 M KCl in buffer A , followed by a second gradient from 0.5 M to 1 M KCl in buffer A for 300 ml in which rubredoxin was eluted. Rubredoxin in the eluate was identified by absorbance at ~ 495 and 380 nm. Fractions containing rubredoxin were pooled and dialysed against 2 x 5 L of buffer A for at least 3 h each.

The protein was then brought to 35% $(NH_4)_2SO_4$ saturation and loaded onto a hydrophobic interaction column (Phenylsepharose, ~ 300 ml, Pharmacia) pre-equilibrated with buffer A containing 35% $(NH_4)_2SO_4$. Protein was eluted in a gradient of 35-0% $(NH_4)_2SO_4$ saturated buffer A. Fractions containing samples with A_{280}/A_{497} ratio of 6.5:1 or less were pooled and concentrated using centrifugal filtration with a 10 kDa cut-off (Millipore, Biljerica, USA). Concentrated protein was dialysed exhaustively against buffer A to remove any salts and stored at -20 ^{o}C in 50% glycerol.

As rubredoxin is purified in the one iron form, iron can be inserted into the second iron binding site by precipitation and refolding of the protein in the presence of iron [50, 80]. A 10 mg sample of rubredoxin as purified above was precipitated by the addition of trichloroacetic acid (TCA) to a final concentration of 10% (w/v) at room temperature. The precipitate was harvested by centrifugation (10 min at top speed in

a bench-top centrifuge) and transferred to anaerobic glove box (Bell Technology, UK). Once in the glove box, the protein precipitate, which was now very pale having lost its iron, was dissolved in oxygen-free 0.5 M Tris base, 0.5 M 2-mercaptoethanol to give a final protein concentration of 5-10 mg/ml. The mixture was incubated at room temperature, under anaerobic conditions, for 3 h. The protein was then precipitated as before by addition of TCA to 10% (w/v). Precipitate was harvested by centrifugation as before and incubated **on ice** for 30 min before re-suspension in 0.5 M Tris base, this time containing ferrous ammonium sulphate ($(NH_4)_2SO_4FeSO_4$ $6H_2O$) to a 5 fold molar excess over protein. The protein solution, now a deep green, was further incubated for 1 h on ice before gradual introduction of air via a needle puncture to the microfuge tube, returning the protein to a deep red colour. The refolded protein was desalted and exchanged into 0.05 M potassium phosphate buffer (pH7.5) by passing through a G-25 Sephadex column (Whatman, Maidstone, UK) pre-equilibrated with the buffer.

2.3.2 Expression and purification of rubredoxin reductase

Rubredoxin reductase was expressed in *E. coli* TG1 cell transformed with pKRR5 following the protocol described by Tambraya [79]. Starter cultures (2 x 10 ml LB, containing 100 μg/ml ampicillin) were inoculated from freshly transformed cells and grown overnight at 37 ^oC with vigorous shaking (230 rpm). These overnight cultures were used to inoculate a secondary starter culture of 2 x YT media (500 ml in 2 L Erlenmeyer flask) supplemented with ampicillin to 100 μg/ml which was incubated at 30^oC for 18 – 22 h with vigorous shaking (230 rpm). This secondary starter culture was then used to inoculate 2 x YT media (1 L each in 2 L Erlenmeyer flasks) supplemented with ampicillin to 100 μg/ml, ensuring a final cell density of between OD_{600} 0.075 and 0.08. These cells were grown 20^oC with vigorous shaking until cell density reached OD_{600} of 3.5- 4 (typically 20-26 h). The cells were then harvested by centrifugation, washed and stored overnight as described for rubredoxin (Section 2.3.1).

All subsequent processes were carried out at 4^oC or on ice, unless otherwise stated. Cell pellets were defrosted on ice and re-suspended in buffer B (20 mM potassium phosphate, pH 7.5, 20% v/v glycerol) with the addition of 1 mM PMFS. Cells were lysed using a combination of French press (2 passes at 950 lb/in^2) followed by

sonication at 40% power for 10 x 20 second bursts with 2 minute rest gaps to allow cooling. Unbroken cells and cellular debris were separated from soluble protein by centrifugation for 90 min at 12,000 g (18,000 rpm in a Sorvall RC5B using FAS20C rotor). The supernatant containing rubredoxin reductase was then removed to a clean pre-cooled container ready for purification.

Cell free lysate was fractionated using ammonium sulphate ($(NH_4)_2SO_4$). Lysate was brought slowly to 30% saturation $(NH_4)_2SO_4$ with gentle stirring, the supernatant, containing rubredoxin reductase, was separated from precipitate by centrifugation (10 min at 8,000 g) and the precipitate discarded. The $(NH_4)_2SO_4$ saturation in the supernatant was then increased to 60% and precipitate was again separated by centrifugation. Precipitate of this 40-60% fraction, which contained rubredoxin reductase was kept and the protein gently re-suspended in buffer B (~ 100 ml) and dialysed against 2 x 5 L of buffer B for at least 3 hours each, or overnight prior to chromatography.

The protein was then loaded onto anion exchange resin (Q-Sepharose, ~ 250 ml col. vol. Pharmacia) pre-equilibrated with buffer B. The column was then washed with at least two column volumes of buffer B to remove unbound protein. The column was washed using a gradient of 0 – 0.14 M KCl in buffer B over 300 ml followed by 150 ml holding at 0.140 M KCl in buffer B. Protein was eluted in a second gradient of 0.140 M to 1 M KCl in buffer B over 300 ml. The presence of rubredoxin reductase was monitored by absorbance at 450 nm. Fractions containing rubredoxin reductase were pooled and dialysed against 2 x 5 L of buffer B for at least 3 h each.

The protein was then brought to 35% $(NH_4)_2SO_4$ saturation and loaded onto a hydrophobic interaction column (Phenylsepharose, ~ 300 ml, Pharmacia) pre-equilibrated with buffer B containing 35% $(NH_4)_2SO_4$. Protein was eluted in a gradient of 35-0% $(NH_4)_2SO_4$ saturated buffer B. Fractions containing rubredoxin reductase were pooled and dialysed against 2 x 5 L of buffer B for at least 3 h each.

The protein was then applied to anion exchange column Q-Sepharose, ~ 250 ml col. vol. Pharmacia) pre-equilibrated with buffer B for a second time. The column was washed and protein eluted under the same conditions as before. Presence of rubredoxin reductase was monitored by absorbance as before and purity was analysed

by SDS-PAGE. Fractions containing pure rubredoxin reductase were pooled and concentrated by centrifugal filtration using Centrecon filters with a 30 kDa cut-off (Millipore, Biljerica, USA). Concentrated protein was dialysed exhaustively against buffer B to remove any salts and stored at -80 ^{o}C in 50% glycerol.

2.3.3 Expression and purification of AlkB

After optimisation (discussed in Ch 3) wild-type alkane hydroxylase AlkB was expressed in *E. coli* BL21(DE3)pLysS transformed with pAlkB-3a. Starter cultures (5 ml LB, containing 50 μg/ml ampicillin) were inoculated from freshly transformed cells (glycerol stocks were found to lose plasmid in -80 ^{o}C storage). Cells from the overnight cultures were used to inoculate LB media (500 ml in 2 L baffled flasks) supplemented with ampicillin to 50 μg/ml and chloramphenicol to 34 μg/ml and 3 drops of antifoam A (Fluka, Buchs, Switzerland). After inoculation, cells were incubated and allowed to reach OD_{600} 0.6, whereupon protein production was induced by the addition of IPTG to 1 mM. The temperature was reduced to 30 ^{o}C and cells were incubated for 4-6 h with shaking (230 rpm). Cells were harvested by centrifugation at 10,000 x g for 20 min (5,000 rpm in a Sorvall RC5B using FAS10C rotor) and frozen at -20 ^{o}C overnight.

The histidine tagged alkane hydroxylase (AlkB$(His)_6$) was expressed in *E. coli* C41(DE3) transformed with pAlkBH in the same manner as for the wild-type above.

2.3.3.1 Purification method 1

AlkB (wild-type and his tagged) purification was attempted following the method published by Shanklin *et al*. [74]. All processes were carried out at 4^{o}C or on ice unless otherwise stated. Cells were re-suspended in 40 ml of 50 mM HEPES (pH 8.0) containing $MgCl_2$, 2 mM PMSF, 10 mg DNase I and 10 mg/ml RNase. Cells were broken by passage through a French press (3 x at 950 psi). Broken cells were centrifuged at 40,000 x g for 45 minutes. The clarified supernatant was then placed in ultracentrifuge tubes (Kendro, Bishops Stortford, UK) underlayed with 1.5 ml 50 mM HEPES (pH7.5), 40% v/v glycerol. These were then centrifuged at 240,000 g for 2 h at 4^{o}C in a TH-641 swinging bucket rotor in a Sorvall OTD65B ultracentrifuge to pellet the membranes containing AlkB in the glycerol cushion. Glycerol cushions (containing AlkB) were harvested by careful removal of the upper supernatant layer

then diluted with 50 mM HEPES (pH 7.5), 500 mM urea to 45 ml, before re-centrifugation at 240,000 x g for 1 hour. The supernatant was discarded and the pellets, containing AlkB enriched membranes were gently re-suspended using a small paintbrush in 10 ml 25 mM HEPES (pH 7.5) containing 10% v/v ethylene glycol.

2.3.3.2 Purification method 2

The ultracentrifugation purification of AlkB (wild-type and his tagged) was modified following discussion with Dr David Leys following a research visit to the laboratory of So Iwata (Imperial College, London). All processes were carried out at 4^{o}C or on ice unless otherwise stated. Cells were defrosted and re-suspended in ~ 80 ml 50 mM Tris pH 7.4. Cells were lysed by sonication in the presence of 1 mM PMSF (Power level 40%, 20 x 20 bursts 2 - 5 minute rest gaps to ensure constant temperature). Cell debris and unbroken cells were then separated from protein and membranes by centrifugation 20,000 g for 45 min until the extract appeared clear. The clear extract was then centrifuged at 100,000 g for 1 h (TH-641 swinging bucket rotor in Sorvall OTD65B) to pellet membranes. The resultant supernatant was discarded and the pellets gently re-suspended in 50 mM Tris, 2 M NaCl pH 7.4 using a small paintbrush. The re-suspended pellets were subjected to sonication (3-5 x 10 second bursts at 30%) to break up membrane vesicles and wash undesirable membrane associated proteins from the membranes. The membrane suspension was then centrifuged at 100,000 g for 1 h (TH-641 swinging bucket rotor in Sorvall OTD65B) to re-pellet the membrane and the washing procedure repeated. Membranes were then stored as pellets at –80 ^{o}C.

2.3.3.3 Affinity Chromatography of His tagged AlkB

Membrane pellets (section 2.3.3.2) were resuspended in solubilisation buffer (approximately 1 ml buffer per 1 ml membrane pellet) 50 mM TRIS, 100 mM NaCl, 2% ANAPOE $C_{10}E_9$ (Polyoxyethylene(9)dodecyl ether) (Anatrace, Maume, Ohio) pH 7.4 by stirring at 4 ^{o}C for 1.5 hr. The suspension was loaded onto cobalt affinity resin (TALON, 10 ml col. vol., Clontech, California) pre-equilibrated with the solubilisation buffer. The column was then washed with 2 column volumes of solubilisation buffer followed by 10 column volumes of 50 mM TRIS, 500 mM NaCl, 2% ANAPOE, 80 mM imidazole, before membranes were eluted with the same buffer containing 500 mM imidazole.

2.3.4 Expression and purification of P450 BM3 and its mutants

The full-length and heme-domain of P450 BM3 and the heme-domain of P450 BM3F87G were expressed in TG1 cells using pBM23 , pBM20 and pBMHF87G respectively. Starter cultures (5 ml LB, containing 50 μg/ml ampicillin) were inoculated from either freshly transformed cells or from fresh glycerol stocks (less than 1 month old and stored at -80 ^{o}C). Cells from the overnight cultures were inoculated and grown in 500 ml (2 L flasks) of Terrific Broth (typically 5 L total culture) supplemented with ampicillin to 50 μg/ml . After inoculation with an overnight culture, cells were allowed to grow for 36 hr at 37 ^{o}C with shaking at 230 RPM. Cells were harvested by centrifugation at 10,000 x g for 20 min (5,000 rpm in a Sorvall RC5B using FAS10C rotor) then washed once with TED buffer (50 mM Tris.HCl, 1 mM EDTA pH 7.2). The cell were then re-centrifuged as above to pellet the cells and frozen overnight at -80 ^{o}C.

The full-length P450 $BM3_{F87G}$ was expressed in *E. coli* BL21(DE3) transformed with pBMF87G. Starter cultures (5 ml LB, containing 50 μg/ml ampicillin) were inoculated from freshly transformed cells from fresh glycerol stocks (less than 1 month old and stored at -80 ^{o}C). Cells from the overnight cultures were used to inoculate LB media (500 ml in 2 L Erlenmeyer flasks) supplemented with ampicillin to 50 μg/ml. After inoculation, cells were incubated at 37 ^{o}C and allowed to reach OD_{600} 0.8, whereupon protein production was induced by the addition of IPTG to 1mM. Cells were incubated for a further 6h at 37 ^{o}C with shaking (230 rpm) before being harvested by centrifugation at 10,000 x g for 20 min (5,000 rpm in a Sorvall RC5B using FAS10C rotor). Cells were washed once with TED buffer before centrifugal collection and storage at -20 ^{o}C overnight.

All subsequent processes were carried out at 4 ^{o}C or on ice, unless otherwise stated. Cell pellets were defrosted on ice and lysed in the presence of 1mM benzamidine hydrochloride using a combination of French press (2 passes at 950 lb/in^2) followed by sonication at 40% power for 10 x 20 second bursts with 2 minute rest gaps to allow cooling. Broken cells were then centrifuged to isolate soluble protein from unbroken cells and cellular debris. Typically, 3 x 20 minute spins at 12,000 x g were needed to ensure the lysate was completely clear. The soluble protein-containing extract was then dialysed against 2 x 5 L of TED buffer containing 1 mM benzamidine

hydrochloride for at least 3 hours each, or overnight prior to protein purification by chromatography.

2.3.4.1 Purification of Full-length P450 BM3 and mutants

The full length, holo-enzyme of wild-type and the mutant forms were purified using anion exchange followed by NAD(P)H affinity chromatography.

Following cell lysis and clarification and dialysis into TED buffer, the cell extract was centrifuged (40,000 x g, 4 ^{o}C, 20 min) to remove any precipitate, then loaded onto a DEAE-Sepharose anion exchange resin (~ 250 ml col.vol. Pharmacia) pre-equilibrated with TED buffer containing 1mM benzamidine hydrochloride at 4 ^{o}C. The column was then washed with at least 2 column volumes of TED buffer before the protein was eluted using a linear gradient of 0 – 500 mM KCl in TED buffer over approximately 500 ml.

Fractions were analysed for P450 content spectrophotometrically by comparison of the absorption associated with the P450 (i.e. from the Soret peak (A_{418})) with that from the total protein content (aromatic amino acid absorption A_{280}). The presence of P450 specifically (rather than another cytochrome or cofactor absorbing in this region) was also tested by dithionite reduction and CO binding to ensure a peak shift to A_{450} diagnostic for the P450. Fractions with the highest A_{418}/A_{280} ratio were pooled and concentrated to a volume of approximately 5-10 ml by centrifugal filtration using Centricon filters with a 50 kDa cut off (Millipore, Biljerica, USA). The protein was then dialysed overnight into 2 x 1.5 L of 25 mM potassium phosphate (Kpi, pH 6.5).

Dialysed protein was then loaded onto ATP/NADP+ affinity resin (Mimetic Yellow 10 - 15 ml col. vol., ProMetic Biosciences, Quebec, Canada) pre-equilibrated with 25 mM Kpi pH 6.5. The column was washed with approximately 15-20 column volumes of the same buffer until the total absorbance of the eluate at 280 nm was negligible. Protein was eluted in a single step by application of 25 mM KPi, pH6.5 containing 500 mM KCl and 20 mM 2’5’AMP. Eluate was collected manually in 1-1.5 ml fractions and each was analysed for presence of P450 by spectrophotometry as previously described. Those containing pure protein were pooled and concentrated as described previously then dialysed exhaustively into TED buffer before further

dialysis in TED buffer containing 50% v/v/ glycerol. Aliquots were then stored at –80 ^{o}C.

2.3.4.2 Purification of heme-domain P450 BM3 and mutants

The wild-type and mutant forms of BM3 heme-domain were isolated and purified by liquid chromatography using a three-stage protocol employing anion exchange (weak), ceramic hydroxyapatite and anion exchange (strong).

Following cell lysis, clarification and dialysis into TED buffer, the cell extract was centrifuged (40,000 x g, 4 ^{o}C, 20 min) to remove any precipitate, then loaded onto DEAE-Sepharose (column dimensions as described, Section 2.3.4.1) pre-equilibrated with TED buffer containing 1mM benzamidine hydrochloride at 4 ^{o}C. The column was washed and the protein eluted under the same conditions as described for the full length P450s (Section 2.3.4.1). Fractions were analysed spectrophotometrically as described and those containing P450 were pooled, dialysed and concentrated as for the full length P450s. Once concentrated, the protein was dialysed overnight into 25 mM Kpi, pH6.5.

Dialysed protein was loaded onto ceramic hydroxyapatite resin (~300 ml col. vol. BioRad, Hercules, USA), pre-equilibrated with 25 mM Kpi, pH6.5. The column was washed with at least 2 column Volumes of 25 mM Kpi, pH6.5 before protein was eluted using a linear gradient from 25 mM to 500 mM Kpi (pH 6.5) over approx. 500ml. Fractions were analysed as described previously and those containing P450 were pooled and dialysed against 2 x 5 L TED buffer.

Dialysed heme domain was loaded onto Q-Sepharose anion exchange (15 cm x 2.6 cm column volume, Pharmacia), pre-equilibrated with TED buffer. The protein was washed with at least 2 column volumes of TED buffer before elution using a linear gradient of 0 – 500 mM KCl over approx. 500 ml. Fractions containing pure protein were pooled and dialysed exhaustively into TED buffer. The pure protein was then concentrated by centrifugal filtration as described previously before further dialysis into 2 L TED buffer containing 50% v/v glycerol and storage in aliquots at –80 ^{o}C.

An additional purification step was used when purifying $BM3_{Q403C}$ in an attempt to improve the poor resolution of the protein. Fractions containing heme domain $BM3_{Q403C}$ collected post Q-sepharose anion exchange were pooled and dialysed

exhaustively in 50 mM Tris.HCl, 1 mM EDTA pH 8. Dialysed protein was loaded onto Q-Sepharose anion exchange (15 cm x 2.6 cm column volume, Pharmacia), pre-equilibrated with the same buffer. The protein was washed with at least 2 column volumes of TED buffer before elution using a linear gradient of 0 – 500 mM KCl over approx. 500 ml. Fractions containing $BM3_{Q403C}$ were pooled and the purity of the protein sample assessed by SDS-PAGE before purification of this mutant was discontinued.

2.4 Analytical Methods

2.4.1 SDS-PAGE analysis

SDS-PAGE analysis of proteins was completed using the Laemmli method [81]. Gels were prepared using a mini-gel preparation kit (Bio-Rad, Hercules, USA) following the manufacturer's instructions. Stacking gel and resolving gels were made using the solution components outlined in Table 2.4. The ammonium per sulphate (APS) and tetramethylethlylenediamine (TEMED) was only added immediately prior to pouring the gels. To pour, the glass plates were cleaned using ethanol and allowed to dry. The resolving gel of the appropriate percentage acrylamide was gently poured between the plates and overlain with iso-butanol to exclude air and left to set for 30 min. The iso-butanol was then poured off and any residue removed using filter paper. The stacking gel was then poured between the plates over the resolving gel and an appropriate size comb inserted in the top and left to set for 30 min.

Table 2.4 SDS-PAGE solution components.

	Component volumes (ml) per gel				
	2 ml Stacking Gel	10 ml resolving gels			
Solution components		8%	10%	12%	15%
H_2O	1.4	4.6	4.0	3.3	2.3
30% bis/acrylamide	0.33	2.7	3.3	4.0	5.0
0.5 M Tris (pH6.8)	0.25	n/a	n/a	n/a	n/a
1.5 m Tris (pH8.8)	n/a	2.5	2.5	2.5	2.5
10% SDS	0.02	0.1	0.1	0.1	0.1
10% APS (fresh)	0.02	0.1	0.1	0.1	0.1
TEMED	0.002	0.006	0.004	0.004	0.004

The electrophoresis apparatus (BioRad®, vertical model) was set and the tank was filled with gel running buffer (25 mM Tris, 250 mM glycine, 0.1% SDS).

Protein samples were prepared by mixing with 3 x loading buffer (2 µl per 6 µl sample) (187.5 mM Tris-HCl (pH 6.8 @ 25 °C), 6% (w/v) SDS, 30% glycerol and 0.03% (w/v) phenol red, 40 mM DTT) and the mixture was heated at 95 ^{o}C for ~ 5 min. Samples were then centrifuged (2 min at full speed in a bench-top microfuge) to remove any precipitated protein, before loading onto the gel. Electrophoresis was performed at 150 V for ~ 1 hour, being stopped when the dye front approached the end of the gel.

To visualise the protein bands gels were stained by first 'fixing' the gel by submersion in 50% v/v methanol, 10% acetic acid, 40% dH_2O for approximately 10 min. The gel was then removed from the fixer and submersed in Coomassie Blue Stain (0.25% w/v Coomassie Blue G-250, 50% v/v methanol, 10% acetic acid, 40% dH_20) for 20-30 min with gentle shaking. The gel was then de-stained overnight in 25% v/v methanol, 10% v/v acetic acid, 65% v/v dH_20 before visualisation and image capture using the gel documentation system described previously (Section 2.2.3).

2.4.2 Protein concentration

All UV-visible spectroscopy was carried out on a Varian Cary 50 UV-visible spectrophotometer using a quartz cuvette with a path length of 1cm.

The concentration of rubredoxin was determined from absorbance measurements at 498 nm for 1FeDDR and 494 nm for 2FeDDR forms using the Beer Lambert Law (Equation 1) and the molar extinction coefficients of 6,300 $M^{-1}cm^{-1}$ and 10,600 $M^{-1}cm^{-1}$ for 1FeDDR and 2FeDDR respectively [50, 80]. The concentration of rubredoxin reductase was determined from absorbance measurements at 450 nm using the extinction coefficient of 11,100 $M^{-1}cm^{-1}$[46].

The concentration of cytochrome P450 BM3 and mutants were calculated using the method described by Omura and Sato [82]. Briefly, a sample of the purified P450 protein was reduced by addition of sodium dithionite, and then gently bubbled with CO (approximately 1 bubble per second for 1 minute). Spectra were recorded at each of the following stages; pure enzyme, dithionite reduced enzyme, and CO-bound

enzyme. The dithionite-reduced spectrum was then subtracted from the CO-bound spectrum to obtain a difference spectrum, which was used to calculate the difference between absorbance at 450 nm and 490 nm. The concentration was then calculated using the Beer Lambert Law (Equation 1) and the molar extinction coefficient ($\varepsilon_{450-490}$) = 91,000 M^{-1} cm^{-1}.

$$A=\varepsilon cl$$

Equation 1 Beer Lambert Law.

Where A is the absorbance, ε the molar extinction coefficient (M^{-1} cm^{-1}), c the concentration of the absorbent and l is the path length in cm.

2.4.3 Substrate Binding studies

All binding titrations were carried out using a Cary-50 (Varian) UV-visible scanning spectrophotometer at 30 °C using 25 mM MOPS buffer with 100 mM KCl at pH 7.4 (reaction buffer). The fatty acid arachidonic acid and known P450 inhibitor 4-phenylimidazole were titrated against the heme domains of P450 BM3 and its various mutants (F87G, Q387C, Q397C, Q404C) to determine binding constants (K_d values) from the spectral shift induced [83]. A range of alkenes (hexane, octane and decene with varying C=C bond positions) and styrene were also tested against the heme-domains of P450 BM3 and the F87G mutant. Protein concentrations used in binding studies was typically between 3 and 6 µM.

Each of the substrates was first diluted in ethanol to make stock solutions, (typically 33 mM for arachidonic acid, 50 or 100 mM for alkenes and styrene). Stock solutions for 4-phenylimidazole were made in reaction buffer to a concentration of 50 mM. Care was taken not to exceed a final concentration of 5 % ethanol during the titration.

Absolute spectra were collected for the pure, oxidised P450 samples prior to ligand binding. Spectra were then collected following each addition of the substrate, typically between 250-800 nm. Difference spectra were then generated by subtraction of the original (substrate-free) spectrum from all subsequent spectra. The maximal absorption differences (i.e. those from the peak and trough positions in the difference spectra, computed as the absorption at the former minus that at the latter for the same

wavelength pair throughout) was then plotted against the corresponding substrate concentration. The data were fitted to a rectangular hyperbola (where binding was relatively weak) or to a quadratic equation (where the apparent K_d was less than five times the concentration of P450 used)) to calculate a binding constant (K_d) using the graphical software Origin 6 (OriginLab, Massachusetts).

$$A_{obs} = A_{max} \frac{([E_T] + [S_T] + K_d) - \sqrt{([E_T] + [S_T] + K_d)^2 - 4[E_T][S_T]}}{2[E_T]}$$

Equation 2 Quadratic 'tight binding' equation.

Where A_{obs} is the observed absorption at a given concentration, A_{max} is the maximal absorbance at the given wavelength, E_T is the total enzyme concentration, S_T is the substrate concentration and K_d the apparent dissociation constant.

$$A_{obs} = \frac{A_{max}[S_T]}{K_d + [S_T]}$$

Equation 3 Rectangular hyperbola.

Parameters as given in Equation 2

2.4.4 Redox Potentiometry

All redox titrations were carried out under a nitrogen atmosphere in an anaerobic glove box (Belle technology, Dorset, UK). Spectroscopic measurements were recorded using a UV-visible probe inside the box attached to a Varian Cary 50 UV-visible spectrophotometer. Potentials were measured with a Pt/Calomel electrode (ThermoRussell, Fife, UK) attached to a pH211 microprocessor meter (Hanna Instruments, Leighton Buzzard, UK). Redox titrations were carried out for both wild type heme-domain P450 BM3 and all BM3 mutant heme-domains (in substrate-free and substrate-bound states) as well as for rubredoxin (1FeDDR and 2FeDDR) essentially by the method of Dutton [84]. All buffers were deoxygenated by bubbling extensively with O_2-free argon. Traces of oxygen were removed from the protein samples by passing them through a Bio-Rad Econo-pac 10DG gel filtration column within the glove box, which had been pre-equilibrated with 100 mM KPi at pH 7.0 and contained 10% (v/v) glycerol (redox buffer). Enzyme was diluted in redox buffer

to a concentration of approximately 80 μM and mediators were added to the enzyme solution to speed equilibration between the enzyme and electrode; 1.5 mM methyl viologen, 2.5 mM benzyl viologen, 7 mM 2-hydroxy-1,4-naphthaquinone and 5 mM phenazine methosulfate. The reductant sodium dithionite, in a ~ 10 mM stock, was titrated against the enzyme solution by the addition of small aliquots (0.1-0.2 μl) and the sample mixed using a magnetic stirrer and flea. The sample was left to equilibrate, typically 10 – 15 minutes, the magnetic stirrer switched off and the spectra was collected and the potential recorded. When the enzyme was entirely reduced, potassium ferricyanide was added (0.1-0.2 μl of ~10 mM stock) to re-oxidise it to the start point and a final reading was taken. In substrate-bound titrations, arachidonic acid was added from a 33 mM stock in ethanol until no more high spin enzyme was formed prior, to the reductive titration being started.

Data were analysed by plotting the absorbance at an appropriate wavelength, corresponding to the maximal absorbance change between oxidised and reduced forms, against the potential. Data were fitted to the 1 electron Nernst equation (Equation 4) using Origin software (Microcal) to calculate the mid-point potential.

$$A_{Obs} = \frac{\left(A_{Abs} + B_{Abs} * 10^{\left(\frac{E_0 - X}{C}\right)}\right)}{1 + 10^{\left(\frac{E_0 - X}{C}\right)}}$$

Equation 4 One electron Nernst equation.

Where A_{abs} is the observed absorption of the ferric (oxidised) P450 form, B_{Abs} is the absorbance of the ferrous (reduced) P450, E_0 is the reduction potential for the Fe^{3+}/Fe^{2+} transition, X is the applied potential and c is a constant derived from the universal gas constant (R=8.315 J mol^{-1} K^{-1}), the absolute temperature in Kelvin and the Faraday constant ($9.64853x10^4$ C mol^{-1}) representing the term RT/nF, where n is the number of electrons.

2.4.5 Steady state kinetics of wild-type BM3 & F87G mutant

Steady state kinetic analysis of the full-length BM3 proteins was carried out using the same substrates as used in the binding studies reported above. Activity was measured using the NADPH-dependent assay described by Matson *et al* [85]. All assays were performed at 30 ^oC in 20 mM MOPS, 100 mM KCl, pH 7.4 with BM3 concentrations of typically 200 nM and NADPH at near-saturating concentrations (200 μM).

The rate of enzyme catalysis was measured by monitoring the absorbance change at 340 nm using the extinction coefficient 6.22 $mM^{-1} \cdot cm^{-1}$ for the difference between the reduced and oxidised forms of the coenzyme [86]. Initial rates of NADPH oxidation were measured at varying concentrations of each substrate. These initial rates were then plotted against substrate concentration and fitted to the Michaelis Menten equation (Equation 5) and the K_M and k_{cat} values calculated using Origin software (Microcal).

$$v = \frac{V_{max}[S]}{K_M + [S]}$$

Equation 5 Michaelis-Menten Equation.

Where v is the velocity or reaction rate, V_{max} is the maximal reaction rate, [S] is the substrate concentration and K_M is the Michaelis constant, the substrate concentration at which v is exactly half of V_{max}.

2.4.6 Product Characterisation

For styrene and the alkene that stimulated above-background rates of NADPH oxidation by P450 BM3 and $BM3_{F87G}$, experiments were done to define any reaction products. Full-length BM3 (both wild-type and F87G) were incubated with the substrate and NADPH and the resultant products were recovered by dichloromethane extraction then analysed by GC/MS.

2.4.6.1 Product formation and extraction

All product formation extraction and analysis was performed using the facilities at Avecia, Billingham under supervision by Dr. Robert Holt. Reactions were performed in glass (pre-washed with water and dichloromethane), at room temperature ($23^oC \pm 2^oC$) with gentle agitation on a rolling mixer (Wolf Laboratories, York, UK) using the same buffer as used in the reactions in Section 1.7.3 above, namely 20 mM MOPS, 100 mM KCl ,pH 7.4.

For wild-type P450 BM3, reaction volumes of 5 ml containing 4 µM P450 and 2 mM substrate (stock dilutions in ethanol) were incubated for 5 minutes, whereupon NADPH was added also at 2 mM. Reactions were incubated over-night at room

temperature before 2 ml of each reaction was removed and 1 ml dichloromethane was added to this. The acidification step prior to addition of dichloromethane was omitted to prevent any conversion of epoxide product to alcohol. The mixture was agitated by shaking for ~ 30 s then allowed to settle for 2-3 min a total of 3 times. To aid separation of organic and aqueous layers, each sample was subject to brief (30 s) centrifugation in a bench top microfuge before the lower organic layer was recovered by glass pipette pre-rinsed in water and dichloromethane. Excess water was removed from the extraction by the addition of solid anhydrous sodium sulphate (Na_2SO_4). The sample was then covered with foil and incubated on the bench at room temperture for 10 min to complete the drying process. The liquid extract was then separated from any sediment by glass pipette pre-rinsed in water and dichloromethane and the samples were filtered through a 0.45 μm polypropylene syringe filter (GE Osmonics, Minnetonka, USA) before analysis by GC/MS (section 2.4.6.5).

Products for styrene and the alkene substrates incubated with $BM3_{F87G}$ were analysed in a similar manner. Reactions were performed as above, except that the reaction volume was reduced to 2 ml and protein concentration was reduced to 2 μM due to limited availability of the mutant enzyme.

A series of negative controls were also performed using BM3 and the F87G mutant where enzymes were incubated under identical conditions and DCM extractions were analysed by GC/MS as described below.

2.4.6.2 NADPH recycling using Glucose dehydrogenase

Glucose dehydrogenase (GD) (Sigma) and its substrate, glucose, was tested as a recycling mechanism for NADPH. The activity of GD was given a 11 U, equal to 11 μmoles $NADP^+$/mg enzyme/min. As P450BM3 activity was found to be ~ 8.4 μmol NADPH/mg enzyme/min for the substrate with the highest activity, the same mass of P450 BM3 and GD were used in the reactions to allow competent recycling. A typical reaction contained 4 μM P450 (0.47 mg/ml), 0.5 mg/ml GD, 5 mM substrate, 5 mM glucose and 600 μM NADPH.

The enzymes were incubated with substrate for 5 min prior to addition of NADPH. Reactions were conducted under identical conditions as described for NADPH only

reactions and samples were extracted, recovered and analysed by GC./MS as described.

2.4.6.3 Preparation of m-chloroperoxybenzoic acid (mCPBA)

5 g of crude mCPBA (Aldrich, ~70%) was dissolved in 50 ml dichloromethane (DCM) and washed with 3 x 50 ml buffer solution (100 mM sodium phosphate, pH 7.6). Washing constituted 50 ml of buffer was mixed with mCPBA solution, allowed to settle then the organic layer (lower) recovered. The pH of the discarded buffer was tested and the washing step repeated until the pH was above pH 7.2. The organic layer was recovered from the final wash and any remaining aqueous media (buffer) was removed by the addition of anhydrous sodium sulphate (Na_2SO_4) until the organic phase was clear. Precipitate was removed by filtration and DCM was evaporated under reduced pressure in a rotary evaporator to give ~ 3 g of pure mCPBA which was stored in a sealed container at 4^oC and used within one week.

2.4.6.4 Epoxidation of alkenes using mCPBA

Epoxides of the following the alkene substrates were manufactured using the peracid mCPBA as purified in the preceding section: n-hexene, t2- and t3-hexene, n-octene, t2-, t3- and t4-octene. 3 mmoles of alkene was dissolved in a 10 ml volume of DCM, stirring (magnetic stirrer) in and ice bath. 3.3 mmoles of purified mCPBA was dissolved in a 10 ml volume of DCM. The mCPBA/DCM solution was then added drop-wise to the alkene solution over a period of 10 min. The mixture was then removed from the ice bath and incubated at room temperature with stirring for a further 2 h. Solid sodium sulphite (~3 mmoles) was then added to the mixture to remove any residual peroxide. The solution was then washed (4 x 20 ml) with a 5% sodium bicarbonate solution, followed by water (1 x equal volume), followed by saturated sodium chloride solution (1 x equal volume). The organic layer from the final wash was recovered and any residual aqueous phase removed by the addition of solid (Na_2SO_4) and filtered as described previously (Section 2.4.6.1) . The remaining solvent was removed by rotary evaporation under reduced pressure to yield the alkene oxides present as oil.

2.4.6.5 Gas Chromatography and Mass Spectroscopy

GC/MS analyses of the products from the above reactions were performed on an Agilent 6890 series GC system with an Agilent 5973 Network Mass Selective Detector attached. The System was fitted with a HP5MS, 5% phenyl methyl siloxane capillary column (30.0 m x 250 μm x 0.25 μm) with a maximum run temperature of 325 ^{o}C. All samples (1 μl) were run using the following method: oven temperature was set to 50 ^{o}C with a 2 minute solvent delay and a flow rate of 1 ml/min. The temperature was then increased to 200 ^{o}C at a rate of 20 ^{o}C/min with mass detection set between 20-150 MW. Standard samples of substrates in dichloromethane (DCM) were used to identify retention times and fragmentation patterns of starting material and then checked against the software's internal compound library.

Product identification was achieved by comparison with the internal library and, where possible, by comparison using commercially available compounds. Where a prospective epoxide product was not commercially available, products were chemically manufactured in the laboratory as described (Secction 2.4.6.3).

Chiral resolution of styrene oxide (R- and S-) was achieved using a GC (Agilent 6890N) with an Agilent HP-5, 5% phenylmethyl siloxane column (30m x 320μm x 0.25μm) fitted with a flame ionisation detector. Chiral products were identified by running commercially available standards (styrene oxide, racemic mixture and R-styrene oxide) concurrently to compare retention times.

2.4.7 Quantification of solvent accessible protein sulfhydryls

Solvent accessible sulfhydryls were measured using a modified version of the 'Ellman's test' using 5, 5'-dithiobis-(2-nitrobenzoic acid) (DTNB commonly known as Ellman's reagent) and cystamine as mediator [87, 88]. Protein samples (1-5 nmoles) were diluted in PBS (137 mM NaCl, 10.1 mM Na_2HPO_4, 1.76 mM KH_2PO_4, 1 mM EDTA, adjusted to pH7.4) to a final volume of 1 mL. A 200 μl aliquot of 'strong buffer' (100 mM boric acid, 0.2 EDTA adjusted to pH 8.2 with NaOH) was added to adjust the pH to $\geq$ 8.0. A 20 μl aliquot of DTNB/cystamine reagent (10 mM DTNB, 10 mM cystamine in dissolved in 100 mM NaH_2PO_4, 0.2 mM EDTA adjusted to pH 7.0 with NaOH) was added to the sample and immediately vortexed. The reagent treated samples were incubated at room temperature for 5 min before the absorbance

at 412 nm was measured against a water blank. A protein blank was made by replacing the DTNB/cystamine reagent with 20 µl dH_2O and a reagent blank was made by replacing the protein by PBS only. The amount of sulfhydryl in the protein sample was calculated according to Equation 6, using the standard value $\Delta\varepsilon_{412}$ = 14,150 M^{-1} cm^{-1}.

$$molSH = 0.00122\ L\frac{\left(A_{412s} - A_{412r} - A_{412p}\right)}{\Delta\varepsilon_{412} * 1cm}$$

Equation 6 Determination of sulfhydryls.

Where molSH is the moles of sulfhydryls, A_{412s} is the absorbance of protein after reaction with reagent, A_{412r} is the absorbance of the reagent blank, A_{412p} is the absorbance of the protein blank and ε_{412} is the molar extinction coefficient of DTNB at 412 nm (14,150 $M^{-1}cm^{-1}$)

2.4.8 Redox Potentiometry

All redox titrations were carried out under a nitrogen atmosphere in a Belle technology glove box fitted with a UV-visible probe attached to a Varian Cary 50 UV-visible spectrophotometer. Potentials were measured with a Thermo Russell electrode attached to a Hanna pH211 microprocessor meter. Redox titrations were carried out for both wild type heme domain P450 BM3 and mutant heme domains. Titrations were carried out using the arachidonic acid bound and substrate-free forms of the enzyme essentially by the method of Dutton [89]. All buffers were deoxygenated by bubbling extensively with O2-free argon. Traces of oxygen were removed from the protein samples by passing them through a Bio-Rad Econo-pac 10DG gel filtration column within the glove box, which had been pre-equilibrated with 100 mM KPi at pH 7.0 and contained 5% (v/v) glycerol. Mediators were added to the enzyme solution to speed equilibration between the enzyme and electrode, 1.5 mM methyl viologen, 2.5 mM benzyl viologen, 7 mM 2-hydroxy-1,4-napthaquinone and 5 mM phenazine methosulfate were added to 5 ml of enzyme in 100 mM KPi pH 7.0, with the enzyme concentration approximately 80 µM. The reductant sodium dithionite, in a 10 mM stock, was titrated against the enzyme solution, and the enzyme sample was left to equilibrate, typically 10 – 15 minutes, prior to the spectrum being collected and the potential being noted at each titration point. When the enzyme was entirely reduced, potassium ferricyanide was added to re-oxidise it to

the start point and a final reading was taken. Data were analysed by plotting the absorbance at an appropriate wavelength corresponding to the maximal absorbance change between oxidised and reduced forms against the potential, a Nernst function was then fitted to the data and the midpoint potential calculated from it. In substrate-bound titrations, arachidonate was added from a 33 mM stock in ethanol until no more high spin enzyme was formed prior to the reductive titration being started.

2.4.9 Electron paramagnetic resonance (EPR) spectroscopy

Spin labelling of P450 BM3 and Q/C mutant heme-domains and subsequent EPR spectra was carried out by Louise Ottignon under the supervision of Dr Myles Cheesman (Dept. of Chemistry, University of East Anglia).

2.4.9.1 Spin-labelling using MTSL

Each sample (~0.1 μmol) protein was diluted to 2.5ml with buffer. (20mM Hepes, pH7). The reducing agent dithiothretol (DTT) was added (1 mg) to each sample under anaerobic conditions to remove any disulphide bridges. Each sample was then passed down a PD10 desalting column pre-equilibrated with the Hepes buffer to remove the DTT. The proteins' UV-visible spectra were recorded to determine the protein concentration before the addition of a 10-fold molar excess of the spin-label *S*-(2,2,5,5-tetramethyl-2,5-dihydro-1H-pyrrol-3-yl)methyl methanesulfonothioate (MTSL). The samples were incubated in the dark at room temperature for 4 h. Unbound label and was removed from the samples by passing down a PD 10 column, then samples were concentrated and their UV-visible spectra recorded to determine their concentration.

2.4.9.2 Collection of EPR spectra

Continuous wave EPR spectra were recorded at room temperature on a Bruker ER-300D series electromagnet and microwave source interfaced with a Bruker EMX control unit (Bruker, Coventry, UK). Spectra were collected under the following conditions: microwave frequency, 9.741 GHz, microwave power 2 mW.

3 Isolation of the trans-membrane alkane hydroxylase from *Pseudomonas putida*.

3.1 Outline

The alkane hydroxylase from *Pseudomonas putida* (AlkB) is a trans-membrane, non-heme, di-iron enzyme. It catalyses the mono-oxidation of alkanes using a single oxygen atom derived from the activation of molecular oxygen. Information regarding the structure of the enzyme is limited to its topology as deduced from studies of hydrophobicity and analysis of AlkB/alkaline phosphatase and AlkB/β-galactosidase fusion proteins. One avenue of investigation for shedding light on enzyme function is through structural characterisation. Thus far, there has been no reported success of crystallisation of the enzyme for structural studies. To this end a histidine tagged construct encoding the alkane hydroxylase was made and expressed in *E. coli*. Methods of separating AlkB enriched membranes were investigated and efforts were made to isolate AlkB using solubilisation in detergent and immobilised metal affinity chromatography. Despite reasonable enrichment of membranes containing AlkB, attempts to solubilise and purify the membrane protein to homogeneity were unsuccessful.

3.2 The alkane hydroxylase system of Pseudomonas putida

The alkane hydroxylase system of *Pseudomonas putida GPo1*[1] (TF4-1L; ATCC 29347) is the first stage of an inducible enzyme system that enables the organism to utilise *n*-hexane and other short chain alkanes as its sole carbon source [35]. Originally termed the ω-hydroxylation system because of its strict selectivity for hydroxylation of the terminal methyl group of fatty acids and alkanes [90, 91], the system consists of three proteins: NADH- rubredoxin reductase (*AlkT*), a flavoprotein which serves to transfer electrons from NADH to the rubredoxin [46, 92]; rubredoxin (*AlkG*), a non-heme iron-containing electron transfer protein [44]; alkane hydroxylase (*AlkB*), a membrane bound iron containing mono-oxygenase [93]. All three components are essential for oxidation of the substrate [94]. The genes coding for all three proteins are found on the transmissible OCT-plasmid, which also encodes the genes for other proteins involved in the alkane oxidation pathway [36]. The *n*-alcohol products of alkane mono-oxygenase are subsequently acted on in turn by alcohol dehydrogenase (*AlkJ*), aldehyde dehydrogenase (*AlkH*) and acyl-CoA synthetase (*AlkK*) to convert them into fatty acids which are then used by the normal functions of the cell to produce energy (Figure 3.1).

The OCT plasmid contains two gene clusters; the first operon encodes the genes for the membrane-bound alkane hydroxylase *alkB*, two rubredoxins *alkF* and *alkG*, an aldehyde dehydrogenase *alkH* [41], an alcohol dehydrogenase *alkJ*, an acyl coenzyme A (CoA) synthetase *alkK* and an outer membrane bound protein of unknown function

[1] *Pseudomonas putida* GPo1 is synonymous with *Pseudomonas oleovorans* GPo1 and both terms are used in the literature.

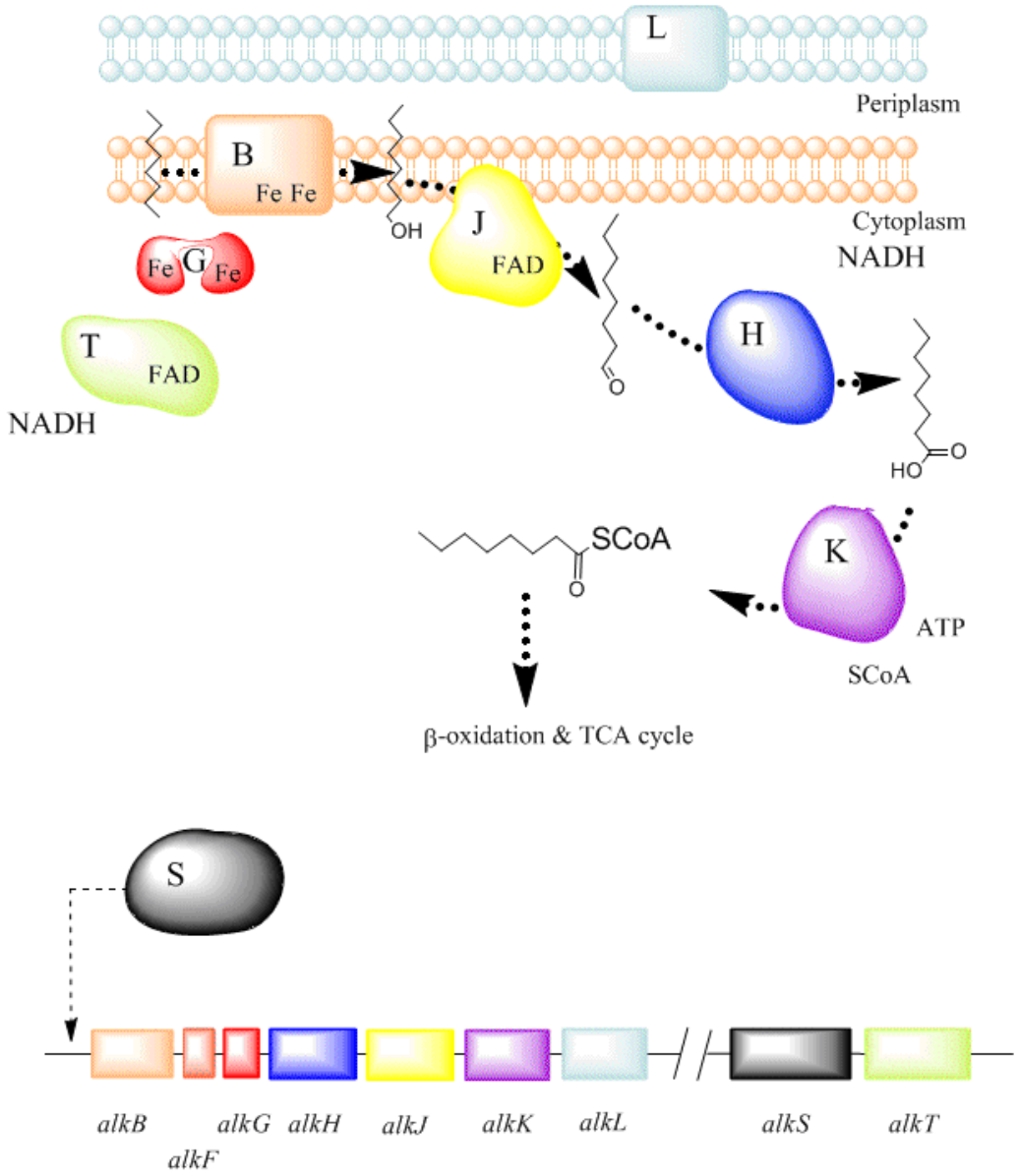

alkL [95]. The second operon encodes a regulatory protein *alkS* and a rubredoxin reductase *alkT* [40, 47].

Figure 3.1 The function and cellular location of the gene products (a) encoded by the OCT plasmid (b) from *P. putida* GPo1.

The expression of the *alkBFGHJKL* genes is positively regulated by the product of *AlkS*. Key: *AlkB*, alkane hydroxylase; *AlkG*, rubredoxin; *AlkH*, aldehyde dehydrogenase; *AlkJ*, alcohol dehydrogenase; *AlkK*, acyl coenzyme A (CoA) synthetase; *AlkT*, rubredoxin reductase; neither *alkF*, non essential rubredoxin nor *alkL*, outer-membrane protein of unknown function, are needed for alkane oxidation to continue [39, 95].

Homologous genes forming similar alkane oxidation systems have more recently been isolated from other *Pseudomonads* and *Acinetobacter* as well as some gram-positive bacteria [21, 96, 97]. In fact, two AlkB homologues have been functionally identified in *P. aeruginosa* although, interestingly, the genes are contained within the genome rather than on a transmissible plasmid. However, expression of the alkane hydroxylase system in both *P. aeruginosa* and *P. putida* is regulated by the presence of alkanes in the growth medium and absence of any other carbon source [39].

3.2.1 Rubredoxin

The rubredoxin encoded by *alkG* was the first component of the system to be isolated and characterised and is required for catalysis [43, 44, 94]. The rubredoxin encoded by *alkF*, although structurally related to the product of *alkG* is not required for electron transport in the system and is thought to be the result of some gene duplication event [41]. Rubredoxins are a family of non-heme iron-sulphur proteins which contain a single iron tetrahedrally co-ordinated by 4 cysteine residues commonly associated with electron transport [48]. At 19 kDa, the functional rubredoxin from *P. putida* is significantly larger than the majority of known rubredoxins which are typically just 6 kDa [48, 52]. However, sequence alignment and cleavage studies show that this protein contains two rubredoxin-like iron-binding domains separated by an unstructured ~70 amino acid linker region [49, 98] and is commonly termed double domain rubredoxin (DDR) [50, 53]. The two-iron form (2FeDDR), although believed to be the physiological form [80], is less readily isolated and requires the unfolding and refolding of the one iron form (1FeDDR) in the presence of iron [50]. The solution structure [53] shows each iron binding domain contains a 3-stranded anti-parallel β–sheet and several tight turns, that correlate well with the 3-dimensional structures of other rubredoxins solved by crystallography. Both 1FeDDR and 2FeDDR are known to be comparably redox active in complex with either the natural electron donor, rubredoxin reductase, or with spinach ferredoxin reductase [49, 51, 53, 80, 98].

The gene encoding the double domain rubredoxin, *alkG,* from *P. putida* has previously been sequenced and cloned into the expression vector pKK223-3 to create the recombinant plasmid pKR10 [38, 47]. The recombinant, one-iron form of double domain rubredoxin (1FeDDR) is readily isolated from *E. coli* TG1 cells transformed

with plasmid pKR10 and its expression and purification has been well documented [50].

3.2.2 Rubredoxin reductase

Encoded by the *alkT* gene, rubredoxin reductase was first isolated in the early 1970s [47]. This 55 kDa protein contains 2 ADP-binding sites as determined by the amino acid sequence; each matching that typical of a Rossmann fold and the phosphate binding consensus sequence G-x-G-x-x-G associated with nucleotide binding proteins [99, 100]. The nucleotide binding site closest to the N-terminus binds FAD, one per mole of protein [46], whilst the second, towards the centre of the sequence, binds one unit of NAD(H) [47].

The gene encoding rubredoxin reductase has been sequenced and cloned into pKK223-3; producing the recombinant plasmid pKRR5V [47, 51]. The expression and purification of the recombinant form of the protein has been documented [98]. However, rubredoxin reductase is far less stable than rubredoxin and prone to losing its FAD cofactor [92]. Spectral characterisations show it is able to accept two reducing equivalents from NADH and can transfer them to rubredoxin as expected, but also to ferricyanide. It is also capable of reducing cytochrome c but only in the presence of rubredoxin; and it forms a complex with rubredoxin in a 1:1 ratio in solution [46].

3.2.3 Alkane hydroxylase (AlkB)

AlkB belongs to a large family of oxygen activating, non-heme iron enzymes, the majority of which are soluble but a sub-family of which includes the membrane bound mono-oxygenases [101]. Even though the gene was not sequenced until 1989 [41], the alkane hydroxylase from *P. putida* (AlkB) is arguably the most studied of this growing class of trans-membrane, metallo-proteins [22]. AlkB contains non-heme iron, which if removed eliminates the enzymes mono-oxygenase activity [93]. Activity can be restored to the apo-enzyme by addition of ferrous ions (e.g. ferrous ammonium sulphate) but not ferric ions or other metal ion substitutes e.g. Mn^{2+}, Cu^{2+} [102]. Originally thought to contain just one atom of iron per polypeptide chain [103], Mössbauer studies on AlkB enriched membrane vesicles indicate the alkane

hydroxylase contains a di-iron cluster at the centre of its active site. Although it contains iron, it has a fairly non-descript UV/visible spectra which shows no real perturbations on addition of redox active components such as dithionite or substrates and removal of iron appears to make no significant UV/visible difference either [102, 103]. It cannot, therefore, be analysed by UV/visible spectroscopy. Neither does EPR afford any real insight into the protein as the signal doesn't change on addition of substrate and completely disappears on addition of dithionite [102].

The *alkB, alkG, alkS* and *alkT* genes, essential for regulation and expression of the three component system (*alkS* code for the regulatory protein), have been cloned and inserted into pLAFR1 to construct the plasmid pGEc47, which has been used to transform various *E. coli* host organisms [39]. Expression of the alk genes is easily controlled by the use of n-alkanes or dicyclopropylketone (DCPK) [37]. AlkB in particular is expressed to high levels in *E. coli*; from 1.5 to 2% (w/w) of total cell protein in *E. coli* DH1 [39] to 10–15% of total cell protein in *E. coli* W3110 [104]. This increase in AlkB synthesis in *E. coli* is concomitant with an increase in membrane synthesis. Indeed, AlkB enriched membrane vesicles can be seen in freeze-fracture micrographs of *E. coli* W3110 upon induction [104]. Whilst *alkB* gene expression rates in some *E. coli* are higher than in the native host, degradation rates are also high; with a reduction in half life from over 50 h in *P. putida* to 15-20 h for *alkB* in *E. coli* W3110. The specific activity of AlkB in these *E. coli* strains is also 5-6 times lower than in the native host [105, 106].

Hydrophobicity plots of the amino acid sequence indicate eight hydrophobic stretches long enough to span the cytoplasmic membrane [41]. However, gene fusions of AlkB to either alkaline phosphatase or β-galactosidase reveal the enzyme is more likely to contain 6 trans-membrane helices with both the N- and C- terminal domains located in the cytoplasm [107] (Figure 3.2). AlkB shares 25% sequence similarity with the membrane bound xylene mono-oxygenase (Xmo) from *P. putida* PaW1, which catalyses the oxidation of xylenes and toluene [108]. Whilst not displaying sequence similarity to the integral membrane fatty acid desaturase (FAD) family, both AlkB and Xmo share a distinct histidine rich consensus sequence in relation to the hydrophobic regions, which implies they are structurally related to the fatty acid desaturases (Figure 3.3) [109]. Conversion of any one of the eight histidine residues

to alanine in Steroyl-CoA desaturase results in an inactive enzyme [110] and preservation of the histidines is thought to play a vital role in co-ordination of the di-iron centre. Further structural information about this or related proteins has not been published and nothing is known about the spatial arrangement of the helices in the membrane or how the enzyme determines substrate specificity. More than 80 putative AlkB homologues have been identified in over 40 strains of gram negative and gram positive bacteria, acquired from sources as diverse as Alaskan sediments [111], arctic and Antarctic soil [112], clinical isolates [97] and fuel oil-contaminated sites [113]. Fewer than half of these have been shown to code for functional proteins as shown by either gene knockouts or heterologous expression (Table 3.1).

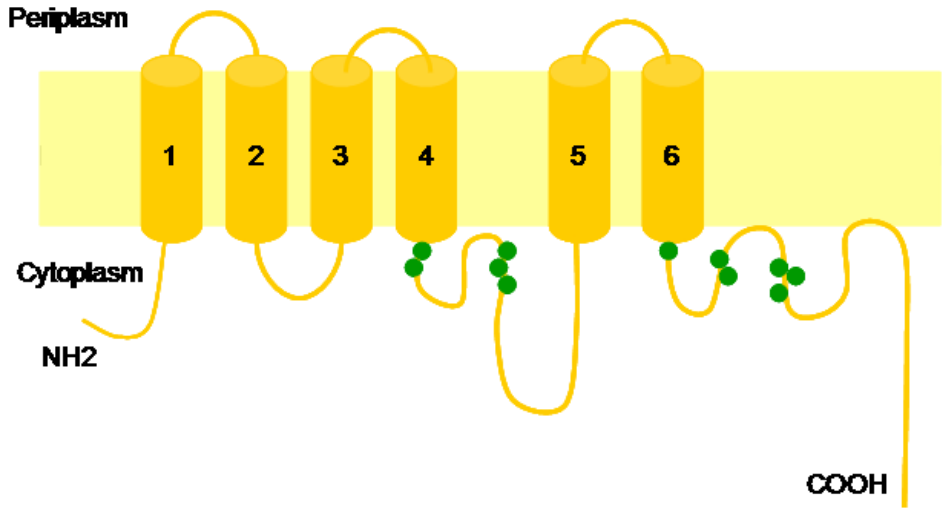

Figure 3.2 Schematic of the proposed topology of AlkB.

Trans-membrane helices are shown as cylinders, conserved histidine residues are shown as green circles. AlkB is believed to consist of six trans-membrane helices with both the N- and C- terminal domains on the cytoplasmic side of the membrane. The three histidine rich motifs ($HX_{(2,3)}H$, $HX_{(2,3)}HH$ and $HX_{(2,3)}HH$) AlkB shares with xylene mono-oxygenase and the membrane bound fatty acid desaturase (FAD) family are thought to co-ordinate the di-iron centre is located in the cytoplasm [95].

```
ALKB_PSEOL,    1 MLEKHRVLDSAPEYVDKKKYLWILSTLWPATPMIGIWLANETGWGIFYGLVLLWWYG-----ALPLLDAMFGEDFNNPPEEVVP 79
XYLM_PSEPU,    1 M---------------DTLRYYLI-----PVVTACGL-------IGFYYG-GYWWWLGAATFPALMVLDVILPKDFS--ARKVSP 55

ALKB_PSEOL,   80 KLEKERYYRVLT-YLTVPMH---YAALIVSAWWVGTQPMSWLEIGALALSLGIVNGL-ALNTGHELGHKKETFDRWMAKIVLAV 158
XYLM_PSEPU,   56 ------FFADLTQYLQLPLMIGLYGLLVFGVENGRIELSEPLQVAGCILSLAWLSGVPTLPVSHELMHRRHWLPRKMAQLLAMF 133

ALKB_PSEOL,  159 VGYGHFFIEHNKGHHRDVATPMDPATSRMGESIYKFSIREIPGAFIRAWGLEEQRLSRRGQSVWSFDNEILQPMIITVILYAVL 242
XYLM_PSEPU,  134 YGDPNRDIAHVNTHHLYLDTPLDSDTPYRGQTIYSFVISATVGSVKDAIKIEAETLRRKGQSPWNLSNKTYQYVALLLALPGLV 217

ALKB_PSEOL,  243 LALFGPKMLVFLPIQMAFGVWVQLTSANYIEHYGLLRQKMEDGRYEHQKP---HHSVWNSNHIVSNLVLFHLQRHSDHHAHPTRSY 323
XYLM_PSEPU,  218 SYLGGPALGLVTIASMIIAKGIVEGFNYFQHYGLVR--------DLDQPILLHHAVWNHMGTIVRPLGCEITNHINHHIDGYTRF 293

ALKB_PSEOL,  324 QSLRDFPGLPALPTGYPGAFLMAMIPQWFRSVMDPKVVDWAGGDLNKIQIDDSMRETYL---KKFGTSSAGHSSSTSAVAS    401
XYLM_PSEPU,  294 YELRPEKEAPQMPSLFVCFLLGLIPPLWFALIAKPKLRDW-----DQRYATPGERELAMAANKKAGWPLWCESELGRVASI    369
```

Figure 3.3 Pairwise alignment of the amino acid sequence of AlkB and xylene mono-oxygenase.

The hydrophobic 'trans-membrane' regions are coloured blue with white text; conserved histidine motifs are boxed.

Table 3.1 Functional homologues of the *AlkB* gene of *P. Putida* GPo1.

Strain	***No of homologues**	**Chain-length specificity**	**Ref**
Alcanivorax borkumensis	1(2)	C8-C12	[34]
Burkholderia cepacia RR10	1	C10-16	[113]
P. fluorescens	1	C12-C16	[34]
P.aeruginosa ATCC 17423	3	C8-C18	[114, 115]
P.aeruginosa NCIMB 8704	3	C8-C18	[114, 115]
P.aeruginosa NCIMB 9581	3	C8-C18	[114, 115]
Acinetobacter calcoaceticus EB104	1	C6-C18	[34]
Acinetobacter sp. Strain ADP1	2	C12-C18	[116, 117]
Acinetobacter sp. Strain M-1	2	C22-C40 C16-C22	[96]
Mycobacterium tuberculosis H37Rv	1	C12-C16	[34, 118]
Prauserella rugosa NRRL B-2295	1	C8-C14	[97, 119]
Rhodococcus erythropolis NRRL B-16531	1(4)	C6-C36	[21, 120, 121]
Rhodococcus erythropolis Q15	1(4)	C8-C32	[21, 120, 121]
Nocardioides sp. strain CF8	1	C6-C16	[32]

*Numbers shown are known functional homologues, numbers in brackets () denote the total number of alkB homologues found in that strain that have not yet been proven functional.

AlkB is known to catalyse the hydroxylation of *n*-alkanes, transferring one atom of oxygen from molecular dioxygen to the substrate and the other to water:

$$\mathbf{R\text{-}CH_3 + O_2 + NADH + H^+ \rightarrow R\text{-}CH_2OH + H_2O + NAD^+}$$

Although its most preferred substrates are short chain linear aliphatic alkanes [122], AlkB from is known to have a broad substrate specificity. Amongst its capabilities are the hydroxylation of cycloalkanes, functionalised hydrocarbons (alkenes and alkynes) and some aromatic compounds [24]. It is also able to epoxidate the double bonds of unsaturated hydrocarbons and perform stereo-selective sulfoxidation of methyl thioether substrates (Figure 3.4) [123]. Despite this broad range of activity, AlkB is able to perform many of the reactions in a stereo- and regio-specific manner [124]. Comparison of the size of substrates that are and are not catalysed by AlkB, and the location of the oxidation has enabled the elucidation of an approximate size of the active site of the enzyme, this being approximately 5 Å high and 8 Å wide [124].

3.2.4 Aims

The rubredoxin and rubredoxin reductase components of the system have been isolated and characterised, but so far the structure of AlkB has not been solved. This is partly due to the common problems involved with isolation and crystallisation of membrane proteins. A more detailed understanding of the substrate binding site and amino acids involved in stereo-selectivity would greatly enhance the possibility of biotechnological exploitation of the system and may lead to improvements in activity.

The preliminary aim of the work on the alkane hydroxylase system is the isolation and structural characterisation of the AlkB component with a secondary aim of characterising its interaction with the electron transfer components of the system. As rubredoxin is the most well characterised component of the alkane hydroxylase system, the production of 1FeDDR and 2FeDDR was taken as a starting point for the reconstitution of alkane hydroxylase activity of the membrane bound AlkB.

The expression constructs, pKR10, pKRR5v and pAlkB-3a, used as the basis of this work were kindly donated by Winston Tambyrajah in Professor Nigel Scrutton's laboratory (Dept. of Biochemistry, University of Leicester).

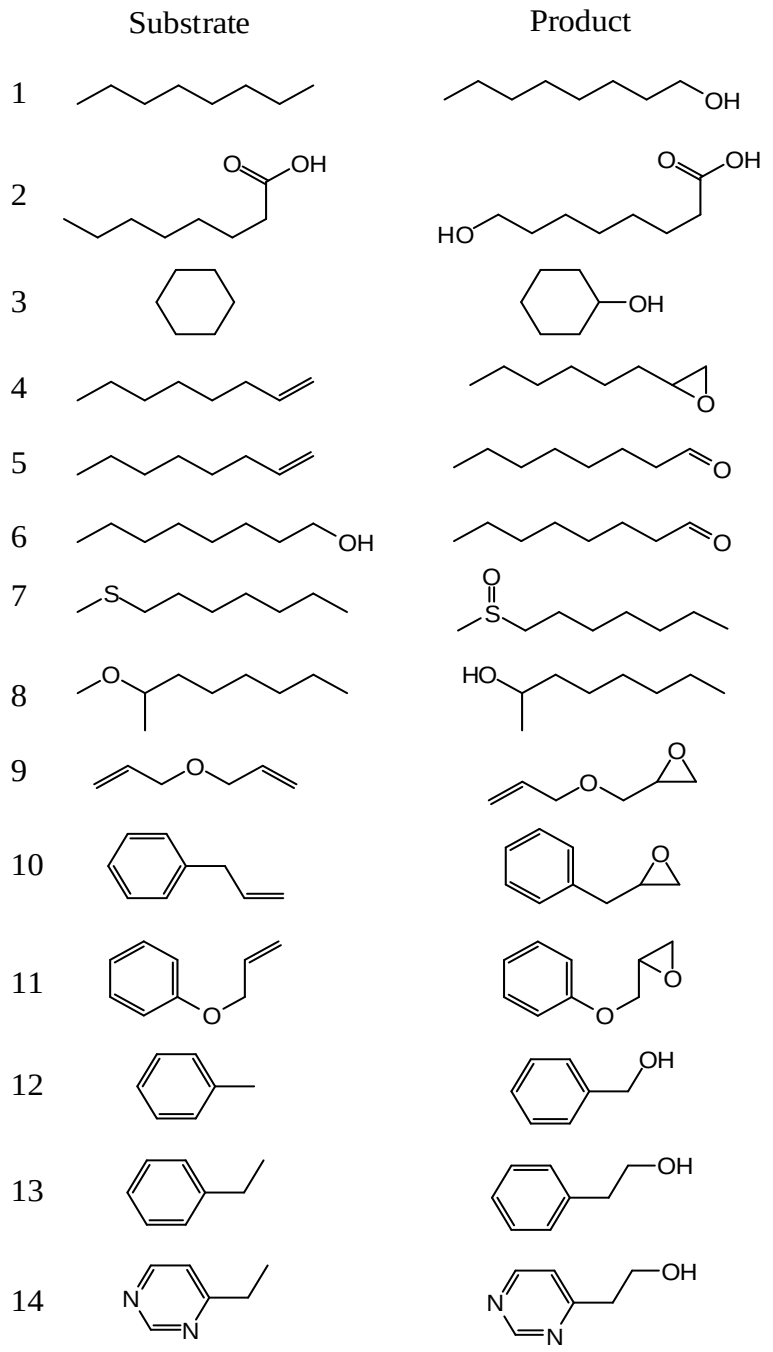

Figure 3.4 The catalytic range of the alkane hydroxylase system from *P. putida*.

Only examples of each class of compounds are shown. ω-hydroxylation of C6-C12 alkanes (1) and fatty acids (2), hydroxylation of cyclohexane to cyclohexanol (3), epoxidation of C3-C12 alkenes (4), and oxidation of 1-octene (5) and 1-octanol (6) to 1-octanal, sulfoxidation of methyl heptyl thioethers (7), demethylation of branched ethers to alcohols (8), epoxidation of diallyl ethers(9), epoxidation of allylbenzene (10), ring substituted allyl phenyl ethers (11) and substituted allyl benzyl ethers (12), hydroxylation of toluene (13), ethylbenzene (14) and ethyl-substituted heterocyclic 5- and 6-membered aromatic rings (15). Adapted from [124].

3.3 Results

3.3.1 Verification of plasmids pKR10, pKRR5 and pAlkB-3a

A sample of the pAlkB-3a plasmid was subject to analysis by restriction digest to verify that the size and restriction pattern was as expected based on the DNA sequence. Figure 3.5 shows the fragmentation pattern of pAlkB-3a digested with either *BamH*I or *Ase*I separated by agarose gel electrophoresis. As expected, the *BamH*I digest yielded two fragments of 5.21 kb and 0.53 kb. Similarly, the *Ase*I digest yielded three fragments of sizes 3.2 kb, 2.2 kb and 0.3 kb.

Restriction digest were also performed on the donated plasmids pKR10 and pKRR5v, encoding rubredoxin and rubredoxin reductase respectively. The plasmid pKR10 was digested with *EcoR*V and *Sca*I in a double digest and yielded two fragments of 4.2 and 0.95 kb which matched expectations (data not shown). The plasmid pKRR5v was digested with *Msc*I to yield two fragments of 3.75 and 1.98 kb in size, also as expected (data not shown).

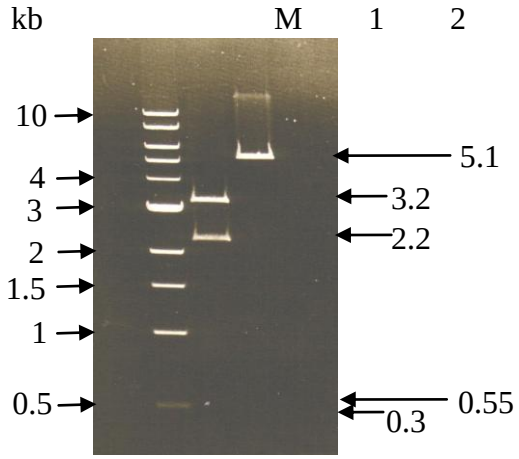

Figure 3.5. Analysis of restriction digest of pET3aAlkB using *BamH*I and *Ase*I.

A 2 µl sample of the plasmid pET3aAlkB was incubated with *Ase*I (lane 1) or *BamH*I (lane 2), in separate reactions as described in Methods. A 10 µl aliquot of each restriction digest was loaded onto a 0.8% agarose gel alongside a 1 kb DNA ladder marker (M) and subject to 150 V for approximately 30 min. The gel was visualised under UV light and fragment sizes estimated by comparison with the marker. Fragments obtained with the *Ase*I digest were: 3.2 kb, 2.2 kb and 0.3 kb; and with *BamH*I digest were: 5.1 kb, 0.55 kb. The smaller fragments are difficult to detect clearly on this digital image but were visible under UV light. According to the sequence of pET3aAlkB, digestion with *Ase*I should yield fragments of 3188, 2245 and 384 base pairs whilst digestion with *BamH*I should yield fragments of 5189 and 528 base pairs. The data presented are consistent with those expected. Representative of n = 2. Similar analysis was performed on the plasmid pKR10 (encoding Rubredoxin) using *EcoR*V and *Sca*I in a double digest to yield fragments of ~4.2 kb and 1 kb (data not shown).

3.3.2 Expression and purification of recombinant double domain rubredoxin from *P. putida*

Recombinant rubredoxin was isolated in preparation for use in activity assays during the subsequent purification and characterisation of the membrane bound AlkB. The 1FeDDR was expressed in TG1 *E. coli* transformed with pKR10 and purified following the protocol described in Methods. Samples were taken at all stages of purification and analysed by SDS-PAGE to assess the homogeneity of the final protein sample (Figure 3.6).

SDS-PAGE analysis shows two distinct bands of protein at 19 and 24 kDa that are progressively enriched during the purification. There are some minor contaminants in the final sample. Rubredoxin is known to migrate as two bands during electrophoresis. This phenomenon is attributed to the formation of disulphide bridges and can be reduced by the addition of 2-mercaptoacetic acid to the gel running buffer [50]. This level of purity was deemed acceptable, as the primary use of this protein was as a marker for activity of alkane hydroxylase.

3.3.3 Conversion of one-iron rubredoxin to two-iron rubredoxin

A sample of the purified 1FeDDR (section 3.3.2) was converted to 2FeDDR by unfolding the protein then refolding in the presence of excess iron as described in Methods. Samples of both forms were then examined and compared by UV/visible spectroscopy (Figure 3.7). The absorption spectrum of 1FeDDR shows the protein absorbs maximally at 497, 377 and 280 nm with an A_{280}/A_{497} ratio of 6.8 which is comparable to that previously reported for pure 1FeDDR (6.4) [50]. The absorption spectrum of 2FeDDR shows absorbance maxima at 494, 378 and 280 nm with an A_{280}/A_{497} ratio of 4.0 which is also in good agreement with previously reported values of pure protein (4.0 – 4.3) [50]. Protein concentrations were calculated from the absorbance at 497 nm and 494 nm using the extinction coefficients 6,300 M^{-1} cm^{-1} and 10,600 M^{-1} cm^{-1} for 1FeDDR and 1FeDDR respectively [80].

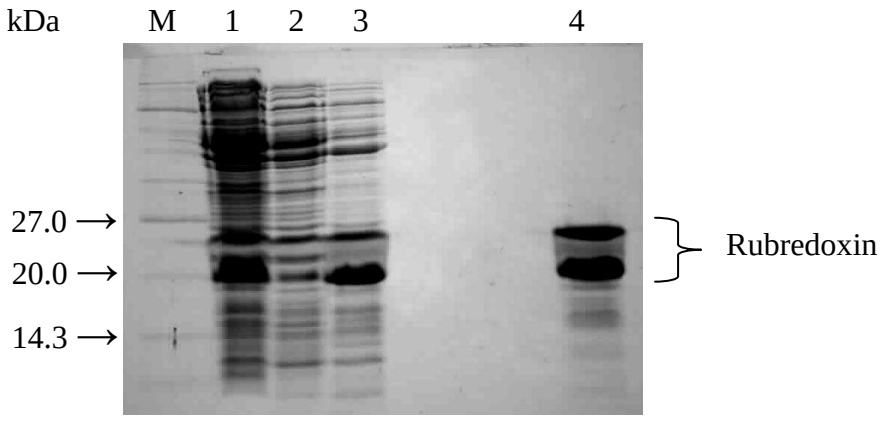

Figure 3.6. Purification of 1Fe rubredoxin from *E. coli* TG1 transformed with plasmid pKR10.

The transformed *E. coli* were grown in 2 x YT media for a period of 24 h at 37 ^{o}C, harvested by centrifugation and frozen at -20 ^{o}C as described in Methods. Once thawed, cells were sonicated in the presence of 1 mM PMSF and cell debris removed by centrifugation. Rubredoxin was purified from the cell free lysate using a combination of ammonium sulphate fractionation, anion exchange chromatography and hydrophobic interaction chromatography (see Methods and text for details). Samples from each step were prepared for analysis by SDS-PAGE as described in Methods. Each sample was loaded onto a 15% polyacrylamide gel alongside a standard protein size marker (M) and subject to 150 V over a period of approximately 1 h. The gel was then fixed and stained with Coomassie Blue as described in Methods. Lanes: M) marker; 1) soluble fraction of cell lysate; 2) post ammonium sulphate fractionation (40-60%); 3) post anion exchange chromatography; 4) post hydrophobic interaction chromatography in two different amounts. Rubredoxin is a 19 kDa protein and at high concentrations pure rubredoxin migrates as two bands, as can be seen here at 19 and 23 kDa. This phenomenon is attributed to the formation of disulphide bridges during electrophoresis and can be reduced by using smaller amounts or by the addition of 2-mercaptoacetic acid to the gel running buffer.

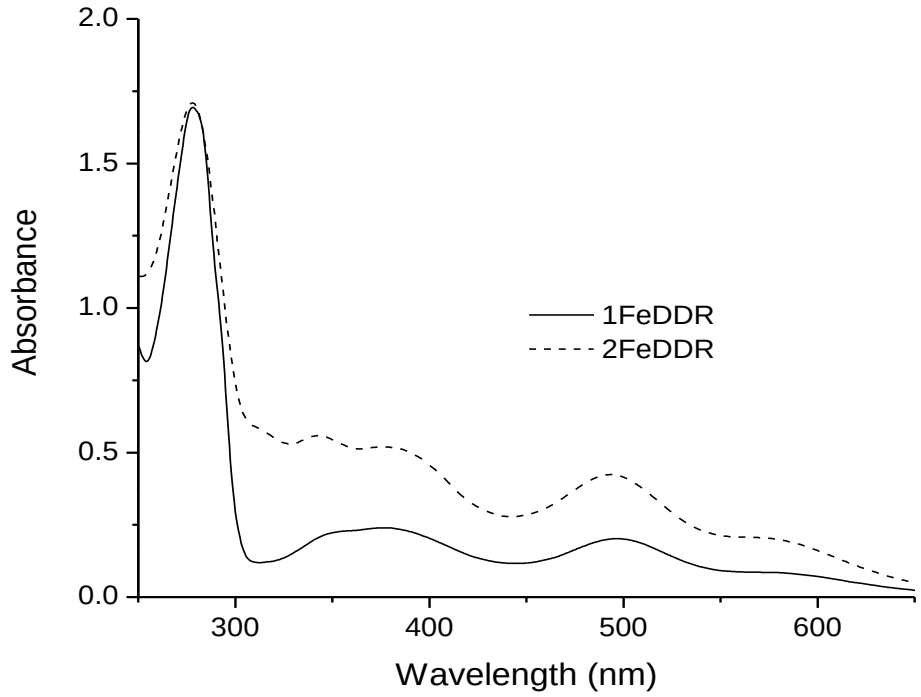

Figure 3.7. UV/visible spectroscopy of pure 1Fe and 2Fe rubredoxin.

The rubredoxin is purified in the one iron (1Fe) form but its native state in vivo is the two iron 2Fe) form. The second iron can be replaced by unfolding and refolding the protein in the presence of iron without loss of activity [50]. A proportion of 1FeDDR from the purification described in section 3.2.1 was unfolded and refolded in the presence of ferrous ammonium sulphate under anaerobic conditions as described in Methods. A 40 μM sample of 1Fe rubredoxin was diluted in 50 mM potassium phosphate buffer, pH 7.5 at room temperature and absorbance measurements were recorded over the wavelength range 250 – 800 nm. The spectrum of 2Fe rubredoxin was obtained in the same way and overlaid for comparison.

3.3.4 Redox Potentiometry

Determination of the mid-point potential of a redox enzyme can provide crucial information required to understand electron transfer within the system of interest. A reliable and well documented method of measuring redox potentials involves the use of a platinum (Pt)/calomel electrode in combination with UV/visible spectroscopy to record changes in the electronic absorption spectra [84]. The (Pt)/calomel electrode consists of a solution of potassium chloride in contact with solid mercurous chloride (calomel) and mercury containing a platinum wire. The resulting redox potentials are expressed relative to the normal hydrogen electrode (NHE) with a correction factor of +244 mV. Due to the globular nature of proteins, their redox centres are often buried within the protein or shielded from solution. To speed the reduction and re-oxidation reaction, small organic or inorganic molecules are used which act a redox mediators, to shuttle electrons between the surface of the electrode and the proteins redox centre.

Determination of the mid-point redox potential of rubredoxin was performed by titrating small amounts of oxidant or reductant to the protein in solution and recording the spectral changes at the observed potentials. Reductive titrations were performed under anaerobic conditions on both the 1FeDDR and 2FeDDR as described in Methods. The spectral changes observed when 1FeDDR was reduced are shown in Figure 3.8. When fully oxidised the enzyme displayed typical absorption spectra for rubredoxin as described previously (Figure 3.7). As the sample was reduced the absorbance values at 386 nm and 495 nm decreased to almost zero. A mid-point redox potential of -3 mV was calculated from the plot of maximal absorbance change versus the corresponding potential measurement (inset Figure 3.8). Reductive titration of 2FeDDR yielded a mid-point redox potential of -9 mV (Figure 3.9 Spectral changes in 2FeDDR during reductive titration and calculation of the mid-point potential.Figure 3.9). Both values are in good agreement with the reported redox potentials of -6 mV and -8 mV for 1 and 2 FEDDR respectively [50].

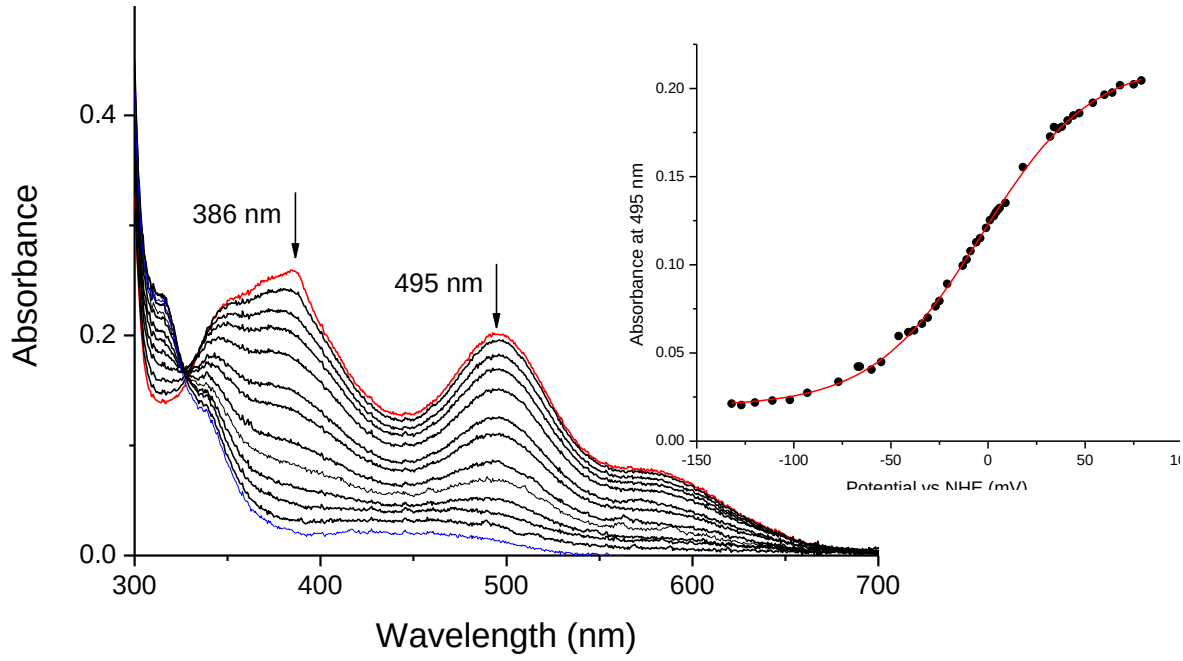

Figure 3.8 Spectral changes in 1FeDDR during reductive titration and calculation of the mid-point potential.

Under anaerobic conditions, 1FeDDR in 100 mM KPi (pH 7.0) containing 10% (v/v) glycerol was incrementally reduced then re-oxidised as described in Methods. Spectra were recorded (250 nm – 800 nm) at each reductive/oxidative addition along with the corresponding potential. The absorbance measurements at the wavelength showing the maximal absorbance changes were then plotted against the corresponding potential measurement corrected against the normal hydrogen electrode (NHE) by the addition of +244 mV. Data were then fit to the 1-electron Nernst equation (n) to calculate the midpoint potential. The starting spectrum (red) shows ~30 μM of oxidised 1FeDDR. The final spectrum (blue) shows the enzyme following the addition of sodium dithionite to full reduction. A number of example intermediate spectra are shown in black. Arrows show the direction of the absorbance change as the enzyme is reduced. Inset shows a plot of absorbance at 495 nm against the normalised potential measurement, yielding a mid-point reduction potential of -3 ± 0.5 mV. The error shown is the estimate from graphing software (Origin 6; OriginLab, Massachusetts) of the fit of the data to the 1-electron Nernst equation (n) from a single potentiometric titration.

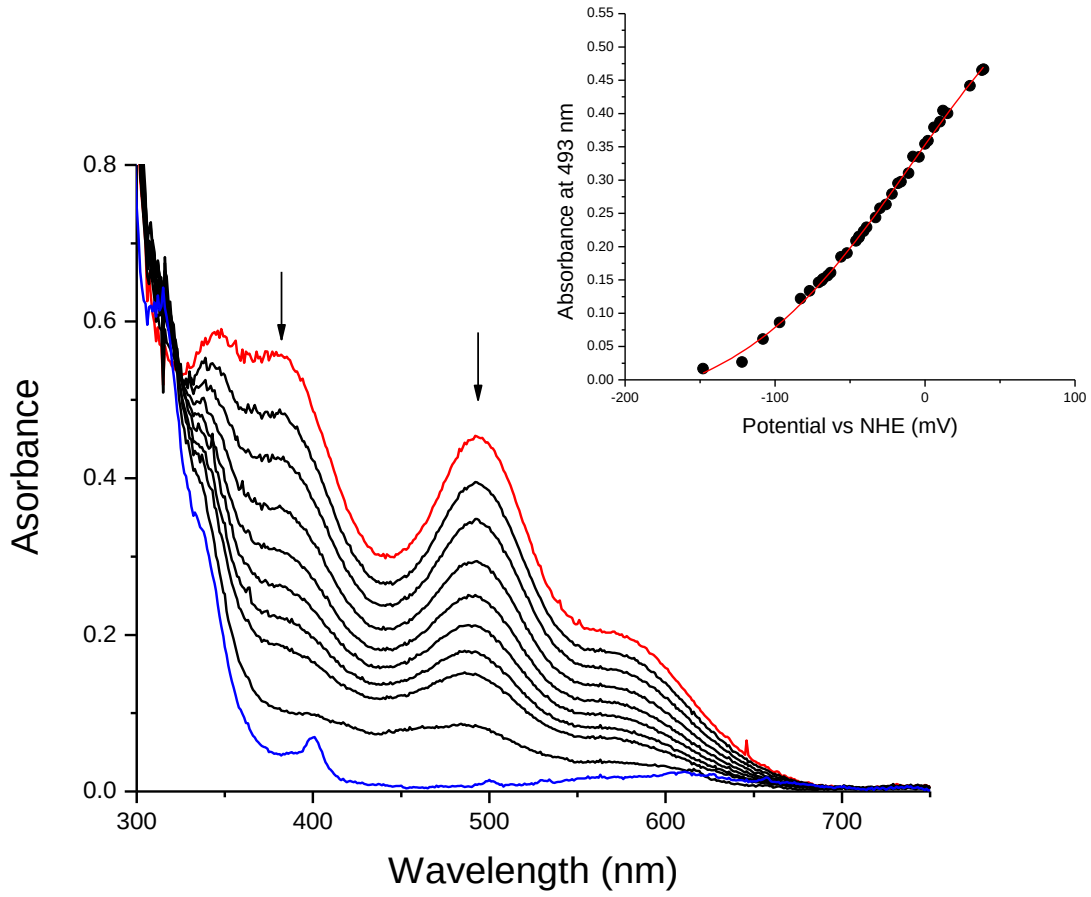

Figure 3.9 Spectral changes in 2FeDDR during reductive titration and calculation of the mid-point potential.

Under anaerobic conditions, 2FeDDR in 100 mM KPi (pH 7.0) containing 10% (v/v) glycerol was incrementally reduced then re-oxidised as described in Methods. Spectra were recorded (250 nm – 800 nm) at each reductive/oxidative addition along with the corresponding potential. The absorbance measurements at the wavelength showing the maximal absorbance changes were then plotted against the corresponding potential measurement corrected against the normal hydrogen electrode (NHE) by the addition of +244 mV. Data were then fit to the 1-electron Nernst equation (Equation 4) to calculate the midpoint potential. The starting spectrum (red) shows ~30 μM of oxidised 2FeDDR. The final spectrum (blue) shows the enzyme following the addition of sodium dithionite to full reduction. A number of example intermediate spectra are shown in black. Arrows show the direction of the absorbance change as the enzyme is reduced. Inset shows a plot of absorbance at 493 nm against the normalised potential measurement, yielding a mid-point reduction potential of -9 ± 5 mV. The error shown is the estimate from graphing software (Origin 6; OriginLab, Massachusetts) of the fit of the data to Equation 4 from a single potentiometric titration.

3.3.5 Expression and purification of recombinant rubredoxin reductase from *P. putida*

Expression and purification of recombinant rubredoxin reductase was performed to enable the reconstitution of the full electron transfer chain of the alkane hydroxylase system to monitor activity during purification of AlkB. Rubredoxin reductase was expressed in TG1 *E. coli* transformed with pKRR5 and purified following the protocol described in Methods. The presence of reductase in samples was monitored using UV/visible spectroscopy and the purity was analysed by SDS-PAGE (Figure 3.10). The purification was successful as indicated by the absence of any significant amounts of other proteins, even when the gel was overloaded. However, during preparation of protein for storage and spectroscopic analysis the reductase appeared to lose its FAD cofactor. At this stage it was decided to suspend attempts to isolate rubredoxin reductase in favour of using the commercially available spinach ferredoxin reductase as an electron donor for rubredoxin in activity studies planned for alkane hydroxylase and rubredoxin.

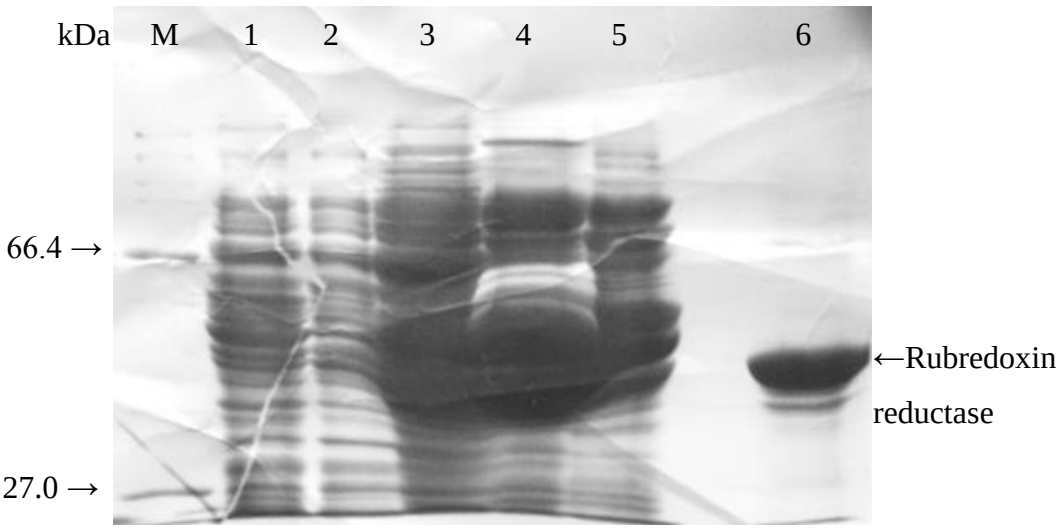

Figure 3.10. Purification of recombinant rubredoxin reductase from *E. coli* TG1 transformed with plasmid pKRR5.

Transformed *E. coli* were grown as described in Methods, harvested by centrifugation and frozen at -20 ^{o}C. Once thawed cells were lysed by French Press in the presence of 1 mM PMSF and cell debris removed by centrifugation. Rubredoxin reductase was purified using a combination of ammonium sulphate fractionation followed by anion exchange chromatography (see Methods). Samples from each step were loaded onto a 10 % polyacrylamide gel alongside a standard protein size marker (M) and subject to 150 V for approximately 1 h. The gel was fixed and stained with Coomassie Blue as described in Methods. Lanes: 1) soluble fraction of cell lysate; 2) post ammonium sulphate fractionation (30 – 60 %); 3-5) post Phenysepharose; 6) post anion exchange chromatography (Q-sepharose).

3.3.6 Engineering an N-terminal (His)6 tagged AlkB (AlkB$(H)_6$)

3.3.6.1 Blunt-end cloning

The gene for AlkB contained within pAlkB-3a was amplified by PCR using the primers ANF and ASR and *Pfu* DNA polymerase under the conditions described in Methods. The PCR fragments generated were separated from any remaining template DNA and potential primer dimers by agarose gel electrophoresis and examined under UV light. The sample contained DNA of various lengths indicated by smearing over the size range 0.5 to 2 kb (data not shown). PCR amplification was repeated with the following alterations; template DNA increased from 2 to 5 ng and annealing time increased from 1.5 to 1.75 min. The product was then separated by electrophoresis as before. Figure 3.11a shows the product of this PCR reaction migrating at 1.2 kb with no smearing indicating successful amplification of the gene.

The blunt-ended *Pfu* DNA polymerase-generated fragments were purified and subject to an A-tailing reaction before ligation into pGEM-T and subsequent transformation into *E. coli* JM109 as described in Methods. Fewer than 10 white colonies grew (data not shown) so all were selected for analysis of their recombinant plasmid. Each colony was used to inoculate 5 ml of LB media supplemented with 50 mg/ml ampicillin and incubated over-night at 37 ^{o}C. The resultant plasmid DNA was isolated using the Qiagen mini-prep kit as described in Methods. Each DNA sample was then subject to restriction digest with *BamH*I and analysed by agarose gel electrophoresis. Figure 3.11b shows plasmid samples of greater than 5 kb with no 528 bp fragment that was expected, indicating the procedure had not been successful.

To eliminate degradation of communal stock laboratory reagents in the A-tailing reaction as the possible cause of error, fresh dNTP solution was mixed and fresh *Pfu* DNA-Polymerase was purchased. A-tailing and ligation procedures were repeated, with similar results.

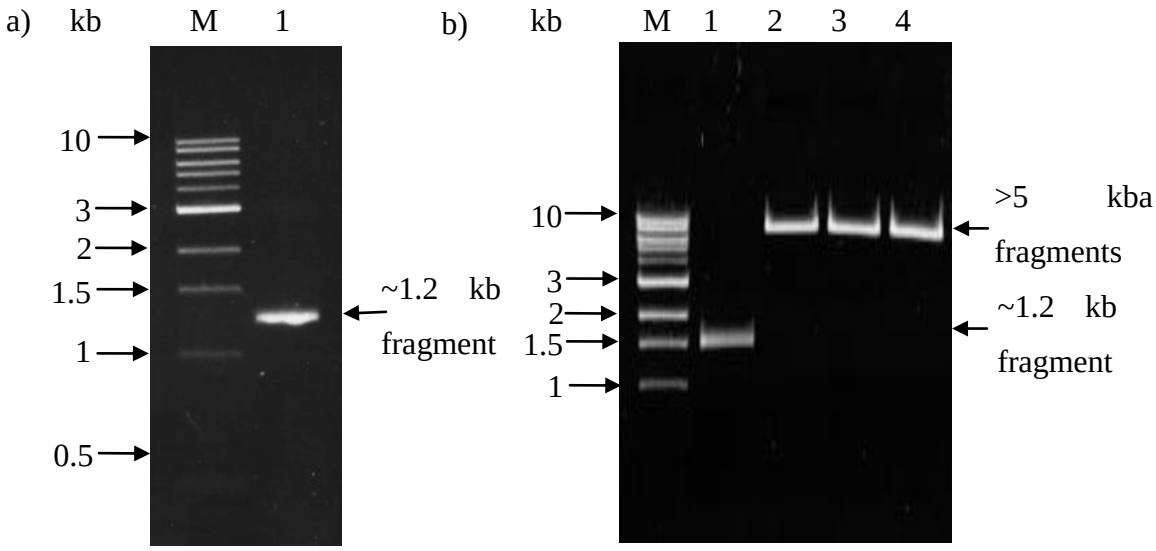

Figure 3.11. Analysis of cloning of pAlkB-3a to engineer a $(His)_6$ tag to the N-terminal of AlkB.

Panel a) PCR products obtained with pAlkB-3a as a template using oligonucleotide primers ASR and ANF detailed in Methods. Lanes: M) 1kb DNA marker; 1) amplified insert. Panel b) *BamH*I restriction digest of DNA prepared from *E. coli* JM109 transformed with the ligation product of pGEM-T/A-tailed AlkB PCR product. Lanes: M) 1kb DNA marker; 1) amplified insert; 2 – 4 examples of digested plasmids from *E. coli*. Digestion with *BamH*I was expected to yield fragments of 5189 and 528 base pairs. These data suggest that the ligation was unsuccessful as there is only a single fragment of >5 kbp. This protocol was followed twice more with similar results leading to a reassessment of approach and application of alternative method (Section 3.3.6.2).

3.3.6.2 Site-directed mutagenesis

Mutagenic PCR was performed on pAlkB-3a to construct a (His)6 tag and stop codon in the C-terminus of AlkB. PCR was performed using primers AHF and AHR under the conditions described in Methods. The resultant sample was subject to digestion with *Dpn*I and analysed by agarose gel electrophoresis as described in Methods. Figure 2.8a shows little digested DNA indicating the presence of PCR amplified plasmid. The plasmid, now termed pAlkBH, was then used to transform *E. coli* NOVABlue cells and DNA preparations were made from a selection of single colonies and then subject to agarose gel electrophoresis as before. Figure 2.8b shows a band of DNA at approximately 3 kb which is as expected for a circular plasmid of almost 6kb.

Sequencing analysis for the samples from 3 isolates from the site-directed mutagenesis identified one plasmid that had been successfully mutated to include a $(His)_6$ tag and stop codon at the N-terminal with no secondary, unplanned mutations located in the rest of the gene sequence. There appeared an ambiguous nucleotide, denoted by 'N' in the stop codon. However, upon examination of the chromatogram (Figure 3.13) it is clear that the nucleic acid at this position was an A and therefore the stop codon was correct (i.e. TAG).

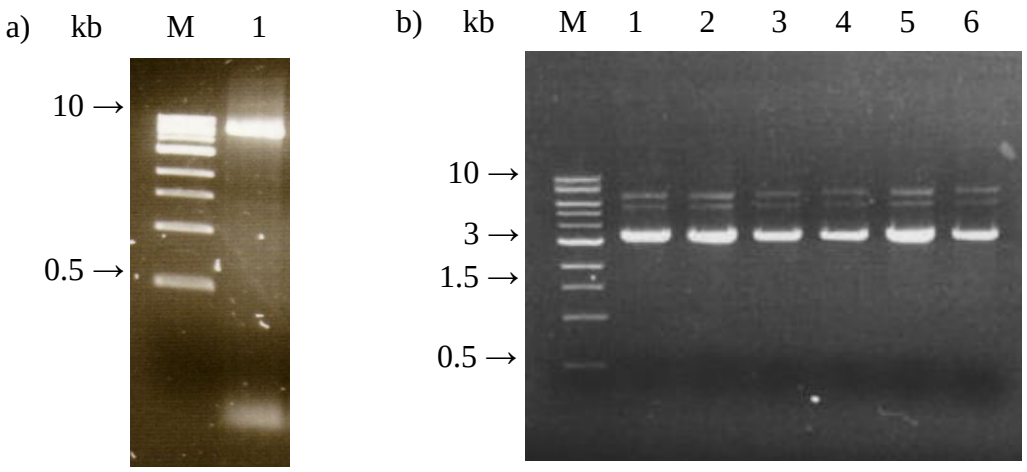

Figure 3.12 Analysis of PCR performed on pAlkB-3a to insert a N-terminal $(His)_6$ tag.

Panel a) The plasmid pAlkB-3a was incubated with the AHF and AHR under the conditions described in Methods. The resultant PCR product was subject to digestion with *Dpn*I restriction endonuclease as per the manufacturer's instructions. A 10 µl aliquot of the digest was loaded onto an 0.8% agarose gel alongside a 1 kb DNA ladder marker (M) and subject to 150 V for approximately 30 min. Panel b) The product of the PCR reaction in panel a was used to transform *E. coli* NOVABlue, plated out onto agar plates containing ampicillin (100 µg/ml) and incubated at 37^{oc} for ~12 h. Single transformant colonies were used to prepare DNA ready for sequencing as described in Methods. Samples of each DNA preparation were analysed by agarose gel electrophoresis to confirm presence of plasmid and estimate DNA concentration prior to selecting two for sequencing. Both gels were visualised under UV light.

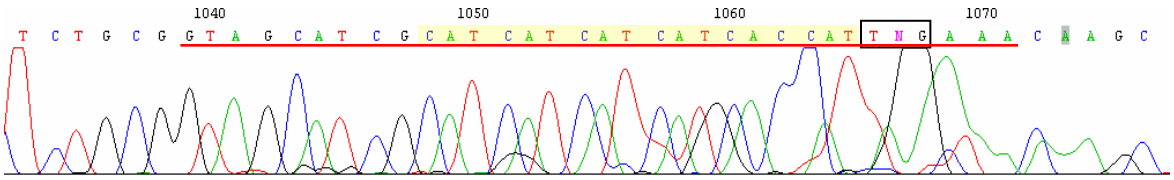

Figure 3.13. Part of the chromatogram of sequenced plasmid pAlkB-3H to show the insertion of a $(His)_6$ tag and stop codon at the N-terminal of AlkB.

The sequenced plasmid was checked by alignment with the pET3aAlkB sequence using ClustalW to ensure no unplanned mutations had occurred in the plasmid or insert sequence. There appears an ambiguous 'N' in the stop codon. However, upon examination of the chromatogram it is clear that the nucleic acid at this position is an A and therefore the stop codon is correct, i.e. TAG. The primer sequence (AHF) is underlined in red, the $(His)_6$ tag insert highlighted in yellow and the engineered stop codon is boxed in black.

3.3.7 Expression of recombinant AlkB and AlkB(H)$_6$

E. coli BL21(DE3)pLysS were transformed using either pAlkB-3a (wild-type) or pAlkBH (His-tagged). Protein expression trials were performed in LB media under the conditions described in Methods. Protein expression was induced using IPTG, samples were taken at timed intervals pre- and post-induction and analysed by SDS-PAGE. Comparison of induced versus un-induced in the wild-type, clearly demonstrates a band of protein at 41 kDa that developed after induction with IPTG, with no such band present in the un-induced sample (Figure 10). According to the entry on the Swiss-Prot database (www.expasy.org/uniprot/P12691), the expected mass of Alkb based on its amino acid sequence is 45.8 kDa. However, it is known from previous work that the protein migrates at an apparent 41 kDa on SDS-PAGE [41].

Induction of cells transformed with pAlkBH lead to rapid cell lysis (within 2-4 h). Reduction in temperature to 25 or 20^{o}C at induction did not significantly slow or prevent lysis. The mutant *E. coli* strain C41(DE3) was investigated as an alternative host [72]. This mutant of *E. coli* BL21(DE3) has increased resistance to toxic effects, a significantly improved expression of membrane proteins, and a reduction in the proportion of protein in inclusion bodies [125-127]. It has also been shown to affect support proliferation of intracellular membranes when expressing membrane proteins. So much so, that the membrane structures were visible on electron micrographs of thin section of the cells [126].

E. coli C41(DE3) was transformed using pAlkBH and tested as an alternative expression host following the same protocol as used for the wild-type. SDS-PAGE analysis shows a clear band of protein at 41 kDa that developed after induction. Furthermore, cell lysis was not a problem even at 16 h post-induction (Figure 3.15). Un-induced cells showed no such protein band.

In an effort to improve protein yield by increased aeration, *E. coli* C41(DE3) transformed with pAlkBH were incubated in LB media in baffled conical flasks with all other variables remaining constant. Figure 3.16 shows increased levels of a protein at 41 kDa within the same time span when compared with those from cells incubated in Erlenmeyer flasks.

Taking into account the results of these expression trials the protocol for the expression of AlkB and AlkB$(H)_6$ is described in methods. Briefly, starter cultures of either BL21(DE3)pLysS/pAlkB-3a or C41(DE3)/pAlkBH for AlkB and AlkB$(H)_6$ respectively were used to inoculate LB media (0.5 L in 2 L baffled flasks) supplemented with the appropriate antibiotics. Once cell density reached 0.6-8 OD_{600} expression was induced by the addition of 1 mM IPTG and harvested after 4 h.

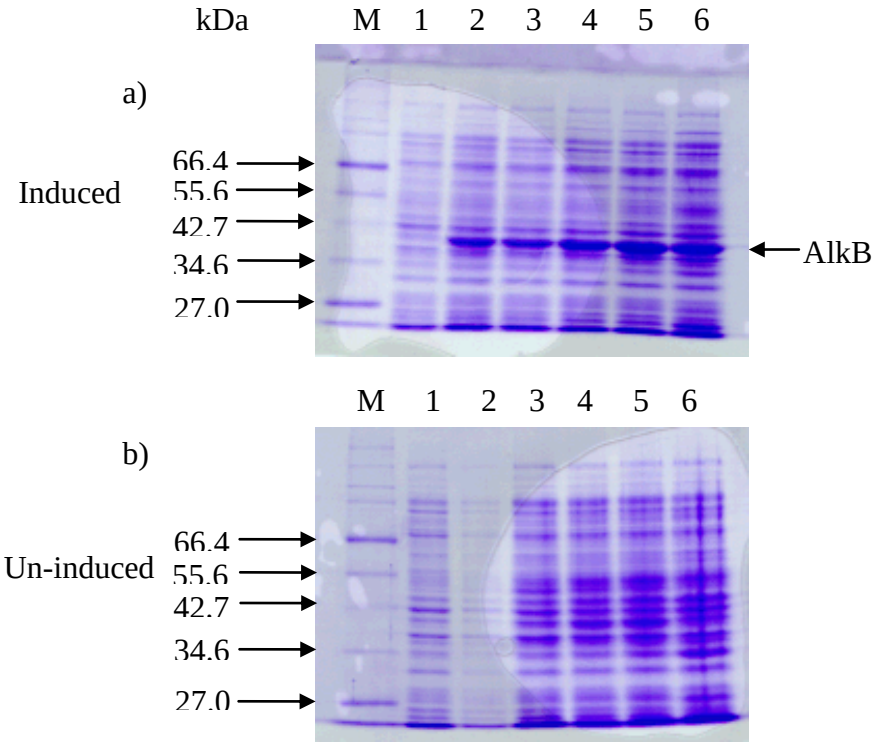

Figure 3.14 Protein expression by *E. coli* BL21 (DE3) pLysS transformed with pAlkB-3a.

Cells were grown in 2 L capacity Erlenmeyer flasks containing 0.5 L LB liquid media supplemented with ampicillin to 100 μg/ml and chloramphenicol to 34μg/ml. Cultures were grown at 37°C to an OD_{600} of ~0.8 whereupon cells were either induced by the addition of 1 mM IPTG (a) or left to grow with no induction b), in both cases temperature was reduced to 30 °C. Samples of the transformed *E. coli* were taken at time intervals before and after induction, normalised against the OD_{600} as described in Methods and frozen at -20 °C overnight. Samples were thawed and sonicated in the presence of 1 mM PMSF and 20 μl of each were prepared for SDS-PAGE analysis as described in Methods. Samples were loaded onto a 10% polyacrylamide gel alongside a standard protein size marker (M) and subject to 150 V over a period of approximately 1 h. The gel was then fixed and stained with Coomassie Blue as described in Methods. For the induced cells (a) Lanes: 1) *E. coli* at t = 0 pre-induction with IPTG; 2-6 post-induction at; 2) t = 2 h; 3) t = 4 h; 4) t = 6 h; 5) t = 9 h; 6) t = 12 h. For the uninduced cells b) lanes are 1) *E. coli* at t = 0 where OD_{600} = 0.8; 2) t = 2 h; 3) t = 4 h; 4) t = 6 h; 5) t = 9 h; 6) t = 12 h. According to the entry on the Swiss-Prot database, the expected mass of AlkB based on its amino acid sequence is 45.8 kDa. However, it is known from previous work that the protein migrates at an apparent 41 kDa on SDS-PAGE [41].

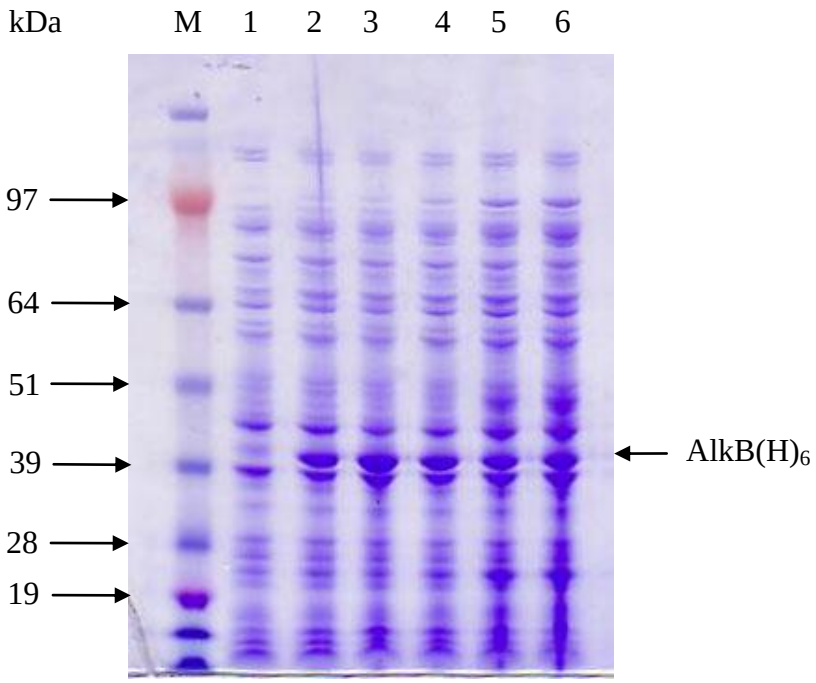

Figure 3.15 Protein expression by *E. coli* C41 cells transformed with pAlkB3H.

Cells were grown in LB liquid media supplemented with ampicillin to 100 µg/ml and chloramphenicol to 34 µg/ml with shaking at 37^{o}C to an OD_{600} of ~0.8 whereupon cells were induced by the addition of 1 mM IPTG and growth continued at 30 ^{o}C. Samples of the transformed *E. coli* were taken at time intervals before and after induction, normalised against the OD_{600} as described in Methods and frozen at -20^{o}C overnight. Samples were prepared and analysed by SDS-PAGE in the same way as detailed in Figure 3.11. Lane: 1) E. *coli* at OD_{600} 0.8 pre-induction with IPTG. Lanes: 2-6 post induction at; 2) t = 2 h; 3) t = 4 h; 4) t = 6 h; 5) t = 9 h; 6) t = 12 h.

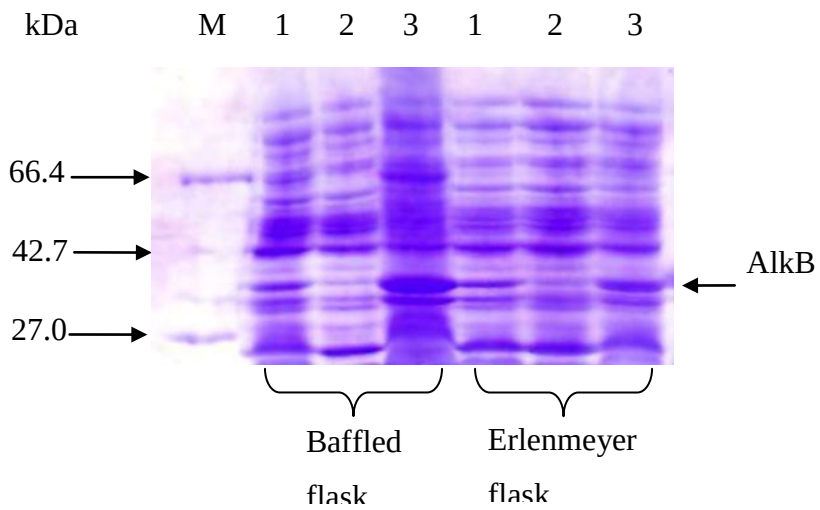

Figure 3.16 Protein expression by *E. coli* BL21 (DE3) pLysS transformed with pAlkB-3a grown in baffled or Erlenmeyer flasks.

Cells were grown in 0.5 L LB liquid media supplemented with ampicillin to 100 μg/ml and chloramphenicol to 34μg/ml at 37^{o}C in either 2 L capacity baffled flasks (lanes 1-3) containing anti-foaming agent or 2 L Erlenmeyer flasks. In both cases, cells were grown to an OD_{600} of ~0.8 whereupon cells were induced by the addition of 1 mM IPTG and growth continued at 30^{o}C for 4 h. Cells were harvested by centrifugation and frozen at -20^{o}C overnight. Samples were thawed and sonicated in the presence of 1 mM PMSF and cell lysate was subject to centrifugation 8000 x g for 15 min to separate cell debris. The resulting supernatant was subject to further centrifugation at 100,000 x g to separate soluble proteins from AlkB-containing membranes. A 20 μl aliquot of each cell lysate (1), soluble protein (2) and membrane pellet (3) were prepared for SDS-PAGE analysis as described in Methods. Samples were loaded onto a 10% polyacrylamide gel alongside a standard protein size marker (M) and subject to 150 V over a period of approximately 1 h. The gel was then fixed and stained with Coomassie Blue as described in Methods.

3.3.8 Purification of AlkB

The final component of the alkane hydroxylase system, the membrane bound AlkB, was expressed in *E. coli* BL21(DE3)pLysS following the optimised protocol described in Methods. AlkB enriched membranes were isolated using the protocol described in Methods as method 1. Briefly, after sonication in the presence of PMSF, cell debris and insoluble proteins were separated by low speed centrifugation. Membranes were isolated by differential ultracentrifugation using a 40% v/v glycerol cushion, followed by urea treatment. The enrichment process was followed by analysing the samples by SDS-PAGE.

SDS-PAGE (Figure 3.17) shows a 41 kDa protein present in both the insoluble and soluble fractions (lanes 3 and 4 respectively). There were two dense bands of protein at 37 kDa and 41 kDa present in the glycerol cushion (lane 6) whereas there were no such bands in the buffer fraction (lane 5) indicating an efficient isolation of the AlkB enriched membranes. Examination of the supernatant (lane 7) and pellet (lane 8) post urea treatment showed a large number of proteins present in both fractions including bands at 39 and 41 kDa. However, the pellet fraction contained a larger proportion of protein at 39 and 41 kDa.

An alternative method of membrane fractionation was investigated (Method 2) in order to simplify the protocol and negate the possibility of the urea treatment irreversibly denaturing the enzyme. Harvested cells were broken and cell debris removed by centrifugation as described for method 1. Membranes were isolated from cell-free lysate by ultracentrifugation without glycerol, then washed twice in a 1M NaCl solution to remove membrane associated and aggregated proteins (see Methods for details). Figure 14 shows significant enrichment of two bands of protein at 39 and 41 kDa. As the lower mass protein appears to be expressed in uninduced cells of both *E. coli* BL21(DE3) and C41(DE3) (Figure 3.14 Figure 3.15) it was considered to be a membrane protein native to these strains.

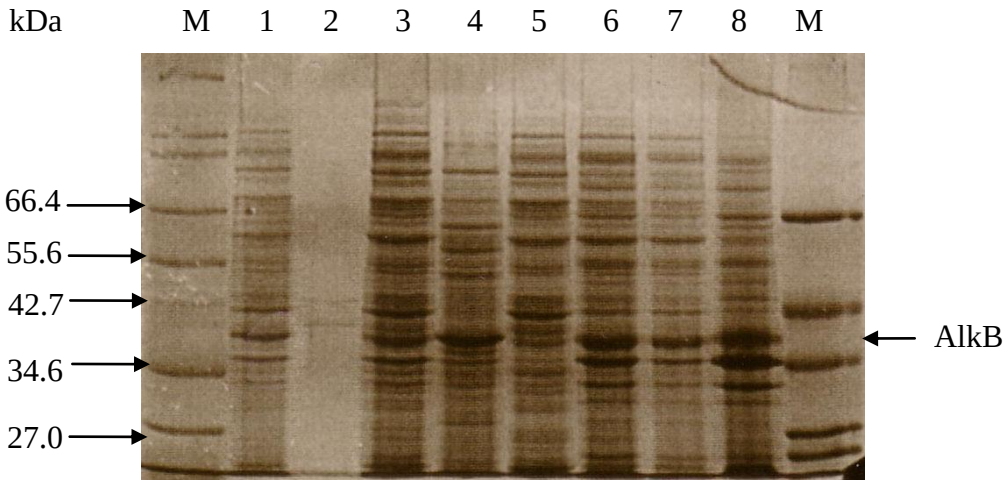

Figure 3.17 SDS-PAGE analysis of differential ultracentrifugation (Method 1) for isolation of AlkB-rich membranes.

E. coli BL21(DE3)pLysS cells transformed with pAlkB3a were grown in 2 L baffled flasks containing 0.5 L LB liquid media supplemented with ampicillin to 100 μg/ml, chloramphenicol to 34 μg/ml and antifoaming agent with shaking at 37^{oc}. Cells were induced when growth reached an OD_{600} of ~0.8 by the addition of 1 mM IPTG and growth continued at 30^{oc} for 4 h. Cells were harvested by centrifugation and membranes isolated following the differential protocol described in Methods as method 1. Briefly, harvested cells were sonicated in the presence of 1 mM PMSF to break up cells. Cell lysate was subject to centrifugation at 8000 x g for 15 min to separate cell debris (pellet) from soluble proteins and membrane vesicles (supernatant). The resultant supernatant was underlain with buffer containing 40% v/v glycerol and subject to ultracentrifugation at 240,000 x g for 120 min to separate membranes (glycerol cushion) from soluble proteins (supernatant). Urea was added to the glycerol fraction to a concentration of 0.5 M before being subject to ultracentrifugation at 240,000 x g for a further 60 min. Samples from each centrifugation step were prepared and analysed by SDS-PAGE as described previously (Figure 3.6). Lanes: M) protein marker; 1) cell lysate; 2) empty; 3) supernatant and 4) pellet from centrifugation at 8000 x g; 5) supernatant and 6) glycerol cushion from differential ultracentrifugation; 7) supernatant and 8) pellet from ultracentrifugation of the glycerol cushion post urea treatment.

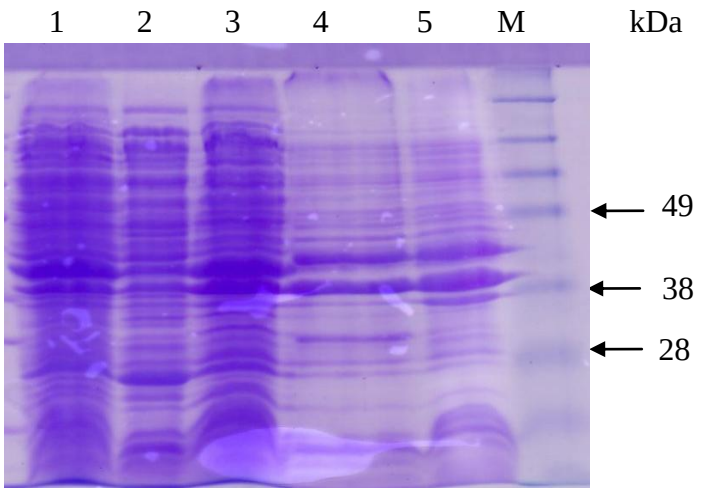

Figure 3.18 SDS-PAGE analysis of alternate ultracentrifugation protocol (Method 2) for isolation of AlkB-rich membranes.

BL21(DE3)pLysS cells transformed with pAlkB3a were grown and harvested as described. The AlkB-rich membranes were isolated following an alternate ultracentrifugation protocol described in Methods as method 2. Briefly, harvested cells were sonicated in the presence of 1 mM PMSF to break up cells. Cell lysate was subject to centrifugation at 8000 x g for 15 min to separate cell debris (pellet) from soluble proteins and membrane vesicles (supernatant). The resultant supernatant was subject to ultracentrifugation at 100,000 x g for 90 min so separate membranes (pellet) from soluble proteins (supernatant). Membrane pellets were re-suspended in 50 mM Tris-HCl, 1 M NaCl, pH 7 to wash the membranes of associated proteins and subject to a second ultracentrifugation. This wash step was repeated and the final membrane pellets stored at -20^{oc}. Samples from each step were prepared and analysed by SDS-PAGE as described previously (Figure 3.6). Lanes: 1) cell lysate; 2) supernatant from centrifugation 8000 x g; 3) membrane fraction after ultracentrifugation; 4) membrane fraction after 1st wash; 5) membrane fraction after 2nd wash; M) marker.

3.3.9 Purification of AlkB$(H)_6$

AlkB$(H)_6$ was expressed in *E. coli* C41(DE3) under control of the T7 promoter as described (Figure 3.14). AlkB$(H)_6$-enriched membranes were isolated using the salt-based ultracentrifugation method described and samples from each purification stage were analysis by SDS-PAGE as described previously (Section 3.3.2). Clear bands of protein at 39 and 41 kDa were enriched during the ultracentrifugation (Lanes 1-5, Figure 3.15). The sample was then solubilised in 2% ANAPOE (polyoxyethylene(a)dodecyl ether) (Anatrace, Maumee, Ohio) and applied to cobalt affinity resin (Talon, Clontech), washed with solubilisation buffer and eluted in a high concentration of imidazole (10 mM). Samples (2ml) were collected and analysed by SDS-PAGE (Figure 3.19). Lanes 6-9 show samples collected as the protein sample was loaded onto the column. Lanes 6-8 shown no protein present as expected for the buffer however, lane 9 shows a mixture of proteins similar in profile to the starting sample indicating unbound protein passing through the column. Lanes 10 and 11 show the samples as salt buffer and low imidazole concentration is washed through, little or no protein is present. Lane 12 is the sample collected as the high imidazole buffer is washed through. Two faint bands of protein at 39 and 41 kDa can be seen but the majority of the protein appears to have not bound to the resin and been washed through with buffer.

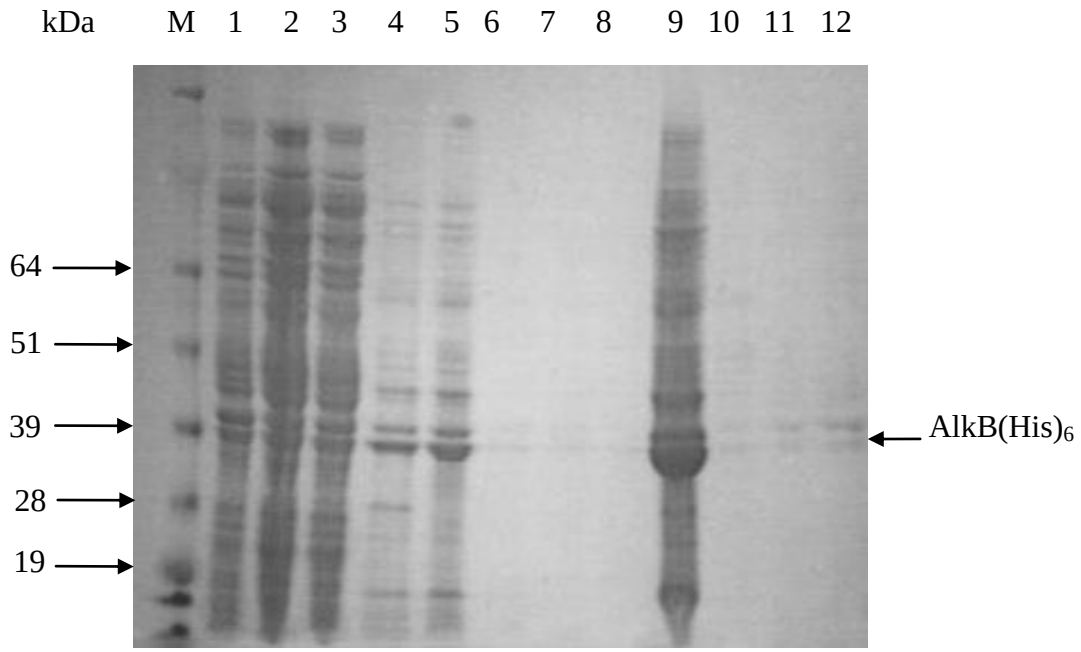

Figure 3.19 SDS-PAGE analysis of AlkB(His)$_6$ at various stages of purification using ultracentrifugation and affinity chromatography (Method 2).

The (His)$_6$-fusion AlkB was grown and harvested from *E. coli* C41 cells transformed with pAlkB3H as described for the wild-type (Figure 3.16). Membranes were isolated from the cell lysate using Method 2 (Figure 3.18). The AlkB(His)$_6$ enriched membranes were then solubilised in detergent (2% Anapoe) and applied to a cobalt affinity resin (see text and Methods for details). Lanes 1-6 show the stages of membrane isolation: M) marker; 1) cell lysate from *E. coli* C41 cells harvested at 4 hrs post induction; 2) supernatant from 8000 x g centrifugation; 3) membrane fraction after ultracentrifugation; 4) membrane fraction after 1st wash; 5) membrane fraction after 2nd wash. Lanes 6-12 show the affinity chromatography stages of the purification: 6-9) run-through from column as the membranes were applied; 10-12) washes of increasing imidazole concentrations (10 – 400 mM) to elute any bound protein. Samples taken at each purification step were loaded onto a 10% polyacrylamide gel alongside a standard protein size marker (M) and subject to 150 V over a period of approximately 1 h. The gel was then fixed and stained with Coomassie Blue as described in Methods.

3.4 Discussion

The expression and purification, by published methods [51-53], of rubredoxin and rubredoxin reductase have been described. Rubredoxin was successfully isolated in the one-and two-iron forms, both of which display UV/visible spectra and mid-point redox potentials comparable to that of published data [50]. Rubredoxin reductase is known to be rather unstable and at glycerol concentrations of less than 20% (v/v) has a tendency to lose its FAD cofactor; rendering the enzyme catalytically inactive [79]. Despite, successful isolation, the rubredoxin reductase lost its cofactor during concentration of the preparation for storage. It is possible that the centrifugal concentration of the protein caused local fluctuations in the glycerol content of buffer caused the enzyme to release FAD into the buffer. Due to the relative instability of the reductase, the extended time and resources required to complete purification and the fact that there is a readily available substitute, efforts to isolate the rubredoxin reductase were terminated in favour of using the commercially available spinach ferredoxin reductase.

The crystal structure of the electron transfer complex rubredoxin-rubredoxin reductase of *Pseudomonas aeruginosa* has been recently published [128]. These constitutively expressed, genomicaly encoded proteins can replace their homologues in the *P. putida* system [97, 129]. Considering the reductase component of the *P. aeruginosa* system was able to be crystallised in conjunction with the reductase component, it may be a more robust enzyme and therefore may be a viable alternative to commercially bought spinach ferredoxin reductase.

Using the donated plasmid, pAlkB-3a, as a template a histidine tag was successfully engineered onto the C-terminal of AlkB using site-directed mutagenesis. Expression trials were conducted to establish optimum conditions for expression of both the wild-type and his-tagged AlkB proteins. It was found that in contrast to the wild-type, expression of AlkB$(H)_6$ caused cell lysis of the expression host *E. coli* BL21(DE3). Literature searches identified a mutant of the *E.* coli strain BL21(DE3) which has been used and documented as an expression host for other toxic membrane proteins [72, 125-127]. The use of this mutant *E. coli* C41(DE3) enabled expression of AlkB$(H)_6$ without cell lysis. It may also be worth examining whether *E. coli*

C41(DE3) could be used to express AlkB wild type a previous work on the *E. coli* inner membrane, enzyme acyl-acyl carrier protein synthase (acyl-ACP) shows that although the protein is not in toxic to *E. coli* BL21(DE3), expression of acyl-ACP in *E. coli* C41(DE3) improves the yield of active protein 3- to 4-fold and reduces the proportion of inactive protein in inclusion bodies [125]. A second generation mutant derived from *E. coli* C41(DE3), *E. coli* C43(DE3), has been shown to have improved plasmid stability over C41(DE3) and enhanced membrane proliferation [126, 127] so it may also be with exploring its use as an expression host. It would also be interesting to see if expression of AlkB and AlkB$(H)_6$ affected membrane biogenesis in this mutant host as has occurred with the expression of the b subunit of F_1F_o ATP synthase in C41(DE3) [126].

Two methods for isolation of AlkB enriched membranes were investigated. The first using differential centrifugation and urea treatment as outlined by Shanklin and co-workers [74]; the second using an alternate ultracentrifugation technique involving high salt washing of the membranes to remove spurious membrane associated proteins. Both methods appear to enrich AlkB membranes reasonably well with little difference in the purity between both methods. However, the protocol using salt washes is less labour intensive than using differential ultracentrifugation with the glycerol cushion. It is interesting to note that AlkB (either wild-type or his tagged) expressed in either *E. coli* BL21(DE3) or C41(DE3) appears to be co-purified alongside a native *E. coli* protein of a similar size and neither the urea treatment nor salt washes is able to remove this contaminant. Further to the earlier comments regarding expression hosts, although in theory, the contaminant should be easy to eliminate from the AlkB$(H)_6$ upon successful employment of metal affinity chromatography, it may be necessary to investigate alternative expression host that are not derived from BL21 (DE3) to eliminate this contaminant in AlkB wild-type preparations.

Based on subsequent analysis of literature, were work to continue on purification of AlkB for the purposes of crystallisation there are several alterations that could be recommended. It is known that induction of the *alk* genes in both *P. putida* and *E. coli* increases the requirement for iron; if iron is limited, induction causes reductions in cell density when compared to cells that have not been induced [130]. The specific

activity of AlkB is also reduced when expressed in cells without additional iron in the growth medium [130]. The addition of iron in the growth medium to greater than 2.5 μM ($FeSO_4$) leads to increased cell densities comparable to that of uninduced cells and restoration of AlkB specific activity [130]. To ensure sufficient bio-availability of iron for AlkB expression growth medium was supplemented with 100 mg/L $Fe^{(II)}SO_4$ upon induction with IPTG. Preliminary tests of this modification to the protocol demonstrated that not only was wet weight of harvested cells doubled, from approximately 5.5g/L to approximately 11g/L. It was also noted that harvested cells grown in the presence of additional iron took on a distinct blue tint which turned a vivid green colour upon freezing of the cells. Additional alterations which seem common to the literature regarding isolation of membrane proteins are a reduction of temperature to 25 ^{o}C on IPTG induction [126] and removal of the freezing step after cell harvesting [131].

It was disappointing that the initial solubilisation and affinity chromatography experiments described here failed. There are several variables that may have contributed to this initial failure and would warrant further exploration. Membrane proteins are prone to aggregation, a feature which is heavily dependent upon the choice of detergent [132]. Ineffective solubilisation will have meant that many of the histidine tags may have been buried and inaccessible to bind to the IMAC resin. Alternative detergents, as well as improvements in solubilisation techniques e.g. sonication and removal of large protein aggregates by centrifugation could lead to vast improvements in the purification of his-tagged AlkB. It may also be worthwhile investigation whether the addition of glycerol to buffer would aid purification. Glycerol reduces the concentration of water, thus increasing the hydrophobicity of the buffer and has previously been shown to help keep membrane protein in a monomerically dispersed state. It has also been show to be crucial in maintaining activity in some membrane proteins [132]. This last feature may have implication for the reconstitution f the three component system as rubredoxin reductase also requires 20% glycerol to maintain its activity.

Other factors which may contribute to the success of IMAC in this instance are the size of the histidine tag and the choice of metal ion. Although exposed histadine groups will form complexes with many transition metal ions, binding effect will vary

depending on the ion [133]. The choice of cobalt affinity resin in this instance was a preventative measure. Nickel-based resins have been shown to strip functional iron from iron containing proteins as well as bind to histidines not located on the proteins histadine tag [134] which could interfere with the active site of AlkB as it contains a di-iron centre co-ordinated by several histidines. It is entirely possible the interaction between this his-tag and the cobalt resin is not strong enough and an alternative metal ion would be more suitable. Increasing the size of the His tag from 6 to 10 has also been shown to increase the affinity of a histidine tagged protein for IMAC media and may well be worth exploring [131].

3.5 Conclusion

Until recently, few alkane hydroxylase were known about and even fewer characterised in any great detail. The advent of new technology capable of screening large genome libraries for consensus sequences and motifs has enabled the identification of a great number putative AlkB homologues and homologues of soluble alkane hydroxylases such as cytochromes P450 and butane and methane mono-oxygenases. Novel AlkB homologues continue to be identified in undefined bacterial populations from sources as varied as deep sea sediments and shore lines of areas affected by oil spillages [23]. For example, analysis of a meta-genomic library of deep-sea sediment has identified 2 homologous AlkB genes present within this population. Cloned and functionally expressed, these membrane-bound enzymes contain the histidine rich motif and are able to catalyse the mono-oxidation of C5-C16 alkanes [135].

Despite the identification of over 40 functional AlkB homologues, the divergence of sequences across populations has not allowed identification of the amino acids involved in substrate recognition or binding on sequence comparison alone. Since completion of the work presented here, forced evolution studies have provided some insight into those amino acids responsible for chain-length specificity. Mutation and recombinant selection techniques have identified AlkB mutants from *P. putida* (W55S and W55C) and from *A. borkumensis* (W58S and W58L) which have altered their bacterial host's preference for growth on mid-chain alkanes (C6-C12) to longer chain alkanes (C10-C16). The wild type forms of both enzymes contain a tryptophan residue at position 55 or 58 in *P. putida* or *A. borkumensis* respectively. The transformant colonies carrying AlkB forced to grow on longer chain alkanes (C14 or C16) produced mutants which contained either serine, cysteine or lysine at this position [136]. In contrast, replacement of the equivalent residue in *M. tuberculosis* AlkB (L69) with either tryptophan or phenylalanine pushed the host's preference towards shorter chain alkenes [107]. The recently identified AlkB homologues from deep sea sediment contain either serine or glycine at the equivalent residue position which correlates to their extended chain length specificity (C5-C16) [135]. These data are growing evidence that this residue, located towards the centre of the

membrane on the putative trans-membrane helix 2, is key to the substrate selectivity of this group of enzymes.

It is postulated that the six trans-membrane helices of AlkB are distributed in a hexagonal arrangement which define a deep pocket that protrudes into the membrane. The side chain of the tryptophan found in those AlkB homologues specific for the shorter chain alkanes, is thought to project into the cavity and obstructs the pocket for longer chain alkanes [135]. It is likely there are more residues lining this pocket that interact with substrate and confer selectivity or specificity in some way. It may be possible to use the 'forced evolution method' to produce mutants with preference for cyclic or heterocyclic substrates to elucidate more information regarding the substrate specificity and selectivity.

Considering the inherent difficulties in crystallising membrane proteins, it may be more fruitful to investigate alternative methods of structural characterisation. Spin label relaximetry could potentially be used to study the 3D structure of AlkB by site-specific labelling of cysteine residues and measurement of the EPR signal in the presence of oxygen or spin relaxing agents like chromium oxalate (CROX) [137, 138]. The location of the spin-label within or exterior to the membrane can be calculated by the amount of exposure to hydrophobic or hydrophilic spin-relaxing agents. It is even possible to calculate the secondary structure and immersion depth of a membrane-exposed side chain by mutating consecutive residues and measuring their accessibility to oxygen or CROX. A spin-label on the exterior of a protein and exterior to the membrane will show sensitivity to oxygen and CROX, whilst a spin-label on the exterior of protein but interior to the membrane will only show sensitivity to oxygen. Site directed spin labelling has even been used to observe conformational events in membrane proteins [139, 140]. Application of this technique to AlkB may provide insight into the arrangement of the trans-membrane helices in relation to one another and identify residues which are likely to interact with the substrate.

From a biocatalysis view point the structural characterisation of alkane hydroxylase was rather ambitious; whilst a crystal structure would undoubtedly shed light on the catalytic mechanism and interaction with substrates, in practice the structural characterisation of AlkB truly deserves to be tackled in a structural biology laboratory. The original scope of the project, towards robust and specific enzymatic

oxidation of hydrocarbons, would not have been best served by continuing this route. Therefore, a strategic decision was taken to discontinue work on the alkane hydroxylase in favour of cytochrome P450 BM3. It would appear too, that interest in the system has waned somewhat as the number of publications arising from work on AlkB has dropped quite significantly over the last few years. Recent interest has focused on the growing number of novel alkane hydroxylases, many of which are soluble and thus far more amenable to studies of structure function relationships [30, 141, 142].

Since the work presented here was concluded, AlkB$(H)_6$ from the construct described in this thesis has been isolated in a detergent solubilised form (Dr Anna Roujeinikova, Structural Biology, University of Manchester). However, it is not known if the solubilised AlkB$(H)_6$ contains its full complement of iron or whether it is active; neither have crystallisation trials been performed.

4 Cytochrome P450 BM3 from *Bacillus megaterium*: $BM3_{F87G}$ mutant alters *stereo*- and *regio*-selectivity of olefin oxidation

4.1 Outline

Cytochrome P450 BM3 utilises NADPH and dioxygen to hydroxylate mid- to long-chain fatty acids at sub-terminal positions. Mutation studies have been shown to alter the enzymes substrate specificity towards short-chain fatty acids and alkanes as well as alkenes (olefins) and polycyclic aromatic hydrocarbons (PAH). The active site residue phenylalanine 87 (F87) has been demonstrated to be key in effecting the enzymes specificity in regio- and stereo-specific manner. As a starting point for the development of the enzyme as a useful biocatalyst for the epoxidation of alkenes and PAH the activity and selectivity of wild-type P450 BM3 is compared with the active site mutant $BM3_{F87G}$. Whilst the mutation increases the NADPH-driven activity towards these substrates, it also pushes the regio-selectivity further away from the ω-terminal position and displays a propensity for the epoxidation reaction as opposed to hydroxylation. Interestingly, the mutation also alters the stereo-selectivity of the enzyme, increasing the enantiomeric excess of *R*-styrene oxide by a factor of 3.

4.2 Cytochromes P450

Cytochromes P450 are one of the most abundant and diverse families of metalloenzymes found in nature [143]. Since their discovery in the late 1950s, cytochrome P450 (CYP) genes and their products have been found in almost every form of life and in all five kingdoms; from archea, through eubacteria to fungi, plants and animals [144-146]. The only exceptions appear to be parasitic and free-living platyhelminths and nematodes, where cytochrome P450 genes or gene products have yet to be identified [147].

Over 7000 CYP genes have been named and sequenced from across the animal and plant kingdoms as well as the majority of prokaryotic organisms [148]. They display a huge diversity in substrate specificity and selectivity and are involved in reactions varying from the breakdown of xenobiotic compounds to the biosynthesis of complex hormones in plants and mammals [149-151]. Whilst cytochromes P450 are well known as mono-oxygenases, these enzymes are able to catalyse a range of oxidative and non-oxidative reactions such as dehydrogenation, isomerisation and dehydrations in some organisms [152]. As this thesis deals with oxidative biotransformations, this introduction will only focus on the mono-oxidations typically performed by cytochromes P450.

The designation ‘P450’ originates from their distinctive spectral properties as observed upon their discovery in the late 1950s. It was observed that, when the liver extracts, of rat [153] and pig [154], were reduced with dithionite and allowed to react with carbon monoxide (CO), a pigment absorbing light at 450 nm was formed (Figure 4.1). This was considered a novelty in the context of contemporary knowledge of heme-containing enzymes, which absorb light at approximately 420 nm. It was later observed that only the reduced form of the enzyme could bind CO and similarly to other heme-containing enzymes, were also capable of binding nitric oxide (NO) [82, 155].

This unusual and distinct spectral feature arises from their unique heme ligation state. In many heme b containing enzymes, like haemoglobin and myoglobin, the iron (Fe) of the heme-prosthetic group (protoporphyrin IX) is ligated to a histidine residue. Spectroscopic [156] and resonance Raman studies [157] in the early 1980s suggested

a cysteine-thiolate ligation for P450's, which was later confirmed by x-ray crystallography when the first crystallographic structure of a cytochrome P450 was solved [158]. This cystinate ligation is universally conserved across the cytochrome P450 superfamily [144, 159].

For the historical reasons outlined above, these enzymes are commonly referred to as cytochromes P450 but due to their wide sequence diversity, as low as 20% in some cases, assortment of reactions and the multiplicity of substrates, they should more accurately be referred to as 'heme-thiolate proteins'; based on their only really universal feature, namely the presence of heme and its thiolate ligation, as recommended by the Nomenclature Committee of the International Union of Biochemistry [160]. However, considering cytochromes P450 are not the only proteins to be classified as heme-thiolate proteins, for consistency and simplicity they will, henceforth be referred to as P450s.

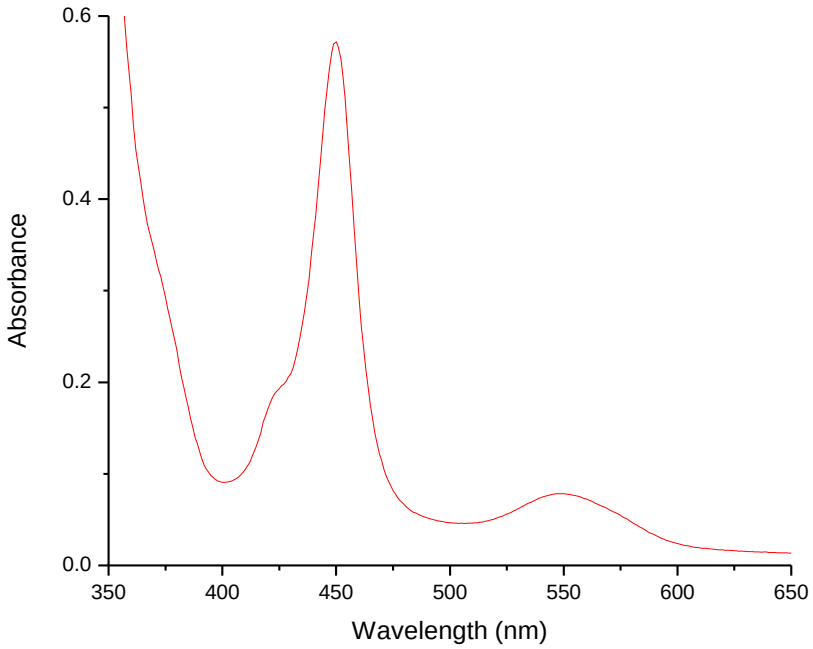

Figure 4.1 UV-visible absorption spectrum of a cytochrome P450/carbon monoxide complex demonstrating the characteristic Soret peak at 450 nm.

These data were collected from a sample of heme-domain P450BM3 as described in Methods. The wavelength of the reduced/CO bound Soret peak varies slightly around 450 nm depending on the protein source [161].

4.3 P450 mono-oxidation reactions

P450s catalyse the reductive scission of molecular oxygen, coupling it to the insertion of one oxygen atom into a hydrocarbon substrate, the other being reduced to water with the incorporation of two electrons and two protons [146]. Reactions typically performed are therefore C-H hydroxylation or C=C epoxidation but also *N*- *O*- and *S*-dealkylation (Figure 4.2). The general mono-oxidation reaction scheme is outlined below where RH denotes the substrate.

$$RH + O_2 + NAD(P)H + H^+ \rightarrow ROH + H_2O + NAD(P)^+$$

Cytochromes P450 as a family are known to act on a broad spectrum of substrates to fulfil a myriad of physiological functions (Figure 4.3). They oxygenate a variety of complex organic molecules in the synthesis of steroid hormones, bile acids, sterols and fat soluble vitamins in plants and animals [162]. They also play a crucial role in detoxification of xeno- and endobiotics by converting these often lipophilic compounds into more water soluble forms to facilitate excretion [143, 150, 151]. P450s also participate in the synthesis and metabolism of fatty acids and contribute to the breakdown of hydrocarbons to enable microbial populations to utilize these otherwise recalcitrant compounds as sole carbon and energy sources [146]. Their functional diversity and specificity of action places them in a unique position for exploitation as biocatalysts.

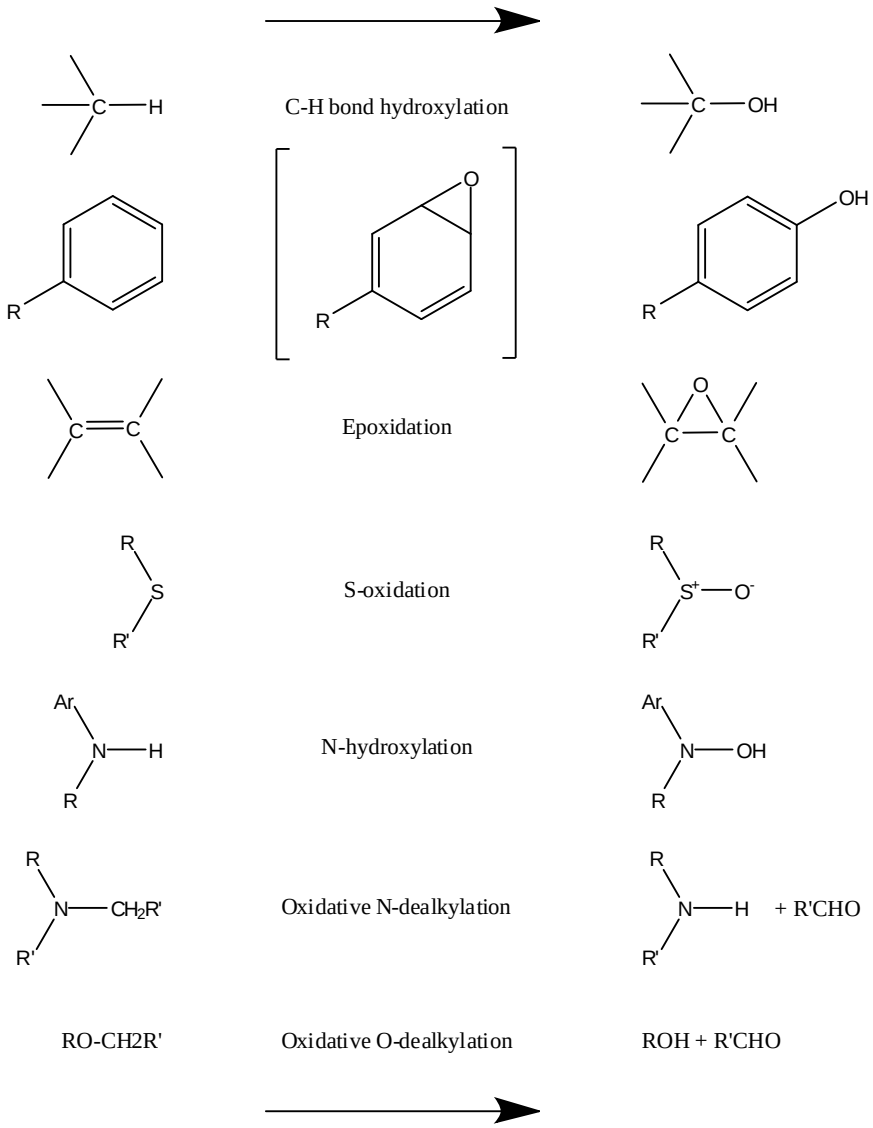

Figure 4.2 Cytochrome P450 catalysed mono-oxidation reactions [152, 163].

P450s catalyse the reductive scission of molecular oxygen and couple it to the insertion of one oxygen atom into the substrate. The reactions typically performed are C-H bond hydroxylation, C=C bond epoxidation and N-, O- and S-dealkylation.

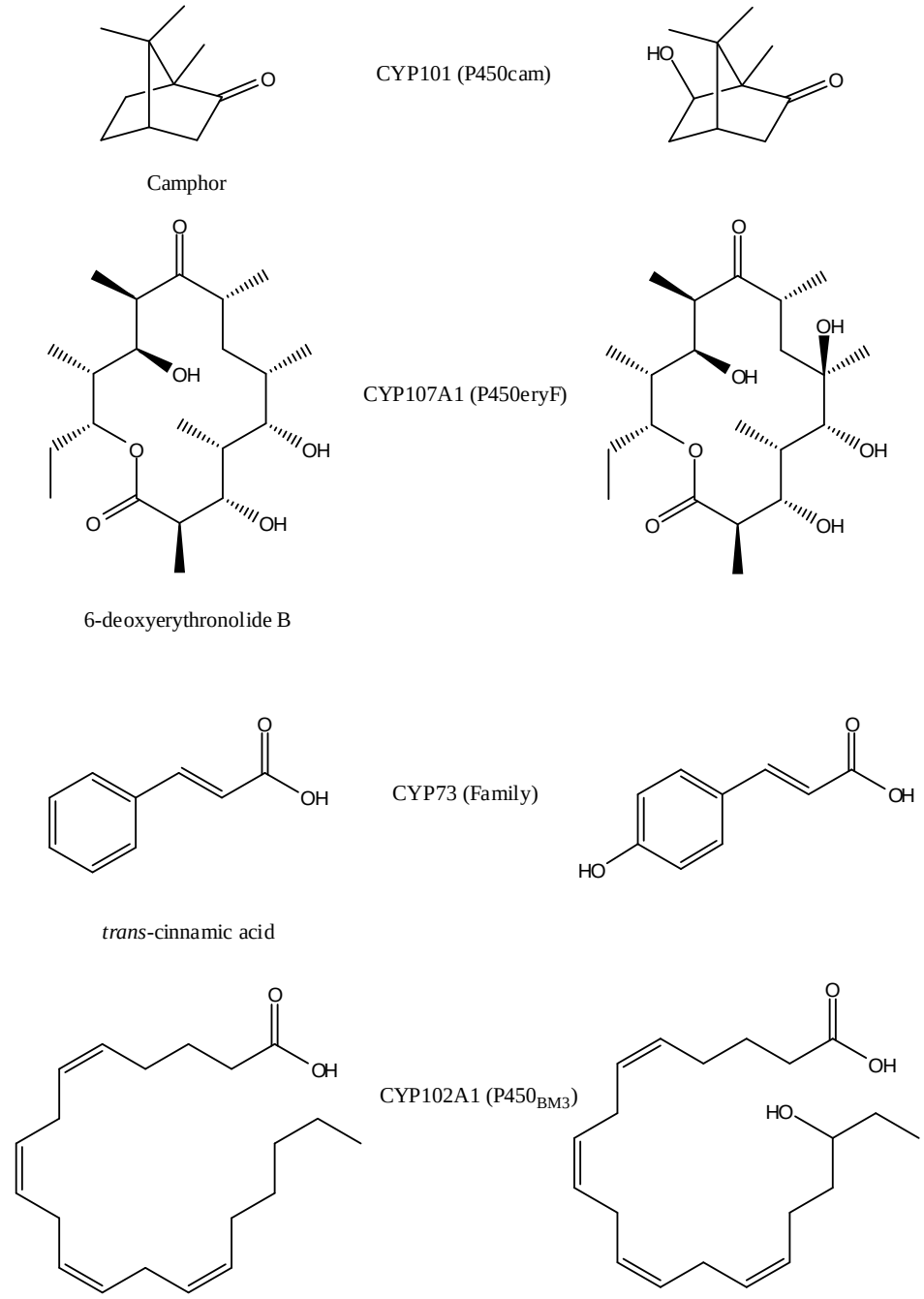

Figure 4.3 The structural variations in cytochromes P450 substrates.

Substrates acted upon by P450s as a superfamily include straight chain, branched chain, aromatic and poly-cyclic hydrocarbons. P450s are involved in the synthesis and catabolism of a huge variety of compounds: CYP101 from *P. putida* is involved in utilisation of camphor as a carbon source [164]; CYP107A1 from *S. erythrea* is involved in the biosynthesis of the erythromycin; the CYP73 in plants are crucial to many metabolic pathways [165, 166] and Cyp102A1 acts on mid- to long-chain fatty acids.

4.4 Cytochrome P450 Redox Partners

With a few notable exceptions virtually all P450s rely on a separate redox partner protein to sequentially deliver the two electrons needed for the reaction and they can be categorised into groups or classes depending on the type of redox partner system employed (Figure 4.4). For many years P450s were thought to belong to one of two groups; the Class I, characteristically bacterial or mitochondrial in origin and Class II, which are associated with microsomal membranes in eukaryotes. However, the last decade has seen an explosion in the number of P450 genes identified, accompanied by the discovery of some novel and very interesting redox partner arrangements, prompting a radical rethink of this classification system.

The class I P450 is exemplified by the soluble P450cam (CYP101A1) from *P. putida* [146]. P450cam catalyses the 5-exo hydroxylation of camphor as the first step in the organism's use of camphor as a carbon and energy source [164]. The P450cam redox system consists of three components: a NADH-dependent, FAD containing putidaredoxin reductase, an iron-sulphur putidaredoxin and the heme-containing P450. The path of electrons flows from NADH to the FAD of the reductase, the putidaredoxin then shuttles the electrons from the reductase to the heme.

The class II P450 is typified by the two component, microsomal system. Electron transfer to the heme is mediated by a membrane-bound, NADPH-specific cytochrome P450 reductase (CPR), containing a flavin mononucleotide (FMN) and a flavin adenine dinucleotide (FAD) cofactor. Electrons are transferred first to the FAD cofactor, then to the FMN cofactor. Docking of the P450, which is also anchored to the membrane, enables the transfer of electrons to the heme. Due to the associated difficulties with purification and crystallisation of membrane bound proteins, structural characterisation of class II P450s and their redox partners has been slower to develop, with the first crystal structure of human CYP2C9 emerging in 1999, more than a decade after the first bacterial P450 structure [158, 167].

This simple classification was accepted as standard until the discovery and characterisation of P450 BM3 (CYP102A1) [55, 62, 168, 169]. This P450, isolated from the soil bacterium *Bacillus megaterium*, was found to be entirely soluble and not reliant on a separate redox partner protein; P450 BM3 has its heme and reductase

domains fused, so that both are located on a single polypeptide chain [170]. Amino acid sequence comparison of this sub-terminal, fatty acid hydroxylase revealed the heme domain of P450 BM3 to be closest to the mammalian microsomal family CYP4 [171] while the reductase domain shares a commonality to eukaryotic CPR proteins [170]. In terms of its redox system, P450 BM3 is a Class II enzyme but this novel fusion is completely soluble and entirely catalytically self-sufficient and therefore was hailed as the first of a new class [62].

For almost ten years, P450 BM3 remained the solitary member of its class; other self-sufficient P450s were not discovered until 1996 when P450foxy (CYP505) was isolated from the fungus *Fusarium oxysporum* [172]. Another sub-terminal fatty acid hydroxylase, it shares 40% and 35% amino acid similarity to the heme and reductase domains respectively of P450 BM3 [173]. Other P450 BM3 homologues have since been isolated from *Bacillus subtilis* (CYP102A2 and CYP102A3) [174] and putative P450 BM3 homologues have been identified in the genomes of *B. cereus*, *B. anthracis* and *Streptomyces avertimetilis* [175-177].

A fourth class has more recently been identified where electron transfer is mediated by a covalently linked phthalate family oxygenase reductase (PFOR)-like domain [178]. Other examples of this novel redox partner fusion have been isolated and characterised from the gram-negative *Rhodococcus erythropolis* and *Ralstonia metallidurans* [175, 179]. The reductase domains of this novel class of P450s contain a FMN and iron-sulphur cluster and show sequence homology to the reductases of the phthalate oxygenases [178, 180].

Even more diverse types of systems employing, for example, interaction with flavodoxins (P450BioI from *B. subtilis*) or direct heme reduction by NADH (P450nor from *Fusarium oxysporum*) have also been recognised [181, 182]. There is even a P450 from *B. subtilis* (CYP152A1) which appears to interact directly with hydrogen peroxide, employing the peroxide shunt pathway (Section 4.6) in order to oxygenate fatty acid substrates, without the need for additional cofactors or redox partner proteins [183, 184].

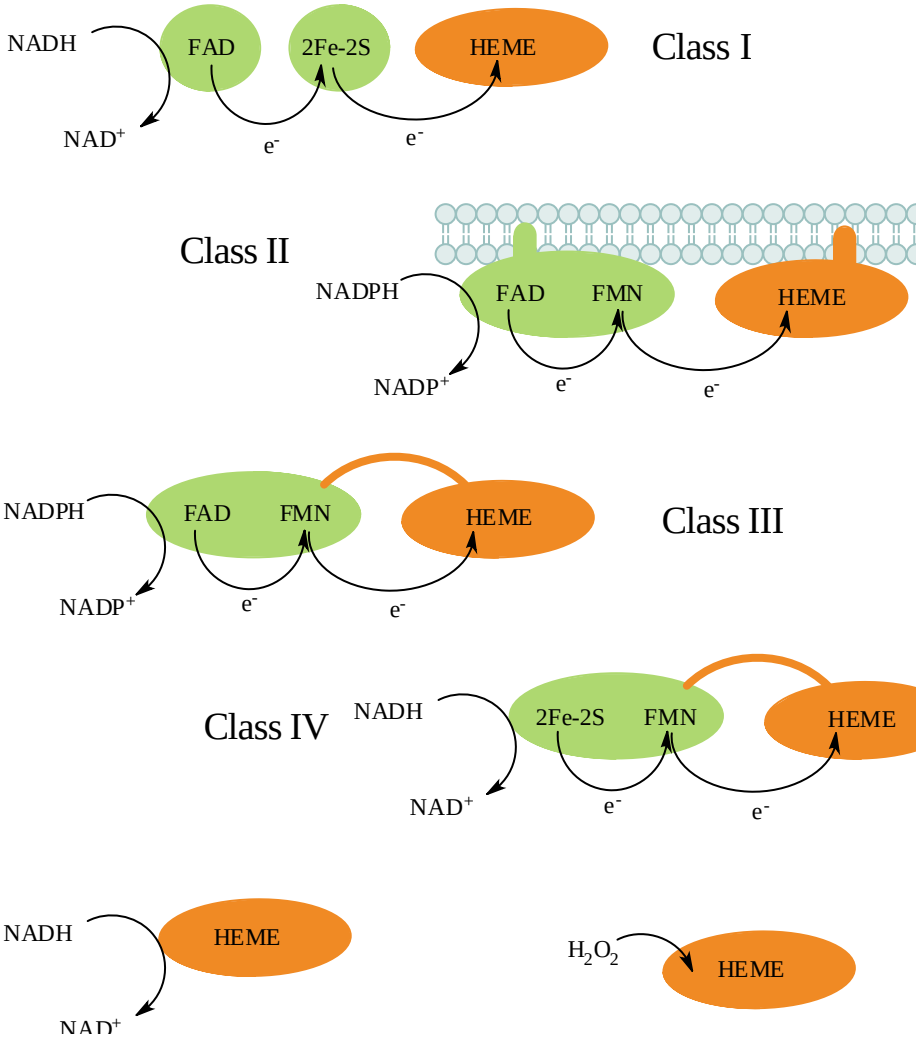

Figure 4.4 Classification of P450s based on redox partners.

Arrows show the path of electrons from NAD(P)H to the heme. Heme containing components are coloured orange, reductase components are coloured green. Classifications are detailed in the text.

4.5 Classification and nomenclature

Due to the tremendous volume and diversity of P450s in nature, a standard nomenclature system based on their structural homology (amino acid identity) and phylogeny has been in use since 1989 [149, 185]. This classification system systematically assigns a P450 to a family and sub-family depending on the level of homology it shares with others in that family. In general, sequences sharing ≥ 40% homology fall into the same family and sequences sharing ≥ 55% homology are grouped in the same sub-family [159]. The root of all P450 names are CYP, (derived from Cytochrome P450), a number denoting the family to which it belongs followed by a letter denoting the subfamily and finally a second number denoting the individual gene and/or protein e.g. CYP2D6 (Figure 4.5). An additional level of classification has since been added, which groups families by potential common ancestors, referred to as clans. However these are not used in the naming of individual genes [144].

CYP families tend to be divided according to taxonomy with families grouped thus: CYP 1-49, 51, 301-353 found in Metazoa; CYP 51, 71-99, 701-766 found in the plant kingdom; CYP 51-69, 97, 501-699, 5001-5121 found in the lower eukaryotes and CYP 51, 101-281 found in bacteria. The only P450 to be found across all kingdoms is the sterol demethylase CYP51 [144, 149]. There are currently more than 7000 named CYP sequences available across a total of 781 families excluding variants and psuedogenes [148] and the number is still growing.

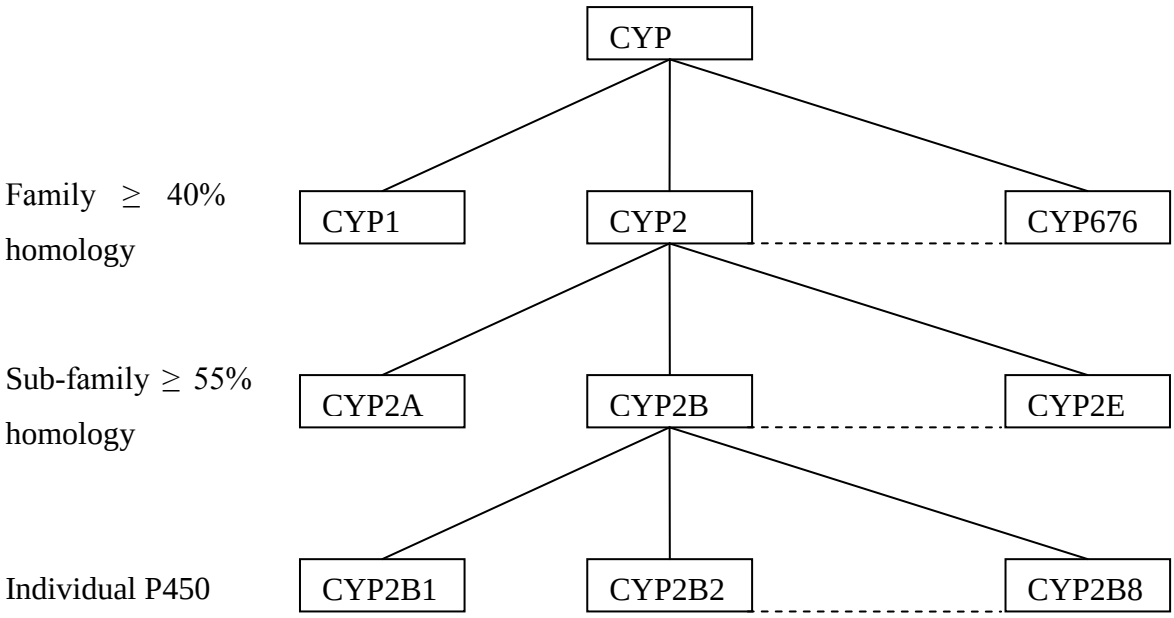

Figure 4.5 Homology based classification of cytochromes P450.

Individual P450s are classified into families and subfamilies based on their sequence homology and allocated an alpha-numerical designation using the following protocol; CYP (root), 1 (family), A (sub-family), 1 (individual gene or protein) **[186]**.

4.6 Cytochrome P450 catalytic cycle

The catalytic mechanism of cytochromes P450 is complex in nature involving a variety of conformational and redox state changes. Although some of the intermediates are still only postulated the catalytic cycle is generally accepted to proceed as follows [54, 187, 188]. In its native resting state, with no substrate bound, the heme iron spin-state equilibrium is held towards the (Fe^{3+}) low-spin (S=1/2) form, with a weakly bound water molecule forming the 6^{th} distal axial ligand (Figure 4.6, 1) [189-191]. Docking of a substrate leads to formation of an enzyme/substrate complex, which results in conformational changes in the protein (Section 4.7) and alteration of the heme iron spin-state, pushing the equilibrium towards the high-spin (S=5/2) form (Figure 4.6, 2). Substrate binding also alters the mid-point redox potential of the heme, causing a positive shift of between 130 and 140 mV [192, 193]. In a system like that of P450 BM3, where the redox chain consists of NADPH, FAD and FMN with redox potentials of -324 mV, -292 mV and -270 mV respectively, the very negative redox potential of the substrate free enzyme (-370 mV in P450BM3) halts the passage of electrons to the heme [194]. On binding of substrate the redox potential becomes more positive; -235mV in the case of arachidonic acid [195] and therefore lifts the redox barrier, allowing the first reducing equivalent to enter the system (Figure 4.6, 3). This switching of redox potential acts as a gating mechanism, exerting powerful control over the catalytic cycle and preventing entry of electrons into the system in the absence of any substrate.

In its reduced, ferrous form (Fe^{2+}), the heme iron remains high-spin. This electron rich state is highly attractive to the electron deficient dioxygen molecule, thus promoting the formation of an enzyme/oxygen/substrate ternary complex which quickly rearranges to form the ferric dioxygen species (Figure 4.6, 4).

The initial substrate and oxygen binding steps are relatively long-lived, such that each have been observed by various spectroscopic methods [196]. The subsequent steps are rather more short lived and have proved difficult to observe [187, 197] but the following are generally considered to be the prevailing species responsible for the scission of molecular oxygen and the incorporation of oxygen into the substrate. A second reducing equivalent is delivered to the heme, promoting formation of a ferric

peroxoanion (Figure 4.6, 5a) which is rapidly protonated, thereby converting to ferric hydroperoxo (Figure 4.6, 5b) [198]. A second protonation leads to creation of 'compound I' and formation of one molecule of water (Figure 4.6, 6). Compound I is the high valent iron-oxo species widely considered to be responsible for the catalysis of the majority of P450-dependant oxidation reactions; attacking the substrate and effecting the incorporation of molecular oxygen (Figure 4.6, 7) [199, 200]. Dissociation of the product enables water to rebind, thus returning the enzyme to its resting, low-spin ferric state.

Uncoupling of the electron transfer process, where electrons are lost as radical oxygen species rather than being used to create product, can and does occur under physiological conditions. These result in branch points in the catalytic cycle (Figure 4.6). If an electron is not delivered to the ferrous dioxygen complex (Figure 4.6, 4) quickly enough, the complex can dissociate, releasing a superoxide radical anion and reverting back to the substrate-enzyme complex (Figure 4.6, 2). This is termed as the 'auto-oxidation shunt'. A second branch point exists, the peroxide shunt, where either the ferric peroxo or hydroperoxo complexes dissociate from the iron, leading to the formation of peroxide and return of the enzyme to the substrate-enzyme complex (Figure 4.6, 2). Interestingly, the peroxide shunt can also function in the opposite direction in some instances, enabling the enzyme to use peroxide as reducing equivalent in a similar fashion as peroxidases, bypassing the need for NAD(P)H and any associated redox partner proteins [64, 183, 201-203]. A third pathway exists after the second protonation step where instead of incorporation into the substrate, oxygen dissociates to form water, known as the oxidase shunt [164, 204].

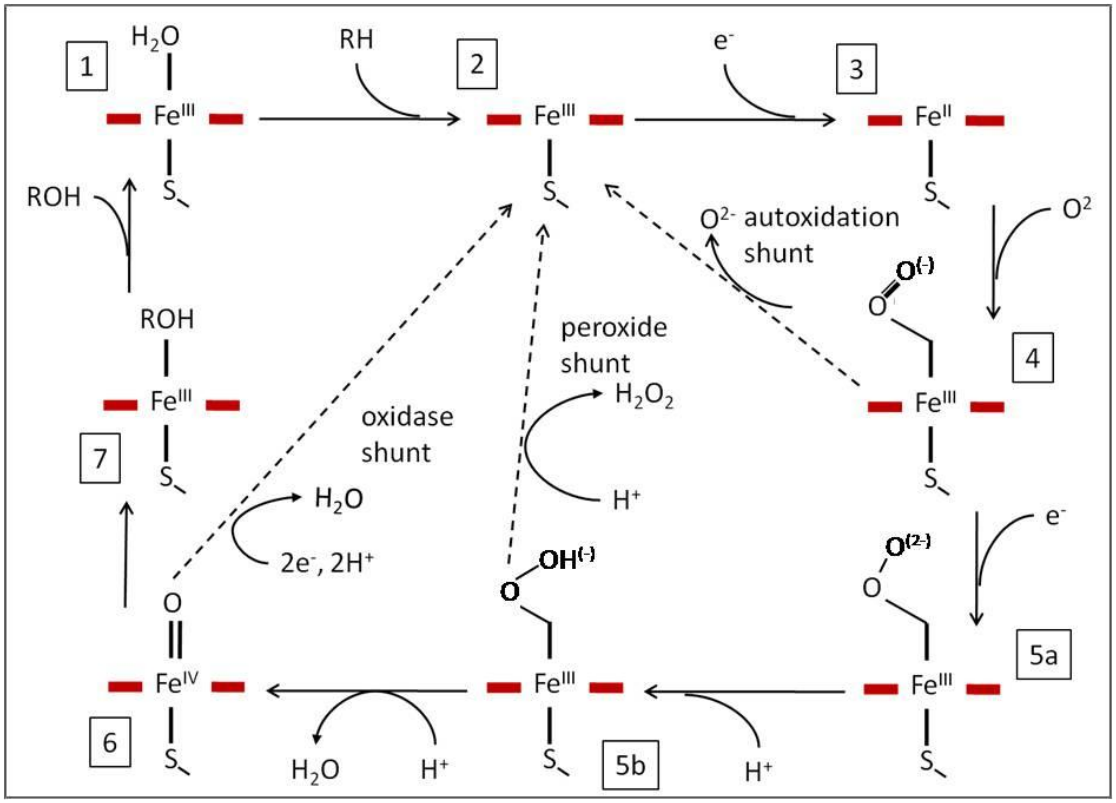

Figure 4.6 Cytochrome P450 catalytic cycle.

The reaction intermediates are: resting with the iron (Fe) in low-spin with water bound (1); substrate-bound forcing the spin-state equilibrium towards high-spin and lowering the redox potential (2); the first electron is introduced via a redox partner converting the iron to ferrous (Fe^{2+}) form (3) and; the subsequent binding of molecular oxygen (4). Introduction of the second electron leads to formation of the peroxoanion (5a) followed by sequential protonation forming first the hydroperoxo species (5b) and then compound I (6). Finally oxygen is incorporated into the substrate (RH) and the product (ROH) dissociates (7). The uncoupling reactions (discussed in the text) are shown as dotted lines.

4.7 Structure

Despite their wide sequence diversity and the size and shape of substrates P450's act upon, they share a number of common structural features including several well-conserved sequence motifs and their general topology and three-dimensional structure. At the heart of all P450s is the *b*-type heme. Heme *b* contains an iron atom, co-ordinated equatorially by the four nitrogens of a protoporphyrin ring. The 5th axial ligand is provided by the thiolate of an invariant cysteine residue [157] whilst water occupies the 6th axial position in the substrate-free enzyme [189, 205] (Figure 4.7). It is the negatively charged thiolate ligand provided by the cysteine that confers the very low redox potential observed in substrate free P450s [187]. This effect can be replicated in histidine-ligated heme-b proteins like myoglobin by engineering the amino acid to a cysteine [206].

In comparison to the number of P450 sequences identified, only 21 individual atomic structures have been solved to date. Despite their often low sequence homology, all structures solved so far display a common topology and three-dimensional structure. A P450s secondary structure commonly consists of 5 β-sheets and 14 α-helices (A-L) arranged thus: an α-helix rich domain which contains the heme binding motif and a β-sheet rich domain often associated with substrate recognition and docking [165, 207] (Figure 4.8). The three-dimensional fold resembles that of a triangular prism with the heme buried in the hydrophobic core (Figure 4.9). Examination and comparison of P450 structures coupled with structure-guided mutation strategies has facilitated the identification of the residues involved in substrate recognition and specificity, those involved in redox partner binding and proton relay pathways. For example, mutation of the well conserved threonine in the I helix to alanine causes uncoupling of the catalytic cycle of P450cam (CYP101) and examination of the crystal structure implicates this residue as the endpoint in a proton delivery pathway leading to the heme (CYP101, Lys178/Arg186, Asp251) [208].

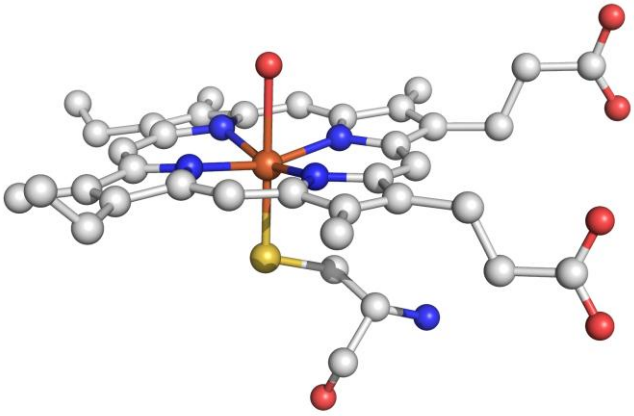

Figure 4.7 The heme b prosthetic group of cytochrome P450.

The iron (orange) is co-ordinated equatorially by four nitrogen atoms of the protoporphyrin IV. The 5th and 6th axial ligands are a cysteine residue on the proximal face and a water on the distal face (in the substrate free enzyme). Image rendered in PyMOL [209] using atomic structure of substrate free CYP101 from *P. putida*, 2CPP [158]. Atoms are coloured according to CPK colour convention.

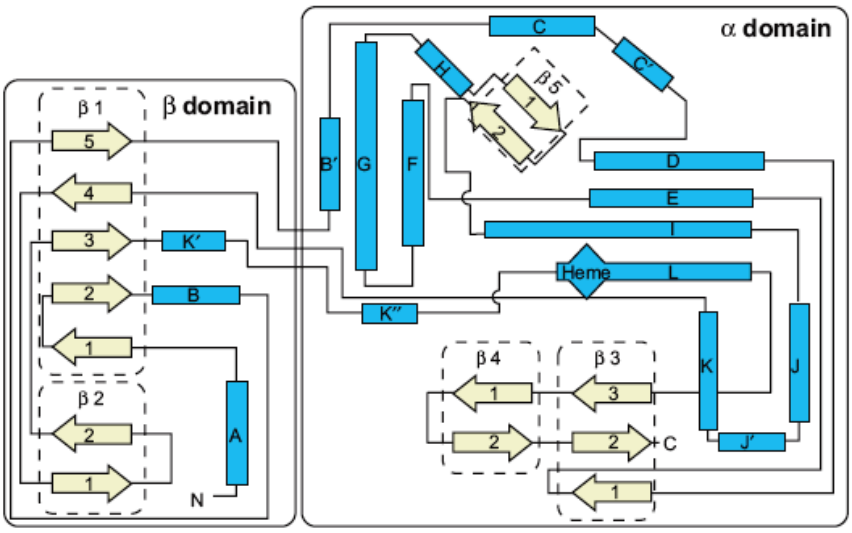

Figure 4.8 A topographic map of the secondary structure of CYP102A1 (P450BM3)

The α-helices are shown as blue rectangles, β-sheets as yellow arrows [207, 210]. The random coils and loops are represented by lines between the structural elements mentioned above. The size of secondary structural elements are not in proportion to their length in the primary sequence. Image adapted from [210].

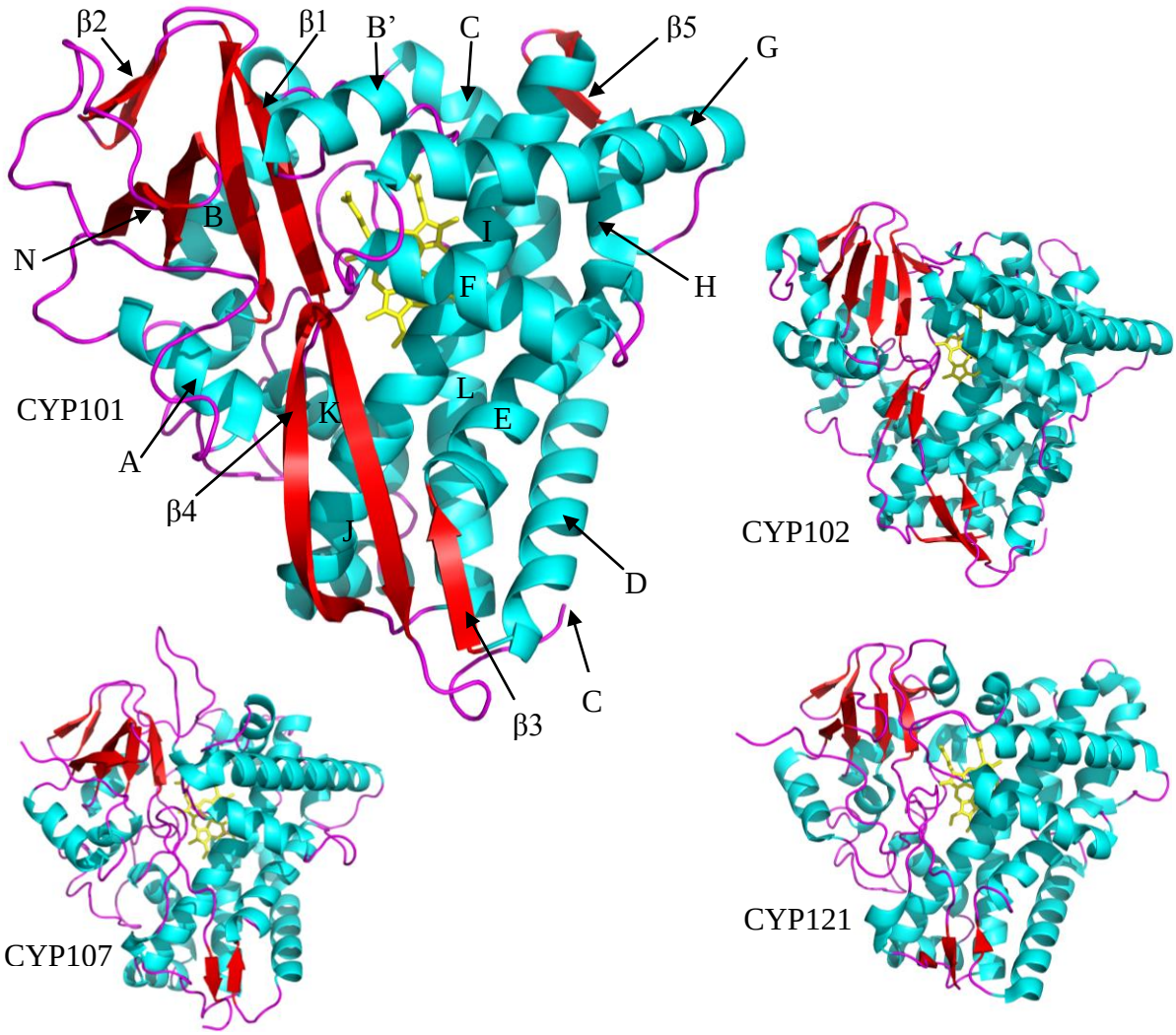

Figure 4.9 The tertiary structure of cytochromes P450.

The 3D-fold of four of the cytochrome P450 atomic structures solved to date: CYP101 from *P. putida*, 2CPP [158]; CYP102A1 from *B. megaterium*, 1BU7 [211]; CYP107A1 from *S. erythraea* 1OXA [165]; CYP121 from *M. tuberculosis*, 1N40 [212]. α-helices are shown as cyan ribbons, β-sheets as red arrows, loops in purple and the heme is represented as yellow sticks in each case. Helices and sheets are numbered as in Figure 4.9. Images were rendered in PyMOL [209].

Amino acid sequence can vary dramatically between members of different families with the most divergent sequences showing less than 20 % identity in pair wise alignments over the length of the protein [159]. The areas that show the most sequence conservation are those which interact with the heme: on the proximal side of the heme, immediately preceding the L helix, the heme binding loop contains the invariant cysteine residue flanked by additional conserved residues FXXGXR/HX**C**XG (Figure 4.10); also on the proximal side of the heme a second consensus motif exists on the K helix, a glutamic acid and arginine separated by two non-specific residues, EXXR; a third sequence motif is located on the I helix which lies over the distal side of the heme, [A,G]GX[D,E]T[T,S] containing an important threonine residue thought to be important in oxygen binding [207, 213].

Areas of sequence showing the most divergence are thought to be associated with substrate and redox partner binding. Comparison of the mammalian CYP2 family with that of P450cam lead to the identification of hyper-variable regions which are commonly referred to as substrate recognitions sites (SRS) [214]. These are numbered SRS-1 to SRS-6 and their locations are labelled in Figure 4.11.

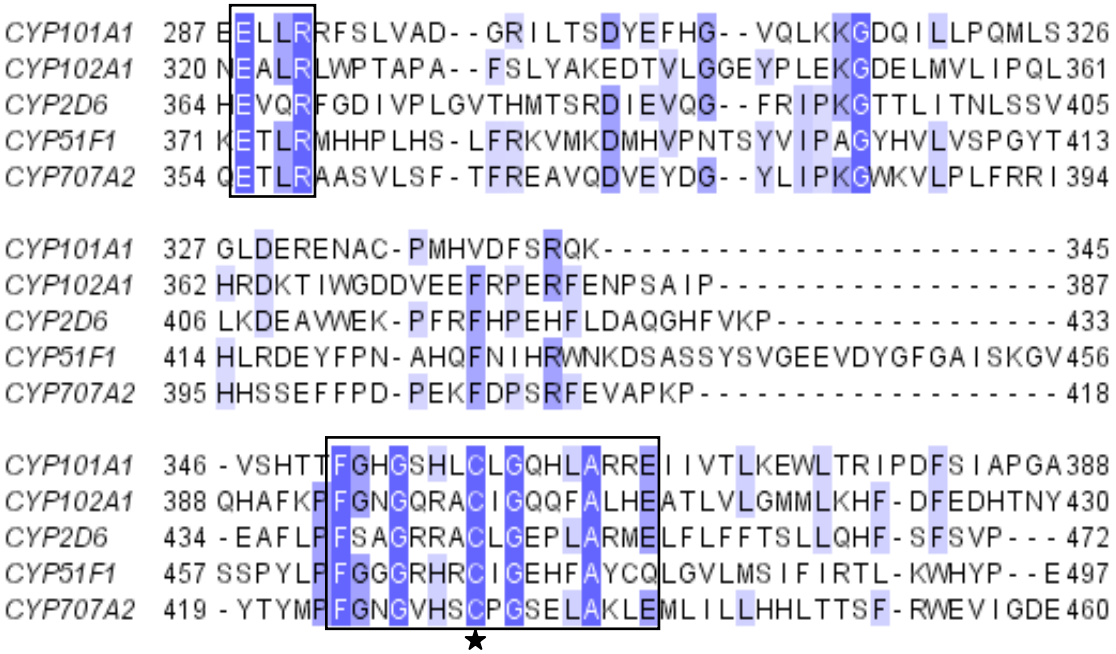

Figure 4.10 The conserved heme binding domain of cytochromes P450.

The degree of conservation is shaded from white to blue with absolutely conserved residues as white text on blue background. Consensus sequences are boxed, the heme ligating cysteine is starred (★). Sequences obtained from Protein Knowledgebase (UniProtKB): CYP101A1 from *Pseudomonas putida* (P00183); CYP102A1 from *Bacillus megaterium* (P14779); CYP2D6 from *Homo sapiens* (Q2XND0); CYP51 from *Saccharomyces cerevisiae* (P10614); CYP707A2 from *Arabidopsis thaliana* (O81077).

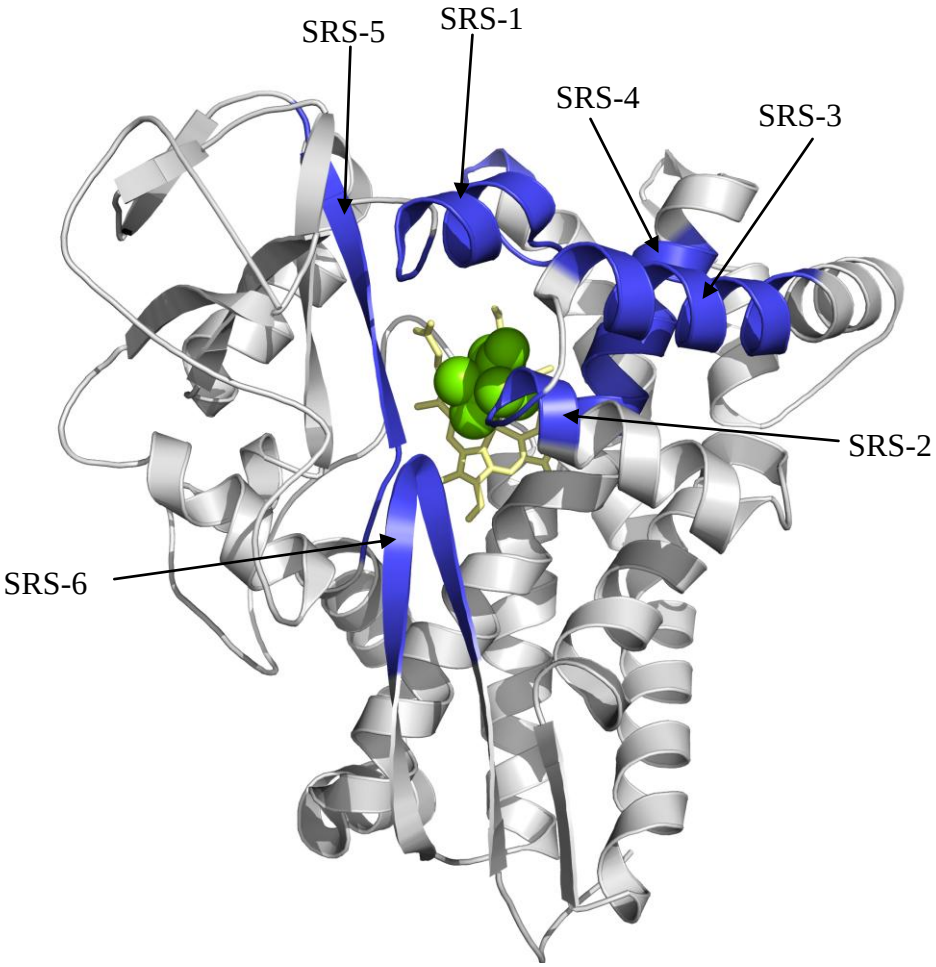

Figure 4.11 3D structure of CYP101A1 showing location of substrate recognition sites.

α-helices, β-sheets and loops are shown as grey cartoons, the heme is represented as yellow sticks, bound camphor is shown as green space-fill. Substrate recognition sites are coloured blue and labelled SRS-1 to 6. Images were rendered in PyMOL [209].

The amazing biodiversity of P450 systems and the stereo-and regio-specificity they display has lead to much interest in their use as industrial biocatalysts. Fundamental targets for bioengineering are the soluble bacterial systems like P450cam. Arguably the most studied of all P450s [164, 215], the substrate specificity of P450cam has been engineered away from camphor towards higher value substrates like styrene and ethylbenzine with some success [216, 217]. The substrate selectivity of various other P450s have been pushed towards non-natural substrates by a range of techniques including structure-guided rational mutagenesis [58, 217-219] and directed evolution methods [25, 26, 201, 220].

One of the problems encountered with the majority of P450 mono-oxidation systems are their reliance upon separate redox partner proteins. Requirement for these adds a level of complexity to their expression in heterologous hosts and almost inhibits their use for *in vitro* biotransformations due to the need to purify not just one but 2 or even 3 proteins. One P450 that precludes these difficulties is P450 BM3. P450 BM3 is capable of extremely high rates of activity and the whole redox system can be expressed in heterologous hosts and purified relatively easily. These qualities, combined with the wealth of literature regarding its structure and mechanism of action make P450 BM3 an excellent target for exploitation as a biocatalyst.

4.8 Cytochrome P450BM3

4.8.1 P450 BM3 enzymology

There has been much interest in the use of cytochrome P450 BM3 in the biotechnology and bioremediation industries. This is due to its extremely high levels of activity coupled with the fact that it is covalently attached to its very own electron donor protein. It was first isolated from *B. megaterium* in the late 1980s upon exposure of the organism to phenobarbital and other barbiturates, although this compound is not a substrate for this enzyme [55].

The stereo- and regio-specificity of P450 BM3 on a range of hydrocarbon substrates has been well characterised. The native enzyme is known to catalyse sub-terminal hydroxylation of mid- to long-chain saturated fatty acids at ω-1, ω-2 and ω-3 positions [169, 221, 222]. The rate of BM3 turnover is 100-1000 times that of most other P450s [168] with rates of up to 4600 min^{-1} with the best saturated fatty acid substrates and rates of > 15 000 min^{-1} with the unsaturated arachidonic acid [146]. It shows highest catalytic activity, based on both NADPH and oxygen consumption in the presence of C14-18 fatty acids [168, 223]; and at limited substrate concentrations, BM3 is capable of performing multiple, sequential hydroxylations on the same molecule, incorporating up to 3 oxygen atoms in the hydroxylated product [223, 224]. BM3 is also capable of epoxidation reactions, attacking at the internal double bounds of unsaturated substrates [222, 225] such as arachidonic acid.

BM3 is also highly active in the presence of fatty acid aldehydes (ω-oxo fatty acids), converting them to the corresponding dicarboxylic acid with chain length specificity analogous to that of the best fatty acid substrates. Using oxygen consumption as a measure of activity, BM3 shows a rate of 1200 min^{-1} in the presence of 16-oxohexadecanoic acid, approaching that in the presence of palmitic acid [226]. When compared to other P450s the extremely high reaction rates, make P450 BM3 an excellent candidate for exploitation as a biocatalyst.

Unusually, when BM3 is pre-incubated with its reducing co-factor, substrate dependent activity when measured via either oxygen or NADPH consumption is inhibited. This peculiarity has been observed by several laboratories upon initial

characterisation of the enzyme [168]. Although the enzyme is unable to hydroxylate substrate in these conditions, the addition of artificial electron acceptors, such as cytochrome *c* or ferricyanide, allow fatty acid hydroxylation to continue, showing this inhibition is fully reversible [227]

4.8.2 P450 BM3 structure

P450BM3 is twice the size of the average P450 having its C-terminal reductase domain (64 kD) fused to the N-terminal heme domain (54 kD) by a linker region rich in charged amino acid residues [62, 228]. The high catalytic rates observed for BM3 are thought to be directly related to this redox partner fusion as when the two domains are expressed separately and reconstituted *in vitro* the activity is significantly lower in the intact enzyme [168, 228, 229].

Although crystallisation of the full length enzyme has proven elusive, the atomic structure of the isolated heme domain has been solved many times over; in the substrate free (SF) and substrate bound (SB) forms as well as a number mutant forms [211, 230-234]. In contrast to the substrate free form of P450cam, the substrate access channel in SF P450BM3 is clearly visible in the crystal structure [211]. The substrate access channel (SAC) is a long funnel shaped opening, leading from the protein surface to the distal face of the heme, lined almost exclusively by hydrophobic residues. Arginine 47 sits at the entrance to the SAC, facing outwards (Figure 4.12). Being the only charged residue in the active site it was predicted to be a key residue in substrate selectivity by controlling access to the SAC. Mutation studies later proved it to be critical in substrate recognition and binding, alongside Y51, both of which interact with the carboxylate of the fatty acid substrate [60]. At the opposite end of the SAC, close to the heme prosthetic group lies a phenylalanine (F87) which has been proven to be crucial in controlling the regio-and stereo-selectivity of the enzyme [60, 64, 67, 219, 235-240].

In 1993 the first high-resolution crystal structure of the heme domain of BM3 emerged [211]. Crystallised in the substrate free form, the structure revealed the identity of potential targets for mutation studies within the active site. Located close to the heme at the end of the substrate access channel (SAC), the aromatic residue F87 was predicted to play a crucial role in catalysis [211]. When the palmitoleic acid

bound structure was solved a few years later, it provided even greater insight into the mechanism of substrate binding in the enzyme. In the substrate free structure, F87 lies almost perpendicular to the heme (Figure 4.12a). Upon substrate binding the active site closes around the substrate bringing residues R47 and Y51, amongst other key residues, closer contact with the carboxylate of the fatty acid. A most interesting conformational change is that of the F87. F87 changes its orientation to lie parallel to the plane of the heme, forcing the alkyl tail of the fatty acid substrate to curl away from the heme (Figure 4.12b) and thus preventing the ω-terminal methyl group from approaching the catalytic centre [230]. The terminal methyl is pushed into a lipophilic pocket created by F87 itself plus L75, V78, I263 and A264 protecting it from hydroxylation.

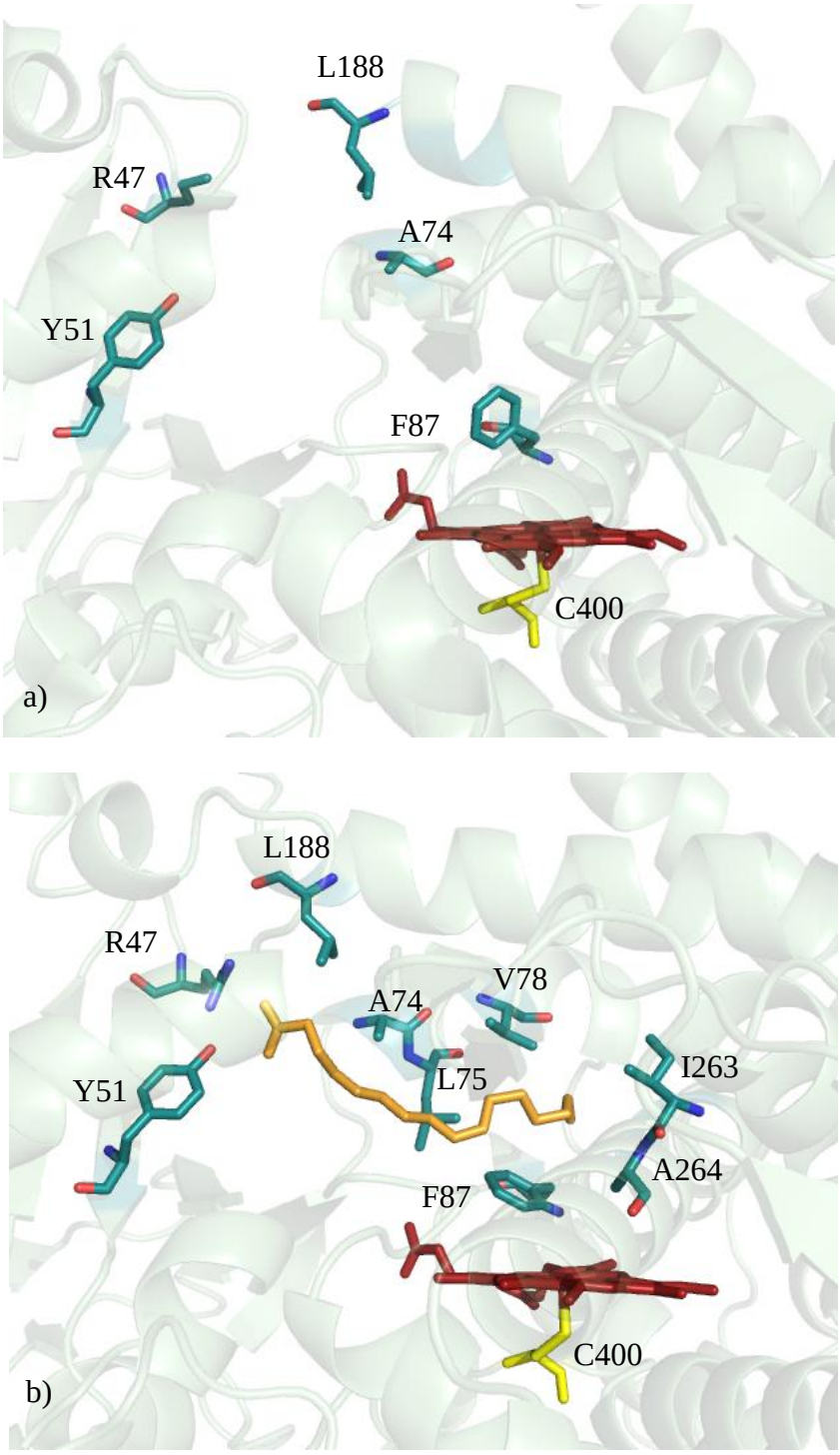

Figure 4.12 Atomic structure of the active site of P450 BM3.

Showing the substrate free (a) and palmitoleic acid bound (b) structures of P450 BM3 (2IJ2 and 1FAG respectively). Key active site residues are shown as atom coloured sticks, palmitoleic acid is shown in orange, the heme (red) and ligated cysteine (yellow) are also shown. Images were rendered in PyMOL [209].

4.8.3 Engineering P450 BM3 for biocatalysis

The main focus of the exploitation of P450 BM3 as a biocatalyst has been on altering the specificity away from mid- to long-chain fatty acids to encompass a wider range of hydrocarbon molecules (Figure 4.13); much of this work has highlighted the importance of residue F87, either through effects observed from site-directed mutagenesis or by the residue emerging as a key mutation in directed evolution studies. For example, directed evolution via successive rounds of mutation created a triple mutant containing the F87V substitution alongside L188Q and A74G [220] which demonstrated significant alterations in substrate selectivity enabling the enzyme to hydroxylate indole. Analysis of each residue in single point mutants reveals F87 is important in selectivity of the substrate with the other two residues (L188Q and A74G) being important for substrate binding and stabilisation. The triple mutant (F87V/L118Q/A74G) was later found to catalyse hydroxylation of a wide variety of structures including alkanes, alicyclic, aromatic and heterocyclic compounds [25, 238, 241] and the regio-specificity of hydroxylation on lauric and arachidonic acid was pushed further away from the ω-terminal of the substrate [237]. Based on this novel substrate selectivity, the triple mutant has been used in a detection system designed to monitor levels of phosphorothionate pesticides in food [242].

In site-directed mutagenic studies, substitution of phenylalanine at position 87 with the more polar tyrosine maintains the overall funnel shape of the SAC but produces a mutant incapable of metabolizing arachidonic acid or eicosapentaenoic acid [235]. Despite the fact that the F87Y mutant appears spectrophotometrically identical in the substrate-free form, there are no spectral perturbations that would suggest binding on addition of a long-chain (C18) fatty acid substrate; neither can any product or H_2O_2 be detected even though NADPH-dependent oxygen consumption is observed under catalytic conditions. It is postulated that the enzyme is therefore converting the oxygen to water instead of insertion into a substrate. Substantially reduced rates of NADPH oxidation has also been observed for this mutant with shorter fatty acids (C10) [60], with only small amounts of H_2O_2 being detected (8% of total NADPH oxidation). However, it is not know if any product is formed in this reaction.

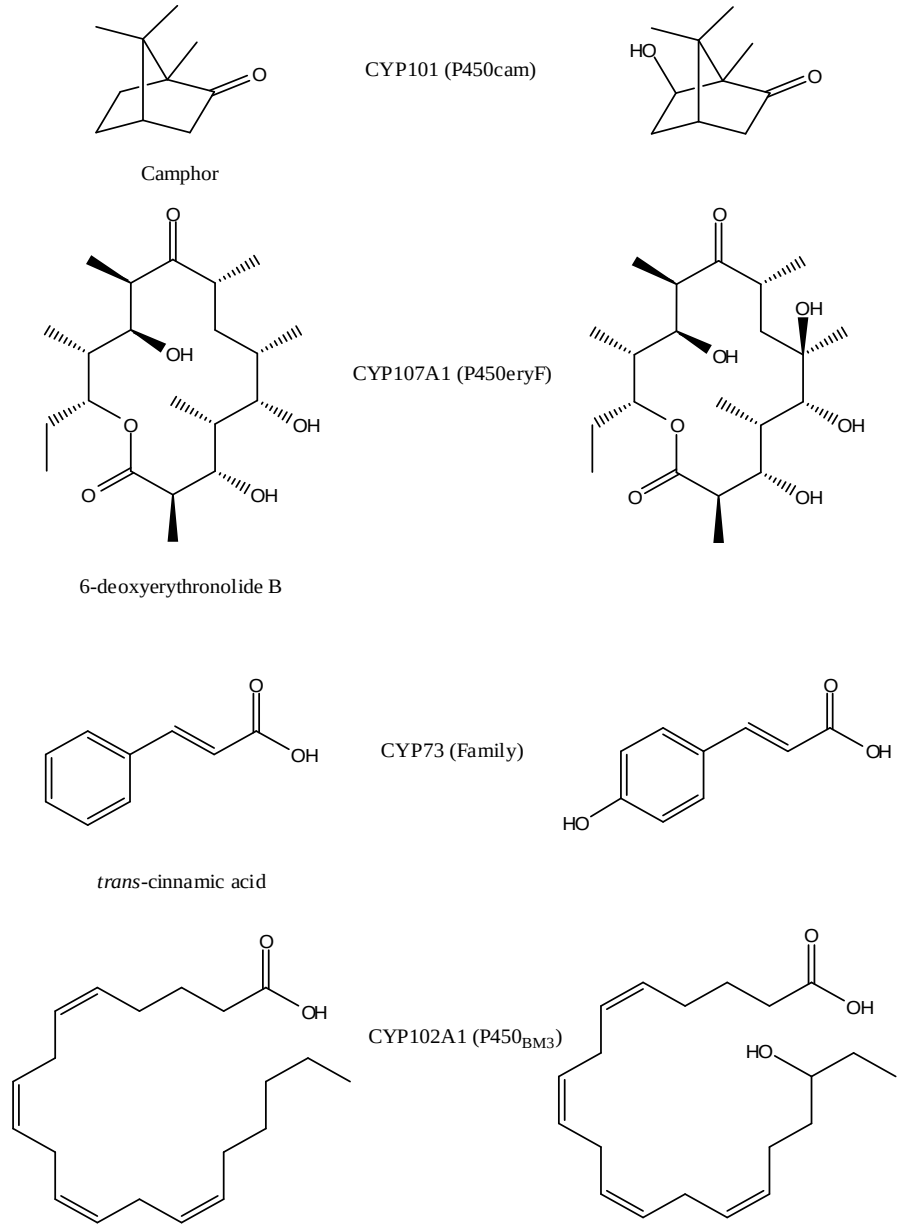

Figure 4.13 Compounds known to be substrates for P450 BM3 or BM3 mutants.

Only examples of each class of compounds are shown. The native form of BM3 is known to catalyse the hydroxylation of mid- to long-chain (C12-C20) saturated fatty acids (1), unsaturated fatty acids (2) and fatty acid aldehydes (3); the triple mutant containing the substitutions F87V, L188Q and A74G is able to catalyse the hydroxylation of shorter chain alkanes (4), alicyclic (5), aromatic (6), heterocyclic (7) and polycyclic, aromatic (8) hydrocarbons [25, 238, 239, 241].

Substitution of F87 with successively smaller residues reveals further information about the regio-selectivity of the enzyme. Replacement with valine, thus increasing the volume of the base of the SAC, whilst maintaining the relatively non-polar environment, alters the regio-specificity of attack on arachidonic acid [224]. Analysis of the products of mono-oxygenation of arachidonic acid by the wild-type reveal two distinct products, 18*(R)*-hydroxyeicosatetranoic acid (80%) and 14(*S*), 15(*R*)-epoxyeicosatrienoic acid ((14*S*,15*R*)-EET) in enantiomeric excesses of 96% or more. The valine mutant yields exclusively (14*S*, 15R)-EET in almost 100% enantiomeric excess under the same conditions. Although the reaction rate is reduced by almost 3 fold, to 1200 min^{-1} [235], this is still very high for a P450 and the mutant also maintains near wild-type coupling efficiency.

Decreasing the size of the F87 substituted amino acid further to alanine decreases NADPH-driven reaction rates and coupling efficiency on fatty acids and, as is the case for the F87V substitution, broadens the regio-specificity of the hydroxylation reaction pushing it further away from the terminal methyl group [64]. This is in direct contrast to earlier findings in which NMR data suggested that removal of the phenylalanine ring at position 87 resulted in almost exclusive ω-terminal hydroxylation [59]. This mutant is also capable of hydroxylation reactions driven by peroxide rather than NADPH with little difference in the rate or regio-selectivity of product distribution [243].

Decreasing the residue size again, to glycine, further reduces the activity of P450BM3 in the presence of lauric acid, but seems not to affect the product distribution [60, 244]. Interestingly, the F87G mutant demonstrates increased binding affinity for the inhibitors 12-(imidozlyl) dodecanoic acid (ImC12) and 1-phenylimidazole (1-PIM), which is postulated to be due to better access to the heme for the imidazole group of ImC12 and the creation of a hydrophobic space for the phenyl group of 1-PIM [60, 244].

As a starting point for developing P450 BM3 as an industrially useful epoxidation biocatalyst, we chose to assess the effect of the F87G mutation on the NADPH-driven catalytic activity and the regio- and stereo-selectivity of the enzyme towards short-chain alkenes and styrene. This was achieved by analysis of binding characteristics,

kinetic parameters and product characterisation in comparison to the wild-type enzyme.

4.9 Results

4.9.1 Plasmid verification

Plasmid pBM20 and pBM23 (Prof. Andrew Munro, Dept. of Biochemistry, University of Leicester) encoding P450 BM3 heme-domain and P450 BM3 full-length respectively were subject to analysis by restriction digest to verify the size and restriction pattern was as expected for the plasmid based on the DNA sequence. Figure 4.14 shows the fragmentation pattern from each plasmid after digestion with *Hind*III and separated by agarose gel electrophoresis. As expected, digested pBM20 yielded three fragments of 3215 bp, 1134 bp and 235 bp and digested pBM23 yielded three fragments of sizes 4469 bp, 1757 bp and 16524.5 bp, also as expected.

Similar restriction digest analysis was performed on the plasmid pBMHF87G (Dr Hazel Girvan, Dept. of Biochemistry, University of Leicester) encoding the heme-domain P450 BM3F87G. A double digest of the plasmid pBMHF87G (*Xba*I and *Kpn*I) yielded two fragments of 3418 bp and 1166 bp as expected (data not shown).

4.9.2 Expression and purification of full-length P450 BM3

The full-length P450 BM3 was expressed in *E. coli* TG1 transformed with pBM23 under the control of its own promoter as described in Methods. On freezing, harvested cell pellets were brown in colour and the cell-free lysate transformed to a deep red/brown colour which remained throughout the purification. Purification was achieved via a two-stage liquid chromatography protocol involving anion-exchange followed by affinity chromatography as described in Methods. Purity was assessed via analysis on 6% SDS-PAGE and via the $A_{280}/A_{419\ ratio}$ of the protein in the native oxidised state. Protein concentrations were measured spectrophotometrically using an extinction coefficient of 91,000 M^{-1} cm^{-1} according to the method described in Methods [155].

SDS-PAGE analysis shows a distinct band of protein at 119 kDa being progressively enriched during the purification with some very minor contaminants in the final sample (Figure 4.15). P450 BM3 was estimated to be approximately 95% of the total protein content and sufficiently pure for enzymatic studies.

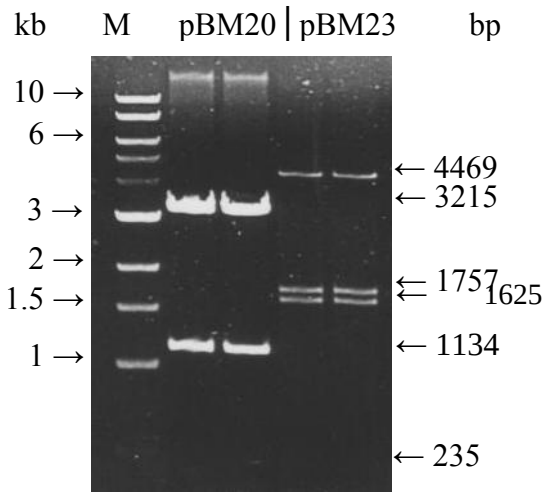

Figure 4.14. Restriction analysis of plasmid constructs for the heme-domain and full-length P450 BM3 (pBM20 and pBM23 respectively).

A 2 ng aliquot of each plasmid was incubated with *Hind*III restriction endonuclease as described in Methods. A 10 µl aliquot of each restriction digest was loaded onto a 0.8% agarose gel alongside a 1 kb DNA ladder marker (M) and subject to 150 V for approximately 30 min. The gel was visualised under UV light and fragment sizes estimated by comparison with the marker. Fragments obtained from digest of pBM20 were: 3215 bp, 1134 bp and 235 bp; fragments obtained for the same digest of pBM23 were: 4469 bp, 1757 bp and 1652 bp. These sizes matched to the expected fragmentation patterns for both plasmids and thus confirm the presence of the plasmid and insert.

4.9.3 Expression and purification of full-length P450 $BM3_{F87G}$

The full-length P450 $BM3_{F87G}$ was expressed in *E. coli* BL21(DE3)pLysS under the control of the T7 promoter using IPTG (1 mM) to induce protein expression. Frozen cell pellets were paler in colour than the wild-type and the cell free lysate was noticeably less intense in colour.

Cell lysate was subject to identical purification procedure as described for the wild-type P450 (Figure 4.15). At each purification stage, the A_{280}/A_{419} ratio of the protein preparation was measured to locate P450 protein and monitor the purification process. The expected A_{280}/A_{419} ratio for pure P450 BM3 should be in the region 1.7 [168, 229] but the observed ratio for the F87G mutant was, at best, 5.5; even after the introduction of an additional size-exclusion step. This was found to be the case for three separate preparations of the enzyme which implies that this mutation causes some kind of disruption affecting heme incorporation or stability.

Figure 4.16 shows a sample of P450 $BM3_{F87G}$ with an A_{280}/A_{419} ratio of 5.5 after DEAE-Sepharose, NAD(P)H affinity and additional size exclusion step. The single band of protein at 119 kDa indicates that the sample has been purified to near homogeneity.

4.9.4 Expression and purification of P450 BM3, and P450 $BM3_{F87G}$ heme domains

The heme-domain of the wild-type and F87G mutant were successfully over-expressed in *E. coli* TG1 as described for the full-length wild-type (Figure 4.15). Proteins were purified by a three step chromatography protocol involving anion exchange and hydroxyapatite resin. Samples from each stage of purification were analysed by 10% SDS-PAGE. Figure 4.17 shows well resolved bands of protein at 54 kDa for both the wild-type and mutant forms of the protein indicating the protein preparation have been purified to near homogeneity. In addition, the A_{280}/A_{419} ratios observed from UV-visible spectroscopy of the samples were in agreement with published values of pure heme domain P450 BM3 at ≤ 0.7 [229].

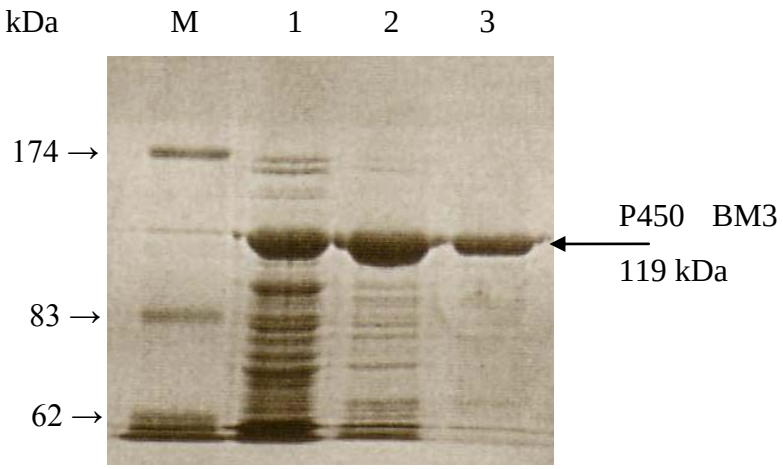

Figure 4.15. SDS-PAGE analysis of full-length P450 BM3 at various stages of the purification process.

The *E. coli* TG1 cells transformed with pBM23 were grown in Terrific broth [70] for a period of 36 h at 37^{o}C, harvested by centrifugation and frozen at -20 ^{o}C as described in Methods. Once thawed, cells were sonicated in the presence of 1mM benzamidine hydrochloride and cell debris removed by centrifugation. P450 BM3 was purified from the cell free lysate using a combination of anion exchange chromatography and ADP Sepharose affinity chromatography as described in Methods. Samples taken at each purification step were loaded onto a 6% polyacrylamide gel alongside a standard protein size marker (M) and subject to 150 V over a period of approximately 1 h. The gel was then fixed and stained with Coomassie Blue as described in Methods. Lanes: 1, soluble fraction of lysate from *E. coli* TG1 cells transformed with pBM23; 2, post anion exchange chromatography; 3, post ADP Sepharose affinity chromatography. These data are representative of 2 similar purifications following the same protocol.

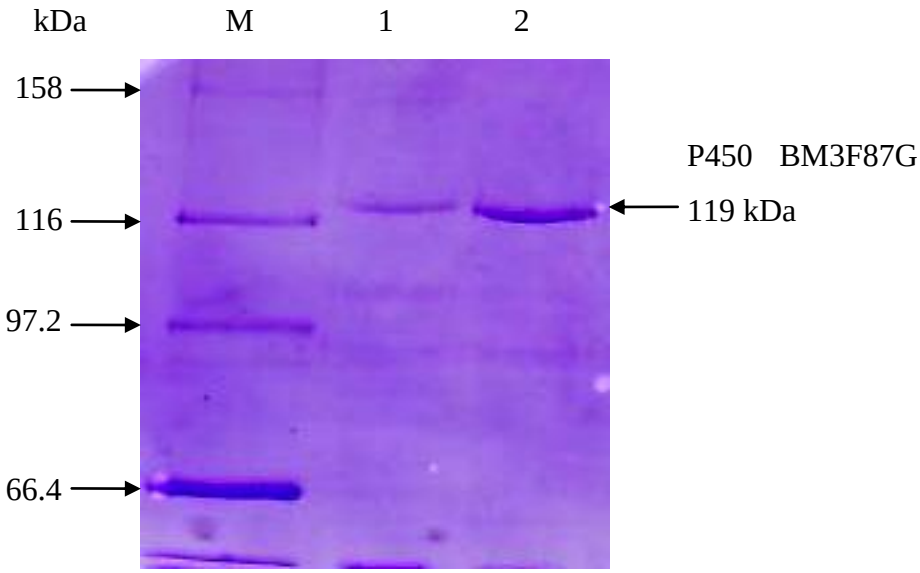

Figure 4.16. SDS-PAGE analysis of the purification of full-length P450 BM3 F87G

Cell lysate from *E. coli* BL21(DE3)pLysS transformed with pTZ18U was subject to the same purification protocol as P450 BM3 with the addition of a final size exclusion chromatography step. Two separate amounts (lanes 1 and 2) of the protein were loaded onto an 8% polyacrylamide gel alongside a protein size marker (M). These data are representative of 3 separate protein preparations.

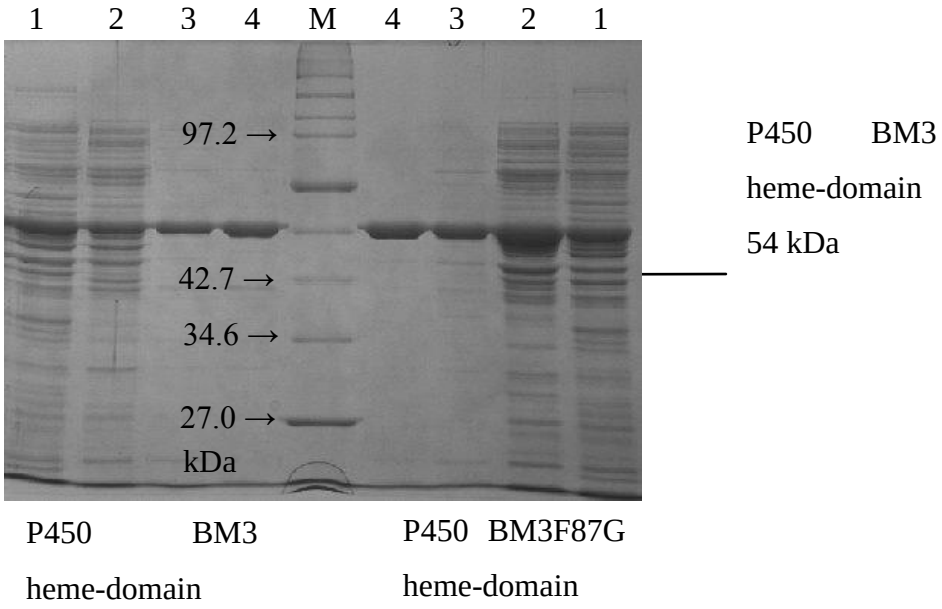

Figure 4.17. SDS-PAGE analysis of P450 BM3 and the F87G mutant heme-domains.

Samples taken at each purification step were loaded onto an 8% polyacrylamide gel alongside a standard protein size marker (M) and subject to 150 V over a period of approximately 1 h. The gel was then fixed and stained with Coomassie Blue as described in Methods. Lanes: M, NEB protein size marker; 1, soluble fraction of lysate from *E. coli* TG1 cells transformed with pBM20 or pBMHF87G; 2, post DEAE Sepharose; 3, post hydroxyapatite; 4, post Q Sepharose. Details of the purification are contained within Methods. For each enzyme, P450 BM3 and F87G, a single growth was prepared but due to the extremely high expression levels, the purification was performed in two batches. These data are therefore representative of the 2 purifications following the same protocol on the same batch of bacteria.

4.9.5 UV-Visible spectral characterisation of P450 BM3 and P450 $BM3_{F87G}$

UV-visible absorption spectra were recorded for both holo-enzyme and heme-domain samples of the wild-type and mutant forms of P450 BM3. For each enzyme, spectra were recorded in the oxidised, reduced and reduced/carbon monoxide bound states over the wavelength range 250 nm to 750 nm.

Figure 4.18 compares the oxidised spectra of the full-length versions of P450 BM3 and the mutant. Both enzymes display a fairly typical cytochrome P450 spectrum, with a peak at 280 nm, the Soret peak at 419 nm and the smaller α and β bands at 538 nm and 569 nm respectively. The ratio of total protein content versus heme content (A_{280}/A_{419}) for the wild-type enzyme was 1.7, fairly typical of pure P450 BM3 with a full complement of heme-cofactor. The same ratio for the F87G mutant however was 5.5, over 3 fold higher. A unique spectral feature of P450 BM3 is the broad absorbance shoulders either side of the Soret peak, attributable to the flavin cofactors (FMN and FAD) [168, 169]. This feature is present in both enzymes but more pronounced in the F87G mutant (Figure 4.18). This combined with the high total protein content versus heme ratio indicates that a significant proportion of the sample is lacking the heme-cofactor. The total protein content versus heme ratio for the heme domain preparations were both around 0.65 which are typical of pure P450 BM3 with a full complement of heme-cofactor (Figure 4.19)

Figure 4.20 compares the effect of sodium dithionite reduction followed by the binding of carbon monoxide (CO) on the spectra of heme-domain and full-length P450 BM3. Reduction of full-length P450 BM3 had the effect of 'bleaching' the flavin signal, thus reducing the apparent width and intensity of the Soret peak. On binding CO in its reduced form the Soret peak shifts to 449 nm, and the α and β bands fuse to give a single maximum wavelength of 545 nm. These reduced/CO bound spectral shifts were mirrored in the heme-domain form of the enzyme.

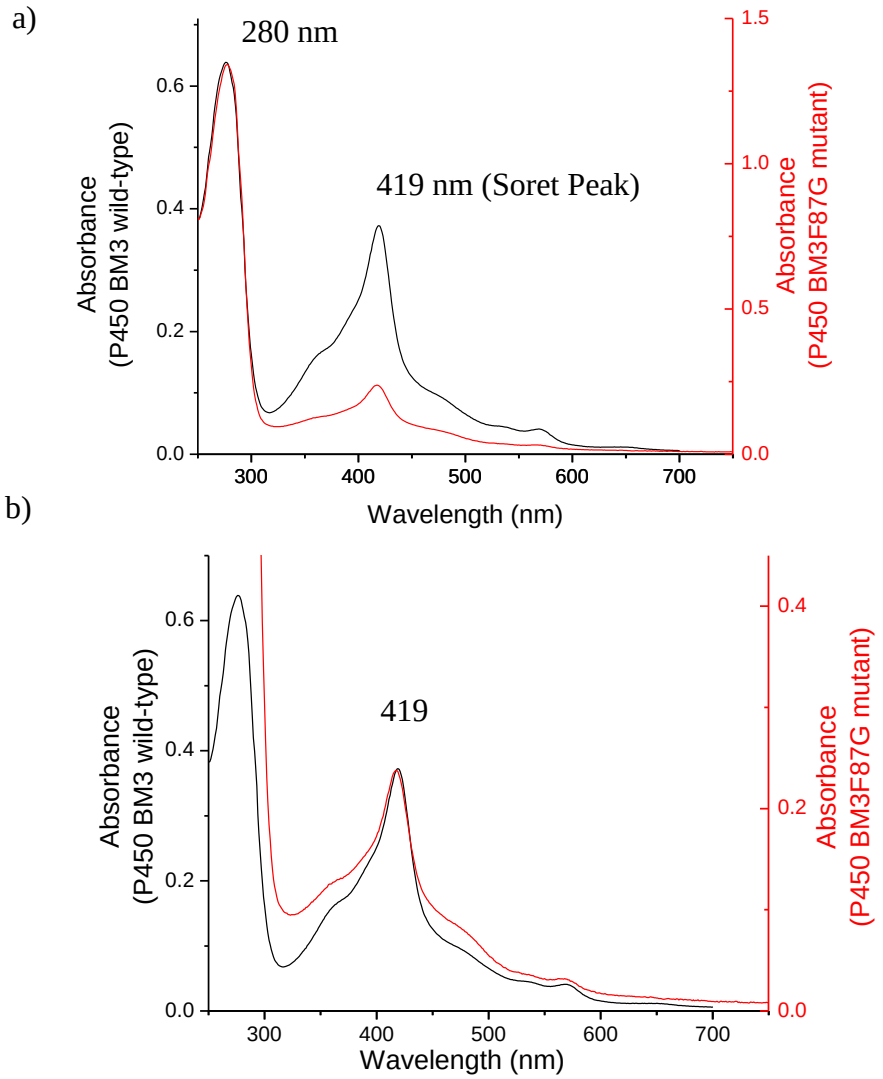

Figure 4.18 UV-visible spectra of full length P450 BM3 wild-type (black) compared to the F87G mutant (red).

Samples from the purifications described in Figure 4.15 and Figure 4.16 were diluted in assay buffer and absorbance measurements taken over the wavelength range 250 – 750 nm. **Panel a)** The A_{280}/A_{419} ratio (total protein content/heme content) of the P450 BM3 (black) preparations was < 1.7, which is in line with published data for pure P450 BM3 [62]. The A_{280}/A_{419} ratio for the 3 preparations of the mutant P450 $BM3_{F87G}$ (red) was much higher, ≥ 5.6, even though SDS-PAGE analysis indicated comparable purity; **Panel b)** The spectra of the wild-type and mutant are overlaid and axes adjusted to compare the shape of the Soret peak.

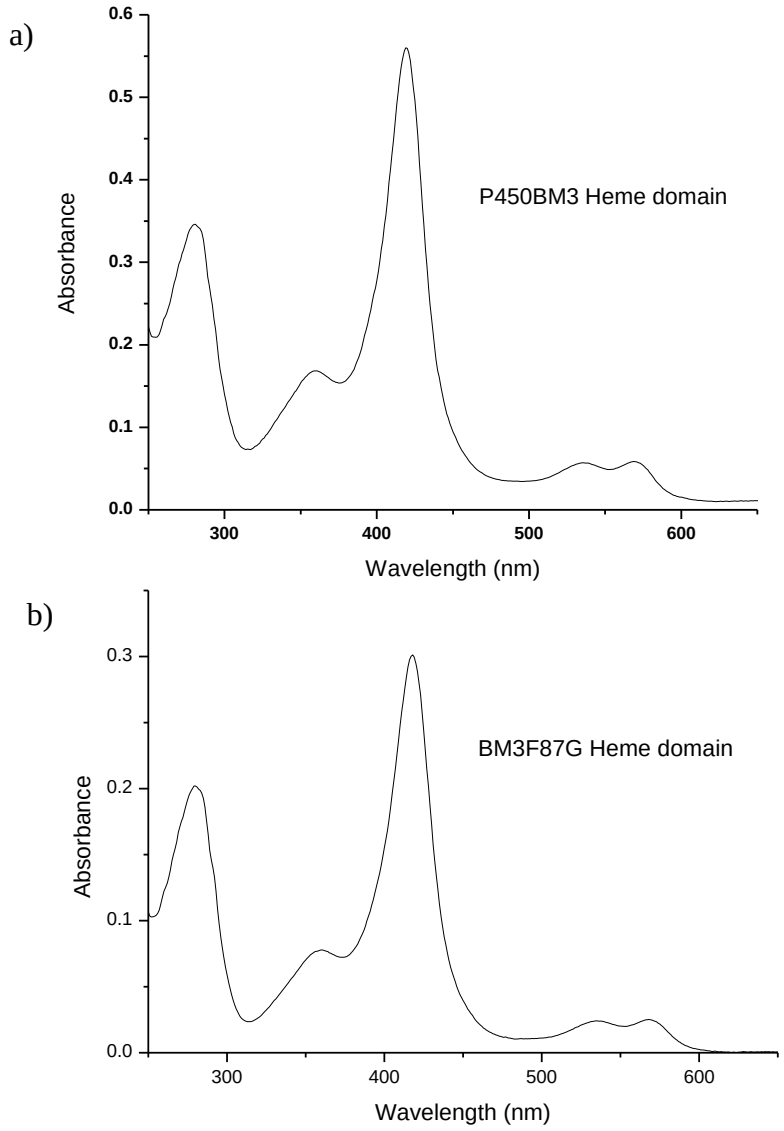

Figure 4.19 UV-visible spectra of heme domains of P450BM3 wild-type (top) compared to the F87G mutant (bottom).

Samples from the purifications described in Figure 4.15 were diluted in assay buffer and absorbance measurements taken over the wavelength range 250 – 750 nm. **Panel a)** The A_{280}/A_{419} ratio (total protein content/heme content) of the P450 BM3 (~ 7.5 μM) preparations was 0.63 which is in line with published data for pure P450 BM3 heme domain [62]. **Panel b)** The A_{280}/A_{419} ratio for the preparation of the mutant P450 $BM3_{F87G}$ (~3 μM) was similar at 0.67.

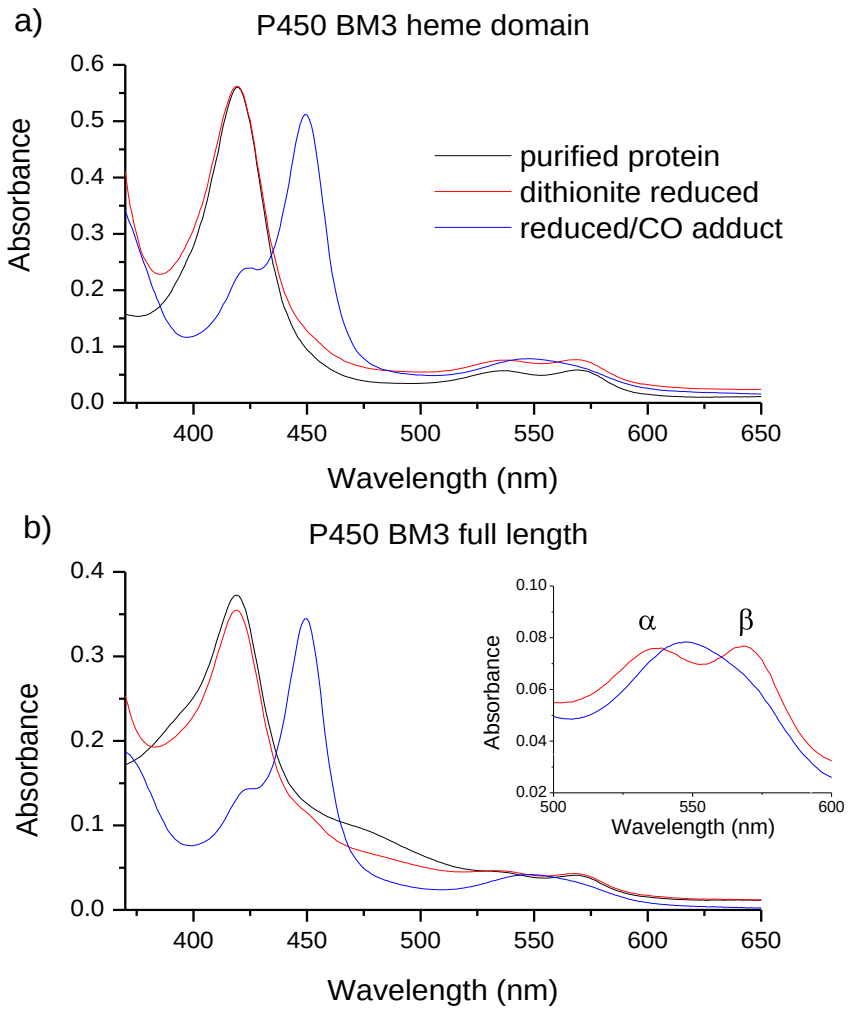

Figure 4.20 Oxidised (black), dithionite reduced (red) and reduced/CO adduct (blue) forms of the heme domain (a) and full length (b) P450 BM3.

Samples of purified protein were mixed with assay buffer to give a final concentration of 3-6 μM and absorbance measurements were taken over the wavelength range 250-750 nm. The samples were then reduced by the addition of excess sodium dithionite (~ 1-5 μM) and the absorbance measurements repeated immediately. Carbon monoxide (CO) was then bubbled gently through the sample for 1 minute and the absorbance measurements repeated. The magnified inset shows the α and β bands at 538 nm and 569 nm respectively are fused in the CO/adduct to form a single absorption peak at 545 nm. These data are representative of at least 3 experiments.

When the same experiment was performed on P450 $BM3_{F87G}$, the mutant would not fully convert to the reduced/CO form. Although the α and β bands were fused, the peak at 449 nm was less pronounced and a shoulder at 422 nm had developed. This was more pronounced in the heme-domain than the full-length form of the enzyme. This can occur when the CO is bubbled through the sample too vigorously, causing a break in the heme ligation, resulting in a peak rising a 422 nm [245]. The dithionite/CO reduction was repeated more than 5 times to ensure this phenomenon was consistent. Not only was it consistent but the mutant enzyme displayed a tendency to revert to the oxidised form over a short period of time. Scans taken at regular intervals after dithionite/CO reduction revealed the mutant re-oxidises over a period of approximately 2 hours (Figure 4.21). The same experiment performed on the wild-type revealed no change in the reduced/CO spectrum after 2 hours and only a mild reversion when left overnight in atmospheric oxygen (data not shown).

Due to the fact that fact that P450 $BM3_{F87G}$ could not be fully converted to the P450 form, calculation of protein concentration using the standard method was not possible. The protein concentration was therefore calculated using the Soret peak of the oxidised enzyme (A_{419}) and the extinction coefficient of 95 mM^{-1} cm^{-1} [60].

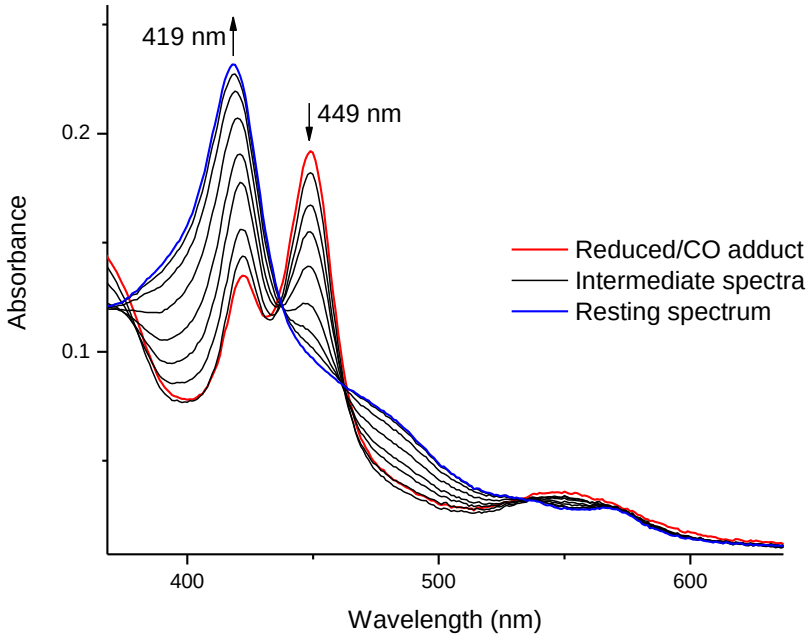

Figure 4.21 The UV-visible spectra of P450 BM3 F87G alters with time after formation of the reduced/CO adduct.

The experiment performed on P450 BM3 described in Figure 4.20 was repeated using P450 $BM3_{F87G}$. Full conversion of the enzyme from the low-spin form (denoted by Soret peak at 419 nm) to the high-spin form (Soret peak at 449 nm) could not be achieved with this mutant. Samples of the purified protein were mixed with reaction buffer to give a final concentration of 3-6 μM before being reduced by the addition of excess sodium dithionite and bubbled gently with CO for 1 minute. Absorbance measurements were taken at 2 min intervals over a period of 2 h. The starting spectrum, immediately after reduced/CO adduct formation (red) shows the incomplete conversion of the enzyme to the reduced, high-spin form denoted by the Soret peak at 449 nm. The intermediate spectra (black) show how the enzyme reverts back to the oxidised, low-spin form (blue) denoted by the decrease in absorbance at 449 nm and a concomitant increase at 419 nm over a period of 112 min (selected intermediate spectra only shown for clarity). These data are representative of 3 similar experiments.

4.9.6 Binding studies

A number of short-chain (C5, C8 & C10) alkenes and the aromatic hydrocarbon styrene were titrated against the heme-domains of P450 BM3 and the F87G mutant (Figure 4.22). As a comparison, the unsaturated fatty acid arachidonic acid (C20), and the inhibitor 4-phenylimidazole were also titrated against the enzymes. Both of these are known to bind tightly to the enzyme and have been shown to induce large spectral changes in the Soret region [246, 247]. Spectra were recorded after each successive addition of the substrate/ligand being tested and the results were analysed to determine the dissociation constant (K_d value).

Titration of the fatty acid induces a shift in the Soret peak from 419 nm to 393 nm (Figure 4.23) commonly referred to as a type I spectral shift; attributable to the substrate affecting the spin-state equilibrium. When the change in absorbance was plotted against the fatty acid concentration, a K_d of 0.39 μM was calculated (Figure 4.24**).** When the fatty acid was titrated against P450 $BM3_{F87G}$ the spectral shift of the Soret peak was visibly diminished which was reflected in the change in K_d to 1.7 μM (Figure 4.25). The plot of maximal absorbance versus arachidonic acid concentration in BM3F87G shows a systematic deviation of the line of fit from the data (Figure 4.25, inset). This may be a result of errors or uncertainty in the estimation of the substrate or enzyme concentration which would lead to the errors in the assumed 1:1 stoichiometry of binding. It could equally be due to an enzyme that is not fully functional with only a proportion of the potential binding sites being accessible. The quadratic equation used in the first instance (Figure 4.25) can be modified to include a parameter in order to scale enzyme concentration to take account of deviations from the 1:1 stoichiometry. If this is applied to the data from BM3F87G/arachidonic acid binding then the line fit indicates the stoichiometry is actually closer to a ration of 0.74 and yields a K_d of 0.38 ± 0.02 (Figure 4.26). These data suggest that only 74% of the binding sites are being occupied or that there are actually less binding site than expected due to errors in protein concentration. It should also be noted that the spectra for the arachidonic acid saturated $BM3_{F87G}$ displayed some heterogeneity, defined by the diffuse Soret peak and shoulder at 413 nm. This indicates that the shift from low- to high-spin has not progressed to completion and a proportion of the enzyme has remained low-spin.

Titration of 4-phenylimidazole, against P450 BM3 caused a shift in the Soret peak in the opposite direction, from 419 nm to 425 nm (Figure 4.27). Known as a type II shift, this is a fairly typical for a P450 inhibitor; pushing the spin state equilibrium lower as the inhibitor ligates the heme.

Titration of the alkenes and styrene against P450 BM3 did not induce any discernable spectral shift. It was therefore not possible to calculate a dissociation constant for these compounds. However, when titrated against the P450 $BM3_{F87G}$, some of the alkenes and styrene had a visible effect on the position and amplitude of the Soret peak, all be it to a much lesser degree than with the fatty acid (Figure 4.28 and Figure 4.29).

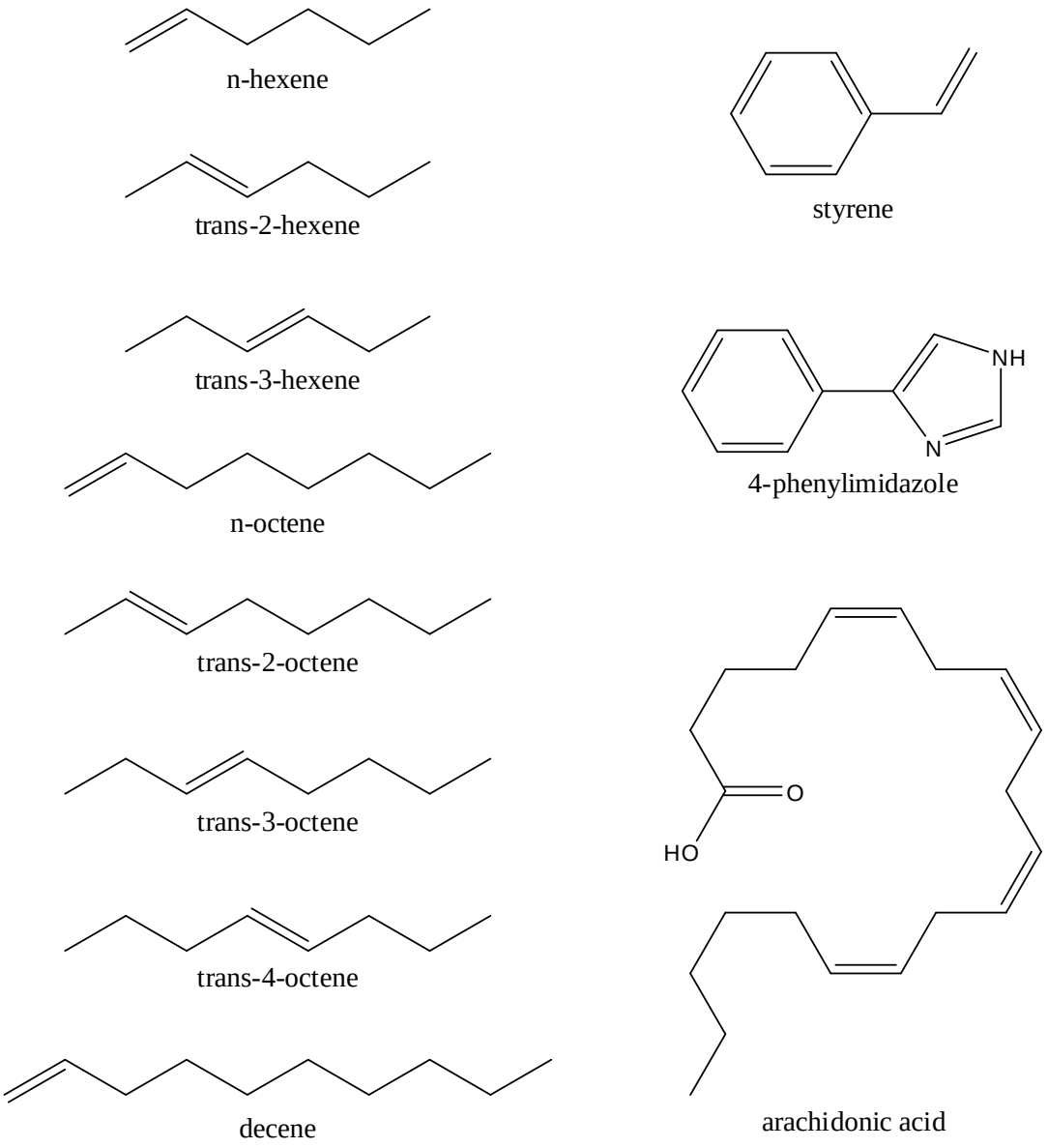

Figure 4.22 Substrates used in binding studies.

A number of short-chain alkenes and the aromatic hydrocarbon styrene were titrated against the heme-domains of P450 BM3 and the F87G mutant. The fatty acid arachidonic acid and the P450 inhibitor 4-phenylimidazole were also titrated against the enzymes as a comparison.

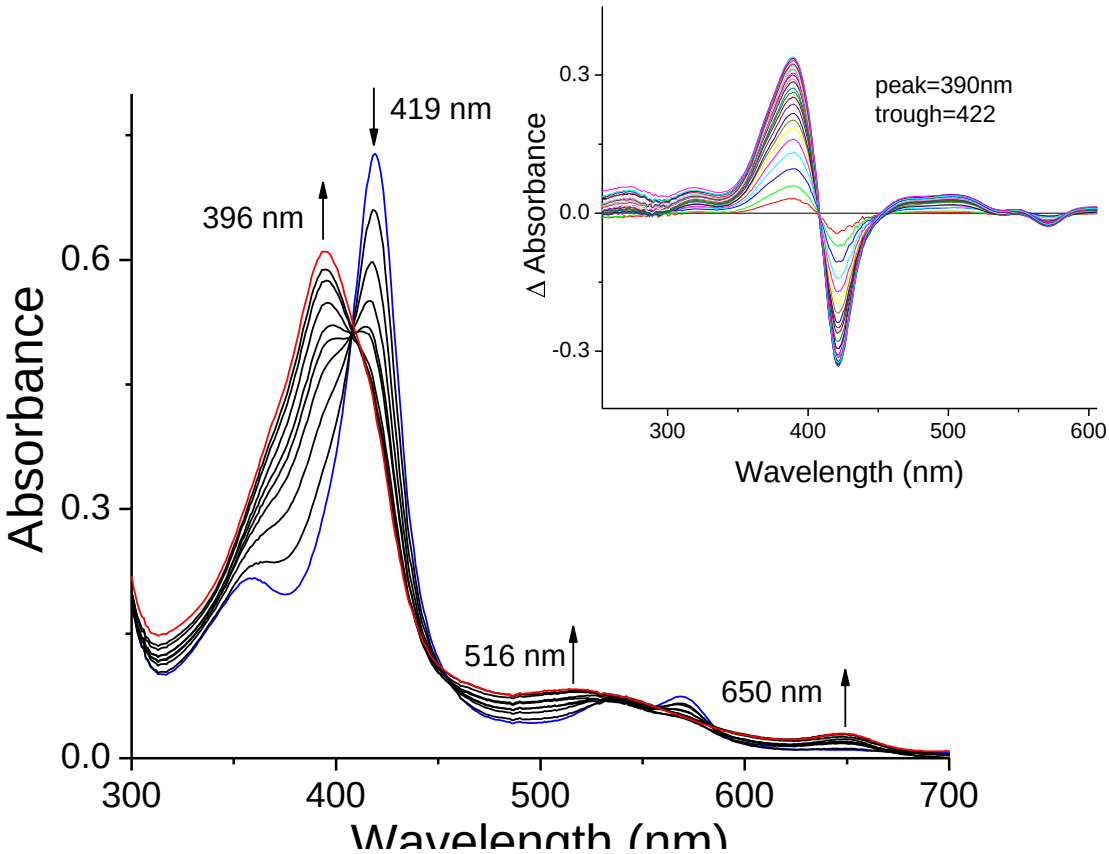

Figure 4.23 Spectral changes induced in P450 BM3 on sequential addition of increasing concentrations of arachidonic acid.

Arachidonic acid (stock solution 33 mM in ethanol) was titrated against P450 BM3 heme-domain as described in Methods. The starting spectrum (blue) shows P450 BM3 in 25 mM MOPS (pH 7.4) 100 mM KCl at a concentration of 4.2 μM. The final spectrum (red) shows the enzyme following the addition of arachidonic acid to a final concentration of 31 μM. A number of intermediate spectra are shown in black. Inset shows the difference spectra generated by subtracting the starting spectrum from each subsequent spectrum. These data are representative of 2 experiments showing similar results.

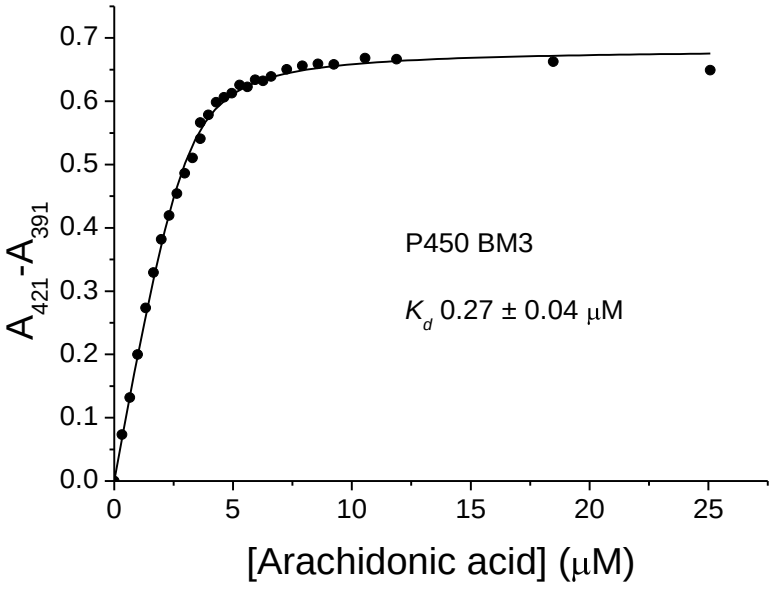

Figure 4.24 Plot of maximal absorbance change against concentration of arachidonic acid.

The wavelength with the largest increase in absorbance was subtracted from the wavelength with the largest decrease in absorbance, 389 nm and 420 nm respectively, derived from the difference spectra described in Figure 4.23. This maximal change in absorbance was plotted against the concentration of arachidonic acid. The plot was then fitted to Equation 2 (quadratic equation), yielding an A_{max} of 0.089 ± 0.007 unit/μM BM3 and a K_d of 0.27 ± 0.04 μM. Data are mean ± SEM, n=3.

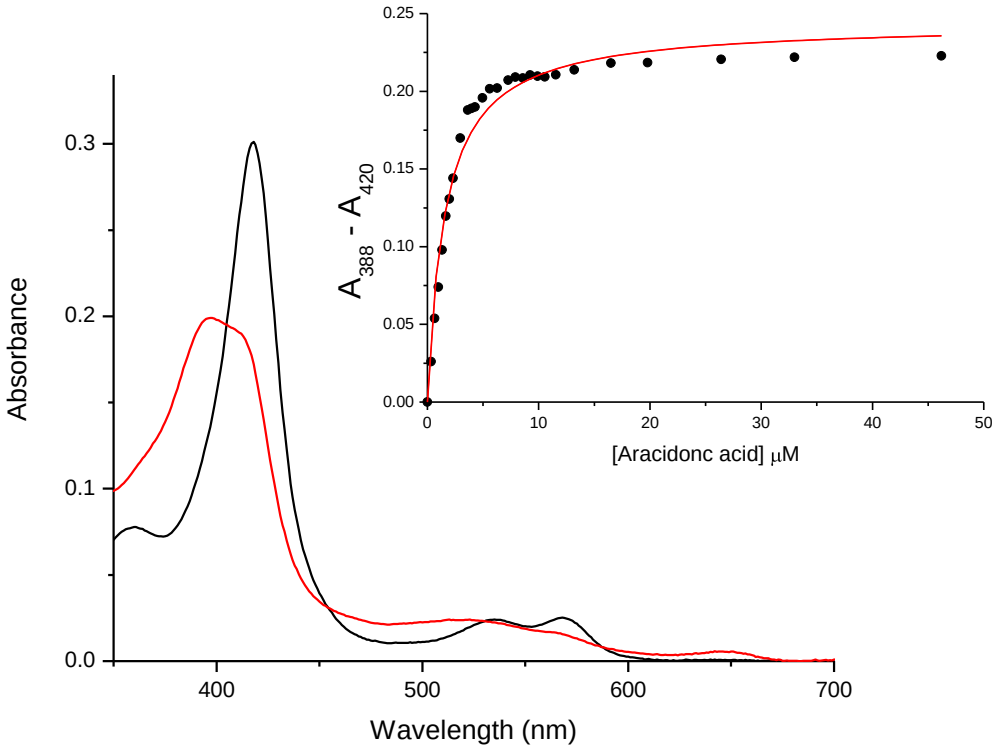

Figure 4.25 Spectral changes induced in P450 BM3$_{F87G}$ on sequential addition of increasing concentrations of arachidonic acid and calculation of K_d.

The black spectrum shows 3.16 μM low-spin P450 BM3$_{F87G}$ heme-domain, the red shows the enzyme following addition of arachidonic acid (stock solution 33 mM in ethanol) to a final concentration of 46 μM, intermediate spectra have been removed for clarity. Inset is the plot of maximal absorbance change against the corresponding arachidonic acid concentration. The data have been fitted to Equation 2 (quadratic equation) with the enzyme concentration set to 3.16 μM yielding an A_{max} of 0.087 ± 0.002 unit/μM BM3 and a K_d of 1.70 ± 0.08 μM.

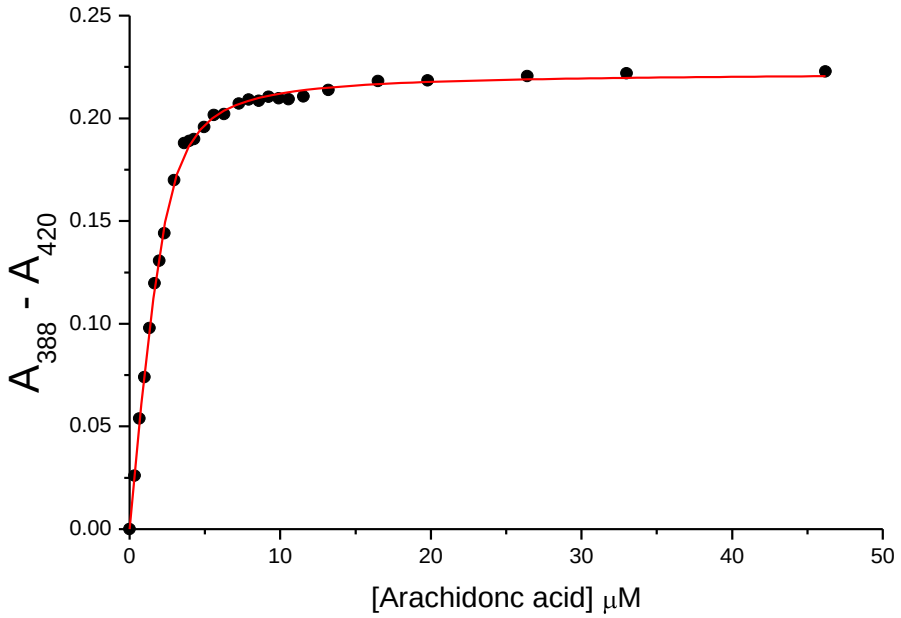

Figure 4.26 Plot of maximal absorbance change against concentration of arachidonic acid taking into account deviation from 1:1 stoichiometry.

A modified quadratic equation which included a stoichiometry factor (*n)* to scale enzyme concentration (*Et*) to account for underestimation in protein concentration due to error or inactivity. The data fit yields a stoichiometry factor of 0.74 estimating the concentration to be 2.34 or that only 74% of binding sites are occupied yielding a new K_d of 0.38 ± 0.02 μM.

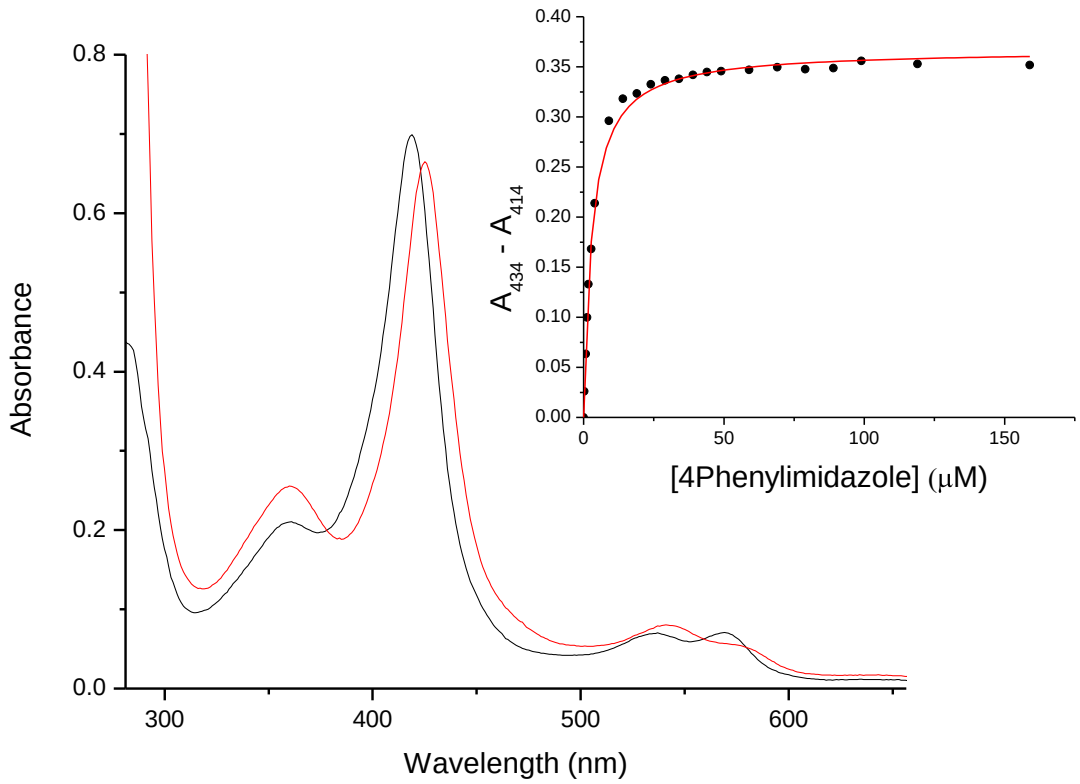

Figure 4.27 Spectral changes induced in P450 BM3 on sequential addition of increasing concentrations of the cytochrome P450 inhibitor 4-phenylimidazole.

The black spectrum shows 6.6 μM of low-spin P450 BM3 heme-domain before addition of the inhibitor, the red spectrum shows the enzyme following the addition of 4-pheylimidazole (stock solution 2.5 mM in assay buffer) to a final concentration of 150 μM. Intermediate spectra have been removed for clarity. Inset is the plot of maximal absorbance change against the corresponding 4-pheylimidazole concentration. The data have been fitted to Equation 2 (quadratic equation) yielding an A_{max} of 0.055 units per μM BM3 and a K_d of 2.95 ± 0.13 μM.

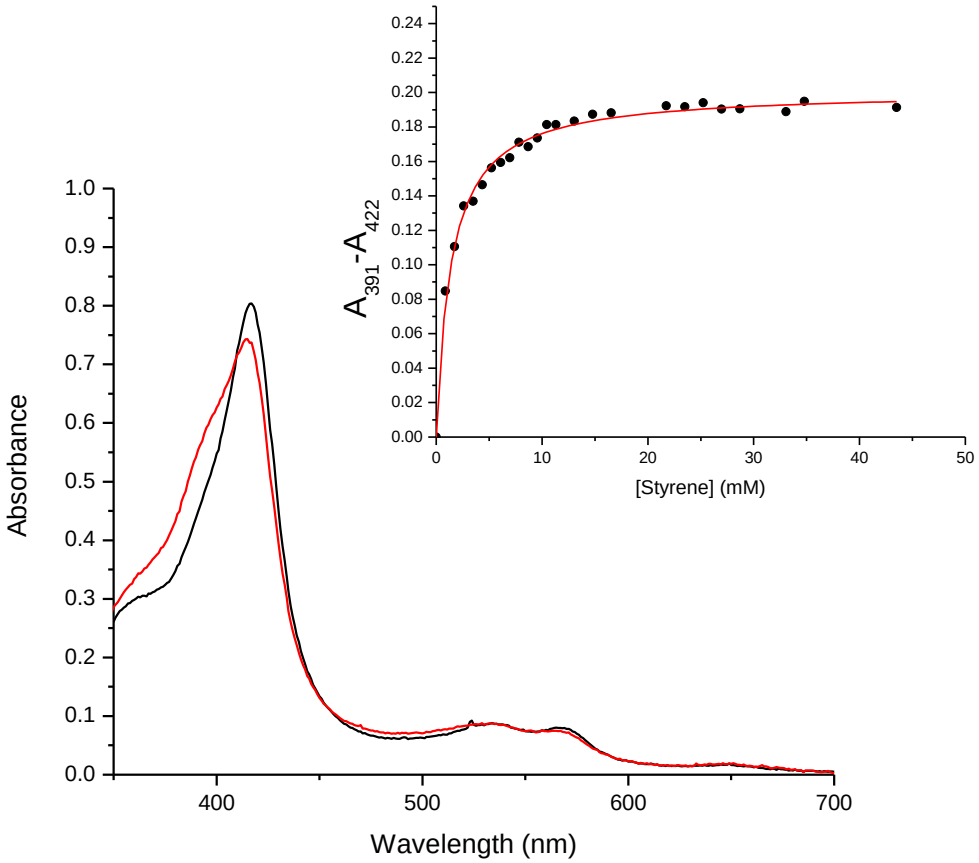

Figure 4.28 Spectral changes induced in P450 BM3$_{F87G}$ on sequential addition of increasing concentrations of styrene.

The black spectrum shows 8 μM of low-spin P450 BM3$_{F87G}$ heme domain, the red shows the enzyme following addition of styrene (stock solution 87 mM in ethanol) to a final concentration of 45 mM, intermediate spectra have been removed for clarity. Inset is the plot of maximal absorbance change against the corresponding styrene concentration. The data have been fitted to Equation 5 (hyperbolic equation), giving an A_{max} of 0.2 and a K_d of 1.42 mM.

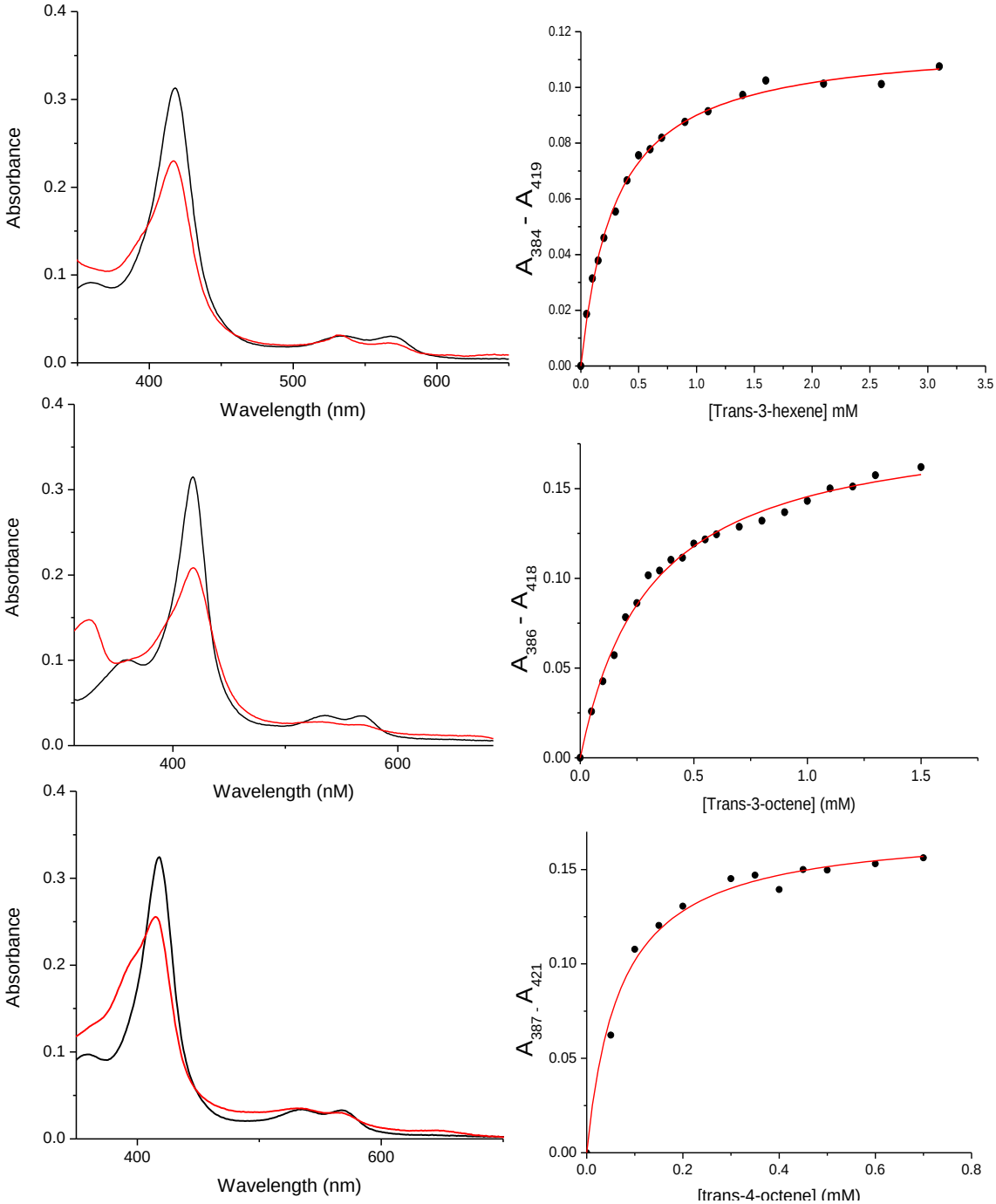

Figure 4.29 Spectral changes induced in P450 BM3$_{F87G}$ on sequential addition of increasing concentrations of a) trans-3-hexene, b) trans-3-octene and c) trans-4-octene.

Black spectra show low-spin P450 BM3$_{F87G}$ heme-domain, red spectra shows the enzyme following addition of the substrate. All data were fitted to Equation 5 (hyperbolic equation) and data are summarized in Table 4.1.

Of the all the substrates tested, excluding the fatty acid, the largest spectral perturbations were induced by styrene. The intensity of the Soret absorbance peak at 419 nm reduced whilst an increase in absorption appears at 397 nm indicating the spin-state equilibrium was being pushed towards high-spin. Although the spectral changes effected on P450 $BM3_{F87G}$ by the short-chain alkenes were less noticeable they were sufficient to calculate apparent dissociation constants (Table 4.1).

In the case of arachidonic acid, the glycine substitution at F87 caused a 4-fold decrease in the apparent affinity for the fatty acid substrate; in contrast there has been a 2 fold increase in the apparent affinity for 4-phenylimidazole. Apparent K_d for the alkene substrates and styrene, where calculated, were in the mM concentration rather than μM which is more typical of P450/substrate interactions.

Substrate	K_d BM3 wt	BM3 F87G
Arachidonic acid	0.27 ± 0.04 μM (0.55 ± 0.05μM)	0.38 ± 0.02 μM
1(n) Hexene	†	†
Trans-2-hexene	†	0.52 ± 0.03 mM
Trans-3-hexene	†	0.30 ± 0.01 mM
1(n) octene	†	†
Trans-2-octene	†	†
Trans-3-octene	†	0.30 ± 0.02 mM
Trans-4-octene	†	0.07 ± 0.01 mM
Decene	†	†
Styrene	†	1.42 ± 0.06 mM
4-Phenylimidazole	2.95 ± 0.13 μM (5.8 ± 1.0 μM)	1.44 ± 0.04 μM

Table 4.1. Dissociation constants calculated for substrate binding to the heme-domain of P450 BM3 and the F87G mutant using the method described in Figure 4.23 toFigure 4.29.

† Spectral changes were not observed or insufficient to enable calculation of dissociation constants. Numbers in brackets are data obtained using similar methods in previous work [248].

4.9.7 Redox Potentiometry

Redox potentiometry was performed on the heme domains of the wild-type and the F87G mutant forms of P450 BM3 to determine whether the glycine substitution had altered the electrochemical environment of the heme. Reductive titrations were performed under anaerobic conditions on both substrate free and fatty acid bound heme-domains of P450 BM3 and P450 $BM3_{F87G}$ as described in Methods. Figure 4.30 shows the spectral changes observed when P450 BM3 was reduced in the presence of arachidonic acid under saturating conditions. When fully oxidised the enzymes heme iron appeared low-spin as indicated by the absorption peak at 392 nm. As the sample was reduced absorbance at 392 nm reduced and absorbance at 409 nm increased. A mid-point redox potential of -240 mV was calculated from the plot of maximal absorbance change versus the corresponding potential measurement. Reductive titration of substrate free P450 BM3 (Figure 4.31) yielded a mid-point redox potential of -388 mV. Both values are in good agreement with the reported redox potentials [195].

Similar potentiometric titrations were conducted on arachidonic acid bound (Figure 4.32) and substrate free (Figure 4.33) P450 $BM3_{F87G}$. In the absence of substrate the Soret peak of $BM3_{F87G}$ shifts towards 409 nm, emulating the transition observed for P450 BM3. However, it should be noted that toward the end of the reductive titration it became increasingly difficult to reduce the potential suggesting that the reduction process had not progressed to completion within the accessible range (~ -420 mV using dithionite as reductant). The mid-point redox potential of BM3F87G was calculated to be -416 ± 8 mV but it is conceivable that the real redox potential could be even more negative. Indeed, if the data are fitted whilst fixing the Nernst factor (or RT/F value) to 59 mV, the slope of a one-electron redox couple at 25 ºC, the mid-point redox potential is estimated to be -424 mV ± 2. In the presence of saturating concentrations of arachidonic acid the starting spectra of $BM3_{F87G}$ shows heterogeneity in the sample as discussed previously (Section 4.9.6) indicating a proportion of the sample is in low-spin. Upon reduction the Soret peak at 396 nm shifts towards 409 reflecting the transition made by P450 BM3 on reduction. The mid-point potential calculated to be -187 ± 16 mV, some 53 mV more positive than

the wild-type. Table 4.2 compares the mid-point potentials calculated for the mutant with those of the wild-type.

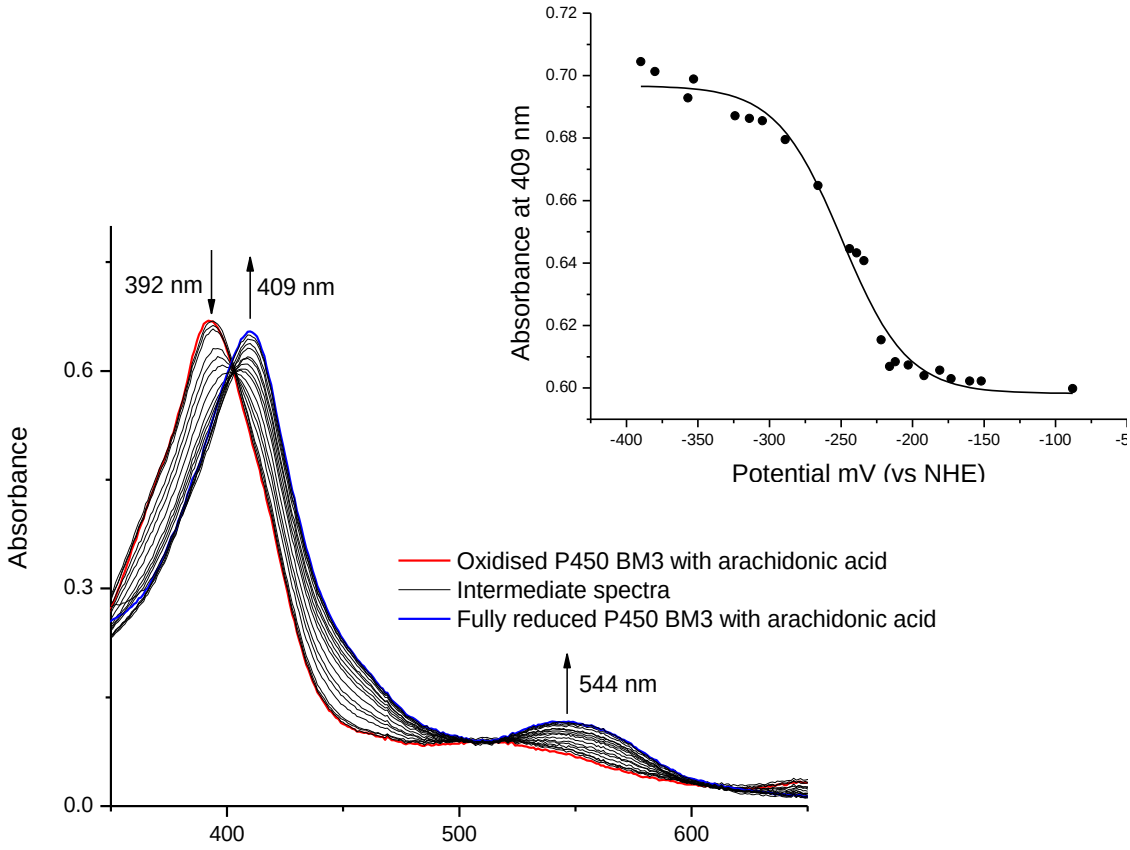

Figure 4.30. Spectral changes in substrate-bound P450 BM3 during reductive titration and calculation of the mid-point potential.

Under anaerobic conditions, the heme-domain of P450 BM3 in 100 mM KPi (pH 7.0) containing 5% (v/v) glycerol was incrementally reduced then re-oxidised in the presence of saturating concentrations of arachidonic acid (at least 80 μM) as described in Methods. Spectra were recorded (250 nm – 800 nm) at each reductive/oxidative addition along with the corresponding potential. The absorbance measurements at the wavelength showing the maximal absorbance changes were then plotted against the corresponding potential measurement corrected against the normal hydrogen electrode (NHE) by the addition of +244 mV. Data were then fit to Equation 4 (1-electron Nernst equation) to calculate the midpoint potential. The starting spectrum (red) shows ~7 μM of oxidised high-spin P450 BM3. The final spectrum (blue) shows the enzyme following the addition of sodium dithionite to full reduction. A number of example intermediate spectra are shown in black. Arrows show the direction of the absorbance change as the enzyme is reduced. Inset shows a plot of absorbance at 409 nm against the normalised potential measurement, yielding a mid-point reduction potential of -249 ± 3 mV. The error shown is the estimate from graphing software (Origin; OriginLab, Massachusetts) of the fit of the data to the 1-electron Nernst equation (equation 4) from a single potentiometric titration.

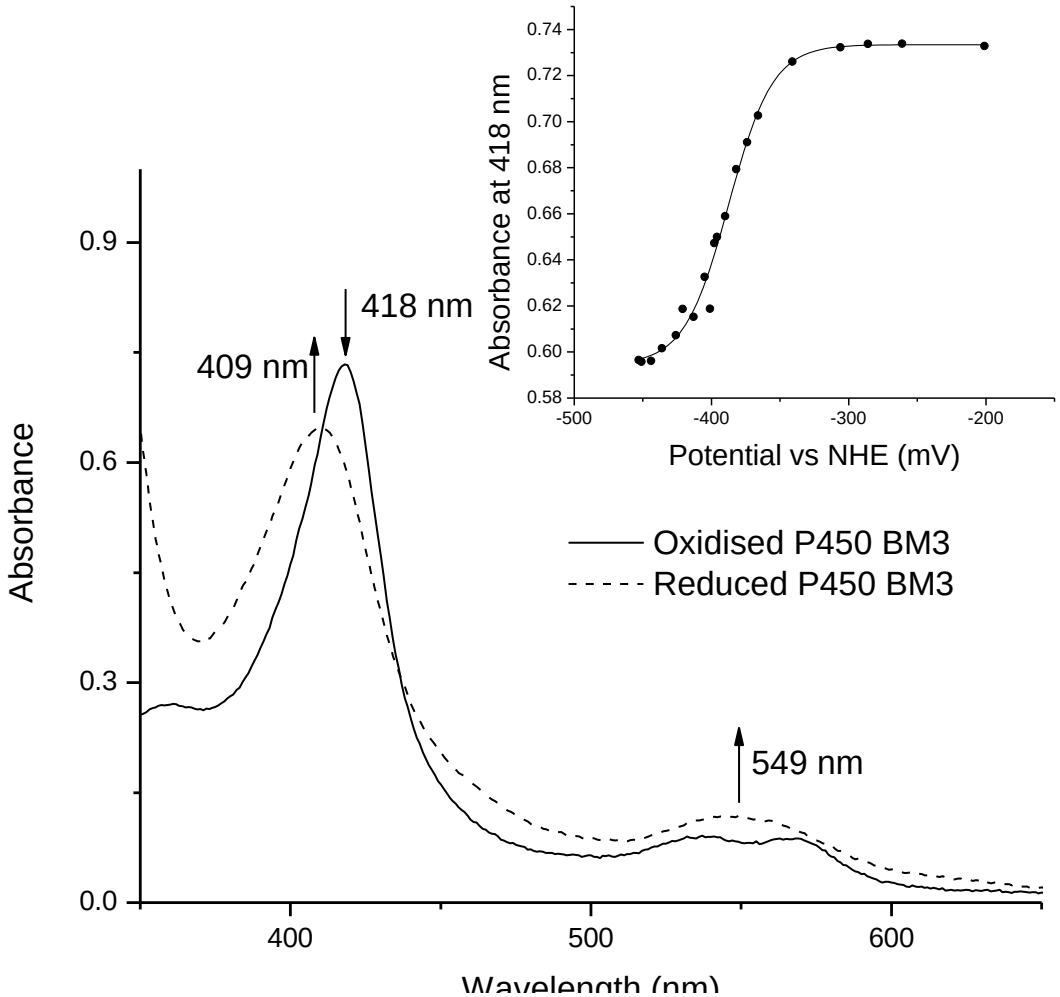

Figure 4.31. Spectral changes in P450 BM3 during reductive titration and calculation of the mid-point potential.

The heme-domain of P450 BM3 was subject to reductive titration as described in with the exclusion of any substrate. The starting spectrum (solid line) shows ~8 μM of oxidised low-spin P450 BM3. The final spectrum (dashed line) shows the enzyme following the addition of sodium dithionite to full reduction. Intermediate spectra are removed for clarity. Inset shows the plot of absorbance at 418 nm against the corresponding potential measurement (mV) corrected against the NHE. These data are fitted to Equation 4 (1-electron Nernst equation) yielding a mid-point reduction potential of -388 ± 2 mV. The error shown is the estimate from graphing software (Origin; OriginLab, Massachusetts) of the fit of the data to equation (n) from a single potentiometric titration.

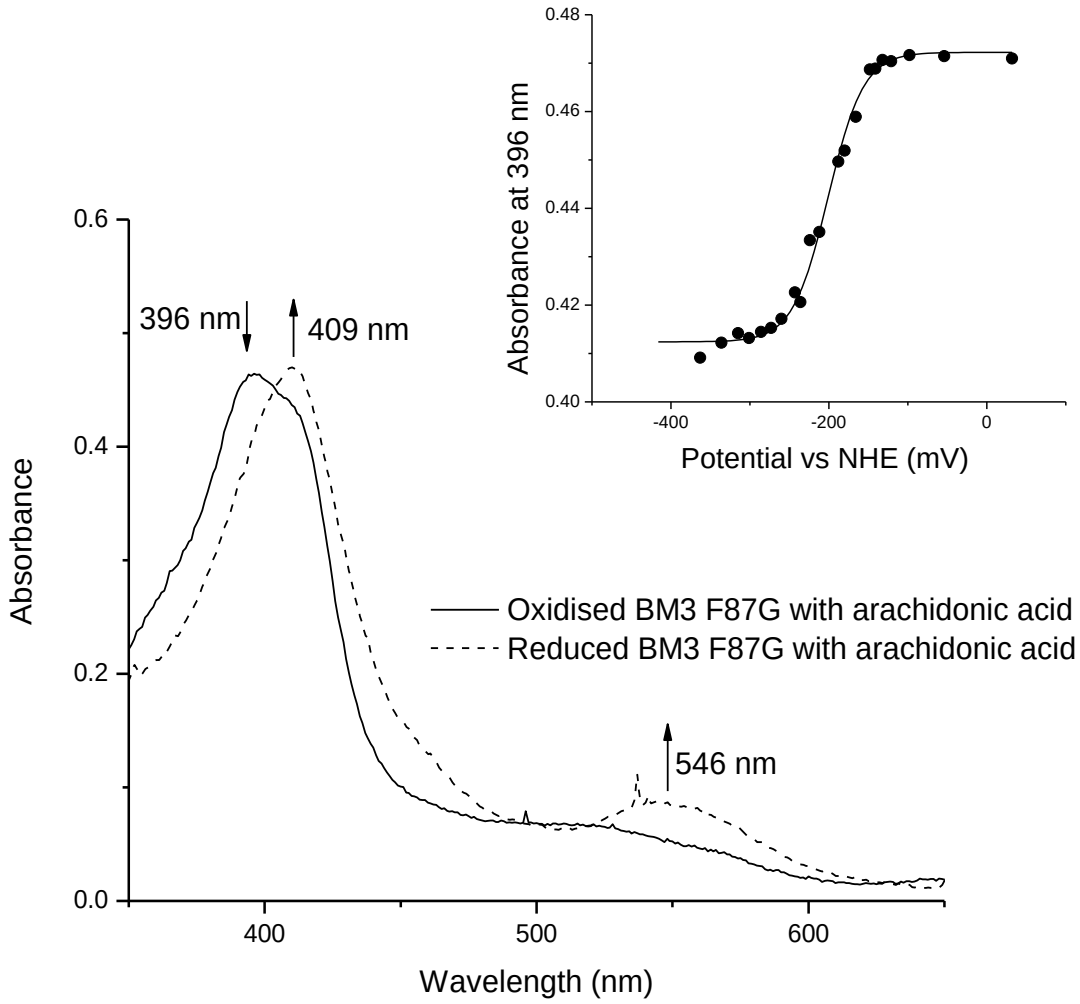

Figure 4.32. Spectral changes in the substrate-bound F87G mutant during reductive titration and calculation of the mid-point potential.

The heme-domain of P450 BM3 F87G was subject to reductive titration as described in Figure 4.31. The starting spectrum (solid line) shows ~5 μM of oxidised high-spin enzyme. The final spectrum (dashed line) shows the enzyme following the addition of sodium dithionite to full reduction. Intermediate spectra are removed for clarity. Inset shows a plot of absorbance at 396 nm (the maximal absorbance change) against the corresponding potential measurement corrected against the NHE. The data are fitted to Equation 4 (1-electron Nernst equation), yielding a mid-point reduction potential of 187 ± 16 mV. Data are mean ± SEM, n=2.

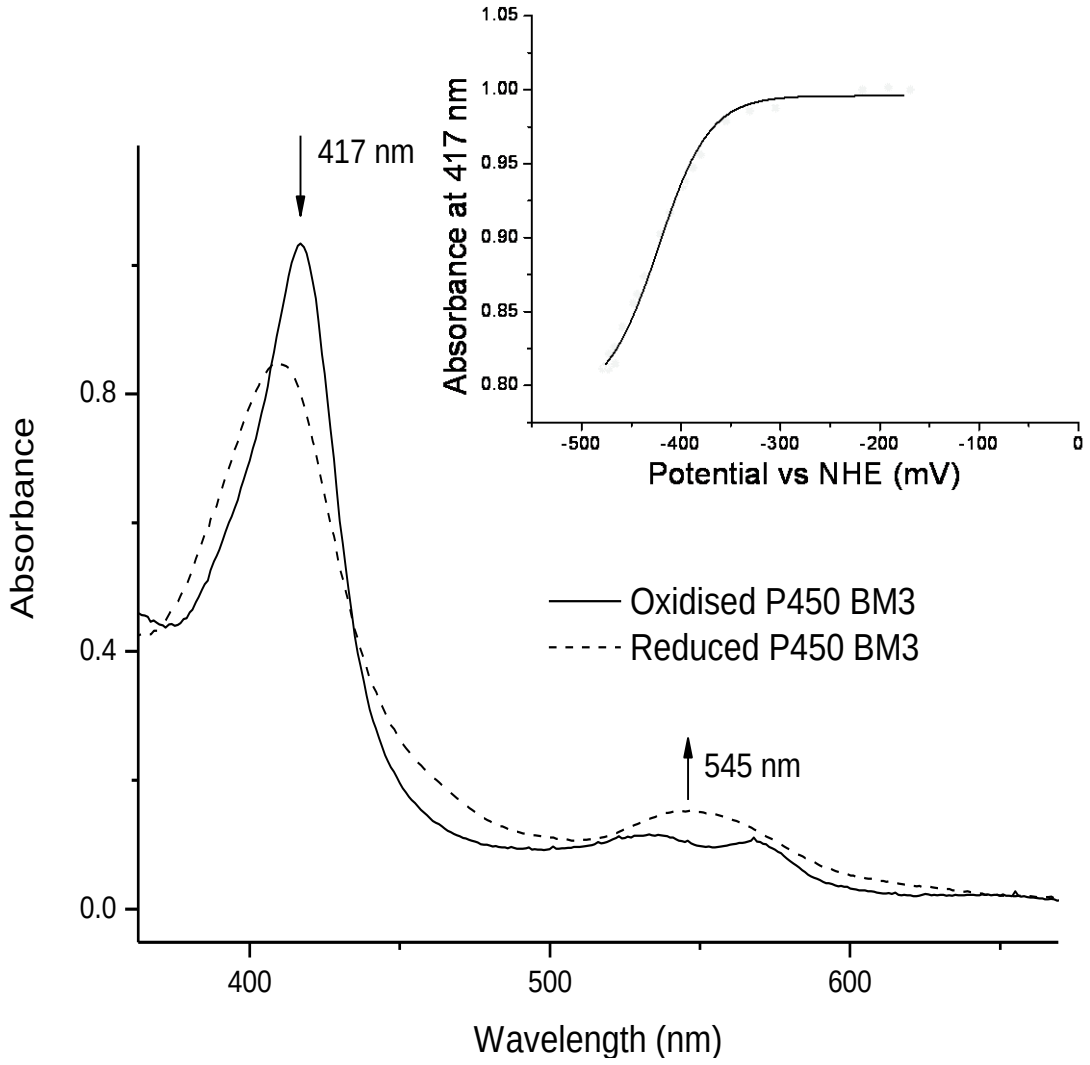

Figure 4.33. Spectral changes in the F87G mutant during reductive titration and calculation of the mid-point potential.

The heme-domain of P450 BM3 F87G was subject to reductive titration as described in Figure 4.31, excluding any substrate. The starting spectrum (solid line) shows 9 μM of oxidised high-spin enzyme. The final spectrum (dashed line) shows the enzyme following the addition of sodium dithionite to full reduction. Intermediate spectra are removed for clarity. Inset shows a plot of maximal absorbance changes at 417 nm against the corresponding potential measurement corrected against the NHE. The data are fitted to Equation 4 (1-electron Nernst equation), yielding a mid-point reduction potential of -416 ± 8 mV.

	Substrate free	Arachidonic acid bound
P450BM3	-388 ± 2 mV	-249 ± 3 mV
	-392 [248]	-283
	-370 [54]	-235
BM3F87G	-416 ± 8 mV *SEM (n=2)*	-187 ± 16 mV *SEM (n=2)*

Table 4.2. Mid-point redox potential of heme-domain P450 BM3 and the F87G mutant with and without arachidonic acid bound.

Potentiometric titrations were performed under anaerobic conditions on the heme-domains of P450 BM3 and its mutant F87G in the presence and absence of the strongly binding substrate arachidonic acid. Enzymes were incrementally reduced using sodium dithionite to full reduction then re-oxidised using potassium ferricyanide as described in Methods. Mid-point reduction potentials were calculated as described in Figure 4.30. For P450 BM3, errors shown are the estimates from graphing software (Origin; OriginLab, Massachusetts) of the fit of the data to the 1-electron Nernst equation (Equation 4) from a single potentiometric titration. For the F87G mutant, two reductive titrations were performed on the same enzyme preparation and an average of the two mid-point potentials was calculated, along with an SEM. Previously published data on the wild type enzyme are also stated for comparison.

4.9.8 Steady-state kinetics

Since binding studies indicated an interaction between the P450 $BM3_{F87G}$ and some of the non-fatty acid substrates, substrate-dependent NADPH-oxidation was examined. Either full-length P450 BM3 or full-length P450 $BM3_{F87G}$ was mixed with the substrates at increasing concentrations whilst monitoring the rate of NADPH oxidation at 340 nm as described in Methods. In the case of the non fatty-acid substrates, it was necessary to increase the amount of enzyme in the reaction mixture (from ~ 50 nM to ~200 nM) to obtain an accurately measurable rate within a reasonable assay time (typically 30 sec). It should be noted that the alkene and styrene substrates are less than 1% soluble in water [249]. To ensure the maximum solubilisation of these substrates, reaction mixtures were mixed by vigorous shaking prior to addition of NADPH to begin the reaction. The data followed a standard rectangular hyperbola and were fit to the Michaelis-Menten (Equation 5) to calculate an apparent k_{cat} and K_m (Figure 4.34).

As expected, the wild-type enzyme showed very high NADPH oxidation activity with arachidonic acid, reaching a maximal rate of over 13000 min^{-1} whereas the maximal rate observed for the F87G mutant was 7.5 fold lower at 1752 min^{-1}. Therefore, although there was little difference in the K_m values (11 μM and 17 μM for wild-type and the mutant respectively) the net effect of this mutation on arachidonic acid-dependent NADPH oxidation was an 11.7 fold reduction in the catalytic efficiency (k_{cat}/ K_m).

Each of the non-fatty-acid substrates tested, with the exception of decene, resulted in substrate concentration-dependent NADPH oxidation in both the wild-type and the mutant enzymes. The kinetic parameters are presented in Table 4.3.

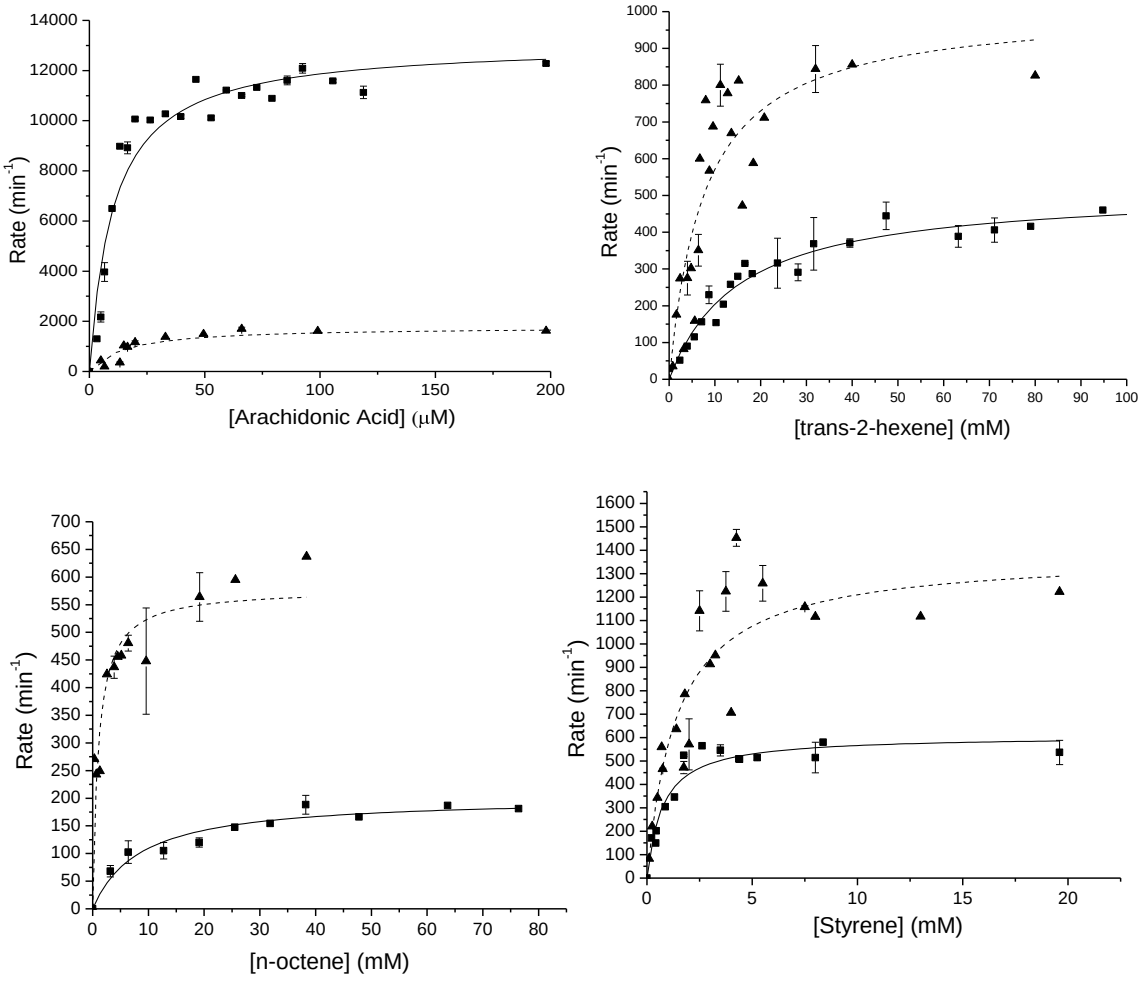

Figure 4.34. Substrate-dependent NADPH oxidation by P450 BM3 and the F87G mutant.

The steady-state kinetics of the enzyme and its mutant were studied by monitoring the oxidation of NADPH by the enzyme at 340 nm in the presence of substrate at various concentrations as described in Methods. Substrates used were the same as those used in the binding studies. Initial rates, expressed as moles of NADPH oxidised per mole of BM3 per minute, were plotted against the corresponding substrate concentration for the full-length P450 BM3 (■) and the F87G mutant (▲). These data were fit to the Michaelis-Menten equation (equation 5) using Origin to calculate the kinetic parameters. Error bars show the mean ± standard error between duplicate measurements. Steady-state kinetic parameters calculated from these data are summarised in Table ??

.

	P450 BM3			F87G mutant		
Substrate	k_{cat} (min^{-1})	K_M (mM)	K_{cat}/K_M	k_{cat} (min^{-1})	K_M (mM)	k_{cat}/K_M
Arachidonic acid	13196 ± 498	0.011 ± 0.002	1.2 x 10^6	1752 ±149	0.017 ± 0.005	0.1 x 10^6
1(n) Hexene	570 ± 62	13.9 ± 3.78	41	306 ±57	0.52 ± 0.63	588.5
Trans-2-hexene	508 ± 25	14.20 ± 2.29	35.8	1251 ± 188	8.92 ± 2.91	140.2
Trans-3-hexene	666 ± 40	2.6 ± 0.50	256.2	1145 ± 134	3 ± 1.4	381.7
1(n) octene	202 ± 12	8.5 ± 2.04	23.8	579 ± 34	1.03 ± 0.30	562.1
Trans-2-octene	877 ± 34	15 ± 1.15	58.5	597 ± 40	1.4 ± 0.36	426.4
Trans-3-octene	1041 ± 66	4.5 ± 1.05	231.3	1366 ± 159	6.23 ± 1.77	219.3
Trans-4-octene	160± 8.7	1.4 ± 0.44	114.3	1710± 125	7.1 ± 1.81	240.8
Decene	†	†		†	†	
Styrene	624 ± 35	0.8 ± 0.18	780	1382 ± 126	1.4 ± 0.44	987.1

Table 4.3. The steady-state kinetic parameters of the interaction of P450 BM3 and the F87G mutant with fatty-acid and alkene substrates.

Apparent K_M, k_{cat} and k_{cat}/K_M for the substrate dependant oxidation of NADPH in the presence of fatty-acid and alkene substrates for wild-type and the F87G mutant are shown. All measurements were made with [enzyme] constant at ~ 100 nM, using 200 μM NADPH in 20 mM MOPS, 100 mM KCl, pH 7.4 as described in Methods. The errors shown are the estimates from Origin of the fit of the data to Equation 5 (Michaelis-Menten equation) calculated from duplicate measurements on the same enzyme preparation. Rates are expressed as moles of NADPH oxidised per mole of BM3 per minute. † Activity above the background rate could not be detected.

4.9.9 Product analysis

To establish whether the observed substrate-dependent NADPH oxidation activity was linked to modification of substrates, enzyme (either full-length P450 BM3 or full-length P450 $BM3_{F87G}$) was incubated overnight at room temperature with each of the non-fatty acid substrates and NADPH; any resulting products and remaining substrate, analytes, were extracted into solvent and analysed by gas chromatography and mass spectroscopy (GC/MS) as described in Methods. All turn-over reactions, extractions and analysis was performed in the laboratories at Avecia under the supervision of Dr Robert Holt.

Identification of analytes in the extracts was achieved by matching their column retention times (RT) and mass spectra with those of standardised substrates and products. The product standards used for comparison were either commercially available hydroxylated alkenes or alkene oxides (epoxides) manufactured in the lab using standard epoxidation chemistry as described in Methods. In the case of styrene; analytes were additionally subject to chiral column chromatography in order to analyse the enantiomeric ratio of the R- and S-styrene oxide products.

Figure 4.35 shows the gas chromatograms of the analytes extracted from P450 BM3 and P450 $BM3_{F87G}$ when incubated with styrene and equimolar ratios of NADPH. The profiles for both enzymes were similar, showing three large peaks with retention times of 8.0, 10.2 and 10.3 min. When compared with the retention times of styrene, a racemic mixture of styrene oxide and a sample of pure *R*-styrene oxide, these peaks can be identified as the starting material, styrene, *R*-styrene oxide and *S*- styrene oxide respectively. Calculation of the area under each peak showed that of the analytes extracted from the wild-type enzyme, 57% was styrene. The remaining 43% had been converted to styrene oxide with the *R*-stereoisomer in 20% enantiomeric excess (e.e.). The same calculation of peak area for the extracts from P450 $BM3_{F87G}$ yielded an 89% conversion to product with the *R*-stereoisomer in 64% e.e.; a two fold increase in conversion to product and a three-fold increase in e.e. for *R*-styrene oxide.

Figure 4.36 shows the gas chromatogram of the analytes extracted from P450 $BM3_{F87G}$ when incubated with trans-2-octene and equimolar ratios of NADPH. Here the RT of two of the peaks matched those of the substrate and epoxide standards that

were chemically manufactured in the laboratory (Methods). The third, much smaller peak could only be identified using the mass spectra by matching the molecular weight and fragmentation pattern with a GC/MS library and was identified as 2-octene-4-ol. Calculation of the area under each peak shows 52% of the substrate was converted to product in a 9:1 ratio in favour of the epoxide. In comparison, only two peaks were extracted from the P450 BM3 reaction; 38% being substrate and 62% was positively identified as the epoxide product.

Figure 4.37 illustrates the structures of the non-fatty acid substrates tested and their oxidised products as identified by GC/MS. P450 BM3 appears to produce only a single hydroxide or epoxide species, with regio-specificity for the w-2 carbon position. In contrast, the F87G mutant generates several product species from a single substrate, displaying less regio-selectivity and attacking the substrate at either ω-1, -2 or -3 position. The percentage of substrate converted to product, as estimated by the area under the curve, calculated from the peaks on the chromatogram, are presented in Table 4.4.

a)

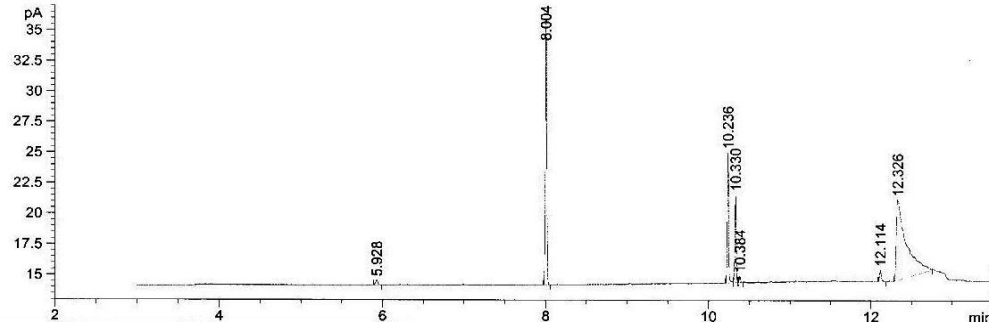

Time (min)

b)

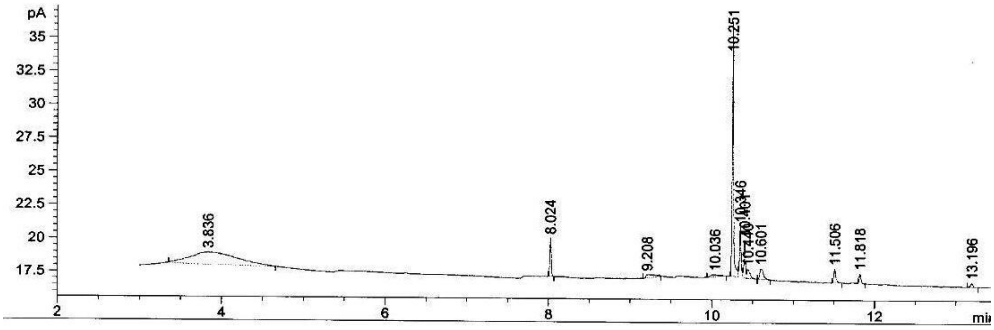

Time (min)

Figure 4.35. Analysis of reaction products from P450BM3 and the mutant F87G using styrene as a substrate.

The enzyme was incubated at room temperature, with agitation, for a minimum of 8 h in the presence of equimolar amounts of styrene and NADPH. Reaction products and any remaining substrate were extracted into dichloromethane and analysed by gas chromatography using a chiral column as described in Methods. The retention times of the constituents of the extracts obtained from (a) P450 BM3 and (b) the F87G mutant were matched against those obtained for the standards (c) styrene, (d) racemic mixture of *S*- and *R*-styrene oxide (e) *R*-styrene oxide (continued over leaf).

c)

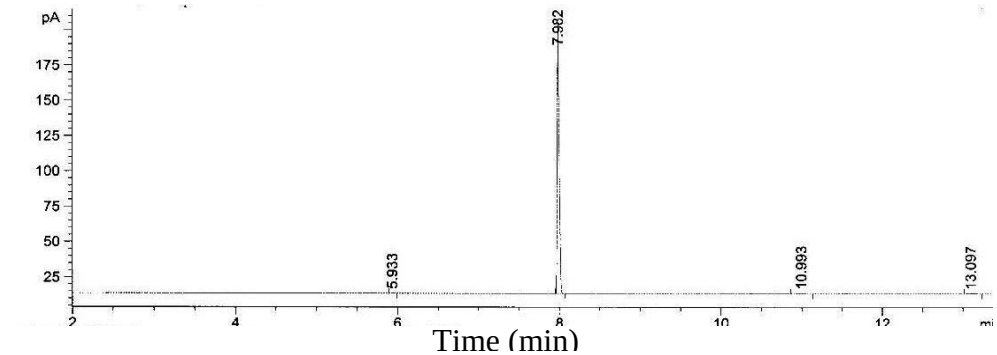

d)

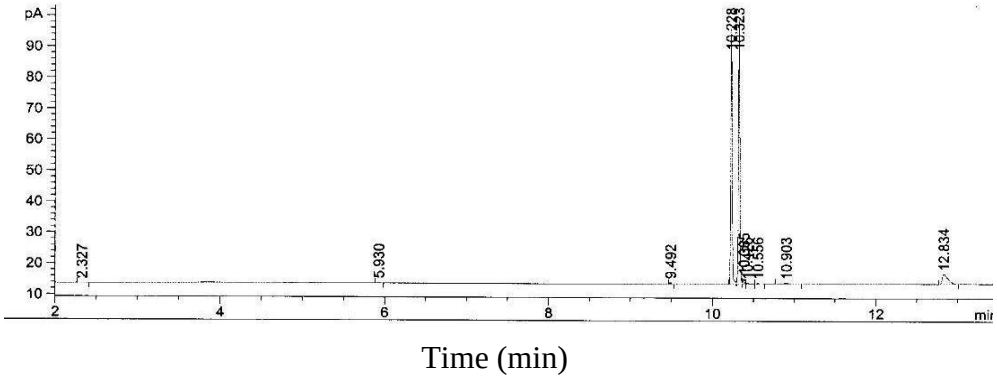

e)

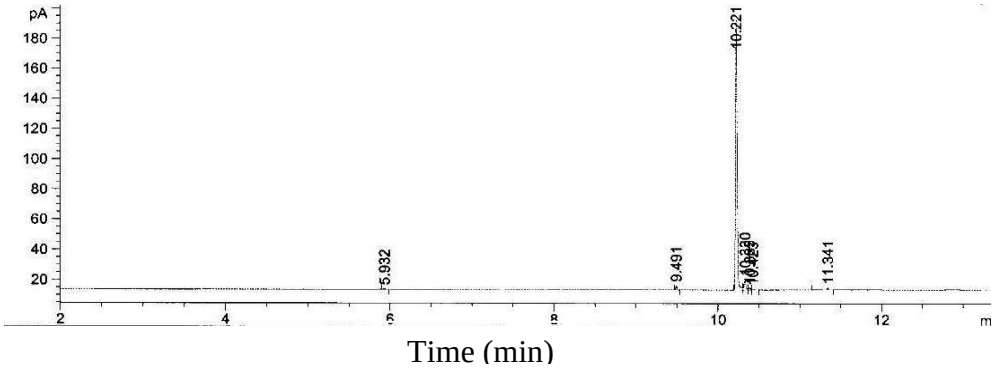

Figure 4.34 Continued.

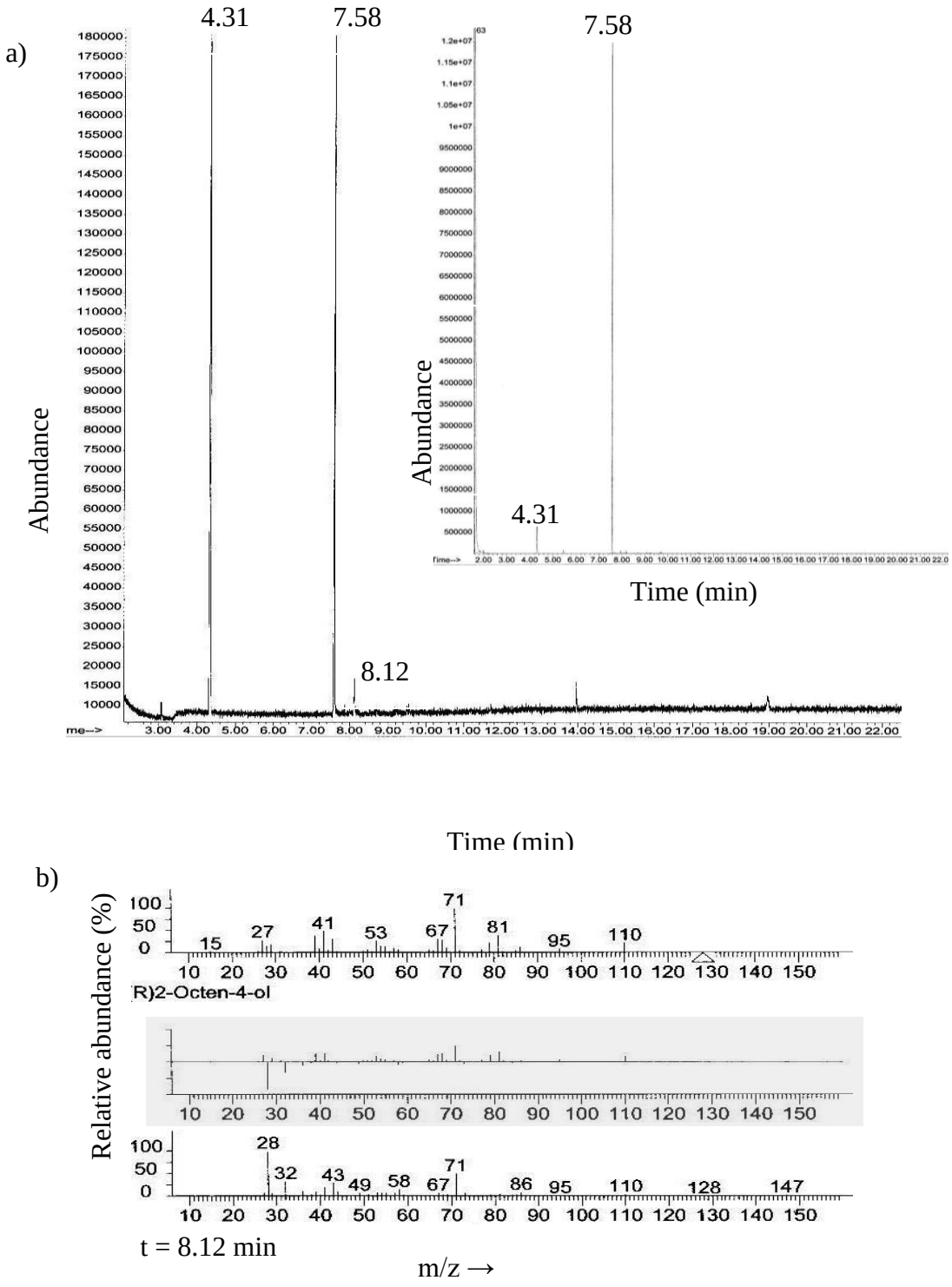

Figure 4.36. Analysis of reaction products from P450BM3 F87G and trans-2-octene in the presence of NADPH.

The enzyme was incubated with trans-2-octene and the products extracted as described previously (Figure 4.33). Extracts were analysed by Gas chromatography and Mass Spectrometry. Panel a) shows the retention times of the analytes separated by gas

chromatography and inset, the retention times of the standards trans-2-octene (4.31) and 2, 3-octene-oxide (7.58). The mass spectra of the GC separated analytes were also compared to the equipments internal library of compounds. Analytes were identified by matching to mass spectra of standard in the compound library; the difference spectra of the library compound subtracted from the unknown is shaded in blue in each case. The best match for the mass spectra of the peak at 8.12 min (b) identified the compound as 2-octene-4-ol.

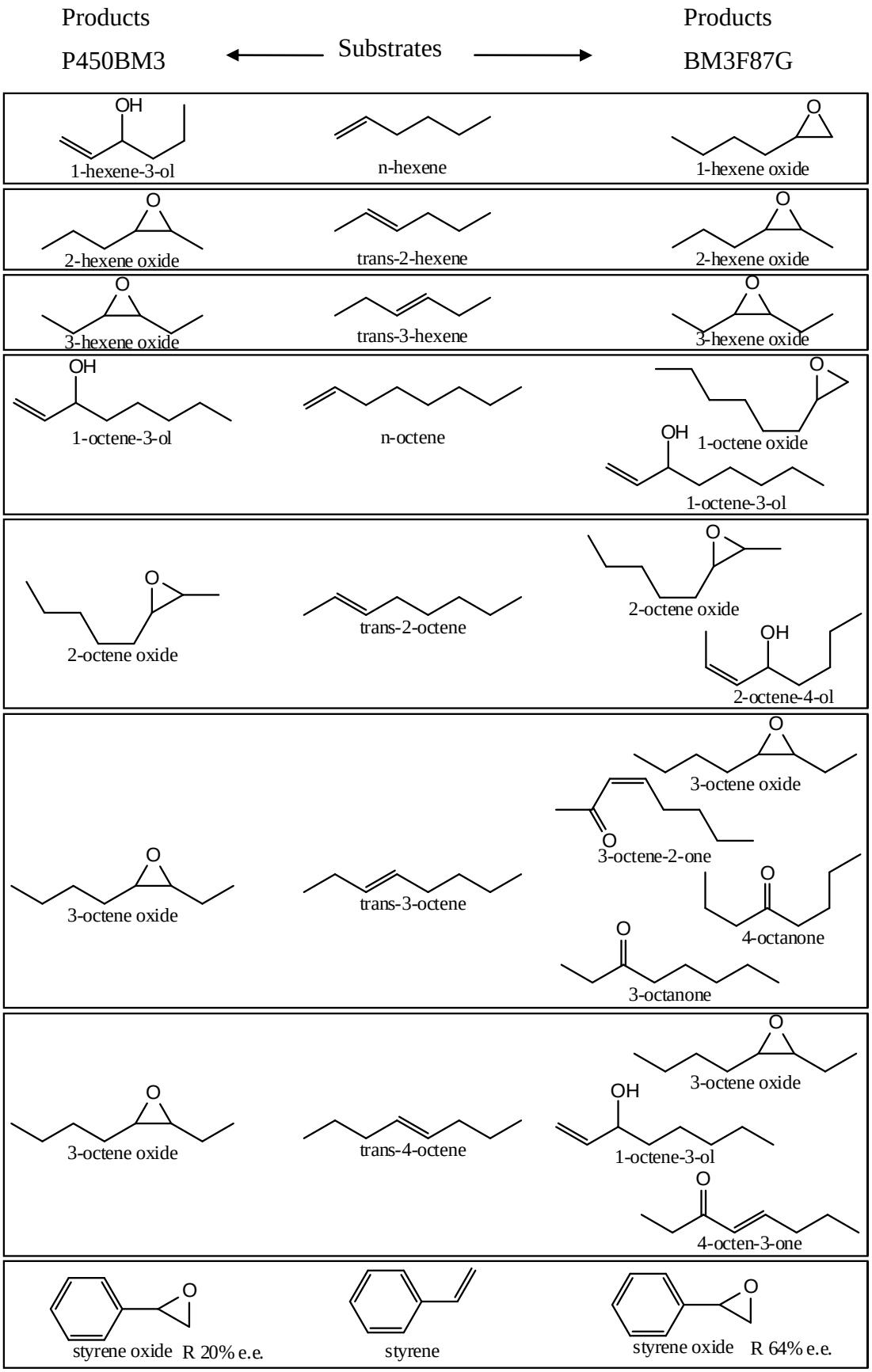

Figure 4.37. Structures of the substrates and their products from P450BM3 (left) and the F87G mutant (right) as identified by GC/MS.

	% converted to product		
Substrate	Product	BM3	F87G
1(n)-hexene	1,2-hexene oxide	*	*
Trans-2-hexene	2,3-hexene oxide	*	*
Trans-3-hexene	3,4-hexene oxide	*	*
1(n)-octene	1-octene-3-ol†	14	6
	1,2-octene oxide	n.d.	6
Trans-2-octene	2,3-octene oxide	62	47
	2-octene-4-ol†	n.d.	5
Trans-3-octene	3,4-octene oxide	79	7
	3 octanone†	n.d.	16
	4 octanone†	n.d.	7
	3-octene-2-one†	n.d.	3
Trans-4-octene	3,4-octene oxide *	80	16
	1-octene-3-ol†	n.d.	22
	4-octen-3-one†	n.d.	7
Decene	n.d.	n.d.	n.d.
Styrene	Styrene oxide	43 (R- 20% ee)	89 (R- 64% e.e.)

Table 4.4. Products identified from extractions.

* % converted could not be calculated, †products identified from GC/MS library only, n.d. no peak detected.

4.9.10 NADPH recycling using glucose dehydrogenase

Cofactor regeneration experiments were performed to establish whether an enzyme driven NADPH regeneration system could be used to drive the P450 reaction. Glucose dehydrogenase from *Cryptococcus uniguttulatus* (Sigma), in conjunction with its substrate glucose, was incubated overnight with the wild-type P450BM, NADPH (600 μM) and substrate (n-hexene, trans-2-hexene, trans-3-octene or styrene) as described in Methods. Any resulting products and remaining substrate were extracted into solvent and analysed by gas chromatography and mass spectroscopy (GC/MS) also as described (Methods).

Identification of analytes in the extracts was achieved by matching their column retention times (RT) and mass spectra with those of standardised substrates and products as well as the RT for the NADPH driven reaction (Figure 4.38). As described previously (section 4.9.9), the product standards used for comparison were either commercially available hydroxylated alkenes or alkene oxides (epoxides) manufactured in the lab using standard epoxidation chemistry as described in Methods.

The retention times for products identified from P450BM3 using the cofactor regeneration system were identical to those identified where NADPH only was used (summarised in Table 4.5).

Table 4.5 Retention times (RT) of products extracted from NADPH driven and Glucose dehydrogenase driven P450 monooxidations using P450BM3.

	NADPH		*Glucose dehydrogenase*	
substrate	RT	Product	RT	Product
n-hexene	3.26	1-hexen-3-ol	3.26	1-hexen-3-ol
trans-2-hexene	3	2-hexene oxide	3	2-hexene oxide
trans-3-octene	5.1	3,4-octene oxide	5.1	3,4-octene oxide
styrene	6.25	styrene oxide	6.26	styrene oxide

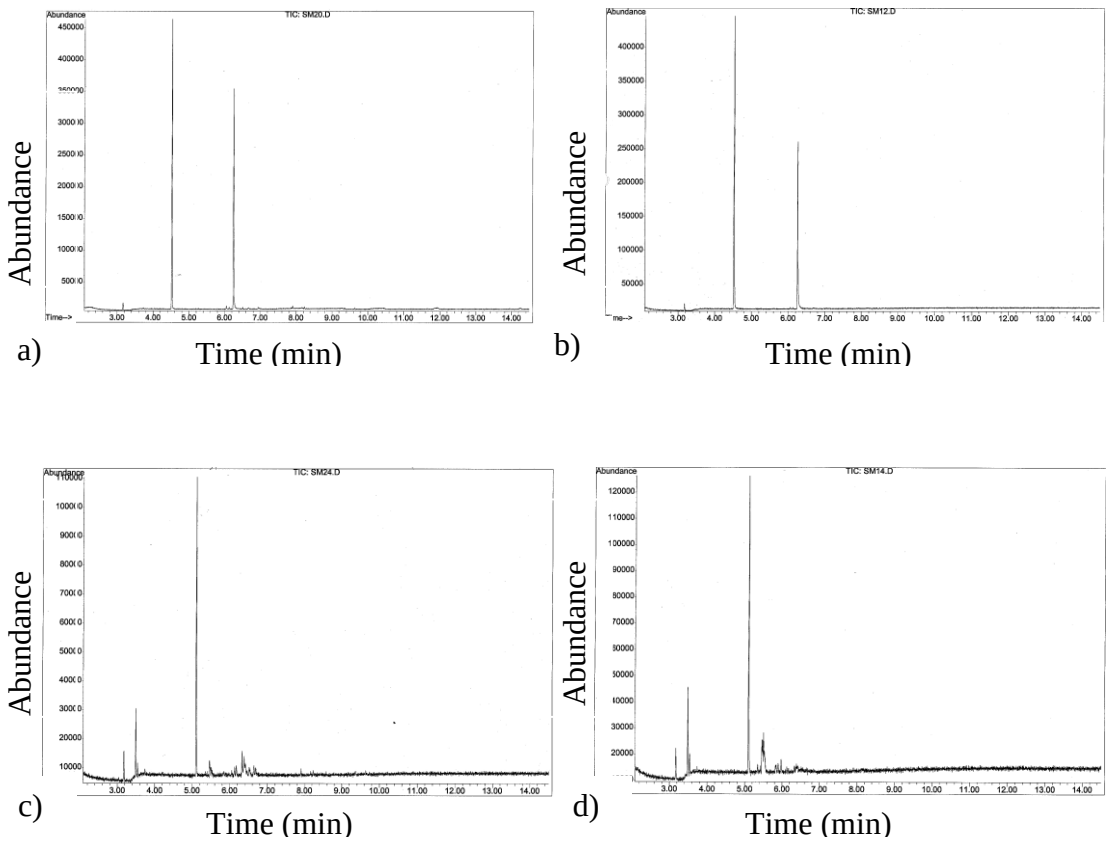

Figure 4.38 Gas chromatograms of products extracted from NADPH driven and Glucose dehydrogenase driven P450 monooxidations using P450BM3.

The retention times of the constituents of the extracts obtained from NADPH driven P450 monooxidation of a) styrene and c) trans-3-octene were matched against those obtained for Glucose dehyrogenase driven P450 monooxidation of b) styrene and d) trans-3-octene.

4.10 Discussion

Potential biotechnological applications for P450 BM3 already reported include, engineering the enzyme's activity towards shorter chain fatty acids (C4-C10) [61], toxic polyaromatic hydrocarbons [250] and short-chain alkanes [251]. The preliminary goal in this work, for development of P450 BM3 as a biocatalyst, was to investigate the enzymes latent potential to catalyse the epoxidation of short-chain alkenes and styrene and explore the effect of the active site mutant, F87G, on this activity.

The full-length and heme-domains of both wild-type and the F87G mutant were isolated and their interactions with alkenes and styrene as substrates examined. Comparison of the UV/visible spectra of the wild-type and the F87G mutant in various oxidation states show little difference in the key spectral features, *i.e.* the location of the Soret peak and α and β bands are the same for both wild-type and mutant (section 4.9.5). This suggests that the mutation has had no effect on either the oxidation state of the enzyme or the local electrical environment of the heme. However, inspection of the near UV end of the oxidised spectrum of F87G reveals a very high total protein/heme ratio despite the relative purity of the sample as judged by SDS-PAGE (Figure 4.18). This would suggest the mutation has effected incorporation and/or stabilisation of the heme within the enzyme and would correlate with observations made by Oliver *et al* on the related mutant BM3 F87A [252]. Purified samples of full-length and heme-domain BM3 F87A contained mixed populations of apo- and holo-enzyme with the primary loss of heme thought to occur during purification. Subsequent enzyme preparations used the addition of imidazole to buffers to stabilise the heme and secure a full complement of holo-enzyme. Heme deficiency was only observed in the full-length preparations of $BM3_{F87G}$ mutant, with low heme signals appearing from the outset of the purification scheme. Samples of heme-domain preparations of $BM3_{F87G}$ appeared to contain holo-enzyme only with no loss of heme signal during purification. It was therefore concluded that the mutation itself was not the probable cause of the loss of heme loss. An alternative explanation could be that the difference is an artefact resulting from the cell type and/or expression construct used. Expression of the $BM3_{F87G}$ full-length mutant is under the control of the T7 promoter and expressed in *E. coli* strain BL21(DE3)pLysS over a

period of less than 4 hours. The full-length and heme-domain of P450 BM3, and the heme-domain of $BM3_{F87G}$ are all under the control of the native promoter and expressed in *E. coli* TG1 over a period of 24-30 hours. It may be that the combination of the T7 vector and BL21(DE3)pLysS cells are less able to synthesise heme at the rate necessary for full heme incorporation. A lower IPTG concentration over a longer induction period could slow protein expression sufficiently to allow the cells time to synthesise enough heme for a preparation with a full heme complement. Addition of iron to the growth medium and/or addition of the heme precursor delta-aminolevulinic acid (δ-ALA) have also been shown to promote the synthesis of holo-enzyme in expression systems where this appears a problem [253, 254].

As these alterations to the protein preparation would increase cost and complexity in industrial scale-up a simpler alternative would be to recreate the full-length $BM3_{F87G}$ using site-directed mutagenesis and pBM23 (wild-type, full-length construct) as the template. Considering the fact that protein concentration is measured using the heme content and therefore based on active holo-enzyme, it was considered reasonable to continue with activity and product analysis in order to proceed in a timely manner. The time taken to create a second construct for expression of full-length $BM3_{F87G}$ would have prevented an opportunity to perform product analysis using GC/MS at Avecia.

A comparison of the reduced/CO spectra of the mutant and wild-type reveal a significant difference in the enzyme's ability to bind CO. In the wild-type, as with most P450's, the reduced heme will reliably bind CO causing a spectral perturbation characterised by a shift of the Soret peak to ~450 nm and fusion of the α and β bands, indicative of thiolate-coordinated (cysteinate) heme iron. The reduced/CO spectra of both the full-length and heme-domain of the F87G mutant shows incomplete conversion to the high-spin form and proved to be unstable as it collapses back to the low-spin form over approximately 2 hr. Formation of the P420 form is the result of protonation to form a neutral cysteine resulting in thiol-co-ordination of the heme iron [245]. It is essential for the cysteine to be de-protonated throughout the catalytic cycle and is required for oxygen activation [156, 163, 255]. The failure of $BM3_{F87G}$ to form a stable CO adduct may indicate that this mutant is more prone to cysteinate

protonation and may impact upon its catalytic activity. However, the rapid collapse of the ferrous heme back to 419 nm indicates this inactivation is reversible.

As mentioned earlier (section 4.9.6) the spectral perturbation observed upon substrate binding is a visual indicator of the alteration of the enzyme's spin state. Upon substrate docking, the axial water ligand is displaced, altering the spin-state equilibrium of the heme from predominantly low-spin *d*-electron configuration (S.1/2) to a primarily high-spin configuration (S.5/2) [192]. This perturbation is characterised by a Soret peak located at approximately 395 nm and a trough at 420 nm, the magnitude of the absorbance change indicating the strength or affinity of the substrate/enzyme complex [256]. Structural studies on CYP101 (P450cam) demonstrate that loosely fitting substrates are less able to displace the axial ligand (water) and thus the spin-state equilibrium remains in the low-spin configuration [193]. As expected wild-type showed very tight binding to arachidonic acid but no spectral perturbation was seen with alkene substrates, reflecting the wild-types known preference for mid- to long-chain fatty acids and demonstrating the alkanes inability to displace the axial ligand. Interestingly the F87G mutant displayed an approximate 3 fold reduction in affinity for the fatty acid and showed increased affinity to the imidazole inhibitor. The non-natural substrates, styrene and the alkenes containing sub-terminal carbon-carbon double bonds, induced measurable spectral perturbations which enabling calculation of an apparent Kd, albeit in the mM range. The Phenyl ring of F87 projects into the base of the active site and lies almost perpendicular to the plane of the heme in the oxidized substrate-free from of the enzyme. The binding data presented here implies that the removal of the bulky phenylalanine from the base of the substrate access channel allows bulkier substrates (styrene and 4-phenylalanine) better access to the active site permitting tighter binding. Work on another F87 mutant, F87A, which used NMR to monitor substrate motion upon binding and reduction, indicated that the methyl terminal of the substrate moved past the position it usually holds in the wild type, ending up approximately 2 Å closer to the heme [59]. This may also be true for the $BM3_{F87G}$ and account for the short-chain alkene substrates apparent increase in affinity.

As previously described, reduction of the mid-point potential (i.e. less negative) is a prerequisite for the binding and subsequent activation of dioxygen (Section 4.6). The

glycine substitution at F87 appears to have increased the redox potential of the enzyme in its resting state, making it more negative and thus providing an even larger barrier to futile electron transfer from FMN to heme in the absence of substrate. However, when fatty acid is bound, the mid-point potential is more than 150 mV less negative than the wild-type. Whilst this provides complete removal of the electro negative barrier, it may have implications for catalytic activity, perhaps removing a level of control over the timing of electron transfer and causing some electrons to be lost, thus reducing the efficiency of the reaction.

Comparison of the stead-state kinetic parameters for the wild-type and F87G mutant reveal an alteration in the enzymes substrate specificity (Table 4.3). Replacement of F87 with glycine has reduced the k_{cat} for arachidonic acid by a factor of 8 and whilst the Km has remained in the same order of magnitude the catalytic efficiency, as measured by Kcat/Km, is reduced by a factor of 12 overall. The glycine substitution has also affected the enzyme activity with the alkene substrates. Whilst in the majority of cases the k_{cat} for F87G with the alkene substrates is increased by a factor of 1.5 - 3 there are more marked differences in the Km which increases the catalytic efficiency by much more. For example the k_{cat}/K_m for F87G with n-hexene and n-octene is 15 and 24 fold higher respectively than that for the wild type. It is interesting the note that as the location of the double bond moves further away from ω- terminal the overall improvement in catalytic efficiency seen with the F87G mutant and the alkene substrates becomes markedly reduced. It is clear from the kinetic data (Table 4.3) that both the wild type and F87G mutant enzymes are active with styrene and these alkene substrates, at least in the sense that they are oxidising NADPH and cycling electrons. The F87G mutant exhibits broadened substrate specificity in favour of the shorter chain hydrocarbons and styrene, with as much as 24-fold increase in catalytic efficiency for *n*-octane. Although the rates recorded are several-fold slower than those with arachidonic acid, they are substantially faster than rates typically reported for most eukaryotic P450s and their favoured substrates [257]. This may relate to the efficiency of the P450 BM3 redox system, i.e. FMN-to-heme electron transfer is rapid in BM3 compared to other class II P450 systems. Thus, electron transferase activity is rapid, even with poorer non-lipid substrates.

Due to circumstances beyond my control the time available for completion of experimental work was cut short by a total of 10 weeks during the latter half of the project. As previous analysis of $BM3_{F87G}$ revealed less than 10% uncoupling of NADPH oxidation from fatty acid oxidation a strategic decision was taken to prioritise the analysis of reaction products ahead of measuring reaction efficiency. Analysis of products generated by the enzymes confirmed that not only are the wild type and mutant enzymes oxidising NADPH but that they are generating specific products which are different from one another. These data clearly demonstrate that, in the case of the wild-type, where a double bond is located at the terminal position or at position 4 (in the case of trans-4-octene), P450 BM3 hydroxylates the alkene at the third carbon (ω-2), when the double bond is located at position 2 or 3 the wild-type enzyme performs an epoxidation reaction, yielding a single product from each substrate. This is in agreement with its know function as a sub-terminal fatty acid mono-oxygenase [223]. The F87G mutant on the other hand appears to have lost some regio-selectivity, yielding a much wider range of products from a single substrate, performing a hydroxylation or epoxidation reaction at ω-1, ω-2 or ω-3. This is consistent with the known effects of other F87 mutants (F87A/V) which exhibit similar loss in regio-selectivity [251]. This would indicate that whilst the removal of the phenylalanine ring allows the alkene substrates to approach closer to the heme, the substrate is now less restricted within the active site, thus allowing presentation of alternate activation sites to the oxygenated heme. In both cases the enzymes demonstrate a preference for oxidation at the end closest to the location of the double bond. This would indicate that the substrates proceed into the active site with the double bond end leading first.

Possibly the most interesting result is the effect this mutation has on the affinity for and activity towards styrene. Not only does styrene cause detectable perturbation of the UV/visible spectra and show some increased catalytic activity in $BM3_{F87G}$ (a 2 fold increase in k_{cat}) but the product analysis shows this mutation increases the percentage of substrate converted to product from 43% to 89% and significantly increases the amount of *R*-styrene oxide from just 20% ee to 64% ee. These data compare well with documented findings that this mutation increases the stereo-selectivity to a similar compound, 3-chlorostyrene, as well as increasing catalytic activity towards this substrate [241]. This is economically significant as

enantiomerically pure *R*-styrene oxide is difficult to obtain in large quantities and is, therefore, more expensive than pure *S*-styrene. A biocatalyst that can transform styrene into *R*-styrene oxide in high enantiomeric excess would be extremely useful in chiral synthesis.

4.11 Conclusion

The results reported here show that $BM3_{F87G}$ does indeed alter substrate specificity and regio- and stereo-selectivity of olefin oxidation. As the kinetic and analytical data demonstrate, despite P450 BM3 showing no spectral perturbations when incubated with the alkenes, these substrates clearly interact with the enzyme and are transformed by it. To assess the strength of the interaction, competitive binding experiments could be performed in the presence of the strongly binding arachidonic acid to establish a value for the dissociation constant for each of the non-fatty acid substrates. In addition, fluorescence measurements to monitor the effects of binding on tryptophan residues in the active site could also provide information regarding the nature and strength of the interactions.

Any consideration of further work on this mutant should include an analysis of the reaction efficiency, to measure to what extent electron transfer is being coupled to product formation. As discussed earlier (Section 4.6) it is possible for electron transfer to become uncoupled from substrate oxidation during the P450 cycle, causing the release of reactive oxygen species or water instead of oxygenated product. The extent of electron transfer coupling is typically measured by colorimetric or fluorimetric assays using horse radish peroxidase to detect peroxide [258-260]. However, this would only measure the amount of peroxide formed and would not provide information regarding electrons lost in the form of reactive oxygen species or water. A more indirect but inclusive approach would be to quantify the products formed from the reactions, discussed below.

The product analysis results reported here are primarily qualitative, at best providing an indication of the ratio of product to remaining substrate. Quantification of product requires the use of either an internal standard or a calibration curve. Extraction procedures are not 100% efficient and depend on the combination of the solvent and its volume and the number of times the extraction procedure is applied [261]. The use of an internal standard (introduced prior to extraction) would enabled quantification of substrate/product within the sample and provided an assessment of the extraction procedure efficiency. Additional data regarding reaction rates could also be gained by performing these extractions at timed intervals to determine definitive product

formation rates. Any continuation of work on this mutant should tackle should include determination of the efficiency of the reaction.

It should be noted that the aqueous solubility of the alkene substrates and styrene is very poor, less than half a gram per Litre in all cases [249]. Despite this low solubility the reaction velocities still apparently increased with increasing alkene and styrene concentrations, beyond the limit of their solubility's. If the enzyme were only interacting with the substrate dissolved in the aqueous phase, one would expect the reaction velocity to level off at the same concentration at which the aqueous solubility of the substrate is reached i.e. 0.7 mM for hexene and 0.03 mM for Octene. The Km values reported are significantly higher e.g. between 1.4 -15 mM for the octenes, which would imply that the enzyme is interacting with the substrate in the organic phase. It may be worth investigating whether P450 BM3 and its mutants could perform catalysis in biphasic media and observing the effects on reaction rates and products. Successful in-vitro experiments using Beyer villager mono-oxidises (BVMO) in a two-liquid-phase system (aqueous phase and water –immiscible solvent phase) have been performed using a thermostable alcohol dehydrogenase to recycle NADPH [2]. The solvent acts as a substrate reservoir and product sink, holding the bulk of the hydrophobic substrate and product away from the enzyme. Extraction of the product is made easier from the organic phase and the solvent can be recycled which combine to reduce production costs [122].

It may also be possible for BM3 (or mutants thereof) to perform biotransformations solely in organic solvents i.e. total removal of the aqueous phase. Solvents have been shown to enhance reaction rates [262, 263], improve enzymes stability [264] and most interestingly alter the substrate specificities of enzymes [265] when water has been removed. As de-hydration of the biocatalyst is a necessity in solvent based reaction, the effect of the removal of water as the 6^{th} axial ligand on the redox potential and catalytic control of P450 BM3 would need to be taken into consideration but could potentially yield interesting and informative results.

In order to extend and explore the potential of P450 BM3 as biocatalyst, it would be beneficial to combine this mutant with others known to modify the enzymes specificity in combination that have not been explored previously. For example, the active site mutant BM3A82F has recently been described [234]. Binding studies and

structural data on this mutant demonstrate it has an altered substrate binding mode promoting increased affinity for fatty-acid substrate and increased spin-state shift to high-spin upon substrate binding. The mutant also demonstrates improved catalysis of indole hydroxylation suggesting increase activity toward smaller aromatic substrates. The residue at position 82 lies over F87 in the active site if and the crystal structure of BM3A82F shows F82 to lie between F81 and F87. It is conceivable that a double mutant containing F87G and A82F could substantially alter the activity of P450 BM3 toward small, cyclic and aromatic compounds such as styrene and indole and as such would be worth investigating as a next step in engineering BM3 as a biocatalyst for industrial biotransformation.

5 Modification of P450 BM3 heme domain to allow photo-induced electron transfer

5.1 Outline

A major obstacle to the economical use of cytochromes P450 as biocatalysts is the requirement for stoichiometric amounts of the cofactor NAD(P)H, which is expensive to produce and liable to decompose over time. In the case of P450 BM3 this is confounded by the fact that the enzyme is known to be inhibited by NADPH in the absence of substrate. In an effort to circumvent the necessity for NADPH during *in vitro* catalysis, a structure-guided approach was taken to develop the heme-domain of P450 BM3 for photo-induced electron transfer. A number of non-conserved amino acids were mutated to cysteines in preparation for the attachment of photo-sensitive chemical agents that may allow photo-induced electron transfer to the heme and thus negate the requirement for not only NADPH but also the labile reductase domain. These mutant heme-domains were analysed to assess the impact on the enzyme/substrate functional relationship and to determine whether the mutated residues were accessible to thiol-modifying agents.

5.2 Introduction

As discussed previously in Chapter 4 (section 4.2) the interest in using cytochromes P450 as biocatalysts arises from their ability to catalyse mono-oxygenation reactions on a diverse array of substrates, performing addition of functional groups to inactive hydrocarbon compounds in a stereo- and regio-specific manner. This capacity can and has been utilised in the synthesis of fine chemicals and the detection and detoxification of environmental contamination [3, 5, 266]. One major obstacle to the economical use of cytochromes P450 as biocatalysts is the requirement for stoichiometric amounts of cofactors (e.g. NADPH) which are expensive and prone to time-dependant decomposition. Various methods have been explored in the search for solutions to this problem, encompassing cofactor regeneration and direct or mediated electrochemistry.

By performing biotransformations *in vivo* with microbial cells expressing the recombinant biocatalyst, the cofactors are regenerated by the organisms' metabolism. An additional advantage of whole cell systems is the stabilisation it provides for multi-component systems and membrane bound monooxygenase such as AlkB. Whilst whole cell biocatalysts are in common use [267-269] they are not without their limitations. Stability and efficiency of the cofactor regeneration system requires the use of metabolically active cells [2, 270] and the associated additional nutrient requirements. Reaction products are often toxic to the host organism and there may be significant transport limitations of substrate and/or product across the cell membrane. Further problems are associated with the recovery of the reaction products from fermentation broth and the propensity of further degradation of the reactions products. It has also been shown that, in some cases, the k_{cat} of a biocatalyst expressed in a recombinant system is lower than in the native host, as in the case of membrane bound AlkB [106] and xylene monooxygenase [271] from strains of *P. putida*.

In cell-free biocatalysis, cofactors are regenerated by purified enzymes. For example, formate dehydrogenase which catalyses the oxidation of formate anions to carbon dioxide has been successfully used to recycle NADPH for immobilised P450 BM3 on a small scale [272]. As *in vitro* cofactor recycling protocols require additional

protein(s) ‘self-sufficient’ enzymes like BM3 are ideal as this limits the number of purified proteins required. Recycling of NAD(P)H using indirect electrochemical regeneration of NAD(P)H has also been explored [273].

An alternative approach to reducing the costs associated with using NADPH as cofactor is engineering the NADPH dependant reductase to accept electrons from NADH instead. NADH is significantly cheaper than NADPH, it is more stable and there are a wider variety of cheaper cofactor regeneration enzymes commercially available [274]. Recent developments in switching the preference of human cytochrome P450 reductase and the reductase domain of P450 BM3 enzymes towards NADH have focussed on mutation of a key tryptophan residue,W676 and W1046 in each enzyme respectively, which is conserved across the ferredoxin/ferredoxin reductase family as well as the diflavin reductases, [275, 276]. Whilst the results of these studies are promising, the switch to using NADH is not yet sufficient to find application in industrial biocatalysis.

Although significant advances in cofactor regeneration have been made there are obvious advantages to pursue the development of cofactor independent biocatalysts. A number of P450s are capable of utilising peroxide as a source of oxygen, employing the peroxide shunt pathway; sidestepping the requirement for cofactor (section 4.6) [9, 10]. However, with the exception of CYP152A1, a peroxygenase from B. *subtilis*, the enzymes are quickly inactivated by oxidative damage to the heme [184]. Various attempts have been made to engineer peroxygenase activity into other P450s. For example, the F87A and F88A mutants of P450 BM3 and its *B. subtilis* homologue CYP102A2 respectively improve the initial activity of peroxide driven reaction but activity is quickly depleted by inactivation [201][13, 14]. Successive rounds of directed mutation on P450 BM3 have produced a mutant with almost 20 fold higher activity than F87A, whilst still retaining the same product profile as those of the NADPH driven reactions [243]. Further developments in this area also include the global incorporation of norleucine in place of methionine. Whilst this increased peroxygenase activity, it also reduced thermal stability [277]. Subsequent engineering to improve the thermal stability only reversed the beneficial increase in peroxidase activity [278].

Methods used to drive NADPH *independent* P450 catalysis have included mediated and direct electrode-driven catalysis. Successful mediated electro-catalysis (e.g. cobalt(III) sepulchrate or cobaltocene) using P450cam and CYP4A1 (rat) have both demonstrated hydroxylation initial rates comparable to those achieved with NADPH [279-281]. However, the propensity for the mediators to reduce molecular oxygen at the electrode surface causes formation of peroxide, resulting in heme degeneration and quickly reducing the activity by 90% over 30 minutes [281]. The inclusion of catalase to mop up H_2O_2 reduces the loss of activity to just 30% over 30 min. A degree of success has also been achieved by incorporating P450cam into thin lipid films [282] and polyion layers [66]. The direct electron transfer from electrode to heme needs neither mediator nor redox partner. However, the distance between the proteins and electrode is critical with only those layers closest to the electrode capable of full electro-activity and electron transfer rates are disappointingly ($<0.01s^{-1}$) [66, 282]. The electron transfer rate can be improved by adsorbing the enzyme onto clay coated electrodes, effectively forming a clay-bridge between the electrode and P450cam [68].

The work presented here explores the potential of photo-sensitive chemo-reductants to drive electron transfer as an alternative to cofactor regeneration or direct electro-chemistry. Photosynthetic proteins are able to harness light directly to drive electron-transfer reactions. Modifying non-photosynthetic systems to harness light energy in order to drive biocatalysis could have significant economical benefits in the field. A useful consequence of direct photo-induced electron transfer in photosynthetic systems is the relative ease with which time-resolved intra- and inter-protein electron transfer can be monitored. Traditional measurement of non-photosynthetic biological electron transfer is limited by the time taken to mix reactants, typically 100-500 microseconds for methods like stopped-flow. As electron transfer typically occurs in the in femto- to milli-second time scale these methods hinder time-resolved measurement of electron transfer. The last twenty years has seen improvements in the methodology used to measure electron transfer in non-photosynthetic systems. A variety of external photosensitive agents have been used to initiate electron transfer in these systems including: flavins [283], ruthenium complexes [284-286], zinc substituted porphyrins [287, 288] and more recently the sulfo-aromatic compound thiouredopyrene-3,6,8-trisulfonate (TUPS) [289-292]. It may be possible to adapt the

methodologies used to study electron transfer to drive catalysis by photo-induced electron transfer.

Of the photo-sensitive agents used to study electron-transfer, the use of ruthenium complexes is probably the most common in the literature, particularly in the study of cytochrome c and its interaction with redox partners [285, 293-295]. Ruthenium (Ru(II), in organometallic complexes, can easily be excited by exposure to visible light. In its excited state is acts a strong reducing agent and can be used as a photo-reductant either free in solution or by using Ru(II)-protein derivatives [284, 295, 296]. Modifying proteins in this way, by covalent attachment of the Ru(II) complex to a histidine residue has the benefit of maintaining fixed distances between electron transfer centres. This allows for investigation of distance dependence on electron transfer and eliminates the effect that random interaction in solution may have on electron transfer rates.

More recently, the sulfo-aromatic compound TUPS has been used as an alternative. TUPS is the thioredo adduct form of 1-isothiocyanatopyrene-3,6,8-trisulphonate (IPTS), which is formed when the dye conjugates to an amino acid. Amino acid conjugation to IPTS causes a reduction in the compound's fluorescence intensity and a concomitant rise in phosphorescence. A single photon is able to convert it to its triplet state TUPS* which is an efficient initiator of electron transfer. The efficiency of the reaction is due to the high yield of the triplet state (30% quantum efficiency), its long lifetime (~0.5 ms) and low redox potential [289]. Photo-excitation of TUPS-modified cytochrome c has been shown to be far more efficient than that of ruthenated cytochrome c [291, 293, 294]. The TUPS molecule is also smaller than ruthenium complexes at ~ 7Å in diameter which supports better access to partially buried reaction centres.

Laser driven photo-excitation has been successfully observed in TUPS-modified cytochrome c [297] and azurin [290, 298] as well as between TUPS-modified cytochrome c and cytochrome c oxidase [291]. Photo-excitation of TUPS can be achieved using a short, low energy (2 ns, 3 mJ/pulse) laser pulse. The protein is not damaged by this exposure and it is, therefore, possible to repeat the redox cycle several hundred times without altering the observable electron transfer rates [290]

The proximal face of the heme is the side closest to the protein surface and has been proposed to be the P450 redox partner docking site [211, 299]. The crystallographic data on a complex between the heme and FMN domain of P450 BM3 supports this hypothesis (Figure 5.1). A 967 $Å^2$ area of the proximal side of the heme domain is shown to interact with the FMN domain, bringing the 7-methyl group of the flavin to within 20 Å of the heme and makes close contact (~4 Å) with I385 and Q387. The interaction appears to be specific but not particularly strong owing to the precise positioning of the FMN molecule and the limited direct contacts between the domains: a salt bridge, two hydrogen bonds and a few water mediated contacts [300]. It is likely that attachment of any photosensitive chemo-reductants should occur at this site. Previous work using a ruthenium complex has demonstrated that this is possible and shows a strong electronic coupling between residue 387 and the iron [301].

The aim of the work presented in this chapter was to engineer a number of sulfhydryl groups onto the proximal surface of the heme domain of P450 BM3 so as to facilitate attachment of thiol modifying, photo-sensitive agents, e.g. TUPS. The ultimate goal being, to explore the potential for photo-induced electron transfer and light driven biocatalysis.

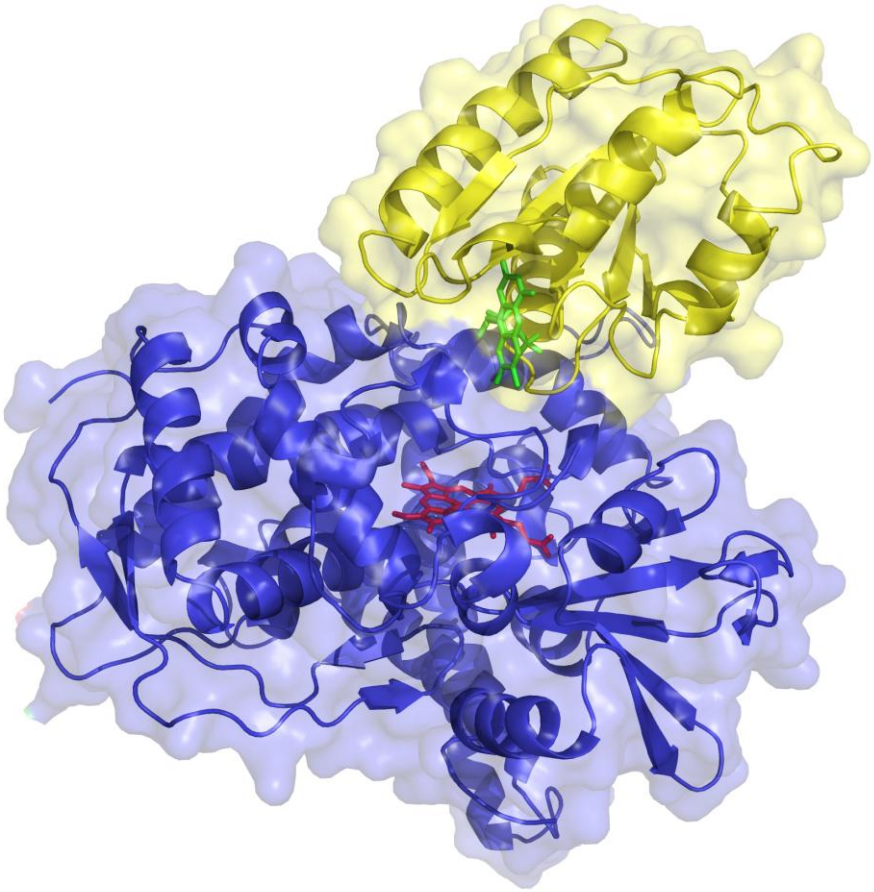

Figure 5.1 Atomic structure of the heme-FMN domain complex of P450 BM3.

Showing the FMN domain (yellow) interfacing with the proximal side of the heme domain (blue) (PDB-ID 1BVY [300]). The heme and FMN are represented as red and yellow sticks respectively. Image rendered using PyMOL [209].

5.3 Results

5.3.1 Design of the P450 BM3 heme-domain mutants

Electron transfer between complexes is mediated by small diffusible molecules like quinones or small electron transfer proteins like cytochrome c [302]. The majority of electron transfer events in biological systems occurs via outer sphere or non-bonded means where electrons hop through space rather than proceed via covalent linkage between redox partners due to the steric hindrance imposed by protein structure on the redox centres. Although the optimum separation distance for redox partners has been calculated to be 6 Å, inter- and intra-protein electron transfer tends to be long-range, occurring over distances greater than 10 Å and in some cases over 30 Å [303]. Therefore, distance must be taken into consideration when choosing the location of any electron donor attachment.

The amino acid cysteine provides an appropriate sulfhydryl group suitable for covalent attachment of TUPS. The sequence of native BM3 contains only three cysteines, one being the invariant heme-ligating cysteine (C400). The other cysteines, C62 and C156, are both solvent accessible, but only C62 is close enough to the heme (well within 20 Å) to potentially support electron transfer. Additional sites chosen for mutation to cysteines were selected on the following criteria: they should not be conserved nor known to be essential for activity; they should be solvent accessible to allow covalent attachment of thiol modifying agent; they should be within a 20 Å sphere of the heme to allow electron transfer.

According to the amino acid sequence (Figure 5.2) and crystal structure of the heme-domain (Figure 5.3), a number of non-conserved residues within the heme-binding loop approach close enough to the heme in the three-dimensional structure, 387, 397, 403 and 404. The distances from the heme iron to the α–carbon of each of the residues ranges from 5.8 Å to 18.6 Å and coincidentally, all the chosen residues are glutamine residues in the native enzyme.

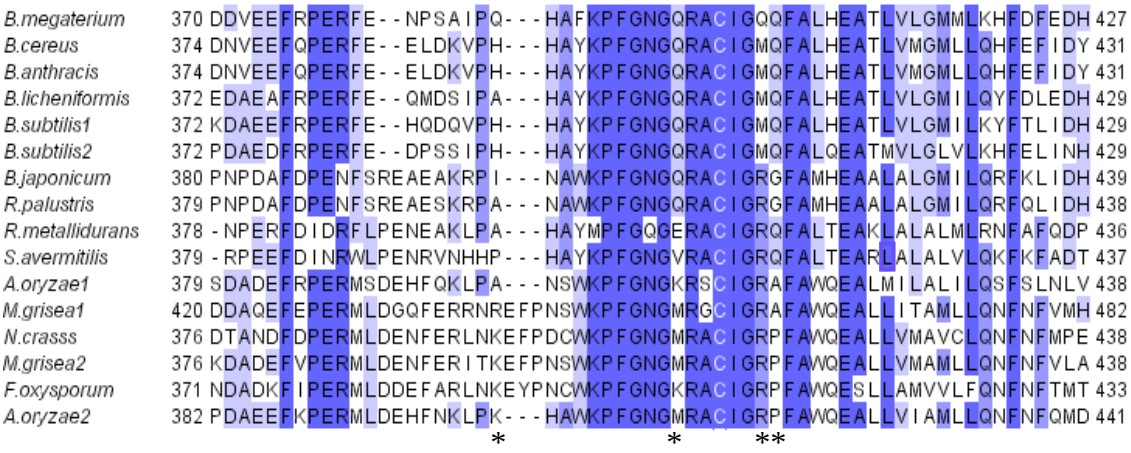

Figure 5.2 Sequence alignment of P450 BM3 with homologous proteins found in other organisms.

The alignment shows the section either side of the heme-ligated cysteine (C400 in BM3). Sequence conservation is indicated by shades of blue with dark blue for completely conserved to white for non-conserved residues. The conserved cysteine (C400 in BM3) is shaded blue with white text. Stars (*) indicate the location of the non-conserved residues within 14 Å of the heme. Sequences are ordered according to pairwise alignment to P450 BM3 from B. megaterium. The sources of the data are as follows; *Bacillus megaterium* [25], *Bacillus cereus* [26], *Bacillus anthracis ames* [27], *Bacillus licheniformis* (strain DSM 13 / ATCC 14580) [28], *Bacillus subtilis* [29], *Bradyrhizobium japonicum*[304], *Rhodopseudomonas palustris* (strain BisB5) [305], *Ralstonia metallidurans* (strain CH34) [305], *Streptomyces avermitilis* [306], *Aspergillus oryzae*, *Neurospora crassa* [307], *Magnaporthe grisea* (Rice blast fungus) [308], *Fusarium oxysporum* [173]. Sequences aligned using ClustalW2 [78], image produced using Jalview [309].

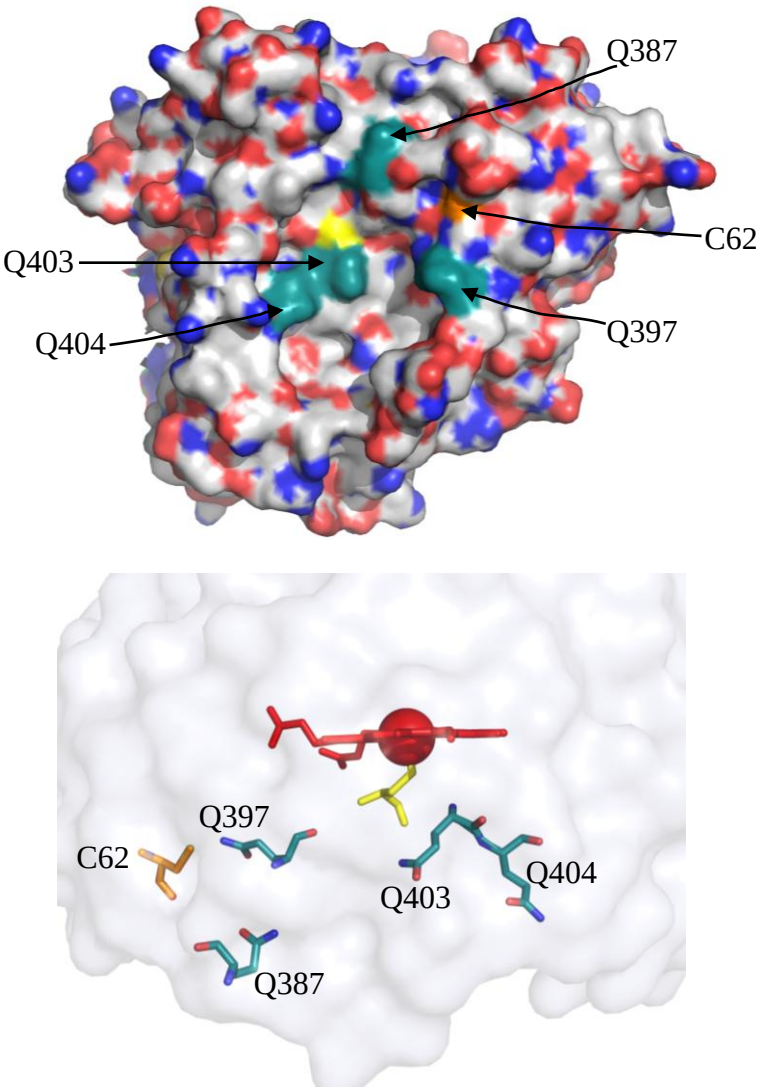

Figure 5.3 Structure of the heme domain of P450 BM3 showing location of the proposed sites for incorporation of sulfhydryl groups.

GRASP diagram (Graphical Representation and Analysis of Surface Properties) from the proximal side of the heme (A) and view along the plane of the heme (B) showing the position of C62 and the four non-conserved glutamine residues within 20 Å of the heme. Heme is shown as red sticks with the iron as a sphere; heme ligated cysteine (C400) is shown as yellow sticks; C62 and the four glutamine residues (Q387, Q397, Q403 and Q404) are shown as orange and cyan coloured sticks respectively. Distances of heme–iron to α-carbon: Q403 = 5.8 Å, Q404 = 9.4 Å, Q387 = 18.6 Å, Q397 = 12.4 Å, C62 = 16.9 Å. Image rendered in PyMOL [209] using PDB-ID 1FAG [230].

5.3.2 Site-directed mutagenesis

The amino acid sequence [62] for the heme domain was used to locate the codons for the four glutamine residues Q387, Q397, Q403 and Q404 that would be mutated to cysteines. For the purposes of stability during the annealing process a minimum of 9 base pairs were selected either side of each of the four codons and all primers were designed to end in GC. As a result of these requirements, the incorporation of a silent mutation to engineer a unique restriction site to enable a simple verification step based on restriction analysis was not possible. A sequencing primer (TUPSeq), which matched the sequence immediately preceding the mutated sections, was therefore designed to allow sequencing verification of the mutation. The oligonucleotide primers are described in Table 5.1.

Mutation	*Primer Name*	**Primer Sequence (5'→ 3')**
$BM3_{Q387C}$	Q387CF	CCAAGTGCGATTCCG**TGT**CATGCGTTTAAACCG
	Q387CR	CGGTTTAAACGCATG**ACA**CGGAATEGEACTTGG
$BM3_{Q397C}$	Q397CF	GCGTTTAAACCGTTTGGAAACGGT**TGT**CGTGCGTGTAT CGG
	Q397CR	CCGATACACGCACG**ACA**ACCGTTTCCACCAGGTTTAAA CGC
$BM3_{Q403C}$	Q403CF	GCGTGCGTGTATCGGT**TGT**CAGTTCGCTC
	Q403CR	GCGAACTG**ACA**ACCGATACACGCACG
$BM3_{Q404C}$	Q404CF	GCGTGTATCGGTCAG**TGT**TTCGCTCTTCATGAAGCAAC GC
	Q404CR	GCGTTGCTTCATGGAGAGCGAA**ACA**CTGACCGATACAC GC
Sequencing	TUPSeq	GCGTTTAAACCGTTTGGAAACGGTTGTCGTGCGTGTATC GG

Table 5.1 Oligonucleotide primers for site-directed mutagenesis. Codon mismatches are shown in bold.

Mutagenesis was performed on pBM20 using the 'QuickChange' Site-directed Mutagenesis Kit (Stratagene) to construct a total of four, single-point glutamine to cysteine mutants, Q387C, Q397C, Q403C and Q404C. QuickChange allows for site specific mutation without the need for sub-cloning. The plasmid pBM20 was incubated with the relevant primers under the conditions described in Methods. The resultant samples were subject to digestion with *Dpn*I and analysed by agarose gel electrophoresis as described in Methods. In the case of Q397C and Q404C it was necessary to increase the number of PCR cycles from 16 to 18 to achieve sufficient amplification. Agarose gel electrophoresis of the products of QuickChange mutagenesis showed plasmids of the correct size after digestion with *Dpn*I (Figure 5.4a).

The plasmids, now termed $pBM20_{Q387C}$, $pBM20_{Q397C}$, $pBM20_{Q403C}$ and $pBM20_{Q404C}$, were then used to transform *E. coli* NOVABlue cells and DNA preparations were made from a selection of single colonies. Each DNA preparation was then subject to agarose gel electrophoresis and. The plasmid preparations from several colonies transformed with $pBM20_{Q397C}$ were subject to electrophoresis and visualised under UV light (Figure 5.4b). The presence of 5 bands of DNA at approximately 2.3 kbp was as expected for a circular plasmid of almost 4.6 kbp. Similar results were obtained from the transformants of $pBM20_{Q387C}$, $pBM20_{Q403C}$ and $pBM20_{Q404C}$ (data not shown).

A minimum of two DNA preparations for each of the mutations were sent for sequencing to confirm the presence of the mutation at the correct position. Plasmid preparation samples (2-3 of each mutant) were sent for sequencing using the sequencing primer TUPSeq to identify samples containing the correct mutation. Samples containing the correct mutation were then sent for full sequencing using the following primers which span the entire plasmid sequence of pBM20; TACCGGAAGACATGACACG (starting at nucleotide 447); TCCTGCGTTTTCCCTATAT (starting at nucleotide 1009); TTCACACAGGAAACAGCTAT (starting at nucleotide 4553); (Dr Hazel Girvan, Dept. of Biochemistry, University of Leicester). Sequencing results were analysed by alignment with the known DNA sequence of pBM20 to confirm the absence of any unplanned mutations (Figure 5.5).

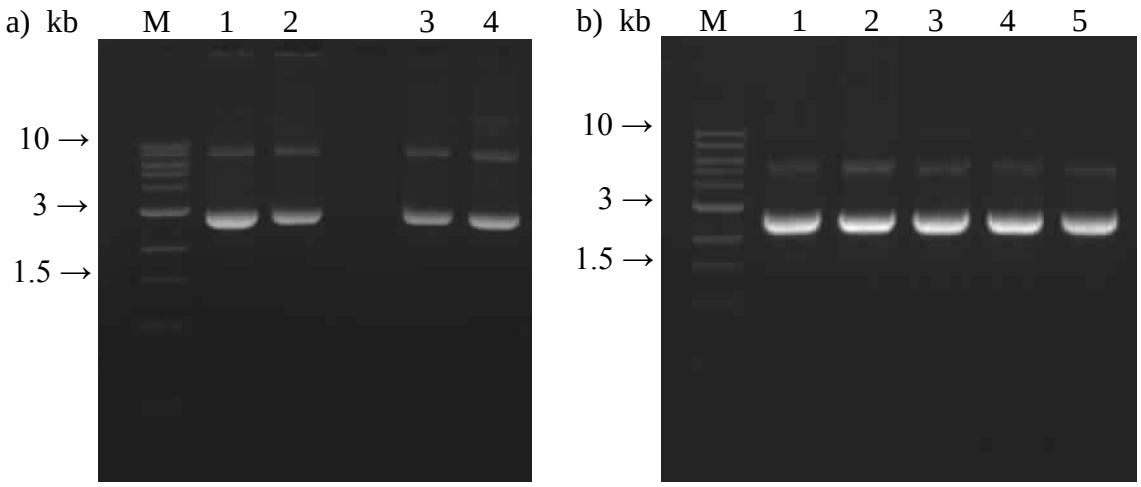

Figure 5.4 Analysis of mutagenic PCR performed on pBM20 to replace glutamine residues Q387, Q397, Q403 and Q404 with a cysteine.

Panel a) The plasmid pBM3 was incubated with the mutagenic primers under the condition described in Methods. The resultant PCR products were subject to digestion with *Dpn*I restriction endonuclease as per the manufacturer's instructions. A 5 µl aliquot of each was loaded onto a 0.8% agarose gel alongside a 1 kb DNA ladder marker (M) and subject to 150 V for approximately 30 min. Lanes: 1) PCR product from Q403C; 2) PCR product from Q404C; 3) PCR product from Q397C; 4) PCR product from Q387C. Panel b) The plasmid product PCR using primer Q397CF/R, pBM20Q397C was used to transform E. coli NOVA Blue, plated out onto agar plates containing ampicillin (100 µg/ml) and 6 single transformant colonies, lanes 1-5 (only 5 shown), were used to prepare DNA ready for sequencing as described in Methods. Samples of each DNA preparation were analysed by agarose gel electrophoresis as described previously (Figure 3.5) to confirm the presence of the plasmid at the expected size (4.6 kb) and to estimate DNA concentration. Each of the mutant plasmids pBM20Q387C, pBM20Q403C and pBM20Q404C were treated in the same way prior to sequencing.

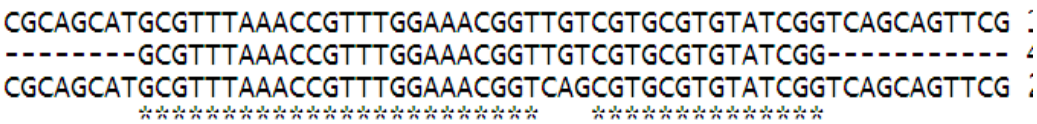

Figure 5.5 DNA sequence analysis of the P450 BM3 heme-domain mutant Q397C.

Samples (0.6 μg) from three of the mutagenic PCR DNA products purified from the transformations were selected for sequencing to screen for insertion of the correct mutation. The sequence alignment of $pBM20_{Q397C}$ (top), Q397CF/R primer (middle) and pBM20 (bottom) with the conserved residues denoted by *. Once the presence of the correct mutation was confirmed, the entire gene was sequenced to ensure no other mutation had occurred. Each of the mutant plasmids $pBM20_{Q387C}$, $pBM20_{Q403C}$ and $pBM20_{Q404C}$ were sequenced following the same protocol to confirm the presence of only the intended mutation. All sequence alignments were performed using ClustalW [78].

5.3.3 Protein purification

The heme-domains of the four cysteine mutants were successfully over-expressed in *E. coli* TG1 as previously described for the wild-type construct (Figure 4.15). As with the wild-type, frozen cell pellets prior to purification were deep red/brown in colour for $BM3_{Q387C}$, $BM3_{Q397C}$ and $BM3_{Q404C}$. However, the cell pellet for $BM3_{Q403C}$ remained a pale buff colour and the cell-free lysate was noticeably less red.

Proteins were purified following the same protocol as for the wild-type heme-domain as described previously (section 2.3.4.2). Samples from each stage of purification were analysed by 10% SDS-PAGE. Purification of the three mutants, $BM3_{Q387C}$, $BM3_{Q397C}$ and $BM3_{Q404C}$ showed a large dominant band at 54 kDa with a few minor contaminants (Figure 2.6).

During purification of the mutant $BM3_{Q403C}$, some notable differences were observed. The cell-free lysate appeared markedly paler in colour than either wild-type or the other mutants. The traditional purification methods appeared to be less effective at separating the enzyme from contaminants, in particular, the strong anion exchange step, Q Sepharose. SDS-PAGE analysis of samples from purification showed the presence of significant amounts of contaminants in the sample even after an additional anion exchange step at an increased pH (pH8) and an additional hydrophobic interaction step Figure 5.7. Due to time constraints, the purification for this mutant was discontinued and no further analysis was performed.

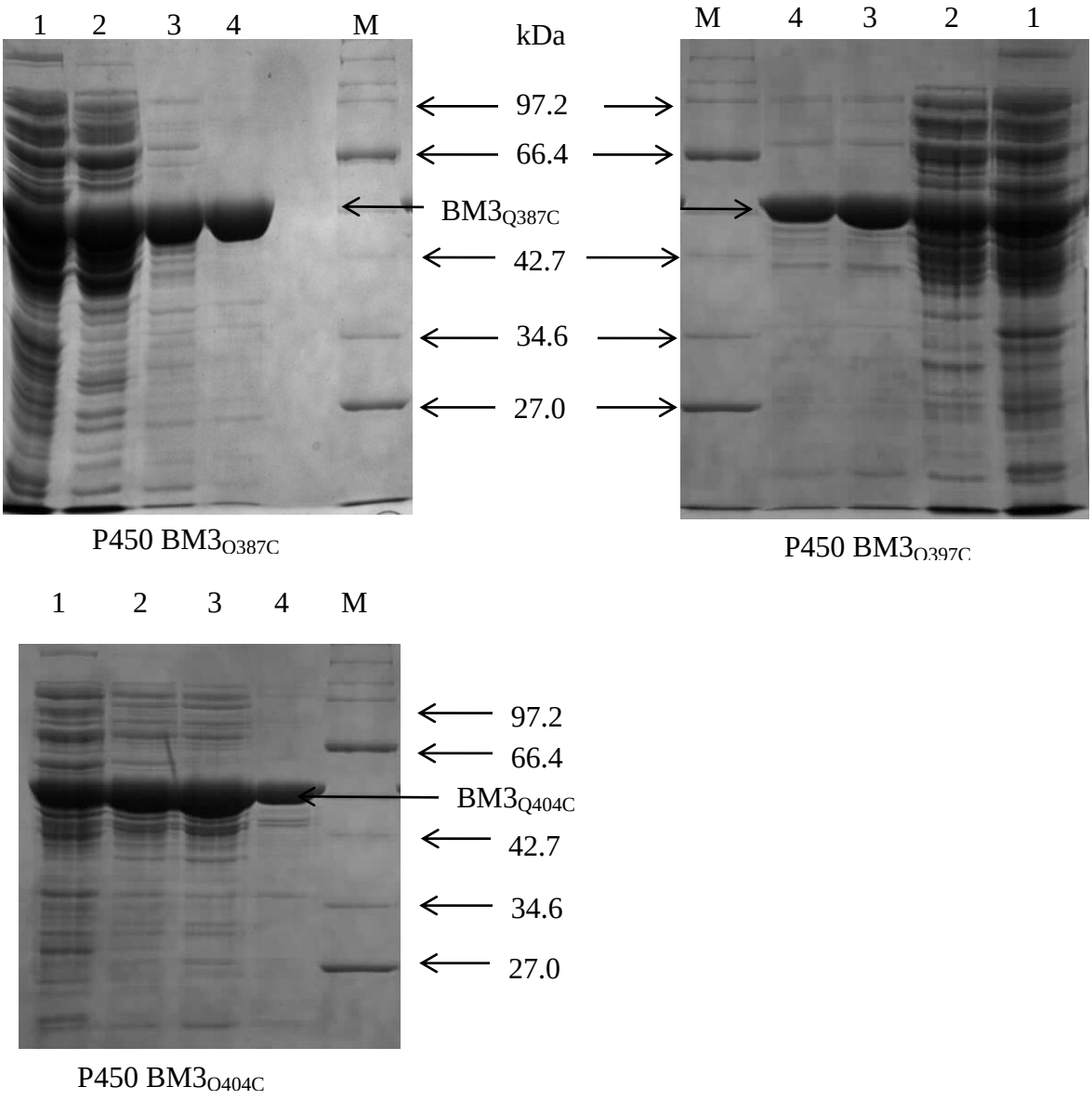

Figure 5.6 SDS-PAGE analysis of P450 BM3 heme-domain mutants Q387C, Q397C and QBM3$_{Q404C}$ at each purification stage.

Cell lysate from *E. coli* TG1 cells transformed with either pBM20$_{Q387C}$ pBM20$_{Q397C}$, or pBM20$_{Q404C}$ were subject to the same purification protocol as described for the heme-domain P450 BM3 (section 2.3.4.2). Samples taken at each purification step were analysed by SDS-PAGE as described previously (Figure 4.17). **Lanes:** M) protein size marker; 1) soluble fraction of lysate from transformed *E. coli* TG1 cells; 2) post DEAE Sepharose; 3) post hydroxyapatite; 4) post Q Sepharose.

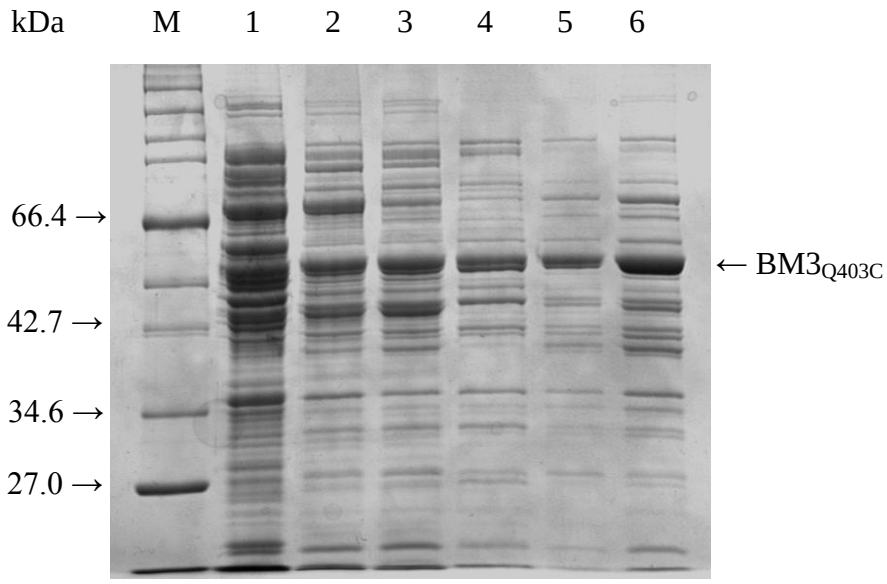

Figure 5.7. SDS-PAGE analysis of P450 BM3 heme-domain mutant P450 BM3$_{Q403C}$.

Cell lysate from *E. coli* TG1 cells transformed with pBM20$_{Q403C}$ were subject to the same purification protocol as described for the heme-domain P450 BM3 (Figure 4.17). Samples taken at each purification step were analysed by SDS-PAGE as described previously (Figure 4.17). **Lanes:** M) protein size marker; 1) cell lysate; 2) post-DEAE; 3) post-hydroxyapatite; 4) post-Q-Sepharose at pH 7.2; 5) post-Q-Sepharose at pH 8; 6) post-phenyl Sepharose.

5.3.4 UV/visible spectroscopy

Samples (4-8 μM) of each of the heme-domain mutants, $BM3_{Q387C}$, $BM3_{Q397C}$ and $BM3_{Q404C}$ were analysed by UV/visible spectroscopy and compared to the wild-type heme-domain. All three mutants displayed identical spectral characteristics to the wild-type in both the oxidised and reduced forms. For example, the oxidised spectra of $BM3_{Q387C}$ showed the Soret peak at 419 nm with the α and β bands at 538 nm and 569 nm respectively. Reduction with sodium dithionite had no effect on the Soret wavelength and caused only minor increase in absorbance of the α and β bands. The spectrum of the reduced/CO bound enzyme displayed a stable shift of the Soret peak to 449 nm and fusion of the α and β bands to form a peak and 549 nm. Spectral analysis of $BM3_{Q397C}$ and $BM3_{Q404C}$ were also indistinguishable from the wild-type indicating that all three mutants had no effect on the spin state of the heme-iron (data not shown).

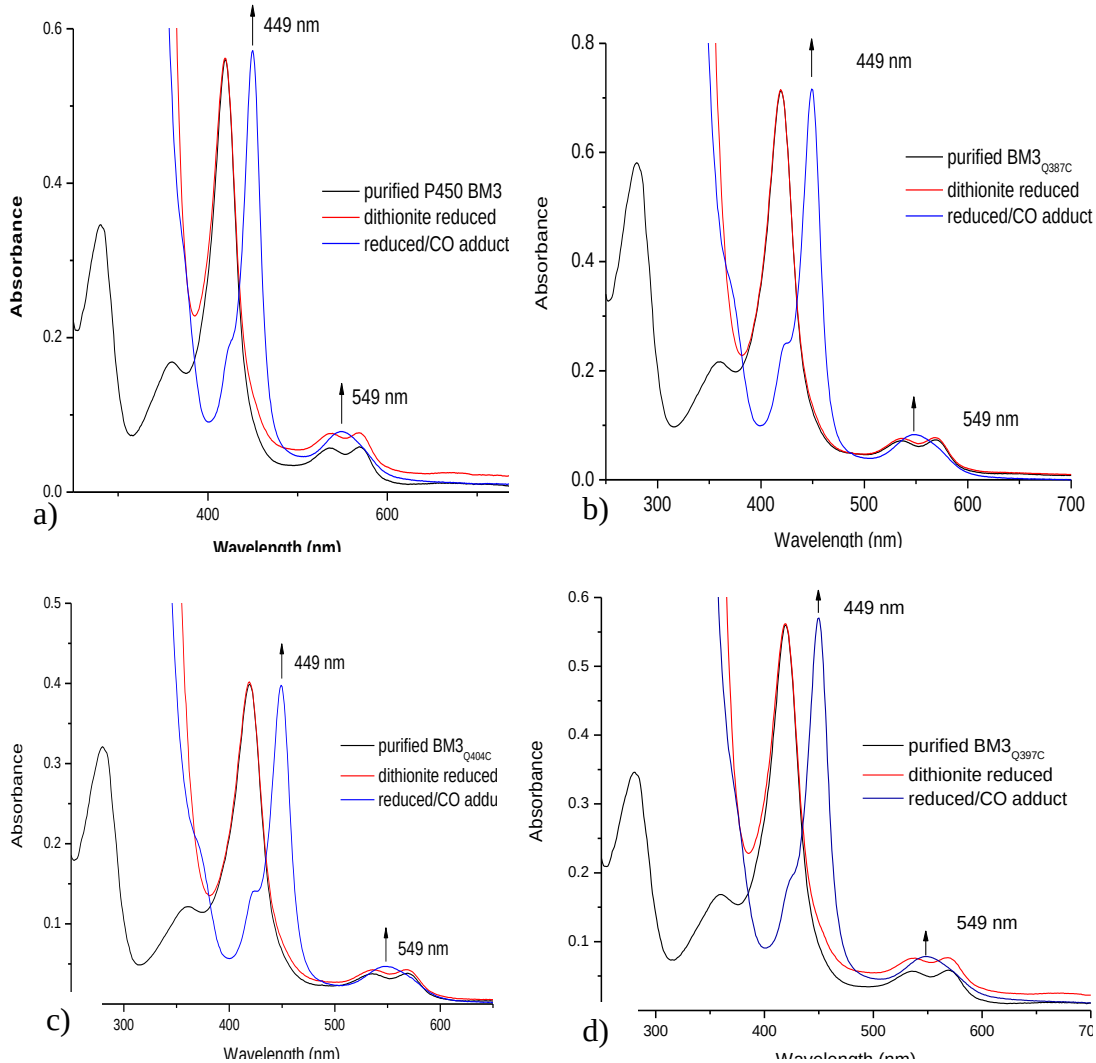

Figure 5.8. Oxidised (black), dithionite reduced (red) and reduced/CO adduct (blue) forms of P450 BM3 and the cysteine mutants.

Samples of purified protein were mixed with assay buffer to give a final concentration of 4-8 μM and absorbance measurements were taken over the wavelength range 250-750 nm. The samples were then reduced by the addition of a few grains of solid sodium dithionite and the absorbance measurements repeated immediately. Carbon monoxide (CO) was then bubbled gently through the sample for 1 minute and the absorbance measurements repeated. Panels are a) P450BM3 b) $BM3_{Q387C}$ c) $BM3_{Q404C}$ d) $BM3_{Q397C}$.

5.3.5 Binding studies

To determine the effect of these mutations on the heme environment, substrate and inhibitor binding was investigated and the results compared to that of the wild-type construct. As mentioned previously (section 4.8) the unsaturated fatty acid arachidonic acid (C20) and the inhibitor 4-phenylimidazole are known to bind tightly to P450 BM3 and induce large spectral changes in Soret region. As described previously (Section 4.9.6), spectra were recorded over the wavelength range 250-750 nm after each successive addition of either the fatty acid or inhibitor to the sample and the results were analysed to determine the dissociation constant (K_d value). Spectral shifts and K_d values obtained were compared with those of the wild-type.

In all cases, titration of arachidonic acid with the mutants induced a type-I spectral shift with the Soret peak shifting from 419 nm to 395 nm ± 1 nm indicating a shift in spin-state equilibrium to high spin. In the case of $BM3_{Q397C}$ and $BM3_{Q404C}$ the α and β bands dissolved and were replaced by an increase in absorbance at 515 nm and ~ 650 nm, matching the spectra of the wild-type. The mutant $BM3_{Q387C}$ displayed only a minor alteration of the wavelength with increases at 518 nm and 645 nm which may imply a slight change in the heme environment.

The tight binding of arachidonic acid was also retained by all three mutants with calculated K_d values of 0.3 ± 0.05, 0.2 ± 0.02 and 0.61 ± 0.1 μM for $BM3_{Q387C}$, $BM3_{Q397C}$ and $BM3_{Q404C}$ respectively with compares well with the K_d value of 0.27 ± 0.04 μM obtained for the wild-type (Table 5.2).

Spectral titrations using 4-phenylimidazole induced a type-II shift in all three mutants shifting the Soret peak from 419 nm to 425 nm and increasing absorbance at 360 nm and 545 nm. These values were indistinguishable from that observed for the wild-type (Figure 5.11 and Figure 5.12). The K_d values calculated from the titrations were also very similar to that obtained for the wild-type (Table 5.2).

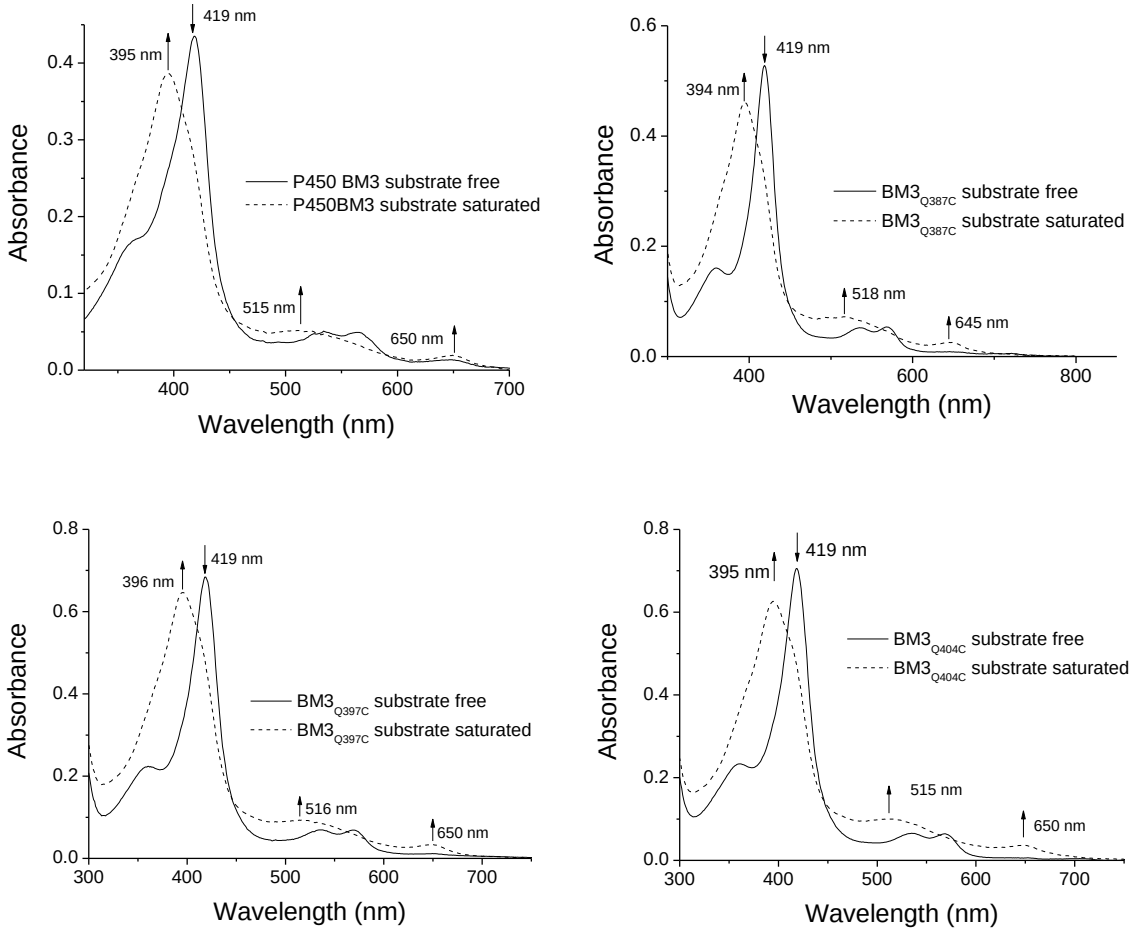

Figure 5.9 Spectral changes induced in the heme-domain of P450 BM3 and the cysteine mutants on sequential addition of increasing concentrations of arachidonic acid.

Arachidonic acid (stock solution, 33 mM in ethanol) was titrated against each of the heme-domains of P450 (BM3, $BM3_{Q387C}$, $BM3_{Q397C}$ and $BM3_{QBM3Q404C}$) as described in Methods. The starting spectra (solid lines) show the enzymes in 25 mM MOPS (pH 7.4) 100 mM KCl at a concentration of between 5 – 8 μM. The final spectra (dashed lines) show the enzyme following the addition of arachidonic acid to a final concentration of between 20 and 30 μM

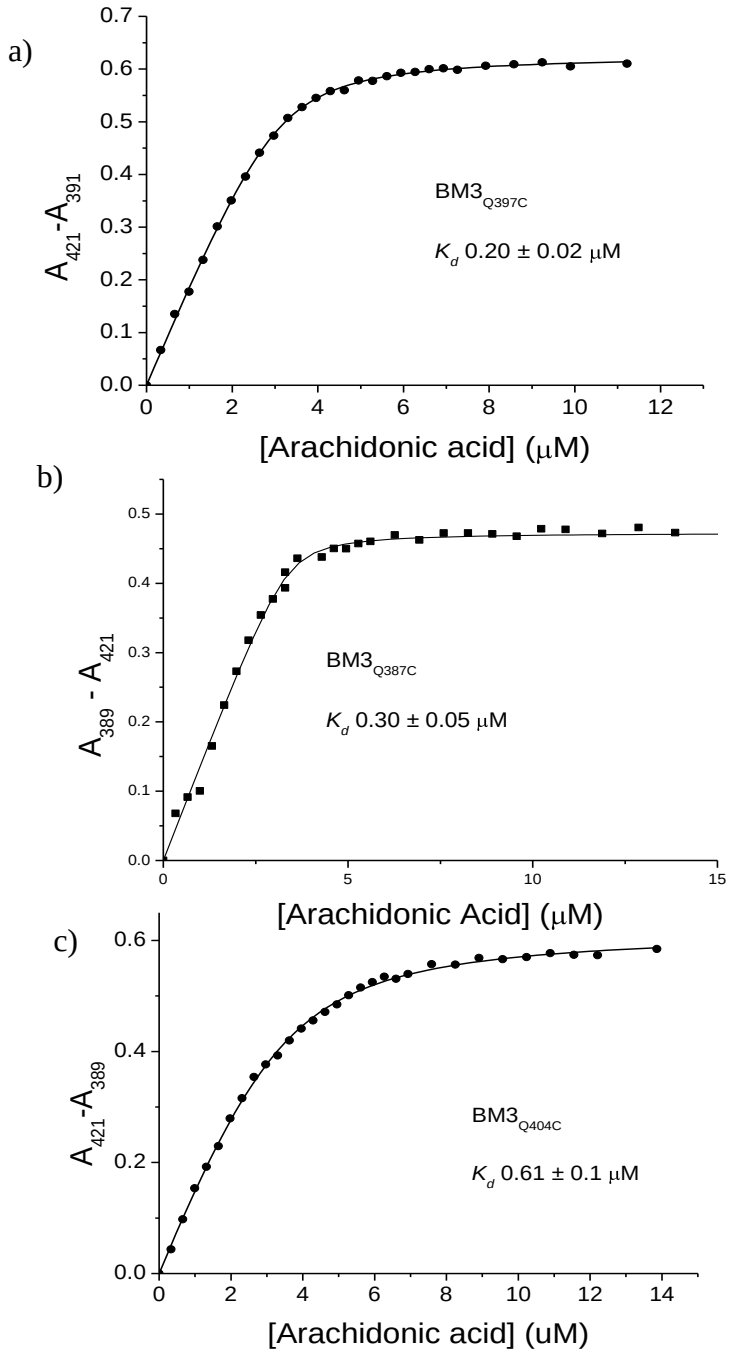

Figure 5.10. Plot of maximal absorbance change against concentration of arachidonic acid for a) BM3$_{Q397C}$, b) BM3$_{Q387C}$ and c) BM3$_{Q404C}$.

The wavelength with the largest increase in absorbance was subtracted from the wavelength with the largest decrease in absorbance, 389 nm and 421 nm respectively, derived from the difference spectra described in Figure 2.9. This maximal change in absorbance was plotted against the concentration of arachidonic acid. The plot was then fitted to Equation 2 (quadratic equation) to yield the dissociation constant, K_d, summarised in Table 5.1.

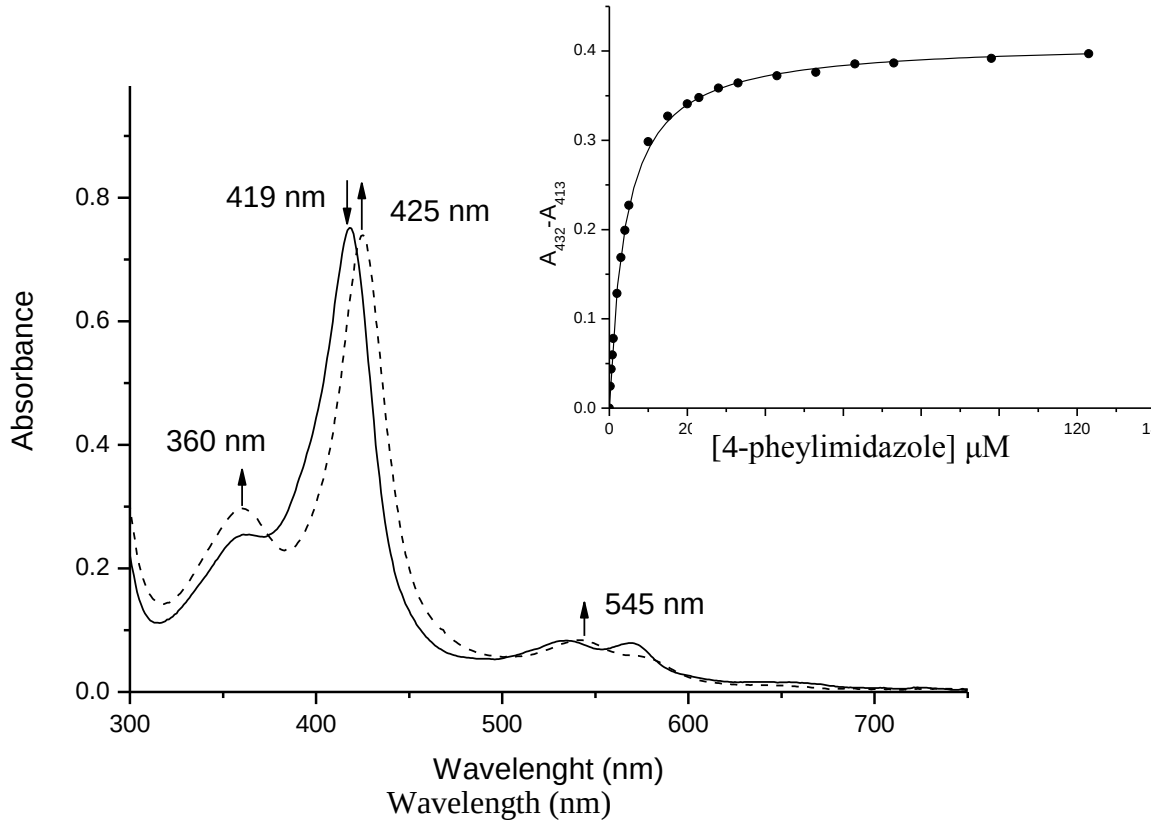

Figure 5.11 Spectral changes induced in P450 BM3$_{Q397C}$ on sequential addition of increasing concentrations of 4-phenylimidazole.

The solid line shows 7 µM of low-spin P450 BM3$_{Q397C}$ heme-domain before addition of 4-phenylimidazole, the dotted spectrum shows the enzyme following the addition of 4-phenylimidazole (stock solution 2.5 mM in assay buffer) to a final concentration of 120 µM. Intermediate spectra have been removed for clarity. Inset is the plot of maximal absorbance change against the corresponding 4-phenylimidazole concentration. The data have been fitted to the quadratic equation n yielding an A_{max} of 0.059 units per µM P450 and a K_d of 4.14 ± 0.1 µM.

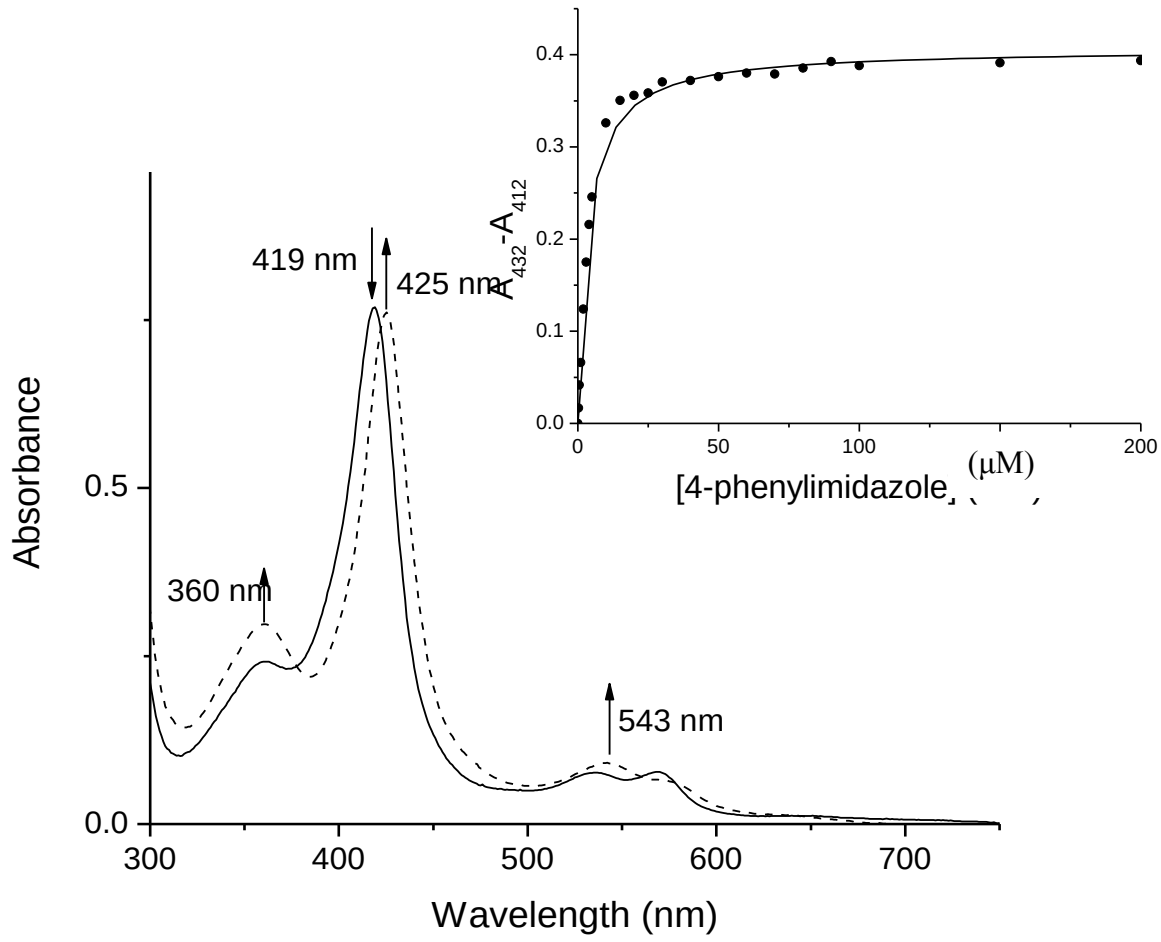

Figure 5.12 Spectral changes induced in P450 BM3$_{Q404C}$ on sequential addition of increasing concentrations of 4-phenylimidazole.

The solid line shows 7.3 μM of low-spin P450 BM3$_{Q404C}$ heme-domain before addition of 4-pheylimidazole; the dotted spectrum shows the enzyme following the addition of 4-phenylimidazole (stock solution 2.5 mM in assay buffer) to a final concentration of 50 μM. Intermediate spectra have been removed for clarity. Inset is the plot of maximal absorbance change against the corresponding 4-phenylimidazole concentration. The data have been fitted to Equation 2 yielding an A_{max} of 0.056 units per μM P450 and a K_d of 3.59 μM ± 0.2

	K_d (μM)	
	Arachidonic acid	4-phenylimidazole
P450 BM3	0.27 ± 0.04	2.95 ± 0.13
$BM3_{Q387C}$	0.30 ± 0.05	3.34 ± 0.2
$BM3_{Q397C}$	0.20 ± 0.02	4.14 ± 0.1
$BM3_{Q404C}$	0.61 ± 0.1	3.59 ± 0.2

Table 5.2 Dissociation constants calculated for substrate binding to the heme-domain of P450 BM3 and the cysteine mutants using the method described in Figure 5.9 to Figure 5.13.

5.3.6 Redox potentiometry

The reduction of P450 BM3 in the substrate free and substrate bound forms and calculation their mid-point redox potentials are shown in Figure 4.27 and Figure 4.30 (section 4.9.7) and discussed therein. The reduction of each of the mutants is described below.

Reductive titrations were performed under anaerobic conditions on both substrate-free and arachidonic acid-bound heme-domains of $BM3_{Q387C}$, $BM3_{Q397C}$ and $BM3_{Q404C}$ as described in Methods to establish their mid-point redox potential. Figure 5.13, for example, shows the spectral changes observed when $BM3_{Q404C}$ was reduced in the substrate-free form. When fully oxidised, the enzyme's heme iron appeared to be high-spin as indicated by the absorption peak at 419 nm. Upon reduction, the sample behaved in a similar manner to the wild-type, following a pattern of reduced absorption at 419 with a concomitant rise at 394 nm. A plot of maximal absorbance change versus the corresponding potential measurement yielded a mid-point redox potential of -355 mV (Figure 5.13 inset).

Reductive titration of the arachidonic acid-bound form of $BM3_{Q404C}$ yielded a mid-point redox potential of -215 ± 3 mV, shifting the potential in the positive direction by 140 mV. Similarly, reductive titration of arachidonic acid-bound and substrate-free $BM3_{Q397C}$ yielded mid-point potentials of -390 mV and -226 mV respectively, a decrease (positive shift) in redox potential of 164 mV. The mid-point reduction potentials of $BM3_{Q387C}$ were -361 mV and 156 mV for substrate free and arachidonic acid bound respectively. These data are summarised in Table 5.3.

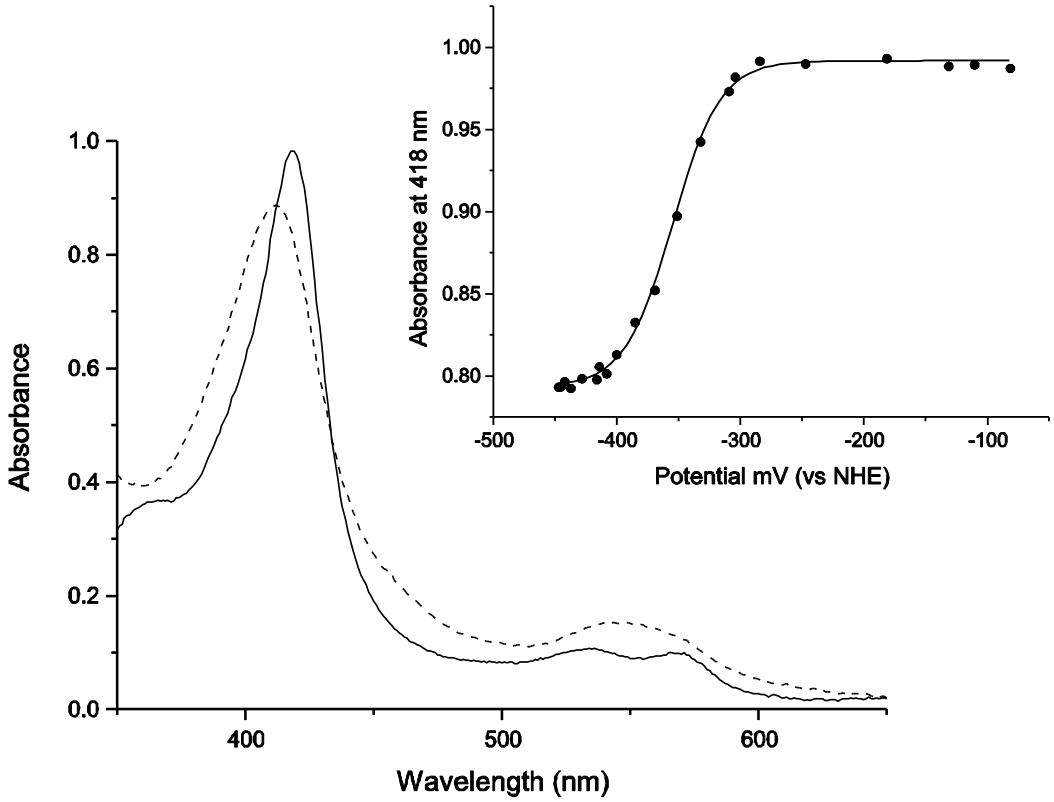

Figure 5.13 Spectral changes in $BM3_{Q404C}$ during reductive titration and calculation of the mid-point potential.

The heme-domain of P450 BM3 was subject to reductive titration with the exclusion of any substrate as described in (section 4.9.7). The starting spectrum (solid line) shows ~9 μM of oxidised low-spin BM3. The final spectrum (dashed line) shows the enzyme following the addition of sodium dithionite to full reduction. Intermediate spectra are removed for clarity. Inset shows the plot of absorbance at 418 nm against the corresponding potential measurement corrected against the NHE. These data were fitted to the 1-electron Nernst equation (Equation 4) yielding a mid-point reduction potential of -355 ± 2 mV. The error shown is the estimate from graphing software (Origin; OriginLab, Massachusetts) of the fit of the data to Equation 4 from a single potentiometric titration.

	Mid-point redox potential (mV *vs* NHE)	
	Substrate free	Arachidonic acid bound
P450 BM3	-388 ± 2	-240 ± 3
$BM3_{Q387C}$	-361 ± 1	-156 ± 3
$BM3_{Q397C}$	-390 ± 2	-226 ± 2
$BM3_{Q404C}$	-355 ± 2	-215 ± 3

Table 5.3 Mid-point redox potential of heme-domain P450 BM3 and the cysteine mutants with and without arachidonic acid bound.

Potentiometric titrations were performed under anaerobic conditions on the heme-domains of P450 BM3 and its mutants $BM3_{Q387C}$ $BM3_{Q397C}$ and $BM3_{Q404C}$, in the presence and absence of the strongly binding substrate arachidonic acid. Enzymes were incrementally reduced using sodium dithionite to full reduction then re-oxidised using potassium ferricyanide as described in Methods. Mid-point reduction potentials were calculated as described in section 4.9.7. Errors shown are the estimates from graphing software (Origin; OriginLab, Massachusetts) of the fit of the data to the 1-electron Nernst (Equation 4) a single potentiometric titration.

5.3.7 Thiol quantification

The number of solvent accessible sulfhydryl groups was measured using 5, 5'-dithiobis-(2-nitrobenzoic acid) (DTNB), more commonly known as Ellman's reagent, and a modified protocol of the standard assay using cystamine as a mediator as described in Methods [88]. The reduction of DTNB is illustrated in (Figure 5.14).

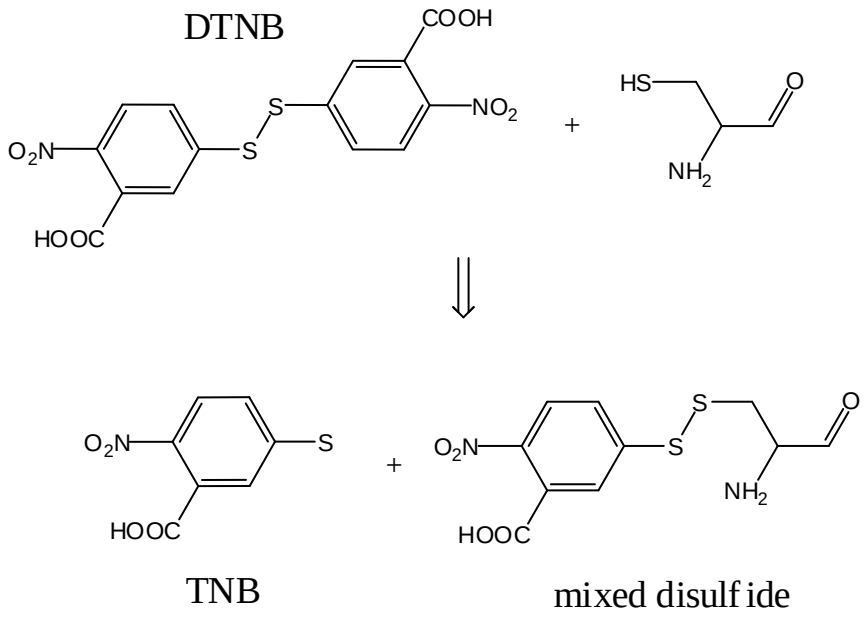

Figure 5.14 Reduction of DTNB

DTNB reacts with a free sulfhydryl group to yield a mixed disulfide and 2-nitro-5-thiobenzoic acid (TNB) which has high molar extinction coefficient in the visible range (412 nm). Each of the heme-domains, P450 BM3 and the mutants $BM3_{Q387C}$, $BM3_{Q387C}$ and $BM3_{Q404C}$, were incubated with both DTNB and cystamine under the conditions described in Methods and the resulting absorbance at 412 nm was measured. The number of sulfhydryls per sample was calculated using Equation 6 then divided by the protein concentration to obtain the number of sulfhydryl groups per mol of protein. Experiments were repeated a minimum of three times for each protein sample. The data are summarized in Table 5.4

Table 5.4 Measurement of protein sulfhydryls in the heme domains of P450 BM3 and the cysteine mutants using DTNB/cystamine assay.

	SH groups per mole of P450	
	Theoretical	DTNB/cystamine
P450 BM3	2	0.5 ± 0.11
$BM3_{Q387C}$	3	0.80 ± 0.1
$BM3_{Q397C}$	3	2.46 ± 0.4
$BM3_{Q404C}$	3	1.09 ± 0.1

Protein samples (typically 1-5 nmole) were incubated with DTNB/cystamine reagent for 5 min as described in Methods. The absorbance at 412 nm was measured alongside that of protein without reagent and reagent without protein and the number of protein sulfhydryls was determined using Equation 6. Experiments were repeated a minimum of three times for each of the mutants and the wild-type, values given are mean ± SEM $n \geq 3$.

Theoretically, the number of solvent accessible sulfhydryls in P450 BM3 is 2, C62 and C156. According to this method, the number of SH groups calculated for P450 BM3 is 0.5 ± 0.1.; in comparison, the available SH groups on the mutants were measured between 0.8 and 2.5, an increase of between 2 and 5 fold that of the wild-type.

The experiments performed here were specifically aimed at determining *surface accessible* thiol groups or cysteines within the protein. To determine the total number or cysteines, it would be necessary to denature the protein using chaotropic agents such at urea (6-8 M) or guanidinium chloride (6 M). This would unfold the protein and expose all possible cysteines, including the heme-ligating cysteine, to the DTNB reaction. This would not, however, provide information about the solvent accessible cysteines available for attachment of thiol-modifying agents to be attached to catalytically active proteins in the future.

5.3.8 EPR spectroscopy

As the determination of the number of solvent accessible sulfhydryl groups had been inconclusive using the DTNB assay an alternative method, using a cysteine specific spin-label reagent and EPR spectroscopy, was used determine whether the mutated residues were accessible to thiol-modifying agents.

EPR is a valuable reporting tool for unpaired electrons e.g. radicals and paramagnetic species such as iron, within a sample and provide information regarding the immediate environment of the species. In heme-containing enzymes, such as P450, the iron provides the paramagnetic ion and EPR on heme-containing enzymes can provide vital clues to the ligation state of the iron.

EPR is annotated by the dimensionless g-factor or gyromagnetic ratio, which can be defined by the following equation:

$$h\nu = g_{obs}\mu_B B_{Res}$$

Equation 7

Where: h = Planck's constant (6.6261 x 10^{-34} J s), ν = the operating microwave frequency of the spectrometer (in Hz), g = g-factor or gyromagnetic ratio, μ_B = electron Bohr magneton (9.2740 x 10^{-24} J T^{-1}) and B_{Res} = magnetic field strength (in Tesla) at which resonance occurs.

The attachment of nitroxide paramagnetic spin labels to proteins prior to EPR can yield even more information about the protein and its environment such as mobility of the side chain, the polarity index for its immediate environment and the distance between the side chain and another paramagnetic centre. All three types of information can be obtained by analysis of the line shape of the EPR spectra [139]. A forth type of information which can be obtained using spin-labelling is the extent of solvent accessibility of the side-chain (whether and how far a side-chain is buried within membrane or protein) to which the label is attached. This latter type of analysis requires the use of power saturation techniques in conjunction with paramagnetic relaxation reagents such as oxygen and nickel or chromium compounds [310]. The spin label used here, methanethiosufonate (MTSL), is specific to cysteine residues (Figure 5.15).

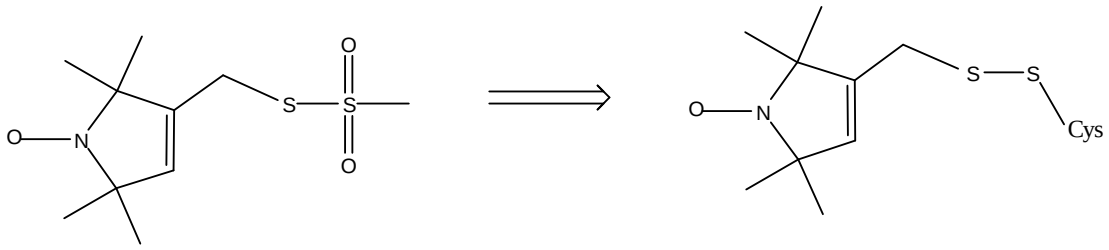

Figure 5.15 Chemical structure of the spin label reagent methanethiosufonate (MTSL), and the reaction to form a disulfide bond with cysteine.

The spin-labelling was performed and EPR spectra were collected by Dr. Louise Ottignon, Department of Chemistry, University of East Anglia using the protein samples prepared as described previously (section 5.3.3). Samples of each of the proteins, P450 BM3 and the three cysteine mutants were labelled using the nitroxide spin-label MTSL according the protocol described in Methods. The room temperature X-band continuous wave EPR spectrum of each protein was then collected. The protein concentrations were determined spectrophotometrically at the Soret band wavelength of 419 nm using the molar extinction coefficient ε^{419} = 95,000 M^{-1} cm^{-1} [60]. The extent of spin label attachment was determined by comparing the double integration of the EPR spectrum to that obtained for an MTSL solution of known concentration. The possible number of cysteines accessible to MTSL in each sample was calculated by dividing the EPR integration by the protein concentration in μM.

EPR integration estimates a total of two cysteine residues accessible to MTSL in the wild-type P450 BM3 and 3 in both $BM3_{Q387C}$ and $BM3_{Q404C}$. However, the integration of the Q397C mutant estimates the total number of spin-labels to be 6 in $BM3_{Q397C}$, indicating a significant increase in solvent accessible sulfhydryl groups (Table 5.5).

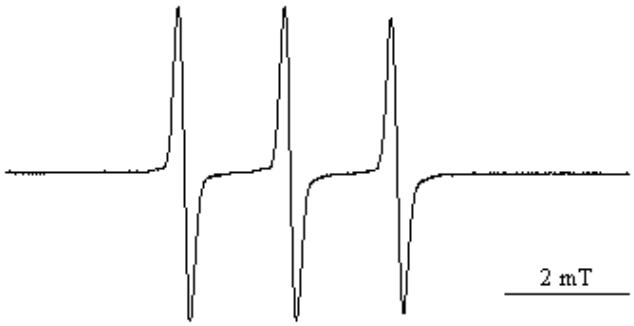

Figure 5.16 Three-line nitroxide EPR spectrum.

Spin labels with the predominant ^{14}N isotope give rise to a three line EPR spectrum. The nuclear spin of the nitrogen $I = 1$ interacts with the unpaired electron, splitting the signal into $2I + 1$. The lines in the spectrum are uniformly spaced with the same intensity showing free rotation of the nitroxide radical [137, 138].

A nitroxide radical with spin quantum number S=1/2, as is the case here, would be expected to give rise to a single derivative signal. However, the nuclear spin of the nitrogen interacts with the electron spin and splits the derivative into three (Figure 5.16) and is generally described by the g-value of the central resonance and the size of the splitting (in Gauss). Restricting the mobility of the nitroxide results in broadening of the lines and decreases in their amplitude. The EPR spectra for all four of the proteins show broad, low intensity lines which indicate the rotational motion of the nitroxide is reasonably restricted (Figure 5.17).

	EPR integration	*P450 [μM]*	*Integration/[μM]*	**Estimated SH groups**
P450 BM3	219	133	1.6	2
$BM3_{Q387C}$	315	115	2.7	3
$BM3_{Q397C}$	2050	345	5.9	6
$BM3_{Q404C}$	370	115	3.2	3

Table 5.5 The number of cysteines accessible to MTSL label as determined by continuous wave EPR spectroscopy.

The number of cysteines was calculated by dividing the EPR integration by the concentration of P450 in the sample.

At room temperature the EPR spectra only captures the signals arising from the nitroxide label(s) and not any signals for the paramagnetic heme iron, which are only observed at low temperature (below 40K). In all the protein sample spectra, there appears to be significant heterogeneity, shown best by the splitting of the outlying resonances or g-tensor elements labelled at 2.019 and 1.98 (Figure 5.18). This indicates that either the nitroxide is adopting different conformations (indicated by differing rotational mobilities of the label) or there is more than one spin label (or both). The spectra for each of the mutants and the wild-type showed the presence of at least three different spin label environments, as indicated by the complicated line shapes with a mixture of low intensity peaks. This is particularly noticeable in $BM3_{Q404C}$ where there is significantly more of the second species relative to the wild-type or $BM3_{Q387C}$. This would suggest that the second species predominantly arises from the label at that site specific mutation i.e. residue 404 (Figure 5.18).

The g-values calculated for each of the spectral features are centred about 2 (Table 5.6), the free electron value, which is as expected for a nitroxide radical. The g-value of species 2 in $BM3_{Q404C}$ is noticeably different than that calculated for the other proteins, additional evidence that this signal predominantly arises from the label on residue C404.

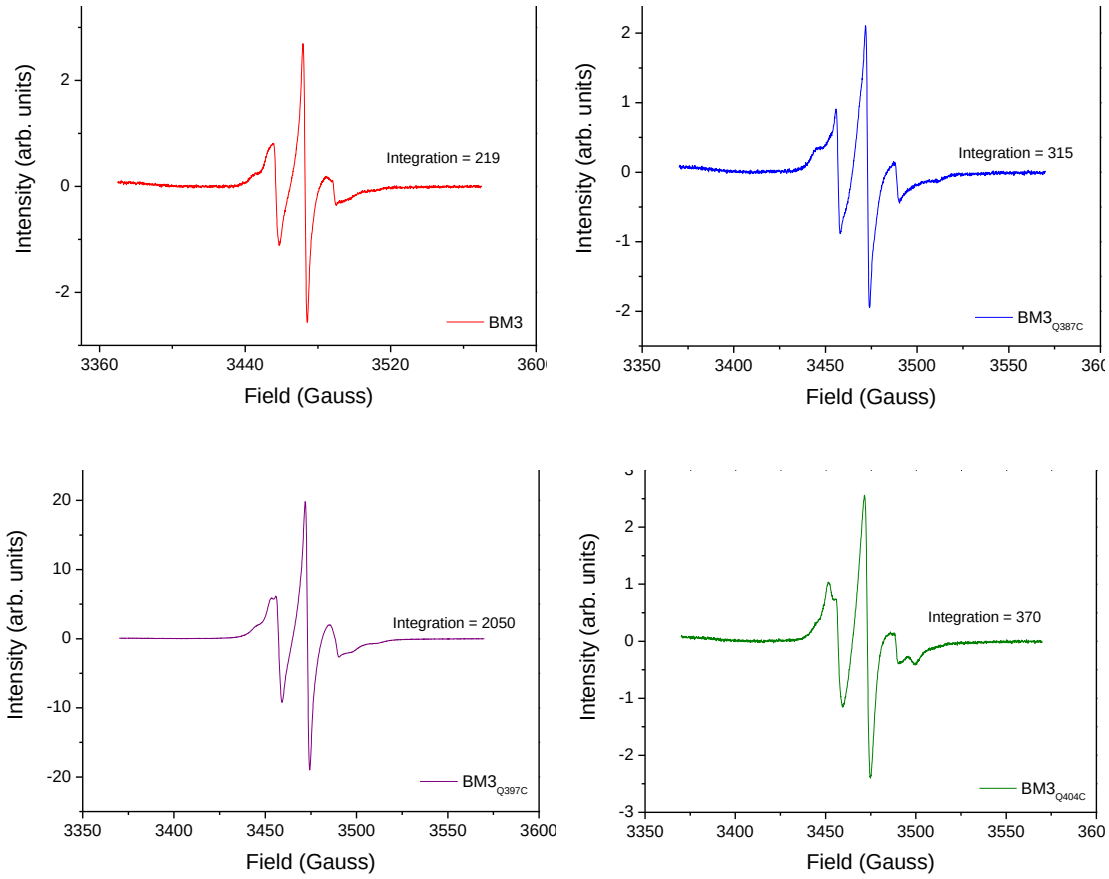

Figure 5.17 EPR spectra for MTSL labelled heme-domain BM3 and cysteine mutants.

Protein samples (~400 μmole) were treated with DTT to remove any disulphide bonds and prevent further disulphide bond formation then labelled with the nitroxide spin label MTSL as described in Methods. Continuous wave EPR spectra were collected at room temperature under the following parameters: microwave power 2mW, X-band frequency 9.741 GHz. Clockwise from top left: P450BM3, $BM3_{Q387C}$, $BM3_{Q404C}$ and $BM3_{Q397C}$.

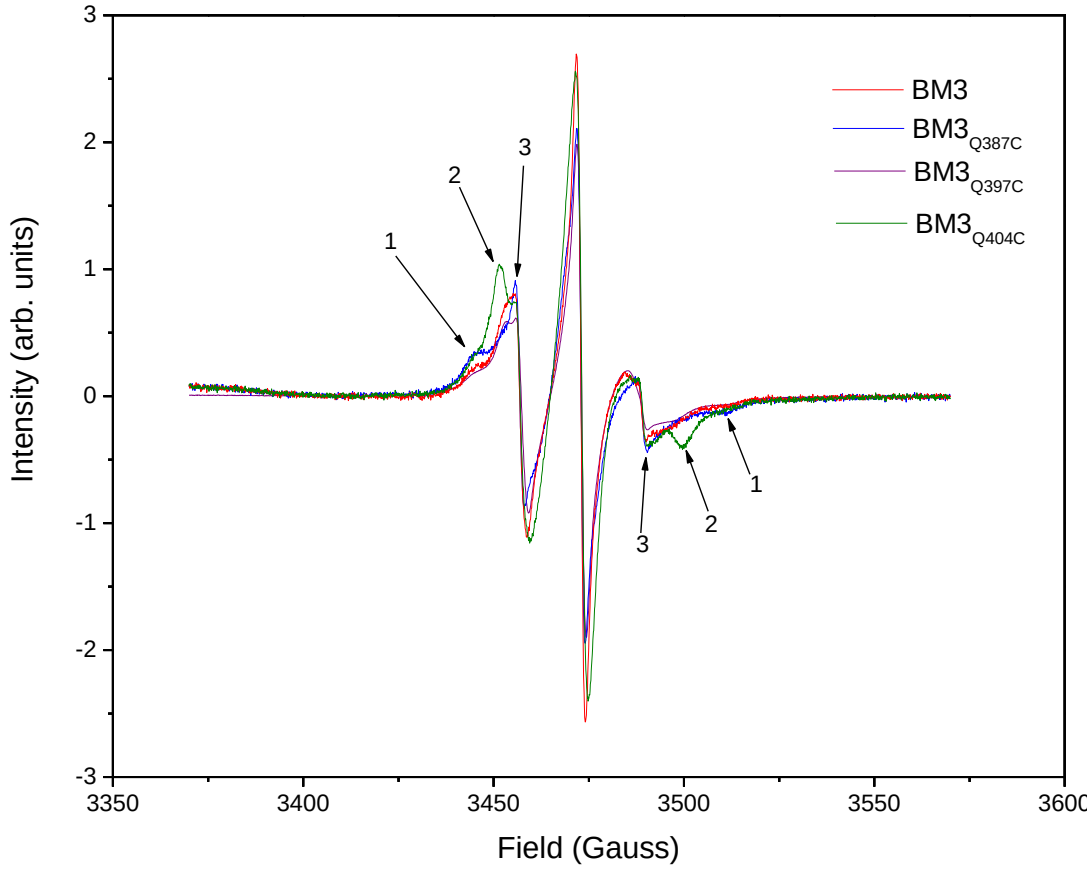

Figure 5.18 EPR spectra of each of the BM3 proteins overlaid on the same scale.

All four proteins display some heterogeneity where the g-tensor elements are split, showing the presence of three distinct species labelled 1, 2 and 3 here. The sample of $BM3_{Q404C}$ shows significantly more of species two suggesting the signal predominantly arises from the label at residue position 404.

	g-values of the nitroxide radical signals					
	1	2	3	3	2	1
P450 BM3	2.0203	2.0156	2.0138	1.9891	1.9902	1.9817
$BM3_{Q387C}$	2.0203	2.0156	2.0138	2.0034	*	1.9817
$BM3_{Q397C}$	2.0203	2.0156	2.0138	1.9942	1.9896	1.9828
$BM3_{Q404C}$	2.0203	2.0167	2.0138	1.9948	1.9885	(~1.9800)

Table 5.6 The calculated g-values of the nitroxide radical signals seen in the spectra.

The g-values were calculated measuring the field strength (in Gauss) of the observed EPR signal peaks and inserting the value into Equation 7. All appear to be centred at g= 2.0x, close to the free electron value. Gaussian splitting were not determined as the positions of the crossover points of the derivatives would require simulation of overlying nitroxide species.

* g-value could not be calculated with any degree of certainty due to diffuse peaks

5.4 Discussion

In an effort to remove the requirement of the expensive cofactor NADPH for biocatalysis performed by BM3, a number of single point mutations were introduced to the heme domain to explore the potential for light induced electron transfer. Four non-conserved residues were mutated to cysteine in preparation for attachment of photo-sensitive chemical agents to allow for light induced electron transfer. Three of the four Q-C mutants behaved similarly to the wild type during expression and purification with high expression levels and well resolved purification protocols. The Q403C mutant was distinctly more problematic to purify. As residue 403 is the closest of the four under investigation at only 5.8 Å from the heme and even closer to the heme-ligating cysteine, it is possible that the introduction of a cysteine here has caused the formation of a disulfide bridge with C400. This, in turn, would affect the protein conformation and heme incorporation and may lead to the production of apo-protein and/or incorporation into inclusion bodies. To investigate this further, it would be necessary to establish to what level the protein was being expressed and whether or not it was accumulating in inclusion bodies. Unfortunately, due to time constraints, further investigation of this mutant was not possible without sacrificing characterisation of the remaining mutants. Therefore, work on this mutant was halted.

Comparison of the observed UV/visible spectra of the remaining Q-C mutants show all three display identical oxidised, reduced and CO/reduced spectral characteristics, implying the mutations have not affected the immediate heme environment. The binding data also confirms these mutations do not significantly affect fatty acid or inhibitor binding suggesting that the mutants have not affected the enzyme's ability to catalyse fatty acid oxidation.

All three mutants show a high mid-point redox potential in the absence of substrate, between -388 mV and -355 mV and, with the exception of $BM3_{Q387C}$, experience a positive shift in of ~ 150 mV when fatty acid is present. These values are consistent with wild-type BM3 and suggest that no major alteration to the electronic environment of the heme has occurred. In the case of $BM3_{Q387C}$, the positive shift is larger at 205 mV. This may imply some electron rearrangement surrounding the heme iron; however, as the substrate bound redox potential is lower (more positive)

than that required for electron transfer it would suggest that will not be a hindrance to electron transfer during catalysis.

Whilst the thiol quantification using DTNB shows $BM3_{Q387C}$ and $BM3_{Q404C}$ to have approximately twice the sulfhydryl concentration when compared to P450 BM3 it estimates the concentration of sulfhydryl groups in $BM3_{Q397C}$ to be almost 5 times that of the wild-type. Whilst the EPR data provide more reasonable estimates of solvent accessible cysteines, the integration of the spectrum of this mutant also estimates an unexpectedly large number in $BM3_{Q397C}$. There are several possible explanations for this observation. Firstly, the values obtained from integration of the EPR spectra may be lower since a spin-coupled interaction between closely spaced spin-labels could quench and therefore reduce the intensity of the signals in the spectra. This would lower the concentration value in the integration and thus underestimate the number of spin-labels. A second suggestion postulated that treatment with DTT prior to the spin labelling had caused the C400-iron bond to break. However, neither of these two explanations would explain the high number of sulfhydryls in the DTNB assay; and had the DTT treatment caused the C400 ligation to break, one would expect the UV/visible spectra to have changed. In this case, the MTSL treated and untreated samples share identical UV/visible spectra.

A third and more plausible explanation is exogenous labelling of impurities within the sample. Re-examination of the UV/visible spectra shows an A_{280}/A_{419} ratio of 0.93 compared to 0.61 and 0.67 for the wild-type and other mutants respectively, indicating contamination of some sort (Figure 5.19). Analysis of a heavily overloaded SDS-PAGE does show other proteins in the sample (data not shown), which would point to contamination as the source of these anomalous results rather than spin-coupling or unintentional labelling of the iron-ligating cysteine.

The integrations of the EPR spectra indicate that MTSL has successfully labelled C156 and C62 in the native enzyme as well as the engineered cysteine in the mutants, which is to be expected. The line shape of the spectra differs from that of a free label in solution (Figure 1.14). The complex line shapes indicate the presence of several overlaying and partially immobilised nitroxide signals. Figure 1.16 shows that there are at least 3 different types of nitroxide signal present in the mutant spectra as a whole (these are shown clearly by on the outlying resonances and labelled 1,2 and 3

in the spectrum and represent species with a resonance at a similar central g-value and different Gaussian splitting). The shape of the signals, distorted from that of free solution (Figure 1.14), indicate that the labels are partially immobilised.

These different types of nitroxide signal could arise from a single label with several mobilities or conformations; or multiple labels in single environments; or these signals may arise from a mixture of both. In this case, the latter is most likely as there is more than one spin label present in each protein, three of which are within 20 Å of one another (Figure 5.20).

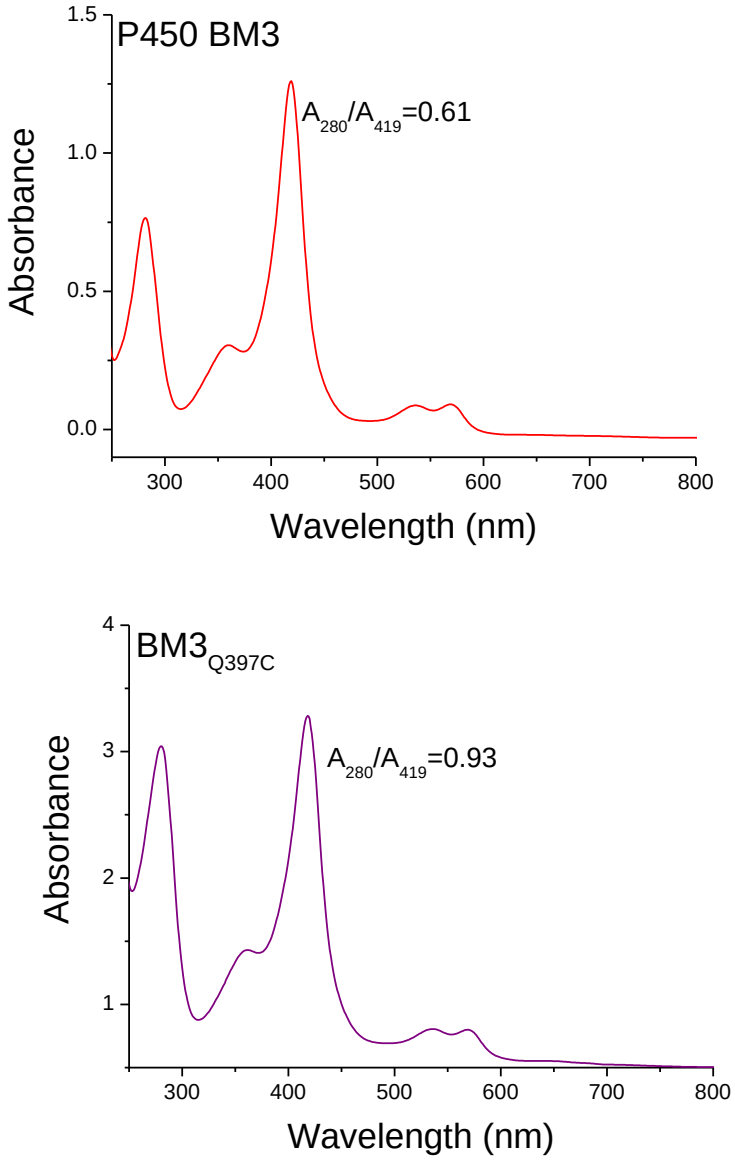

Figure 5.19 UV/visible absorption spectrum after spin label addition.

The UV/visible spectra of each of the samples used for collection of the EPR spectra were recorded to calculate the [P450] of the samples. The total protein/heme ratio for BM3Q397C is almost one, indicating less than pure protein sample.

The possibility of spin-quenching within the labelled samples which may reduce the signal strength of their EPR spectra has already been mentioned. Each of the labels on the mutated cysteines is likely to interact with that of C62. The distance between the alpha-carbon of each residue relative that of C62 is less than 21 Å (Figure 5.20). In the case of the label attached to $BM3_{Q387C}$, the residue points inwards towards C400 which could decrease the distance to C62 and the heme leading to more pronounced quenching. Interaction between the nitroxide label on C156 could probably be discounted as spatially it is over 12 Å from the alpha-carbon of the Q404C and even further from the others and in all cases is shielded by a ridge of protein. If quenching were present it would then mean that the number of estimations of the number of spin labels could have been underestimated. This could partly explain why the integration for $BM3_{Q387C}$ estimated less than 3 labels (2.7) (Table 5.5).

Another source of spin-coupled quenching is the heme iron. Here, we are examining proteins already containing a paramagnetic species, specifically low spin ferric heme iron and it is possible that heme is affecting the nitroxide spin-label signals and adding to the complexities of interpretation of these spectra. The heme iron signal cannot be seen on these spectra at room temperature (iron is observed below 40K). There is, however, the possibility that the spin of the heme iron and nitroxide labels could still interact.

Repeating the experiment at W band (~95GHz) as opposed to X band (~9GHz) would extend the accessible range of time scales and would allow better resolution of the g-tensor components of the nitroxide spin label [311]. An example of where this has been applied are W-band experiments performed by Steinhoff, W-band experiments were able to differentiate motional restrictions of different nitroxide labels where in X-band spectra these were indistinguishable [311]. Probably, in this case, it would be better to first examine mutants that contain a single point for attachment of thiol-modifying agents (removing the native cysteine residues 64 and 152). In addition, perhaps reconstitution of the proteins with zinc-containing hemin to remove potential interaction with a paramagnetic heme would also be of assistance.

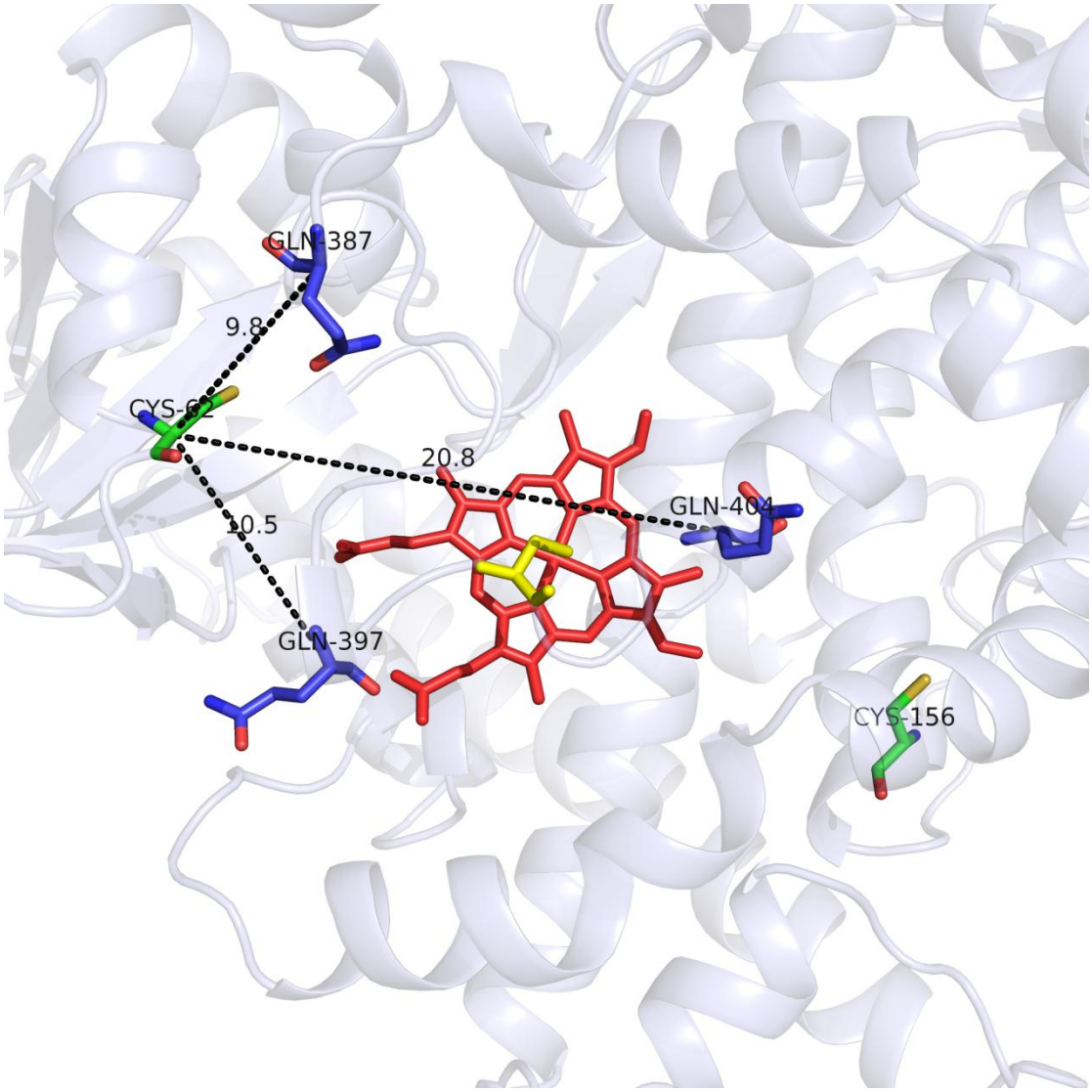

Figure 5.20 Atomic Structure of P450 BM3 proximal face of the protein.

Showing the attachment points for the nitroxide spin labels on relation to each other and the heme-ligating cysteine (C400, yellow sticks). The protein back bone is represented as cartoons, The native cysteines, C62 and C156 are shown as green sticks, the mutated glutamines, Q387, Q397 and Q404 are shown in blue. Distance measurements are defined in Angstroms and identified by black dashed lines (PDB-ID 1FAG). The heme and FMN are represented as red and yellow sticks respectively. Image rendered using PyMOL [209].

5.5 Conclusion

During this study, a number of non-conserved amino acids were mutated to cysteines in preparation for the attachment of photo-sensitive chemical agents that may allow photo-induced electron transfer to the heme and thus negate the requirement for not only NADPH but also the labile reductase domain. These mutant heme-domains were analysed using UV/visible spectroscopy, redox potentiometry and EPR spectroscopy to assess the impact on the enzyme/substrate functional relationship and to determine whether the mutated residues were accessible to thiol-modifying agents.

This study ended before any analysis of whether photo-reductive agents could be attached or attempts made to induce electron transfer. However, the EPR data gathered so far does show the feasibility of attachment of thiol-modifying agents to P450 BM3. The proteins have been labelled and the labels are partially immobilised but quantification of the number of labels is questionable as at least one of the samples in not completely pure and there are at least two paramagnetic species in each protein close enough together to spin-couple and quench each other.

In retrospect, mutating out the native cysteines on the proteins surface (C62 and C156) would have prevented any spin-coupling and subsequent signal quenching that may have been caused by the multiple nitroxide radicals. To eliminate the possibility of unwanted spin-label interaction in any further EPR studies it would be beneficial to construct a second set of mutants containing a single point for attachment of thiol-modifying agents. Removal of the native cysteines would also negate any potential for multiple attachment of photosensitive agents which might confound any future electron transfer experiments.

6 References

1. Faber, K., *Biotransformations in inorganic chemistry*. 4th ed. 2000, Berlin: Springer-Verlag.

2. Held, M., et al., *Biocatalysis. Biological systems for the production of chemicals.* Pure and Applied Chemistry, 2000. **72**(7): p. 1337-1343.

3. Cirino, P.C. and F.H. Arnold, *Protein engineering of oxygenases for biocatalysis.* Curr Opin Chem Biol, 2002. **6**(2): p. 130-5.

4. Straathof, A.J., S. Panke, and A. Schmid, *The production of fine chemicals by biotransformations.* Curr Opin Biotechnol, 2002. **13**(6): p. 548-56.

5. Gillam, E.M.J., *Engineering Cytochrome P450 Enzymes.* Chem. Res. Toxicol., 2008. **21**(1): p. 220-231.

6. Askin, D., et al., Highly diastereoselective reaction of a chiral, non-racemic amide enolate with (S)-glycidyl tosylate. Synthesis of the orally active HIV-1 protease inhibitor L-735,524. Tetrahedron Letters, 1994. **35**(5): p. 673-676.

7. O'Brien, X.M., et al., Engineering an indene bioconversion process for the production of cis-aminoindanol: a model system for the production of chiral synthons. Appl Microbiol Biotechnol, 2002. **59**(4-5): p. 389-99.

8. Buckland, B.C., et al., Microbial conversion of indene to indandiol: a key intermediate in the synthesis of CRIXIVAN. Metab Eng, 1999. **1**(1): p. 63-74.

9. Crossley, R., The relevance of chirality to the study of biological activity. Tetrahedron, 1992. **48**(38): p. 8155-8178.

10. De Camp, W.H., The FDA perspective on the development of stereoisomers. Chirality, 1989. **1**(1): p. 2-6.

11. Drummond, L., J. Caldwell, and H.K. Wilson, The stereoselectivity of 1,2-phenylethanediol and mandelic acid metabolism and disposition in the rat. Xenobiotica, 1990. **20**(2): p. 159-68.

12. Drummond, L., J. Caldwell, and H.K. Wilson, The metabolism of ethylbenzene and styrene to mandelic acid: stereochemical considerations. Xenobiotica, 1989. **19**(2): p. 199-207.

13. Warhurst, A.M. and C.A. Fewson, *Microbial metabolism and biotransformations of styrene.* Journal of Applied Microbiology, 1994. **77**(6): p. 597-606.

14. Katsuki, T. and K.B. Sharpless, *The first practical method for asymmetric epoxidation.* J. Am. Chem. Soc., 1980. **102**(18): p. 5974-5976.

15. Jacobsen, H. and L. Cavallo, A Possible Mechanism for Enantioselectivity in the Chiral Epoxidation of Olefins with [Mn(salen)] Catalysts. Chemistry, 2001. **7**(4): p. 800-807.

16. Menger, F.M., *Enzyme reactivity from an organic perspective.* Acc. Chem. Res., 1993. **26**(4): p. 206-212.

17. Carrea, G., G. Ottolina, and S. Riva, *Role of solvents in the control of enzyme selectivity in organic media.* Trends in Biotechnology, 1995. **13**(2): p. 63-70.

18. Smits, T.H.M., et al., Molecular screening for alkane hydroxylase genes in Gram-negative and Gram-positive strains. Environmental Microbiology, 1999. **1**(4): p. 307-317.

19. Throne-Holst, M., et al., Utilization of n-alkanes by a newly isolated strain of Acinetobacter venetianus: the role of two AlkB-type alkane hydroxylases. Applied Microbiology and Biotechnology, 2006. **72**(2): p. 353-360.

20. Schmid, A., et al., *The use of enzymes in the chemical industry in Europe.* Curr Opin Biotechnol, 2002. **13**(4): p. 359-66.

21. van Beilen, J.B., et al., *Alkane hydroxylase homologues in Gram-positive strains.* Environ Microbiol, 2002. **4**(11): p. 676-82.

22. Van Beilen, J.B., et al., *Diversity of Alkane Hydroxylase Systems in the Environment.* Oil & Gas Science and Technology, 2003. **58**(4).

23. van Beilen, J. and E. Funhoff, *Alkane hydroxylases involved in microbial alkane degradation.* Applied Microbiology and Biotechnology, 2007. **74**(1): p. 13-21.

24. van Beilen, J.B., J. Kingma, and B. Witholt, *Substrate specificity of the alkane hydroxylase system of Pseudomonas oleovorans GPo1*. Enzyme and Microbial Technology, 1994. **16**(10): p. 904-911.

25. Appel, D., et al., A P450 BM-3 mutant hydroxylates alkanes, cycloalkanes, arenes and heteroarenes. J Biotechnol, 2001. **88**(2): p. 167-71.

26. Farinas, E.T.S., Ulrich Glieder, Anton Arnold, Frances H. , *Directed Evolution of a Cytochrome P450 Monooxygenase for Alkane Oxidation.* Advanced Synthesis & Catalysis, 2001. **343**(6-7): p. 601-606.

27. Fritsche, W. and M. Hofrichter, Aerobic Degradation by Microorganisms, in Environmental Processes II - Soil Decontamination, J. Klein, Editor. 2000, Wiley-VCH.

28. Iida, T., et al., The cytochrome P450ALK multigene family of an n-alkane-assimilating yeast, Yarrowia lipolytica: cloning and characterization of genes coding for new CYP52 family members. Yeast, 2000. **16**(12): p. 1077-87.

29. Hamamura, N., et al., *Diversity in butane monooxygenases among butane-grown bacteria.* Appl Environ Microbiol, 1999. **65**(10): p. 4586-93.

30. Maier, T., et al., Molecular characterization of the 56-kDa CYP153 from Acinetobacter sp. EB104. Biochem Biophys Res Commun, 2001. **286**(3): p. 652-8.

31. Murrell, J.C., B. Gilbert, and I.R. McDonald, *Molecular biology and regulation of methane monooxygenase.* Arch Microbiol, 2000. **173**(5-6): p. 325-32.

32. Hamamura, N., C.M. Yeager, and D.J. Arp, *Two distinct monooxygenases for alkane oxidation in Nocardioides sp. strain CF8.* Appl Environ Microbiol, 2001. **67**(11): p. 4992-8.

33. Sluis, M.K., L.A. Sayavedra-Soto, and D.J. Arp, *Molecular analysis of the soluble butane monooxygenase from 'Pseudomonas butanovora'.* Microbiology, 2002. **148**(Pt 11): p. 3617-29.

34. Smits, T.H., et al., Functional analysis of alkane hydroxylases from gram-negative and gram-positive bacteria. J Bacteriol, 2002. **184**(6): p. 1733-42.

35. Baptist, J.N., R.K. Gholson, and M.J. Coon, *Hydrocarbon oxidation by a bacterial enzyme system. I. Products of octane oxidation.* Biochim Biophys Acta, 1963. **69**: p. 40-7.

36. Chakrabarty, A.M., G. Chou, and I.C. Gunsalus, *Genetic regulation of octane dissimilation plasmid in Pseudomonas.* Proc Natl Acad Sci U S A, 1973. **70**(4): p. 1137-40.

37. Grund, A., et al., *Regulation of alkane oxidation in Pseudomonas putida.* J Bacteriol, 1975. **123**(2): p. 546-56.

38. Eggink, G., et al., Structure of the Pseudomonas putida alkBAC operon. Identification of transcription and translation products. J Biol Chem, 1987. **262**(13): p. 6400-6.

39. Eggink, G., et al., Controlled and functional expression of the Pseudomonas oleovorans alkane utilizing system in Pseudomonas putida and Escherichia coli. J Biol Chem, 1987. **262**(36): p. 17712-8.

40. Eggink, G., et al., Alkane utilization in Pseudomonas oleovorans. Structure and function of the regulatory locus alkR. J Biol Chem, 1988. **263**(26): p. 13400-5.

41. Kok, M., et al., The Pseudomonas oleovorans alkBAC operon encodes two structurally related rubredoxins and an aldehyde dehydrogenase. J. Biol. Chem., 1989. **264**(10): p. 5442-5451.

42. van Beilen, J.B., M.G. Wubbolts, and B. Witholt, *Genetics of alkane oxidation by Pseudomonas oleovorans.* Biodegradation, 1994. **5**(3-4): p. 161-74.

43. Peterson, J.A., et al., Enzymatic ohgr-Oxidation. II. Function of rubredoxin as the elecron carrier in ω-hydroxylation. J. Biol. Chem., 1967. **242**(19): p. 4334-4340.

44. Peterson, J.A. and M.J. Coon, Enzymatic ohgr-Oxidation. III. Purification and Properties of Rubredoxin, a Component of the ω-hydroxylation system of Pseuomonas oleovorans. J. Biol. Chem., 1968. **243**(2): p. 329-334.

45. Boyer, R.F., E.T. Lode, and M.J. Coon, Reduction of alkyl hydroperoxides to alcohols: role of rubredoxin, an electron carrier in the bacterial hydroxylation of hydrocarbons. Biochem Biophys Res Commun, 1971. **44**(4): p. 925-30.

46. Ueda, T. and M.J. Coon, Enzymatic ohgr Oxidation. VII. Reduced diphosphopyridine nucleotide-rubredoxin reductase: Properties and function as an electron carrier in ω-hydroxylation. J. Biol. Chem., 1972. **247**(16): p. 5010-5016.

47. Eggink, G., et al., Rubredoxin reductase of Pseudomonas oleovorans : Structural relationship to other flavoprotein oxidoreductases based on one NAD and two FAD fingerprints. Journal of Molecular Biology, 1990. **212**(1): p. 135-142.

48. Sieker, L.C., R.E. Stenkamp, and J. LeGall, *Rubredoxin in crystalline state.* Methods Enzymol, 1994. **243**: p. 203-16.

49. Lee, H.J., L.Y. Lian, and N.S. Scrutton, Rubredoxin/rubredoxin reductase of Pseudomonas oleovorans: a model system for investigating interprotein electron transfer. Biochem Soc Trans, 1996. **24**(3): p. 447S.

50. Lee, H.J., L.Y. Lian, and N.S. Scrutton, Recombinant two-iron rubredoxin of Pseudomonas oleovorans: overexpression, purification and characterization by optical, CD and 113Cd NMR spectroscopies. Biochem J, 1997. **328 (Pt 1)**: p. 131-6.

51. Lee, H.J., J. Basran, and N.S. Scrutton, Electron transfer from flavin to iron in the Pseudomonas oleovorans rubredoxin reductase-rubredoxin electron transfer complex. Biochemistry, 1998. **37**(44): p. 15513-22.

52. Perry, A., Structural studies fof the two iron rubredoxin of Pseudomonas oleovorans, in Department of Biochemistry. 2000, University of Leicester: Leicester.

53. Perry, A., L.Y. Lian, and N.S. Scrutton, Two-iron rubredoxin of Pseudomonas oleovorans: production, stability and characterization of the individual iron-binding domains by optical, CD and NMR spectroscopies. Biochem. J., 2001. **354**(1): p. 89-98.

54. Lewis, D.F.V., Cytochromes P450: Structure, Function and Mechanism 1996: Taylor & Francis Ltd

55. Narhi, L.O. and A.J. Fulco, Phenobarbital induction of a soluble cytochrome P-450-dependent fatty acid monooxygenase in Bacillus megaterium. J Biol Chem, 1982. **257**(5): p. 2147-50.

56. Munro, A.W., Purification schemes for the constituent domains of cytochrome P450 BM3 in E. coli. Biochem Soc Trans, 1993. **21 (Pt 3)**(3): p. 316S.

57. Munro, A.W., et al., The role of tryptophan 97 of cytochrome P450 BM3 from Bacillus megaterium in catalytic function. Evidence against the 'covalent switching' hypothesis of P-450 electron transfer. Biochem J, 1994. **303 (Pt 2)**: p. 423-8.

58. Oliver, C.F., et al., Engineering the substrate specificity of Bacillus megaterium cytochrome P-450 BM3: hydroxylation of alkyl trimethylammonium compounds. Biochem J, 1997. **327 (Pt 2)**: p. 537-44.

59. Oliver, C.F., et al., A single mutation in cytochrome P450 BM3 changes substrate orientation in a catalytic intermediate and the regiospecificity of hydroxylation. Biochemistry, 1997. **36**(7): p. 1567-72.

60. Noble, M.A., et al., *Roles of key active-site residues in flavocytochrome P450 BM3.* Biochem J, 1999. **339 (Pt 2)**: p. 371-9.

61. Ost, T.W., et al., Rational re-design of the substrate binding site of flavocytochrome P450 BM3. FEBS Lett, 2000. **486**(2): p. 173-7.

62. Miles, J.S., et al., Domains of the catalytically self-sufficient cytochrome P-450 BM-3. Genetic construction, overexpression, purification and spectroscopic characterization. Biochem J, 1992. **288 (Pt 2)**: p. 503-9.

63. Coon, M.J., et al., *Assays for cytochrome P-450 peroxygenase activity*. Methods Enzymol, 1990. **186**: p. 273-8.

64. Cirino, P.C.A., Frances H. , Regioselectivity and Activity of Cytochrome P450 BM-3 and Mutant F87A in Reactions Driven by Hydrogen Peroxide. Advanced Synthesis & Catalysis, 2002. **344**(9): p. 932-937.

65. Reipa, V., M.P. Mayhew, and V.L. Vilker, *A direct electrode-driven P450 cycle for biocatalysis*. 1997. p. 13554-13558.

66. Lvov, Y.M., et al., Direct Electrochemistry of Myoglobin and Cytochrome P450cam in Alternate Layer-by-Layer Films with DNA and Other Polyions. J. Am. Chem. Soc., 1998. **120**(17): p. 4073-4080.

67. Schwaneberg, U., et al., P450 in biotechnology: zinc driven omega-hydroxylation of p-nitrophenoxydodecanoic acid using P450 BM-3 F87A as a catalyst. J Biotechnol, 2000. **84**(3): p. 249-57.

68. Lei, C., et al., *Clay-Bridged Electron Transfer between Cytochrome P450cam and Electrode.* Biochemical and Biophysical Research Communications, 2000. **268**(3): p. 740-744.

69. Sambrook. J, F.F.E.a.M.T., *Molecular cloning a laboratory manual, 2nd ed.* 1989: Cold springs laboratory press.

70. Tartof, K.D. and C.A. Hobbs, New cloning vectors and techniques for easy and rapid restriction mapping. Gene, 1988. **67**(2): p. 169-82.

71. Studier, F.W. and B.A. Moffatt, Use of bacteriophage T7 RNA polymerase to direct selective high-level expression of cloned genes. J Mol Biol, 1986. **189**(1): p. 113-30.

72. Miroux, B. and J.E. Walker, Over-production of proteins in Escherichia coli: mutant hosts that allow synthesis of some membrane proteins and globular proteins at high levels. J Mol Biol, 1996. **260**(3): p. 289-98.

73. Vieira, J. and J. Messing, *Production of single-stranded plasmid DNA.* Methods Enzymol, 1987. **153**: p. 3-11.

74. Shanklin, J., et al., Mossbauer studies of alkane omega-hydroxylase: evidence for a diiron cluster in an integral-membrane enzyme. Proc Natl Acad Sci U S A, 1997. **94**(7): p. 2981-6.

75. Birnboim, H.C. and J. Doly, A rapid alkaline extraction procedure for screening recombinant plasmid DNA. Nucleic Acids Res, 1979. **7**(6): p. 1513-23.

76. Vogelstein, B. and D. Gillespie, *Preparative and analytical purification of DNA from agarose.* Proc Natl Acad Sci U S A, 1979. **76**(2): p. 615-9.

77. Sanger, F., S. Nicklen, and A.R. Coulson, *DNA sequencing with chain-terminating inhibitors.* Proc Natl Acad Sci U S A, 1977. **74**(12): p. 5463-7.

78. Thompson, J.D., et al., The CLUSTAL_X windows interface: flexible strategies for multiple sequence alignment aided by quality analysis tools. Nucleic Acids Res, 1997. **25**(24): p. 4876-82.

79. Tambyrajah, W.S., Purification, inter-protein binding and electron transfer reactions in the alkane hydroxylase system of Pseudomonas oleovorans, in Faculty of Medicine and Biological Sciences. 2003, University of Leicester: Leicester. p. 209.

80. Lode, E.T. and M.J. Coon, Enzymatic omega-oxidation. V. Forms of Pseudomonas oleovorans rubredoxin containing one or two iron atoms: structure and function in omega-hydroxylation. J Biol Chem, 1971. **246**(3): p. 791-802.

81. Laemmli, U.K., Cleavage of structural proteins during the assembly of the head of bacteriophage T4. Nature, 1970. **227**(5259): p. 680-5.

82. Omura, T. and R. Sato, *A new cytochrome in liver microsomes.* J Biol Chem, 1962. **237**: p. 1375-6.

83. Modi, S., et al., Effect of replacement of ferriprotoporphyrin IX in the haem domain of cytochrome P-450 BM-3 on substrate binding and catalytic activity. Biochem J, 1995. **310 (Pt 3)**: p. 939-43.

84. Dutton, P.L., Redox potentiometry: determination of midpoint potentials of oxidation-reduction components of biological electron-transfer systems. Methods Enzymol, 1978. **54**: p. 411-35.

85. Matson, R.S., R.S. Hare, and A.J. Fulco, Characteristics of a cytochrome P-450-dependent fatty acid omega-2 hydroxylase from bacillus megaterium. Biochim Biophys Acta, 1977. **487**(3): p. 487-94.

86. Dawson, R.M.C., *Data for biochemical research*. 3. ed. 1987, Oxford: Clarendon. 13, 580 S.

87. Ellman, G.L., *Tissue sulfhydryl groups.* Arch Biochem Biophys, 1959. **82**(1): p. 70-7.

88. Riener, C.K., G. Kada, and H.J. Gruber, Quick measurement of protein sulfhydryls with Ellman's reagent and with 4,4'-dithiodipyridine. Anal Bioanal Chem, 2002. **373**(4-5): p. 266-76.

89. Dutton, P.L., Redox Potentiometry: Determination of Midpoint Potentials of Oxidation-Reduction Components of Biological Electron-Transfer Systems. Methods in Enzymology. **54**: p. 411-435.

90. Kusunose, M., E. Kusunose, and M.J. Coon, Enzymatic Omega-Oxidation of Fatty Acids. I. Products of Octanoate, Deconate, and Laurate Oxidation. J Biol Chem, 1964. **239**: p. 1374-80.

91. Kusunose, M., E. Kusunose, and M.J. Coon, Enzymatic Omega-Oxidation of Fatty Acids. Ii. Substrate Specificity and Other Properties of the Enzyme System. J Biol Chem, 1964. **239**: p. 2135-9.

92. Ueda, T., E.T. Lode, and M.J. Coon, Enzymatic ohgr-Oxidation. VI. Isolation of homogeneous reduced diphosphopyridine nucleotide-rubredoxing reductase. J. Biol. Chem., 1972. **247**(7): p. 2109-2116.

93. McKenna, E.J. and M.J. Coon, Enzymatic omega-oxidation. IV. Purification and properties of the omega-hydroxylase of Pseudomonas oleovorans. J Biol Chem, 1970. **245**(15): p. 3882-9.

94. Peterson, J.A., D. Basu, and M.J. Coon, Enzymatic ohgr-Oxidation. I. Electron carriers in fatty acid and hydrocarbon hydroxylation. J. Biol. Chem., 1966. **241**(21): p. 5162-5164.

95. van Beilen, J.B., et al., DNA sequence determination and functional characterization of the OCT-plasmid-encoded alkJKL genes of Pseudomonas oleovorans. Mol Microbiol, 1992. **6**(21): p. 3121-36.

96. Tani, A., et al., Gene structures and regulation of the alkane hydroxylase complex in Acinetobacter sp. strain M-1. J Bacteriol, 2001. **183**(5): p. 1819-23.

97. Smits, T.H., B. Witholt, and J.B. van Beilen, *Functional characterization of genes involved in alkane oxidation by Pseudomonas aeruginosa.* Antonie Van Leeuwenhoek, 2003. **84**(3): p. 193-200.

98. Perry, A., et al., Solution Structure of the Two-Iron Rubredoxin of *Pseudomonas oleovorans* Determined by NMR Spectroscopy and Solution X-ray Scattering and Interactions with Rubredoxin Reductase. Biochemistry, 2004. **43**(11): p. 3167-3182.

99. Bellamacina, C.R., The nicotinamide dinucleotide binding motif: a comparison of nucleotide binding proteins. FASEB J, 1996. **10**(11): p. 1257-69.

100. Dym, O. and D. Eisenberg, *Sequence-structure analysis of FAD-containing proteins.* Protein Sci, 2001. **10**(9): p. 1712-1728.

101. Lange, S.J. and L. Que, Jr., *Oxygen activating nonheme iron enzymes.* Curr Opin Chem Biol, 1998. **2**(2): p. 159-72.

102. Ruettinger, R.T., G.R. Griffith, and M.J. Coon, *Characterization of the omega-hydroxylase of Pseudomonas oleovorans as a nonheme iron protein.* Arch Biochem Biophys, 1977. **183**(2): p. 528-37.

103. Ruettinger, R.T., et al., Identification of the omega-hydroxylase of Pseudomonas oleovorans as a nonheme iron protein requiring phospholipid for catalytic activity. Biochem Biophys Res Commun, 1974. **57**(4): p. 1011-7.

104. Nieboer, M., J. Kingma, and B. Witholt, The alkane oxidation system of Pseudomonas oleovorans: induction of the alk genes in Escherichia coli W3110 (pGEc47) affects membrane biogenesis and results in overexpression of alkane hydroxylase in a distinct cytoplasmic membrane subfraction. Mol Microbiol, 1993. **8**(6): p. 1039-51.

105. Staijen, I.E., V. Hatzimanikatis, and B. Witholt, The AlkB monooxygenase of Pseudomonas oleovorans--synthesis, stability and level in recombinant Escherichia coli and the native host. Eur J Biochem, 1997. **244**(2): p. 462-70.

106. Staijen, I.E., J.B. Van Beilen, and B. Witholt, Expression, stability and performance of the three-component alkane mono-oxygenase of Pseudomonas oleovorans in Escherichia coli. Eur J Biochem, 2000. **267**(7): p. 1957-65.

107. van Beilen, J.B., D. Penninga, and B. Witholt, *Topology of the membrane-bound alkane hydroxylase of Pseudomonas oleovorans.* J Biol Chem, 1992. **267**(13): p. 9194-201.

108. Suzuki, M., et al., Primary structure of xylene monooxygenase: similarities to and differences from the alkane hydroxylation system. J Bacteriol, 1991. **173**(5): p. 1690-5.

109. Shanklin, J., E. Whittle, and B.G. Fox, Eight histidine residues are catalytically essential in a membrane-associated iron enzyme, stearoyl-CoA desaturase, and are conserved in alkane hydroxylase and xylene monooxygenase. Biochemistry, 1994. **33**(43): p. 12787-94.

110. Shanklin, J. and E. Whittle, Evidence linking the Pseudomonas oleovorans alkane omega-hydroxylase, an integral membrane diiron enzyme, and the fatty acid desaturase family. FEBS Lett, 2003. **545**(2-3): p. 188-92.

111. Sotsky, J.B., C.W. Greer, and R.M. Atlas, Frequency of genes in aromatic and aliphatic hydrocarbon biodegradation pathways within bacterial populations from Alaskan sediments. Can J Microbiol, 1994. **40**(11): p. 981-5.

112. Whyte, L.G., et al., Prevalence of alkane monooxygenase genes in Arctic and Antarctic hydrocarbon-contaminated and pristine soils1. FEMS Microbiology Ecology, 2002. **41**(2): p. 141-150.

113. Marin, M.M., et al., The alkane hydroxylase gene of Burkholderia cepacia RR10 is under catabolite repression control. J Bacteriol, 2001. **183**(14): p. 4202-9.

114. J. P. Vandecasteele, D.B.J.P.T.A.M.B.L.G., *Enzymology of alkane degradation in pseudomonas aeruginosa.* Acta Biotechnologica, 1983. **3**(4): p. 339-344.

115. Marin, M.M., L. Yuste, and F. Rojo, Differential expression of the components of the two alkane hydroxylases from Pseudomonas aeruginosa. J Bacteriol, 2003. **185**(10): p. 3232-7.

116. Ratajczak, A., W. Geissdorfer, and W. Hillen, Expression of alkane hydroxylase from Acinetobacter sp. Strain ADP1 is induced by a broad range of n-alkanes and requires the transcriptional activator AlkR. J Bacteriol, 1998. **180**(22): p. 5822-7.

117. Ratajczak, A., W. Geissdorfer, and W. Hillen, Alkane hydroxylase from Acinetobacter sp. strain ADP1 is encoded by alkM and belongs to a new family of bacterial integral-membrane hydrocarbon hydroxylases. Appl Environ Microbiol, 1998. **64**(4): p. 1175-9.

118. Cole, S.T., et al., Deciphering the biology of Mycobacterium tuberculosis from the complete genome sequence. Nature, 1998. **393**(6685): p. 537-44.

119. Hou, C.T., et al., *Microbial oxidation of cumene by octane-grown cells.* Applied Microbiology and Biotechnology, 1994. **41**(2): p. 178-182.

120. Whyte, L.G., et al., Biodegradation of variable-chain-length alkanes at low temperatures by a psychrotrophic Rhodococcus sp. Appl Environ Microbiol, 1998. **64**(7): p. 2578-84.

121. Whyte, L.G., et al., Gene cloning and characterization of multiple alkane hydroxylase systems in Rhodococcus strains Q15 and NRRL B-16531. Appl Environ Microbiol, 2002. **68**(12): p. 5933-42.

122. Witholt, B., et al., Bioconversions of aliphatic compounds byPseudomonas oleovorans in multiphase bioreactors: background and economic potential. Trends in Biotechnology, 1990. **8**: p. 46-52.

123. Katopodis, A.G., H.A. Smith, and S.W. May, New oxyfunctionalization capabilities for .omega.-hydroxylases. Asymmetric aliphatic sulfoxidation and branched ether demethylation. J. Am. Chem. Soc., 1988. **110**(3): p. 897-899.

124. Van Beilen, J.B., Alkane oxidation by Pseudomonas oleovorans: Genes and proteins, in Department of Biochemistry. 1994, University of Groningen: Groningen.

125. Shanklin, J., Overexpression and purification of the Escherichia coli inner membrane enzyme acyl-acyl carrier protein synthase in an active form. Protein Expr Purif, 2000. **18**(3): p. 355-60.

126. Arechaga, I., et al., Characterisation of new intracellular membranes in Escherichia coli accompanying large scale over-production of the b subunit of F(1)F(o) ATP synthase. FEBS Lett, 2000. **482**(3): p. 215-9.

127. Dumon-Seignovert, L., G. Cariot, and L. Vuillard, The toxicity of recombinant proteins in Escherichia coli: a comparison of overexpression in BL21(DE3), C41(DE3), and C43(DE3). Protein Expr Purif, 2004. **37**(1): p. 203-6.

128. Hagelueken, G., et al., Crystal structure of the electron transfer complex rubredoxin rubredoxin reductase of Pseudomonas aeruginosa. Proc Natl Acad Sci U S A, 2007. **104**(30): p. 12276-81.

129. van Beilen, J.B., et al., *Rubredoxins involved in alkane oxidation.* J Bacteriol, 2002. **184**(6): p. 1722-32.

130. Staijen, I.E. and B. Witholt, Synthesis of alkane hydroxylase of Pseudomonas oleovorans increases the iron requirement of alk+ bacterial strains. Biotechnol Bioeng, 1998. **57**(2): p. 228-37.

131. Mohanty, A.K. and M.C. Wiener, Membrane protein expression and production: effects of polyhistidine tag length and position. Protein Expr Purif, 2004. **33**(2): p. 311-25.

132. Lundstrom, K.H., *Structural genomics on membrane proteins*. 2006, Boca Raton: CRC/Taylor & Francis. 383 p., [12] p. of plates.

133. GE Healthcare Bio-Sciences., *Affinity chromatography : principles and methods*. 2007, Uppsala: GE Healthcare Bio-Sciences. 155 s.

134. CLONTECH Laboratories., *Protein Purification Products*. 2007, CLONTECH Laboratories: Palo Alto, Calif. p. v.

135. Xu, M., X. Xiao, and F. Wang, Isolation and characterization of alkane hydroxylases from a metagenomic library of Pacific deep-sea sediment. Extremophiles, 2008. **12**(2): p. 255-262.

136. van Beilen, J.B., et al., Identification of an Amino Acid Position That Determines the Substrate Range of Integral Membrane Alkane Hydroxylases. J. Bacteriol., 2005. **187**(1): p. 85-91.

137. Millhauser, G.L., Selective placement of electron spin resonance spin labels: new structural methods for peptides and proteins. Trends Biochem Sci, 1992. **17**(11): p. 448-52.

138. Millhauser, G.L., W.R. Fiori, and S.M. Miick, *Electron spin labels.* Methods Enzymol, 1995. **246**: p. 589-610.

139. Hubbell, W.L., D.S. Cafiso, and C. Altenbach, *Identifying conformational changes with site-directed spin labeling.* Nat Struct Biol, 2000. **7**(9): p. 735-9.

140. Hubbell, W.L., et al., *Watching proteins move using site-directed spin labeling.* Structure, 1996. **4**(7): p. 779-83.

141. Beilen, J.B.v. and E.G. Funhoff, *Expanding the alkane oxygenase toolbox: new enzymes and applications.* Current Opinion in Biotechnology, 2005. **16**(3): p. 308-314.

142. Funhoff, E.G., et al., CYP153A6, a soluble P450 oxygenase catalyzing terminal-alkane hydroxylation. J Bacteriol, 2006. **188**(14): p. 5220-7.

143. Sligar, S.G., *Nature's universal oxygenases: the cytochromes P450.* Essays Biochem, 1999. **34**: p. 71-83.

144. Nelson, D.R., *Cytochrome P450 and the individuality of species.* Arch Biochem Biophys, 1999. **369**(1): p. 1-10.

145. Munro, A.W., et al., Formation of flavin semiquinone during the reduction of P450 BM3 reductase domain with NADPH. Biochem Soc Trans, 1996. **24**(1): p. 18S.

146. Munro, A.W. and J.G. Lindsay, *Bacterial cytochromes P-450.* Mol Microbiol, 1996. **20**(6): p. 1115-25.

147. Precious, W.Y. and J. Barrett, *Xenobiotic metabolism in helminths.* Parasitol Today, 1989. **5**(5): p. 156-60.

148. Nelson, D.R. *Cytochrome P450 Homepage*. [Webpage] 1999 November 29th 2006 [cited 2002-2007]; Available from: http://drnelson.utmem.edu/CytochromeP450.html.

149. Nelson, D.R., et al., P450 superfamily: update on new sequences, gene mapping, accession numbers and nomenclature. Pharmacogenetics, 1996. **6**(1): p. 1-42.

150. Rendic, S. and F.J. Di Carlo, Human cytochrome P450 enzymes: a status report summarizing their reactions, substrates, inducers, and inhibitors. Drug Metab Rev, 1997. **29**(1-2): p. 413-580.

151. Rendic, S., Summary of information on human CYP enzymes: human P450 metabolism data. Drug Metab Rev, 2002. **34**(1-2): p. 83-448.

152. Mansuy, D., *The great diversity of reactions catalyzed by cytochromes P450.* Comp Biochem Physiol C Pharmacol Toxicol Endocrinol, 1998. **121**(1-3): p. 5-14.

153. Klingenberg, M., *Pigments of rat liver microsomes.* Arch Biochem Biophys, 1958. **75**(2): p. 376-86.

154. Garfinkel, D., Studies on pig liver microsomes. I. Enzymic and pigment composition of different microsomal fractions. Arch Biochem Biophys, 1958. **77**(2): p. 493-509.

155. Omura, T. and R. Sato, The Carbon Monoxide-Binding Pigment of Liver Microsomes. I. Evidence for Its Hemoprotein Nature. J Biol Chem, 1964. **239**: p. 2370-8.

156. Dawson, J.H., L.A. Andersson, and M. Sono, Spectroscopic investigations of ferric cytochrome P-450-CAM ligand complexes. Identification of the ligand trans to cysteinate in the native enzyme. J Biol Chem, 1982. **257**(7): p. 3606-17.

157. Champion, P.M., et al., *Resonance Raman detection of an iron-sulfur bond in cytochrome P 450cam.* J. Am. Chem. Soc., 1982. **104**(20): p. 5469-5472.

158. Poulos, T.L., B.C. Finzel, and A.J. Howard, *High-resolution crystal structure of cytochrome P450cam.* J Mol Biol, 1987. **195**(3): p. 687-700.

159. Nelson, D.R., *Cytochrome P450 nomenclature, 2004.* Methods Mol Biol, 2006. **320**: p. 1-10.

160. Palmer, G. and J. Reedijk, Nomenclature Committee of the International Union of Biochemistry (NC- IUB). Nomenclature of electron-transfer proteins. Recommendations 1989. J. Biol. Chem., 1992. **267**(1): p. 665-677.

161. Lewis, D.F., Three-dimensional models of human and other mammalian microsomal P450s constructed from an alignment with P450102 (P450bm3). Xenobiotica, 1995. **25**(4): p. 333-66.

162. Pikuleva, I. and M. Waterman, Cytochromes P450 in synthesis of steroid hormones, bile acids, vitamin D3 and cholesterol. Mol Aspects Med, 1999. **20**(1-2): p. 33-42, 43-37.

163. Sono, M., et al., *Heme-Containing Oxygenases.* Chem Rev, 1996. **96**(7): p. 2841-2888.

164. Mueller, E.J., P.J. Loida, and S.G. Sligar, *Twenty-five years of P450cam research.*, in *Cytochrome P450 Structure, Mechanism, and Biochemistry*, P.R. Ortiz de Montellano, Editor. 1995, Plenum Press.

165. Cupp-Vickery, J.R. and T.L. Poulos, Structure of cytochrome P450eryF: substrate, inhibitors, and model compounds bound in the active site. Steroids, 1997. **62**(1): p. 112-6.

166. Chapple, C., *Molecular-Genetic Analysis of Plant Cytochrome P450-Dependent Monooxygenases.* Annu Rev Plant Physiol Plant Mol Biol, 1998. **49**: p. 311-343.

167. Williams, P.A., et al., Crystal structure of human cytochrome P450 2C9 with bound warfarin. Nature, 2003. **424**(6947): p. 464-468.

168. Narhi, L.O. and A.J. Fulco, Characterization of a catalytically self-sufficient 119,000-dalton cytochrome P-450 monooxygenase induced by barbiturates in Bacillus megaterium. J Biol Chem, 1986. **261**(16): p. 7160-9.

169. Narhi, L.O. and A.J. Fulco, Identification and characterization of two functional domains in cytochrome P-450BM-3, a catalytically self-sufficient monooxygenase induced by barbiturates in Bacillus megaterium. J Biol Chem, 1987. **262**(14): p. 6683-90.

170. Ruettinger, R.T., L.P. Wen, and A.J. Fulco, Coding nucleotide, 5' regulatory, and deduced amino acid sequences of P-450BM-3, a single peptide cytochrome P-450:NADPH-P-450 reductase from Bacillus megaterium. J Biol Chem, 1989. **264**(19): p. 10987-95.

171. Nebert, D.W., et al., The P450 superfamily: update on new sequences, gene mapping, and recommended nomenclature. DNA Cell Biol, 1991. **10**(1): p. 1-14.

172. Nakayama, N., A. Takemae, and H. Shoun, Cytochrome P450foxy, a Catalytically Self-Sufficient Fatty Acid Hydroxylase of the Fungus Fusarium oxysporum. J Biochem (Tokyo), 1996. **119**(3): p. 435-440.

173. Kitazume, T., et al., Fusarium oxysporum Fatty-acid Subterminal Hydroxylase (CYP505) Is a Membrane-bound Eukaryotic Counterpart of Bacillus megaterium Cytochrome P450BM3. J. Biol. Chem., 2000. **275**(50): p. 39734-39740.

174. Kunst, F., et al., The complete genome sequence of the gram-positive bacterium Bacillus subtilis. Nature, 1997. **390**(6657): p. 249-56.

175. De Mot, R. and A.H. Parret, A novel class of self-sufficient cytochrome P450 monooxygenases in prokaryotes. Trends Microbiol, 2002. **10**(11): p. 502-8.

176. Ikeda, H., et al., Complete genome sequence and comparative analysis of the industrial microorganism Streptomyces avermitilis. Nat Biotechnol, 2003. **21**(5): p. 526-31.

177. Ivanova, N., et al., Genome sequence of Bacillus cereus and comparative analysis with Bacillus anthracis. Nature, 2003. **423**(6935): p. 87-91.

178. Roberts, G.A., et al., Identification of a new class of cytochrome P450 from a Rhodococcus sp. J Bacteriol, 2002. **184**(14): p. 3898-908.

179. Warman, A.J., The Molecular Enzymology of Cytochromes P450 of Biotechnological and Medical Interest, in Biochemistry. 2007, Leicester: Leicester.

180. Roberts, G.A., et al., A Self-sufficient Cytochrome P450 with a Primary Structural Organization That Includes a Flavin Domain and a [2Fe-2S] Redox Center J. Biol. Chem., 2003. **278**(49): p. 48914-48920.

181. Green, A.J., et al., Expression, purification and characterization of cytochrome P450 Biol: a novel P450 involved in biotin synthesis in Bacillus subtilis. J Biol Inorg Chem, 2001. **6**(5-6): p. 523-33.

182. Takaya, N., et al., Cytochrome p450nor, a novel class of mitochondrial cytochrome P450 involved in nitrate respiration in the fungus Fusarium oxysporum. Arch Biochem Biophys, 1999. **372**(2): p. 340-6.

183. Matsunaga, I., et al., Enzymatic reaction of hydrogen peroxide-dependent peroxygenase cytochrome P450s: kinetic deuterium isotope effects and analyses by resonance Raman spectroscopy. Biochemistry, 2002. **41**(6): p. 1886-92.

184. Lee, D.S., et al., Substrate recognition and molecular mechanism of fatty acid hydroxylation by cytochrome P450 from Bacillus subtilis. Crystallographic, spectroscopic, and mutational studies. J Biol Chem, 2003. **278**(11): p. 9761-7.

185. Nebert, D.W., et al., The P450 superfamily: updated listing of all genes and recommended nomenclature for the chromosomal loci. DNA, 1989. **8**(1): p. 1-13.

186. Nelson, D.R., *Cytochrome P450 nomenclature.* Methods Mol Biol, 1998. **107**: p. 15-24.

187. Denisov, I.G., et al., *Structure and Chemistry of Cytochrome P450.* Chem. Rev., 2005. **105**(6): p. 2253-2278.

188. Poulos, T.L., *Intermediates in P450 catalysis.* Philos Transact A Math Phys Eng Sci, 2005. **363**(1829): p. 793-806; discussion 1035-40.

189. Lewis, D.F. and J.M. Pratt, *The P450 catalytic cycle and oxygenation mechanism.* Drug Metab Rev, 1998. **30**(4): p. 739-86.

190. Raag, R. and T.L. Poulos, Crystal structures of cytochrome P-450CAM complexed with camphane, thiocamphor, and adamantane: factors controlling P-450 substrate hydroxylation. Biochemistry, 1991. **30**(10): p. 2674-84.

191. McKnight, J., et al., Identification of charge-transfer transitions in the optical spectrum of low-spin ferric cytochrome P-450 Bacillus megaterium. Eur J Biochem, 1993. **213**(2): p. 683-7.

192. Sligar, S.G., Coupling of spin, substrate, and redox equilibria in cytochrome P450. Biochemistry, 1976. **15**(24): p. 5399-406.

193. Ortiz de Montellano, P.R., *Cytochrome P450 structure, mechanism, and biochemistry*. 1995, New York: Plenum Press.

194. Daff, S.N., et al., *Redox control of the catalytic cycle of flavocytochrome P-450 BM3.* Biochemistry, 1997. **36**(45): p. 13816-23.

195. Munro, A.W., et al., Flavocytochrome P-450 BM3: a paradigm for the analysis of electron transfer and its control in the P-450s. Biochem Soc Trans, 1999. **27**(2): p. 190-6.

196. Ortiz de Montellano, P.R., *Cytochrome P450 structure, mechanism, and biochemistry*. 2005, New York: Kluwer Academic/Plenum Publishers.

197. Sligar, S.G., T.M. Makris, and I.G. Denisov, Thirty years of microbial P450 monooxygenase research: peroxo-heme intermediates--the central bus station in heme oxygenase catalysis. Biochem Biophys Res Commun, 2005. **338**(1): p. 346-54.

198. Davydov, R., et al., Catalytic mechanism of heme oxygenase through EPR and ENDOR of cryoreduced oxy-heme oxygenase and its Asp 140 mutants. J Am Chem Soc, 2002. **124**(8): p. 1798-808.

199. Raner, G.M., et al., Spectroscopic investigations of intermediates in the reaction of cytochrome P450(BM3)-F87G with surrogate oxygen atom donors. J Inorg Biochem, 2006. **100**(12): p. 2045-53.

200. Munro, A.W., et al., Cytochrome P450 Redox Partner Systems: Bioidiversity and Biotechnological Implications, in Modern Biooxidation: Enzymes, Reasctions and Applicaitons, R.D. Schmid and V.B. Urlacher, Editors. 2007, WILEY-VCH.

201. Joo, H., Z. Lin, and F.H. Arnold, *Laboratory evolution of peroxide-mediated cytochrome P450 hydroxylation.* Nature, 1999. **399**(6737): p. 670-3.

202. Matsunaga, I., et al., Site-directed mutagenesis of the putative distal helix of peroxygenase cytochrome P450. Arch Biochem Biophys, 2001. **394**(1): p. 45-53.

203. Cirino, P.C., *Laboratory evolution of cytochrome p450 peroxygenase activity*, in *Chemical Engineering*. 2004, California Institute of Technology: Pasadena, California.

204. Loida, P.J. and S.G. Sligar, Molecular recognition in cytochrome P-450: mechanism for the control of uncoupling reactions. Biochemistry, 1993. **32**(43): p. 11530-8.

205. Raag, R., et al., Inhibitor-induced conformational change in cytochrome P-450CAM. Biochemistry, 1993. **32**(17): p. 4571-8.

206. Hildebrand, D.P., et al., Trans effects on cysteine ligation in the proximal His93Cys variant of horse heart myoglobin. Biochemistry, 1995. **34**(36): p. 11598-605.

207. Werck-Reichhart, D. and R. Feyereisen, *Cytochromes P450: a success story.* Genome Biol, 2000. **1**(6): p. REVIEWS3003.

208. Raag, R., et al., Crystal structure of the cytochrome P-450CAM active site mutant Thr252Ala. Biochemistry, 1991. **30**(48): p. 11420-9.

209. DeLano, W.L., *The PyMOL Molecular Graphics System* 2002, DeLano Scientific: Palo Alto, CA, USA.

210. Graham, S.E. and J.A. Peterson, *How similar are P450s and what can their differences teach us?* Arch Biochem Biophys, 1999. **369**(1): p. 24-9.

211. Ravichandran, K.G., et al., Crystal structure of hemoprotein domain of P450BM-3, a prototype for microsomal P450's. Science, 1993. **261**(5122): p. 731-6.

212. Leys, D., et al., Atomic structure of Mycobacterium tuberculosis CYP121 to 1.06 A reveals novel features of cytochrome P450. J Biol Chem, 2003. **278**(7): p. 5141-7.

213. Durst, F. and D.R. Nelson, *Diversity and evolution of plant P450 and P450-reductases.* Drug Metabol Drug Interact, 1995. **12**(3-4): p. 189-206.

214. Gotoh, O., Substrate recognition sites in cytochrome P450 family 2 (CYP2) proteins inferred from comparative analyses of amino acid and coding nucleotide sequences. J Biol Chem, 1992. **267**(1): p. 83-90.

215. Omura, T., *Forty years of cytochrome P450.* Biochem Biophys Res Commun, 1999. **266**(3): p. 690-8.

216. Mayhew, M.P., et al., Improving the Cytochrome P450 Enzyme System for Electrode-Driven Biocatalysis of Styrene Epoxidation. 2000. p. 610-616.

217. Bell, S.G., C.F. Harford-Cross, and L.L. Wong, *Engineering the CYP101 system for in vivo oxidation of unnatural substrates.* Protein Eng, 2001. **14**(10): p. 797-802.

218. Bottner, B., H. Schrauber, and R. Bernhardt, *Engineering a mineralocorticoid- to a glucocorticoid-synthesizing cytochrome P450.* J Biol Chem, 1996. **271**(14): p. 8028-33.

219. Harford-Cross, C.F., et al., Protein engineering of cytochrome p450(cam) (CYP101) for the oxidation of polycyclic aromatic hydrocarbons. Protein Eng, 2000. **13**(2): p. 121-8.

220. Li, Q.S., et al., Directed evolution of the fatty-acid hydroxylase P450 BM-3 into an indole-hydroxylating catalyst. Chemistry, 2000. **6**(9): p. 1531-6.

221. Fulco, A.J., P450BM-3 and other inducible bacterial P450 cytochromes: biochemistry and regulation. Annu Rev Pharmacol Toxicol, 1991. **31**: p. 177-203.

222. Shirane, N., et al., Cytochrome P450BM-3 (CYP102): regiospecificity of oxidation of omega-unsaturated fatty acids and mechanism-based inactivation. Biochemistry, 1993. **32**(49): p. 13732-41.

223. Boddupalli, S.S., R.W. Estabrook, and J.A. Peterson, *Fatty acid monooxygenation by cytochrome P-450BM-3.* J Biol Chem, 1990. **265**(8): p. 4233-9.

224. Capdevila, J.H., et al., The highly stereoselective oxidation of polyunsaturated fatty acids by cytochrome P450BM-3. J Biol Chem, 1996. **271**(37): p. 22663-71.

225. Munro, A.W., et al., Analysis of the structural stability of the multidomain enzyme flavocytochrome P-450 BM3. Biochim Biophys Acta, 1996. **1296**(2): p. 127-37.

226. Davis, S.C., et al., *Oxidation of omega-oxo fatty acids by cytochrome P450BM-3 (CYP102).* Arch Biochem Biophys, 1996. **328**(1): p. 35-42.

227. Murataliev, M.B. and R. Feyereisen, Functional interactions in cytochrome P450BM3. Fatty acid substrate binding alters electron-transfer properties of the flavoprotein domain. Biochemistry, 1996. **35**(47): p. 15029-37.

228. Munro, A.W., et al., Structural and enzymological analysis of the interaction of isolated domains of cytochrome P-450 BM3. FEBS Lett, 1994. **343**(1): p. 70-4.

229. Li, H.Y., K. Darwish, and T.L. Poulos, Characterization of recombinant Bacillus megaterium cytochrome P-450 BM-3 and its two functional domains. J Biol Chem, 1991. **266**(18): p. 11909-14.

230. Li, H. and T.L. Poulos, The structure of the cytochrome p450BM-3 haem domain complexed with the fatty acid substrate, palmitoleic acid. Nat Struct Biol, 1997. **4**(2): p. 140-6.

231. Joyce, M.G., et al., A single mutation in cytochrome P450 BM3 induces the conformational rearrangement seen upon substrate binding in the wild-type enzyme. J Biol Chem, 2004. **279**(22): p. 23287-93.

232. Haines, D.C., A role for the strained phenylalanine ring rotation induced by substrate binding to cytochrome CYP102A1. Protein Pept Lett, 2006. **13**(10): p. 977-80.

233. Girvan, H.M., et al., Structural and spectroscopic characterization of P450 BM3 mutants with unprecedented P450 heme iron ligand sets. New heme ligation states influence conformational equilibria in P450 BM3. J Biol Chem, 2007. **282**(1): p. 564-72.

234. Huang, W.C., et al., Filling a hole in cytochrome P450 BM3 improves substrate binding and catalytic efficiency. J Mol Biol, 2007. **373**(3): p. 633-51.

235. Graham-Lorence, S., et al., An active site substitution, F87V, converts cytochrome P450 BM-3 into a regio- and stereoselective (14S,15R)-arachidonic acid epoxygenase. J Biol Chem, 1997. **272**(2): p. 1127-35.

236. Schwaneberg, U., et al., A Continuous Spectrophptometric Assay for P450 BM-3, a Fatty Acid Hydroxylating Enzyme, and Its Mutant F87A. Analytical Biochemistry, 1999. **269**: p. 359-366.

237. Cowart, L.A., J.R. Falck, and J.H. Capdevila, *Structural determinants of active site binding affinity and metabolism by cytochrome P450 BM-3.* Arch Biochem Biophys, 2001. **387**(1): p. 117-24.

238. Li, Q.S., et al., Engineering cytochrome P450 BM-3 for oxidation of polycyclic aromatic hydrocarbons. Appl Environ Microbiol, 2001. **67**(12): p. 5735-9.

239. Li, Q.S., et al., Rational evolution of a medium chain-specific cytochrome P-450 BM-3 variant. Biochim Biophys Acta, 2001. **1545**(1-2): p. 114-21.

240. Raner, G.M., et al., Regioselective peroxo-dependent heme alkylation in P450(BM3)-F87G by aromatic aldehydes: effects of alkylation on cataysis. Biochemistry, 2002. **41**(30): p. 9601-10.

241. Li, Q.S., et al., Residue size at position 87 of cytochrome P450 BM-3 determines its stereoselectivity in propylbenzene and 3-chlorostyrene oxidation. FEBS Lett, 2001. **508**(2): p. 249-52.

242. Schulze, H., R.D. Schmid, and T.T. Bachmann, Activation of phosphorothionate pesticides based on a cytochrome P450 BM-3 (CYP102 A1) mutant for expanded neurotoxin detection in food using acetylcholinesterase biosensors. Anal Chem, 2004. **76**(6): p. 1720-5.

243. Cirino, P.C. and F.H. Arnold, *A self-sufficient peroxide-driven hydroxylation biocatalyst.* Angew Chem Int Ed Engl, 2003. **42**(28): p. 3299-301.

244. Noble, M.A., et al., Imidazolyl carboxylic acids as mechanistic probes of flavocytochrome P-450 BM3. Biochemistry, 1998. **37**(45): p. 15799-807.

245. Perera, R., et al., Neutral thiol as a proximal ligand to ferrous heme iron: implications for heme proteins that lose cysteine thiolate ligation on reduction. Proc Natl Acad Sci U S A, 2003. **100**(7): p. 3641-6.

246. Munro, A.W., J.R. Coggins, and J.G. Lindsay, *A novel inhibitor of cytochrome P450 BM3.* Biochem Soc Trans, 1993. **21**(4): p. 411S.

247. Munro, A.W., J.R. Coggins, and J.G. Lindsay, Regional saturation mutagenesis as an approach to identification of substrate specificity determinants in cytochrome P450 BM3. Biochem Soc Trans, 1993. **21**(4): p. 409S.

248. Girvan, H.M., Characterisacion of flavocytochrome P450 BM3 site directed mutants with novel heme ligation state, in Biochmistry. 2005, University of Leicester: Leicester.

249. Hyman Yalkowsky, S., Handbook of Aqueous Solubility Data: An Extensive Compilation of Aqueous Solubility Data for Organic Compounds Extracted from the AQUASOL DATABASE. 2003: CRC Press.

250. Carmichael, A.B. and L.L. Wong, Protein engineering of Bacillus megaterium CYP102.The oxidation of polycyclic aromatic hydrocarbons. Eur J Biochem, 2001. **268**(10): p. 3117-25.

251. Peters, M.W., et al., Regio- and enantioselective alkane hydroxylation with engineered cytochromes P450 BM-3. J Am Chem Soc, 2003. **125**(44): p. 13442-50.

252. Oliver, C.F., The role of active site residues in cytochrome P450 BM3 from Bacillus megaterium in Biochemistry. 1998, University of Leicester: Leicester.

253. Delcarte, J., et al., Optimisation of expression and immobilized metal ion affinity chromatographic purification of recombinant (His)6-tagged cytochrome P450 hydroperoxide lyase in Escherichia coli. J Chromatogr B Analyt Technol Biomed Life Sci, 2003. **786**(1-2): p. 229-36.

254. Jansson, I., et al., *Enhanced expression of CYP1B1 in Escherichia coli.* Toxicology, 2000. **144**(1-3): p. 211-9.

255. Dawson, J.H. and S.P. Cramer, Oxygenated cytochrome P-450cam: evidence against axial histidine ligation of iron. FEBS Lett, 1978. **88**(1): p. 127-30.

256. Hlavica, P. and D.F.V. Lewis, *Allosteric phenomena in cytochrome P450-catalyzed monooxygenations.* European Journal of Biochemistry, 2001. **268**(18): p. 4817-4832.

257. Poulos, T.L., *Cytochrome P450.* Curr Opin Struct Biol, 1995. **5**(6): p. 767-74.

258. Brotea, G.P. and R.J. Thibert, *Fluorometric determination of hydrogen peroxide using resorufin and peroxidase.* Microchemical Journal, 1988. **37**(3): p. 368-376.

259. Zhou, M., et al., A stable nonfluorescent derivative of resorufin for the fluorometric determination of trace hydrogen peroxide: applications in detecting the activity of phagocyte NADPH oxidase and other oxidases. Anal Biochem, 1997. **253**(2): p. 162-8.

260. Towne, V., et al., Complexities in horseradish peroxidase-catalyzed oxidation of dihydroxyphenoxazine derivatives: appropriate ranges for pH values and hydrogen peroxide concentrations in quantitative analysis. Analytical Biochemistry, 2004. **334**(2): p. 290-296.

261. Reeve, C. 2003.

262. Kirchner, G., M.P. Scollar, and A.M. Klibanov, *Resolution of racemic mixtures via lipase catalysis in organic solvents.* J. Am. Chem. Soc., 1985. **107**(24): p. 7072-7076.

263. Khmelnitsky, Y.L., et al., Denaturation capacity: a new quantitative criterion for selection of organic solvents as reaction media in biocatalysis. Eur J Biochem, 1991. **198**(1): p. 31-41.

264. Guagliardi, A., et al., Stability and activity of a thermostable malic enzyme in denaturants and water-miscible organic solvents. Eur J Biochem, 1989. **183**(1): p. 25-30.

265. Zaks, A. and A.M. Klibanov, *Substrate specificity of enzymes in organic solvents vs. water is reversed.* J. Am. Chem. Soc., 1986. **108**(10): p. 2767-2768.

266. Kellner, D.G., S.A. Maves, and S.G. Sligar, *Engineering cytochrome P450s for bioremediation.* Curr Opin Biotechnol, 1997. **8**(3): p. 274-8.

267. Li, Z., et al., *Oxidative biotransformations using oxygenases.* Curr Opin Chem Biol, 2002. **6**(2): p. 136-44.

268. Ye Ni, R.R.C., Accelerating whole-cell biocatalysis by reducing outer membrane permeability barrier. Biotechnology and Bioengineering, 2004. **87**(6): p. 804-811.

269. Schewe, H., B.-A. Kaup, and J. Schrader, Improvement of P450BM-3 whole-cell biocatalysis by integrating heterologous cofactor regeneration combining glucose facilitator and dehydrogenase in E. coli. Applied Microbiology and Biotechnology, 2008. **78**(1): p. 55-65.

270. Marcus, R.A., Electron Transfer Reaction in Chemistry: Theory and Experiemnt, Nobel Lecture, December 8, 1992, in NOBEL LECTURES IN CHEMISTRY 1991 - 1995, B.G. Malmström, Editor. 1997, World Scientific Publishing: Singapore. p. 300.

271. Panke, S., et al., Engineering of a stable whole-cell biocatalyst capable of (S)-styrene oxide formation for continuous two-liquid-phase applications. Appl Environ Microbiol, 1999. **65**(12): p. 5619-23.

272. Maurer, S.C.S., Holger Schmid, Rolf D Urlacher, Vlada Immobilisation of P450 BM-3 and an NADP Cofactor Recycling System: Towards a Technical Application of Heme-Containing Monooxygenases in Fine Chemical Synthesis. 2003. p. 802-810.

273. Hollmann, F., A. Schmid, and E. Steckhan, The First Synthetic Application of a Monooxygenase Employing Indirect Electrochemical NADH Regeneration This work was supported by BASF AG. We thank DEGUSSA AG for the gift of chemicals. Angew Chem Int Ed Engl, 2001. **40**(1): p. 169-171.

274. Wu, J.T., L.H. Wu, and J.A. Knight, Stability of NADPH: effect of various factors on the kinetics of degradation [published erratum appears in Clin Chem 1987 May;33(5):724]. Clin Chem, 1986. **32**(2): p. 314-319.

275. Neeli, R., et al., Switching pyridine nucleotide specificity in P450 BM3: mechanistic analysis of the W1046H and W1046A enzymes. J Biol Chem, 2005. **280**(18): p. 17634-44.

276. Gutierrez, A., et al., Trp-676 facilitates nicotinamide coenzyme exchange in the reductive half-reaction of human cytochrome P450 reductase: properties of the soluble W676H and W676A mutant reductases. Biochemistry, 2000. **39**(51): p. 15990-9.

277. Cirino, P.C., et al., Global incorporation of norleucine in place of methionine in cytochrome P450 BM-3 heme domain increases peroxygenase activity. Biotechnol Bioeng, 2003. **83**(6): p. 729-34.

278. Salazar, O., P.C. Cirino, and F.H. Arnold, *Thermostabilization of a cytochrome p450 peroxygenase.* Chembiochem, 2003. **4**(9): p. 891-3.

279. Estabrook, R.W., et al., *Application of electrochemistry for P450-catalyzed reactions.* Methods Enzymol, 1996. **272**: p. 44-51.

280. Udit, A.K., F.H. Arnold, and H.B. Gray, Cobaltocene-mediated catalytic monooxygenation using holo and heme domain cytochrome P450 BM3. J Inorg Biochem, 2004. **98**(9): p. 1547-50.

281. Faulkner, K.M., et al., Electrocatalytically Driven {omega}-Hydroxylation of Fatty Acids Usings Cytochrome P450 4A1. 1995. p. 7705-7709.

282. Zhang, Z.N., A F . Lu, Z. Schenkman,J B. Rusling, J F, *Direct electron injection from electrodes to cytochrome P450cam in biomembrane-like films.* Journal of the Chemical Society, Faraday Transactions, 1997. **93**(9): p. 1769-1774.

283. Jung, J. and G. Tollin, *Transient kinetics of electron-transfer reactions of flavodoxins.* Biochemistry, 1981. **20**(18): p. 5124-5131.

284. Nocera, D.G., et al., Kinetics of intermolecular and intramolecular electron transfer from ruthenium(II) complexes to ferricytochrome c. J. Am. Chem. Soc., 1984. **106**(18): p. 5145-5150.

285. Bechtold, R., et al., Directional electron transfer in ruthenium-modified horse heart cytochrome c. Nature, 1986. **322**(6076): p. 286-288.

286. Bjerrum, M.J., et al., *Electron transfer in ruthenium-modified proteins.* J Bioenerg Biomembr, 1995. **27**(3): p. 295-302.

287. Magner, E. and G. McLendon, Ground-state and excited-state electron-transfer reactions of zinc cytochrome c. J. Phys. Chem., 1989. **93**(20): p. 7130-7134.

288. Zhou, J.S. and N.M. Kostic, Kinetics of static and diffusive electron transfer between zinc-substituted cytochrome c and plastocyanin. Indications of nonelectrostatic interactions between highly charged metalloproteins. J. Am. Chem. Soc., 1991. **113**(16): p. 6067-6073.

289. Kotlyar, A.B., N. Borovok, and M. Hazani, Use of thiouredopyrenetrisulfonate photochemistry for driving electron transfer reactions in aqueous solutions. Biochemistry, 1997. **36**(50): p. 15823-7.

290. Borovok, N., et al., Photoinduced electron transfer in singly labeled thiouredopyrenetrisulfonate azurin derivatives. FEBS Lett, 1999. **457**(2): p. 277-82.

291. Kotlyar, A., et al., Photoinduced intracomplex electron transfer between cytochrome c oxidase and TUPS-modified cytochrome c. Eur J Biochem, 2000. **267**(18): p. 5805-9.

292. Szundi, I., et al., Photoinduced electron transfer in the cytochrome c/cytochrome c oxidase complex using thiouredopyrenetrisulfonate-labeled cytochrome c. Optical multichannel detection. Biochemistry, 2001. **40**(7): p. 2186-93.

293. Liu, R.Q., et al., Design of ruthenium-cytochrome c derivatives to measure electron transfer to cytochrome c peroxidase. Biochimie, 1995. **77**(7-8): p. 549-61.

294. Geren, L.M., et al., Design of a ruthenium-cytochrome c derivative to measure electron transfer to the initial acceptor in cytochrome c oxidase. J Biol Chem, 1995. **270**(6): p. 2466-72.

295. Mayo, S.L., et al., *Long-range electron transfer in heme proteins.* Science, 1986. **233**(4767): p. 948-52.

296. Gray, H.B. and J.R. Winkler, *Electron transfer in proteins.* Annu Rev Biochem, 1996. **65**: p. 537-61.

297. Kotlyar, A.B., N. Borovok, and M. Hazani, Photoinduced electron transfer in singly labeled thiouredopyrenetrisulfonate cytochrome c derivatives. Biochemistry, 1997. **36**(50): p. 15828-33.

298. Berg, A., et al., Triplet Characterization and Dynamics of a Novel Pyrene Derivative Covalently Linked to Azurin. J. Phys. Chem. A, 1999. **103**(42): p. 8372-8374.

299. Hasemann, C.A., et al., Crystal structure and refinement of cytochrome P450terp at 2.3 A resolution. J Mol Biol, 1994. **236**(4): p. 1169-85.

300. Sevrioukova, I.F., et al., *Structure of a cytochrome P450-redox partner electron-transfer complex.* Proc Natl Acad Sci U S A, 1999. **96**(5): p. 1863-8.

301. Sevrioukova, I.F., Immoos, C.E., Poulos, T.L. A1 *Electron Transfer in the Ruthenated Heme Domain of Cytochrome P450BM-3.* Israel Journal of Chemistry, 2000. **40**(1): p. 47-53.

302. Harris, D., *Bioenergetics at a Glance*. 1995, Oxford: Blackwell Science Ltd.

303. Gray, H.B. and B.G. Malmstrom, *Long-range electron transfer in multisite metalloproteins.* Biochemistry, 1989. **28**(19): p. 7499-505.

304. Kaneko, T., et al., Complete genomic sequence of nitrogen-fixing symbiotic bacterium Bradyrhizobium japonicum USDA110. DNA Res, 2002. **9**(6): p. 189-97.

305. Cochrane G., A.R., Aldebert P., Althorpe N., Baldwin A., Bates K., Bhattacharyya S., Bonfield J., Bower L., Browne P., Castro M., Cox A., Demiralp F., Eberhardt R., Faruque N., Hoad G., Jang M., Kulikova T., Labarga A., Leinonen R., Leonard S., Lin Q., Lopez R., Lorenc D., McWilliam H., Mukherjee G., Nardone F., Plaister S., Robinson S., Sobhany S., Vaughan R., Wu D., Zhu W., Apweiler R., Hubbard T. and Birney E., *EMBL DDBJ databases*. 2008.

306. Lamb, D.C., et al., Cytochrome p450 complement (CYPome) of the avermectin-producer Streptomyces avermitilis and comparison to that of Streptomyces coelicolor A3(2). Biochem Biophys Res Commun, 2003. **307**(3): p. 610-9.

307. Galagan, J.E., et al., *The genome sequence of the filamentous fungus Neurospora crassa.* Nature, 2003. **422**(6934): p. 859-68.

308. Dean, R.A., et al., The genome sequence of the rice blast fungus Magnaporthe grisea. Nature, 2005. **434**(7036): p. 980-6.

309. Clamp, M., et al., *The Jalview Java alignment editor.* Bioinformatics, 2004. **20**(3): p. 426-7.

310. Klug, C.S. and J.B. Feix, Methods and applications of site-directed spin labeling EPR spectroscopy. Methods Cell Biol, 2008. **84**: p. 617-58.

311. Steinhoff, H.-J., et al., High-field EPR studies of the structure and conformational changes of site-directed spin labeled bacteriorhodopsin. Biochimica et Biophysica Acta (BBA) - Bioenergetics, 2000. **1457**(3): p. 253-262.